

**UCLA**

**UCLA Electronic Theses and Dissertations**

**Title**

Classification of Static and Driven Topological insulators

**Permalink**

<https://escholarship.org/uc/item/4rw7m1kt>

**Author**

Liu, Xu

**Publication Date**

2020

Peer reviewed|Thesis/dissertation

UNIVERSITY OF CALIFORNIA  
Los Angeles

Classification of Static and Driven Topological insulators

A dissertation submitted in partial satisfaction  
of the requirements for the degree  
Doctor of Philosophy in Physics

by

Xu Liu

2020

© Copyright by  
Xu Liu  
2020

# ABSTRACT OF THE DISSERTATION

Classification of Static and Driven Topological insulators

by

Xu Liu

Doctor of Philosophy in Physics

University of California, Los Angeles, 2020

Professor Rahul Roy, Chair

This dissertation focus on the classification of topological matters in static and periodically driven systems.

First, we build a complete topological classification of local unitary operators in free fermionic systems. This result can be encoded in a periodic table with a period of eight, similar to the periodic table of topological insulators. In our classification, we define two local unitaries in a certain symmetry class to be topologically equivalent if they can be connected via finite time evolutions (locally generated unitaries) without breaking the symmetries of the symmetry class while maintaining locality. In this way, the classification we derive will allow us to distinguish locally generated unitaries from those that cannot be locally generated. Besides, we also how to find possible generating Hamiltonians for locally generated unitaries. These results can be used to study the edge behaviors of Floquet systems.

Second, we propose bulk invariants and edge invariants that are locally computable and improve existing topological invariants by being applicable to systems with disorder. Afterward, we set up a rigorous connection between bulk and edge invariants for Floquet systems belonging to Class AIII and class AII of the Altland-Zirnbauer symmetry classification.

Last, after treating a static system as a Floquet system generated by a constant Hamiltonian, we employ the tools we developed in Floquet systems to classify the edge behaviors in static systems.

The dissertation of Xu Liu is approved.

Stuart Brown

Alexander Levine

Yaroslav Tserkovnyak

Rahul Roy, Committee Chair

University of California, Los Angeles

2020

*To my parents.*

# TABLE OF CONTENTS

<b>List of Figures</b> . . . . .	<b>x</b>
<b>List of Tables</b> . . . . .	<b>xv</b>
<b>Acknowledgments</b> . . . . .	<b>xvi</b>
<b>Vita</b> . . . . .	<b>xvii</b>
<b>1 introduction</b> . . . . .	<b>1</b>
1.1 Floquet Topological phases . . . . .	1
1.1.1 Periodically Driven Systems . . . . .	1
1.1.2 An example: The RLBL model . . . . .	3
1.1.3 Topological invariants . . . . .	6
1.1.4 Periodic table for Floquet topological insulators . . . . .	9
1.1.5 Effective edge unitary . . . . .	10
1.2 Outline of this thesis . . . . .	12
<b>2 Classification of Local Unitary Operators</b> . . . . .	<b>13</b>
2.1 Motivations . . . . .	13
2.2 preliminary discussion . . . . .	16
2.3 Flow of quantum systems . . . . .	18
2.3.1 Nontrivial flow in one dimension . . . . .	18
2.3.2 Equivalence Classes of Unitary Operators . . . . .	20
2.3.3 Mapping from Unitary Operators to Flattened Hermitian Operators . . . . .	23
2.3.4 Flow index in higher dimensional systems . . . . .	24

2.3.5	Three Dimensional Quantum Flow . . . . .	26
2.4	Classification of Unitary Operators with Symmetries . . . . .	27
2.4.1	Symmetry Operators and Symmetry Classes for Hermitian Operators	27
2.4.2	Equivalence Classes of Hermitian Operators . . . . .	29
2.4.3	Symmetry Operators and Symmetry Classes for Unitary Operators .	31
2.4.4	Equivalence Classes of Unitary Operators . . . . .	33
2.5	Classification of Unitary Operators without Chiral Symmetry . . . . .	34
2.5.1	Mapping from Unitary Operators to Flattened Hermitian Operators .	34
2.5.2	Mapping from Flattened Hermitian Operators to Unitary Operators .	37
2.5.3	Topological Classification of Local Unitary Operators . . . . .	39
2.6	Unitary Operators with Chiral Symmetry . . . . .	42
2.6.1	Mapping from Unitary Operators to Flattened Hermitian Operators .	42
2.6.2	Mapping from Flattened Hermitian Operators to Unitary Operators .	44
2.6.3	Topological Classification of Local Unitary Operators . . . . .	47
2.7	Examples of Nontrivial Local Unitary Operators . . . . .	48
2.7.1	One Dimension . . . . .	48
2.7.2	Two Dimensions . . . . .	56
2.8	Conclusion . . . . .	57
	<b>Appendices . . . . .</b>	<b>59</b>
2.A	Deviations of flow index . . . . .	59
2.B	Weak topological invariants of unitary operators . . . . .	61
2.C	Eigenstate Properties of Flattened Operators . . . . .	62
2.D	Local unitary transformation . . . . .	64
2.E	Generating nontrivial unitaries from Hamiltonians . . . . .	67

<b>3</b>	<b>Constructing locally generated unitaries</b>	<b>70</b>
3.1	One-dimensional decoupling theory	70
3.2	One dimensional locally generated unitaries	72
3.3	Higher dimensional decoupling theory	75
3.3.1	Decoupling flattened Hermitian operators	75
3.3.2	Unitary operators without chiral symmetry	76
3.3.3	Unitary operators with chiral symmetry	77
<b>4</b>	<b>Chiral flow in one-dimensional floquet topological insulator</b>	<b>78</b>
4.1	Preliminary Discussion	78
4.1.1	The Flow of a Unitary Matrix	78
4.2	Driven Systems with Chiral Symmetry	82
4.2.1	Chiral Symmetry	82
4.2.2	A Model Drive with Chiral Symmetry	83
4.2.3	Winding Number Invariant	84
4.2.4	Chiral Flow Invariant	86
4.3	Dynamical Edge Modes with Chiral Symmetry	89
4.3.1	Protected Dynamical Edge Modes in the Model Drive	89
4.3.2	Edge Invariants	90
4.4	Bulk-Edge Correspondence	94
4.4.1	Bulk-Edge Correspondence at half period	94
4.4.2	Bulk-Edge Correspondence after a complete cycle	98
4.5	Conclusion	98
	<b>Appendices</b>	<b>101</b>

4.A	Extension to Exponentially Decaying Unitaries . . . . .	101
4.A.1	Bulk Invariants . . . . .	102
4.A.2	Edge Invariants . . . . .	104
4.B	Obtaining a Unitary Loop from a General Unitary Evolution . . . . .	107
<b>5</b>	<b>Bulk edge correspondence in high dimensional class AIII . . . . .</b>	<b>110</b>
5.1	A three-dimensional Model Drive with Chiral Symmetry . . . . .	110
5.2	Edge invariants . . . . .	111
5.3	Bulk invariants . . . . .	113
5.4	Bulk-Edge Correspondence . . . . .	114
5.4.1	truncated edge invariants . . . . .	114
5.4.2	Bulk-Edge Correspondence . . . . .	115
	<b>Appendices . . . . .</b>	<b>117</b>
5.A	Projector Calculus . . . . .	117
5.A.1	Winding number . . . . .	121
5.B	Bulk edge correspondence . . . . .	127
5.B.1	Two differential forms . . . . .	127
5.B.2	Bulk invariants . . . . .	130
5.B.3	Expression bulk invariants in two differential forms . . . . .	131
5.B.4	Two cyclic properties . . . . .	133
5.B.5	Edge invariant . . . . .	134
5.B.6	Express edge invariants in differential forms . . . . .	135
5.B.7	Calculate edge invariants . . . . .	136
5.B.8	Connection between edge invariants and bulk invariants . . . . .	141

<b>6</b>	<b>Classification of class AII</b>	<b>142</b>
6.1	Driven Systems with time reversal Symmetry	142
6.1.1	Time reversal symmetry	142
6.1.2	Examples	143
6.1.3	Zero Kitaev flow	145
6.1.4	Construction of edge invariant	146
6.2	The Edge index	150
6.2.1	Properties of the operator A	150
6.2.2	Robustness of the index	153
6.2.3	Properties of the index	155
6.3	Bulk-edge correspondence	156
6.3.1	Bulk invariant	156
6.3.2	Bulk-edge correspondence	158
	<b>Appendices</b>	<b>166</b>
6.A	Edge invariants deviation	166
<b>7</b>	<b>classification of the edge states in static Hamiltonians</b>	<b>167</b>
7.1	Motivations	167
7.2	Constructing unitary loops from a static Hamiltonian	167
7.3	An example: class A Hamiltonian in two dimensions	169
	<b>Bibliography</b>	<b>170</b>

LIST OF FIGURES

1.1 (a)The driving protocol of the four-step RLBL model described in section 1.1.2. Here the  $A$  and  $B$  sublattices are represented by open and filled circles separately. The Hamiltonian is piecewise constant, and there are four steps in total. During each step, a hopping strength of  $J = 1$  is applied along the highlighted bond, and particles can hop to their neighboring sites with probability 1. (b)A depiction of the movements of states initially localized at single sublattices in an open system. Over a complete cycle, states localized in the bulk return precisely to their original position. Along the upper boundary, states initially localized at a  $A$  orbital are translated to the left by two sites (green arrow). While along the lower edge, states initially localized at a  $B$  orbital shift two sites to the right(red arrow). In this way, there are nontrivial edge modes propagating along the boundary. (Figure adapted from Reference [6] with permission from *Annual Reviews of Condensed Matter Physics*.) . . . . . 5

1.2 The spectrum of the Floquet operator  $U(T)$  for the RLBL model in an open system, as defined in Section 1.1.2. In our case, we already assume the lattice spacing  $a$  to be 1 and set the period  $T$  to be  $2\pi$ . And we use the floquet operator to represent the evolution operator evaluated throughout the entire driving period. In the bulk, the Floquet operator acts as the identity matrix at both sublattice  $A$  and  $B$ , thus creates doubly degenerate flat band at quasi-energy zero(blue lines). On the upper/lower boundaries, the Floquet operator acts as a left-moving/right-moving translation operator at sublattice  $A/B$ . Therefore two edge modes appear in the spectrum(red/green lines). (Figure adapted from Reference [6] with permission from *Annual Reviews of Condensed Matter Physics*.) . . . . . 7

2.1	Illustration of the actions of example unitary operators $U_A$ and $U_B$ defined in Eqs. (2.14) and (2.17). $U_A$ is local and locally generated, and may be interpreted as particle hops between neighbouring sites. $U_B$ is local but not locally generated, and may be interpreted as particle translation in one direction. $U_A$ and $U_B$ belong to different equivalence classes. . . . .	22
2.2	Illustration of the actions of the Hermitian operators $H_{U_A}$ and $H_{U_B}$ defined in Eqs. (2.105) and (2.106). In contrast to the underlying unitary operators (see Fig. 2.1, these Hermitian operators have twice the degrees of freedom. As discussed in the main text, $H_{U_A}$ and $H_{U_B}$ belong to different equivalence classes. . . . .	51
2.3	Spectrum of the unitaries (a) $U_{triv}^{DIII}(k)$ , (b) $U_{top}^{DIII}(k)$ , (c) $U_{triv2}^{DIII}(k)$ and (d) $U_{top2}^{DIII}(k)$ given in the main text. The plots show the complex phase of the eigenvalues $\epsilon$ as a function of momentum $k$ . . . . .	55
2.4	Three-dimensional view of the Dirac cone in gap $\pi$ of the quasienergy spectrum of $U^A(k)$ when $\Delta = 1$ . The dispersion is clearly linear in the neighborhood of the Dirac cone (located approximately at $k_x = \pi$ and $k_y = \pi$ ). . . . .	57
4.1	The flow of a unitary matrix. Vertical dashed green line indicates the coordinate of the cross section $x_0$ , defining regions $L$ and $R$ . Red points indicate 1D lattice sites, while black arrows represent the current between sites $j$ and $k$ across the cut. The flow is defined by summing over all particle currents that cross the cut, as in Eq. (4.3). If the unitary is strictly local, only sites within a distance $\ell$ of the cut will contribute to the flow, delimited by grey dotted lines.(Figure adapted from Reference [37] with permission from the <i>American Physical Society</i> .) . . . .	79

- 4.2 Schematic picture of the model drive given in Eqs. (4.16) and (4.17). (a) Driving protocol. The phase with Floquet edge states is obtained by driving with a trivial Hamiltonian  $H_1$  and a nontrivial Hamiltonian  $H_2$  in turn. Black (gray) points are sites on sublattice A (B). For each Hamiltonian, hopping occurs between sites indicated by red lines. Gray background indicates unit cells. (b) Drive action. Particles in the bulk move in closed trajectories indicated by the blue arrows, while particles on the boundary follow the green arrows and gain a phase of  $\pi$ . (Figure adapted from Reference [37] with permission from the *American Physical Society*. . . . . 84
- 4.3 Schematic picture of the chiral flow for the model drive introduced in Sec. 4.2.2. (a) The chiral flow in the closed system generated by  $U(T/2)$ . Black (grey) circles indicate sublattice A (B). Blue (red) lines show the motion of particles on sublattice A (B) after a half period. (b) The chiral flow in the corresponding open system after a half period. Note that on each edge, particles are forced to hop between sublattices (green arrows). (Figure adapted from Reference [37] with permission from the *American Physical Society*. . . . . 86
- 4.4 Action of the 2D class A drive introduced in Ref. [5]. During each step, particles hop between sites on a bipartite lattice following the paths indicated by red and blue arrows. Sublattices are indicated by gray and black points, while gray shaded regions indicate unit cells. After a complete cycle, a particle in the bulk returns to its initial position, while a particle at the edge is translated by one unit cell. The 1D class AIII model we introduce in Sec. 4.2.2 can be obtained by collapsing this 2D model onto a single chain. (Figure adapted from Reference [37] with permission from the *American Physical Society*. . . . . 88

4.5	Schematic quasienergy spectrum for a Floquet operator $U(T)$ with chiral symmetry. Since quasienergies are defined modulo $2\pi$ , the spectrum may be visualised on the unit circle. The chiral symmetry operator $C$ maps states with quasienergy $\epsilon$ onto states with quasienergy $-\epsilon$ (green band and blue points). In this way, the spectrum is symmetric about $\epsilon = 0$ and $\epsilon = \pi$ . States at these special values map onto states with the same quasienergy under the action of $C$ , and possibly map onto themselves (red points). (Figure adapted from Reference [37] with permission from the <i>American Physical Society</i> . . . . .	91
4.6	Action of the general chiral unitaries $U_c(T/2)$ and $U_o(T/2)$ within the left edge ( $L$ ), middle ( $M$ ) and right edge ( $R$ ) regions of a 1D chain. Sublattices are shown as black and gray points. (a) The unitary action of the closed system $U_c(T/2)$ acts on each sublattice independently. (b) In the open system, the unitary $U_o(T/2)$ acts on each sublattice independently in the bulk but couples the two sublattices in the edge regions. (Figure adapted from Reference [37] with permission from the <i>American Physical Society</i> . . . . .	96
4.7	Calculation of the chiral flow invariant for a local unitary satisfying Eq. (4.51). (a) We split the region near a cut at $x = x_0$ into left ( $L$ ) and right ( $R$ ) pieces. (b) Matrix elements which connect sites across the cut are bounded by an exponentially decaying envelope function. By truncating projectors to sites within a distance $a$ from the cut, we neglect contributions which are of size $O(e^{-a/\ell})$ . By taking $a$ much larger than $\ell$ these errors can be made exponentially small. . . . .	101
4.8	Semi-infinite system used in the construction of truncated edge invariants. (a) Boxed region indicates the region where $P_R^a$ is nonzero, extending from $x = 0$ to $x = a$ . To reduce truncation errors, this should be much larger than the Lieb-Robinson length of the unitary $\ell$ . (b) Edge modes decay exponentially away from $x = 0$ . Truncating to the boxed region means contributions of size $O(e^{-a/\ell})$ are neglected. . . . .	105

- 6.1 The action of the 2D class AII drive introduced in Ref. [5]. (a)Driving protocol. The only nonvanishing hopping amplitudes between sites are represented for each time step. Spin up states moves according to the sequence  $1 \rightarrow 2 \rightarrow 3 \rightarrow 4$  while spin-down states follows the opposite sequence  $4 \rightarrow 3 \rightarrow 2 \rightarrow 1$ . (b)During each step, particles hop between sites on a bipartite lattice, following the paths indicated by red and blue arrows. This is done for spin-up (solid lines) and spin-down (dashed lines). Sublattices are indicated by gray and black points. After a complete cycle, a particle in bulk returns to its initial position, while a particle at the edge is translated by one unit cell. . . . . 143
- 6.2 The flow of a time-reversal symmetric unitary matrix. Vertical dashed green line locates at the cross-section  $x_0$ , separating the regions  $L$  and  $R$ . Red points indicate 1D lattice sites host Hilbert space of even dimensions which includes states( $|\phi\rangle$ ) and their time-reversed partners( $\mathcal{T}|\phi\rangle$ ). The solid black arrow represents the hoppings between states on sites  $j$  and  $k$  across the cut, while the dashed arrow denotes the movement of the corresponding time-reversed partners. For example, in the preceding section, the solid arrow corresponds to spin up states while the dashed arrow is associated with the spin-down states. Since a state moves in the opposite direction compared to its time-reversed partner, their total contribution to the Kitaev flow, associated with the charge pumping from region  $L$  to region  $R$ , is zero. . . . . 147
- 6.3 An illustration of the Eigenvalue spectrum of operator  $A$ . Red dots indicate different eigenvalues, while the dashed lines represent the eigenvectors. The green Arrow symbolizes the action of the mapping  $B$ , and the yellow arrows denote the mapping  $Y^\dagger\mathcal{T}$ , between two eigenvectors with opposite eigenvalues. After these two mappings, a state is mapped to another state with the same eigenvalue. Therefore each energy level between  $-1$  and  $+1$  is double degenerate. . . . . 153

## LIST OF TABLES

1.1	The periodic table for Floquet topological insulators by symmetry class and spatial dimension $d$ in Reference [1]. Each entry is equal to one of the Abelian groups $\{0, \mathbb{Z} \times \mathbb{Z}, \mathbb{Z}_2 \times \mathbb{Z}_2\}$ . If a specific symmetry class in a dimension hosts no nontrivial topological phases, then the corresponding entry is zero. For entry that is not zero, it's composed by two identical factors. The first one represents the classification result of the static component and the second one represents the classification result of the dynamical component. . . . .	11
2.1	Periodic table of topological insulators and superconductors [2]. The leftmost column gives the letter label for each AZ symmetry class. The next three columns indicate the presence / absence of time-reversal symmetry ( $\mathcal{T}$ ), particle-hole symmetry ( $\mathcal{C}$ ) and chiral symmetry ( $\mathcal{S}$ ) for each symmetry class, along with whether they square to $+\mathbb{I}$ or $-\mathbb{I}$ . The rightmost eight columns indicate the topological classification for each symmetry class in dimension $d$ . Note that the classification depends only on $d \bmod 8$ ( $d \bmod 2$ for classes A and AIII) due to Bott periodicity [2]. See main text for details. . . . .	32
2.2	Summary of the mapping between a local unitary operator $U$ and a local, flattened Hermitian operator $H_U$ for each symmetry class. We use the shorthand $U \hat{\oplus} U^\dagger$ to represent the doubled Hermitian operator obtained from $U$ and $U^\dagger$ through Eq. (2.18). For these cases, the Pauli operators $\sigma_j$ are expressed in the chiral basis of $H_U$ . See main text for details. . . . .	40
2.3	Periodic table for local unitary operators. The leftmost four columns define the AZ symmetry classes as described in the main text and in Table 2.1. The rightmost eight columns indicate the topological classification for local unitary operators from each symmetry class in dimension $d$ . Note that this table is a permutation of the periodic table for topological Hamiltonians. See main text for details. . .	49

## ACKNOWLEDGMENTS

First, I would like to thank Prof. Rahul Roy, my research mentor and committee chair, for his support and guidance during my doctoral studies at UCLA. I still remember four years ago when I first joined this group, I had no ideas about doing research and couldn't imagine that I would get more and more excited about research. At that time, he told me how to define a theoretical problem and solve a problem from different perspectives. I have learned a lot from him and got valuable suggestions from him.

Second, I want to thank our former post-doctoral scholar Fenner Harper. He is very nice and willing to help graduate students. We worked together and brainstormed many ideas. My understanding of Floquet systems improved due to the many exciting discussions we had in the past four years. He also spent time working through my paper drafts. From him, I learned how to give presentations and write a scientific paper.

Third, I want to express my gratitude to people within our research group: David Bauer, Albert Brown, Dominic Reiss, Pratik Sathe, Adrian Culver, and Spenser Talkington. They are all smart and friendly. Not only we had a good time doing research, but we were also playing well together.

Fourth, I appreciate the help from my committee for my defense and the review of this thesis.

In my last year, I started learning Fracton topological phases. It was great to collaborate with Wilbur Shirley and Arpit Dua. They had taught me a lot about this new field. This experience helps me realize how much I like doing research and learn new techniques. I am also grateful to Prof. Xie Chen, who helped me start this fracton project and provided valuable research advice.

## VITA

- 2014            BSc. (Physics), University of Science and Technology of China
- 2014-present    Teaching Assistant, Department of Physics and Astronomy, University of California, Los Angeles

## PUBLICATIONS

Liu, X., Harper, F., and Roy, R. *Chiral Flow in One-dimensional Floquet Topological Insulators*. Physical Review B **98**, 165116 (2018).

Harper, F., Liu, X., and Roy, R. *Classification of Local Unitary Operators*. (In preparation, 2020).

Liu, X., Harper, F., and Roy, R. Roy. *Bulk-edge connection in time-reversal invariant Floquet insulators*. (In preparation, 2021).

Liu, X., Harper, F., and Roy, R. *Bulk-edge correspondence in Floquet topological insulators with chiral symmetry*. (In preparation, 2021).

Liu, X., Harper, F., and Roy, R. *Classification of the edge states in Topological insulators*. (In preparation, 2021).

Liu, X., Harper, F., and Roy, R. *Dimensional ladder in Topological insulators*. (In preparation, 2021).

# CHAPTER 1

## introduction

### 1.1 Floquet Topological phases

#### 1.1.1 Periodically Driven Systems

A general time-periodic Hamiltonian satisfying  $H(t + T) = H(t)$  generates the unitary time-evolution operator

$$U(t) = \mathcal{T} \exp \left[ -i \int_0^t H(t') dt' \right], \quad (1.1)$$

where  $\mathcal{T}$  indicates time ordering (and we have set  $\hbar = 1$ ). In a time-independent system, we usually study the eigenstates of a static Hamiltonian in order to obtain information about the underlying topology. In a driven system, however, we are instead interested in the spectrum of the Floquet operator  $U(T)$ , the evolution operator after one complete period of driving. If the drive is topologically nontrivial, then this spectrum (in an open system) should exhibit protected boundary modes. These protected edge modes are driven-system analogues of the edge modes that arise (for example) in the quantum Hall effect or topological insulators.

Using an analogue of Bloch's theorem, the action of  $U(T)$  may be written in terms of time-periodic eigenstates  $|\phi_n(t)\rangle$  as

$$U(T) |\phi_n(0)\rangle = e^{-i\epsilon_n T} |\phi_n(0)\rangle, \quad (1.2)$$

where the quantities  $\epsilon_n$  are known as quasienergies and are defined modulo  $2\pi/T$ . In many cases we can define an effective Floquet Hamiltonian  $H_F$ , which is related to the full-period time-evolution operator through

$$U(T) = \exp(-iH_F T). \quad (1.3)$$

In order for  $H_F$  to be well-defined,  $U(T)$  must be gapped at some quasienergy  $\epsilon_g$  so that a branch can be chosen when taking the logarithm. In addition, the branch cut must respect the underlying symmetries of the system. For topological phases, this feature generally restricts the utility of the Floquet Hamiltonian to closed systems, since open systems may have protected edge modes that lie in or across the quasienergy gap.

In Ref. [1] it was argued that the topology of a general periodic drive can have both dynamical and static components, and that these two components may be isolated from each other by a homotopic deformation of the unitary. We briefly review this construction for the specific case of a Floquet system which is gapped at quasienergy  $\epsilon = \pi/T$  and which has chiral symmetry, as will be assumed throughout this paper. A discussion of the more general construction may be found in Ref. [1].

With these assumptions in mind, we consider a closed-system unitary evolution whose end point is of the form  $U(T) = \exp(-iH_FT)$ , where  $H_F$  is a static and local Hamiltonian and where the branch cut in defining the Hamiltonian is at  $\epsilon = \pi/T$ . Then, we continuously deform the unitary evolution into a composition of a unitary loop  $L$  and a constant Hamiltonian evolution  $C$ , which is an evolution with the static Hamiltonian  $H_F$ . The dynamical component of the evolution is characterised by the loop  $L$ , a unitary evolution which (for a closed system) starts and ends at the identity,

$$U(0) = U(T) = \mathbb{I}. \tag{1.4}$$

In this way, the deformed evolution ( $L$  followed by  $C$ ) is a homotopic deformation of the original evolution.

Overall, the bulk properties of an evolution can be described by studying the components  $L$  and  $C$  independently. The loop part of the evolution may be classified by a topological integer  $n_L$ , while the constant part of the evolution may be classified by a set of integers  $n_{C_i}$ , each associated with the  $i$ th gap in the constant Hamiltonian  $H_F$  [1].

The decomposition introduced above may be extended to an open system by removing terms from the generating Hamiltonian at each point in time that connect sites across a boundary cut. At the end of the evolution, these cuts may lead to nontrivial (protected) edge

modes in the gaps in the quasienergy spectrum. Since the deformation is homotopic, any edge modes in the deformed evolution will be topologically equivalent to the edge modes in the original evolution. There is a one-to-one correspondence between the number of edge modes in each quasienergy gap (labelled  $n_i$ ) and the integers characterising the bulk evolution, given by

$$\begin{aligned} n_\pi &= n_L \\ n_i &= n_{C_i} + n_L, \end{aligned} \tag{1.5}$$

where addition is taken modulo two if necessary [1]. We note that since we have assumed the presence of chiral symmetry, only the gaps at  $\epsilon = 0$  and  $\epsilon = \pi/T$  are physically meaningful, and the spectrum must be symmetric about these points [1]. In particular, the index  $n_\pi$  counts the number of edge modes at  $\epsilon = \pi/T$ , which are inherently dynamical in nature and arise only if the loop component of the evolution is nontrivial. The remaining edge modes at  $\epsilon = 0$  (if present) are similar to edge modes that arise in static Hamiltonians (although they may be affected by the loop component of the evolution).

A classification of evolutions by constant Hamiltonians is equivalent to the classification of static topological insulators and superconductors, and is well understood in the literature [2–4]. Since we are interested in Floquet topological phases, we will instead focus on inherently dynamical evolutions, described by unitary loops, and the associated dynamical edge modes at  $\epsilon = \pi/T$  (hereafter we set  $T = 1$  for simplicity). For this reason, we will assume throughout this paper that there is a bulk quasienergy gap at  $\epsilon = \pi$ , in which edge modes may appear in the open system. In the translationally invariant case, loop evolutions corresponding to all symmetry classes and dimensions were classified in Ref. [1]. In the present work, we will study a certain class of loop evolutions which do not have translational symmetry.

### 1.1.2 An example: The RLBL model

In this section we illustrate the basic ideas in Floquet systems by introducing through the exactly solvable RLBL model [5].

Consider a tight-binding model on a bipartite square lattice with two orbitals at each unit cell, denoted by  $A$  and  $B$ . The evolution is generated by the time-dependent Hamiltonian

$$H(t) = \sum_{\mathbf{k}} \begin{pmatrix} c_{\mathbf{k},A}^\dagger & c_{\mathbf{k},B}^\dagger \end{pmatrix} H(\mathbf{k}, t) \begin{pmatrix} c_{\mathbf{k},A} \\ c_{\mathbf{k},B} \end{pmatrix}$$

where  $c_{\mathbf{k},(A/B)}^\dagger$  creates a particle with crystal momentum  $\mathbf{k}$  completely on sublattice ( $A/B$ ) and  $c_{\mathbf{k},(A/B)}$  is the corresponding annihilation operator. The time-dependent momentum-space Hamiltonian is given by

$$H(\mathbf{k}, t) = - \sum_{n=1}^4 J_n(t) \left( \exp(i\mathbf{b}_n \cdot \mathbf{k}) \frac{\sigma_x + i\sigma_y}{2} + h.c. \right) \quad (1.6)$$

where  $J_n(t)$  controls hopping from each  $B$  orbital to its neighboring  $A$  orbital. It is chosen such that a particle hops to its neighboring site with probability one during each step  $n$ ,

$$J_n(t) = \begin{cases} 1 & \text{if } \frac{(n-1)\pi}{2} \leq t < \frac{n\pi}{2} \\ 0 & \text{otherwise} \end{cases},$$

and the real-space vectors  $\mathbf{b}_n$  are given by  $\mathbf{b}_1 = (1, 0)$ ,  $\mathbf{b}_2 = (0, 1)$ ,  $\mathbf{b}_3 = (-1, 0)$ , and  $\mathbf{b}_4 = (0, -1)$  [5].

Our driving cycle consists of four steps, as depicted in Figure 1.1, with the pairing depending on  $\mathbf{b}_n$ . During each step  $n$ , a state which is completely localized at a particular  $A/B$  sublattice will move to its neighboring  $B/A$  sublattice. We can write down the unitary evolution operator during each complete step  $n$ ,

$$U_n = \sum_{\mathbf{r}} c_{\mathbf{r}+\mathbf{b}_n,A}^\dagger c_{\mathbf{r},B} + c_{\mathbf{r},B}^\dagger c_{\mathbf{r}+\mathbf{b}_n,A}.$$

The motion of particles initialized on a single site in the bulk of the system is visualized in Figure 1.1. We can see that particles in the bulk move in closed trajectories, returning to its initial position after a complete driving cycle. Starting from  $A$  sublattice, a particle follows a counter-clockwise trajectory encircling one plaquette, as depicted in Figure 1.1. Similarly, a particle initially localized at a  $B$  sublattice in the bulk completes a counter-clockwise trajectory encircling one plaquette.

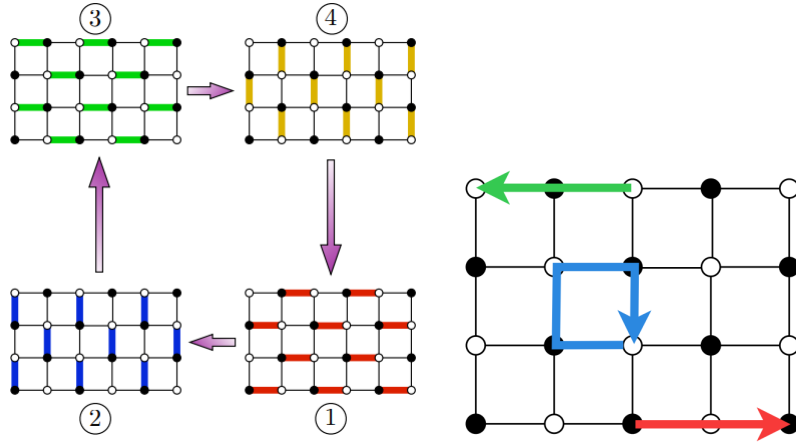


Figure 1.1: (a)The driving protocol of the four-step RLBL model described in section 1.1.2. Here the  $A$  and  $B$  sublattices are represented by open and filled circles separately. The Hamiltonian is piecewise constant, and there are four steps in total. During each step, a hopping strength of  $J = 1$  is applied along the highlighted bond, and particles can hop to their neighboring sites with probability 1. (b)A depiction of the movements of states initially localized at single sublattices in an open system. Over a complete cycle, states localized in the bulk return precisely to their original position. Along the upper boundary, states initially localized at a  $A$  orbital are translated to the left by two sites (green arrow). While along the lower edge, states initially localized at a  $B$  orbital shift two sites to the right (red arrow). In this way, there are nontrivial edge modes propagating along the boundary. (Figure adapted from Reference [6] with permission from *Annual Reviews of Condensed Matter Physics*.)

Therefore, the unitary evolution at the end of a complete cycle in the bulk  $U(T) = \mathbb{I}$ . This can be verified by multiplying four step unitaries together, i.e.  $U_4U_3U_2U_1 = \mathbb{I}$ . In particular, this drive is a unitary loop that starts and ends at the identity. As a result the Floquet Hamiltonian  $H_F$ , defined in Equation (1.3), is identically zero in the bulk. The Chern number associated with its bands is obviously zero. Despite this fact, this system exhibits nontrivial anomalous boundary behavior.

After opening the boundary, we remove terms involving sites beyond the boundary in the real-space representation of the Hamiltonian. When doing this, we need to determine the geometry of the boundary at the beginning. In this example, we consider a strip geometry by applying periodic boundary conditions along one dimension of the underlying lattice ( $y$ -direction) and open boundary conditions in the other dimension ( $x$ -direction). Then we analyze the effect of the boundary by studying the motion of states initially localized near the boundary, which may differ from those in the bulk. The movement of states along the boundary is depicted in Figure 1.1.

Consider how a state initially localized at an  $A$  sublattice moves along the upper boundary. During the first step,  $U_1$  is unmodified since it involves no hopping terms cross the boundary. As shown in Figure 1.1, under the action of  $U_1$ , such a state will be pushed to the  $B$  sublattice to its left. However, during the second step,  $U_2$  drives the states localized in the  $B$  sublattice up, which is allowed in bulk and blocked on the boundary. In this step, this state will stay stationary as  $U_2$  acts as the identity operator. In the third step,  $U_3$  drives this state to its neighboring  $A$  sublattice. Finally, in the last step,  $U_4$  is blocked again and acts as the Identity matrix. After a complete cycle, by adding all four steps, we can see that  $U(T)$  works like a left-moving translation operator on the upper boundary for states initially localized at the  $A$  sublattice, transferring them to another  $A$  orbital.

### 1.1.3 Topological invariants

In the last section, we saw how nontrivial edge modes could appear even if the time-evolution operator is the identity matrix in bulk. As depicted in Figure 1.2, these edge modes wind

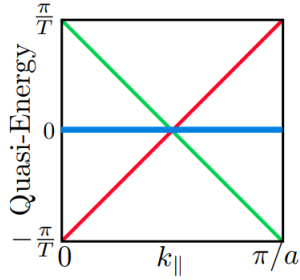


Figure 1.2: The spectrum of the Floquet operator  $U(T)$  for the RLBL model in an open system, as defined in Section 1.1.2. In our case, we already assume the lattice spacing  $a$  to be 1 and set the period  $T$  to be  $2\pi$ . And we use the floquet operator to represent the evolution operator evaluated throughout the entire driving period. In the bulk, the Floquet operator acts as the identity matrix at both sublattice  $A$  and  $B$ , thus creates doubly degenerate flat band at quasi-energy zero (blue lines). On the upper/lower boundaries, the Floquet operator acts as a left-moving/right-moving translation operator at sublattice  $A/B$ . Therefore two edge modes appear in the spectrum (red/green lines). (Figure adapted from Reference [6] with permission from *Annual Reviews of Condensed Matter Physics*.)

around the quasienergy Brillouin zone and thus is robust against small perturbations. In this way, topologically protected edge modes can be hosted even if the effective Hamiltonian is completely trivial (identically zero  $H_F = 0$  in the RLBL model).

The effective Hamiltonian fails to capture the topology of this system due to the loss of the information about the micromotion in the effective Hamiltonian. This micromotion, determined by the evolution unitary  $U(t)$ , records the endpoint of an evolution and how the evolution is completed during each driving period. For example, in the RLBL model, if we reverse the steps(4  $\rightarrow$  3  $\rightarrow$  2  $\rightarrow$  1), we will get an evolution with an opposite circulation direction. This circulation direction determines the propagation direction of the edge states and thus is of crucial importance. However, this chirality information is missing in the effective Hamiltonian since the effective Hamiltonian is zero for both the original and the reversed ones. Therefore, to capture the full topology of a Floquet system, we need to find topological invariants associated with the evolution unitary  $U(t)$ .

The RLBL model presented in Section 1.1.2 is a unitary loop, satisfying the loop condition Equation (1.4). As a result, the bulk time-evolution operator  $U(t, k_x, k_y)$ , is a periodic function of not only  $k_x$  and  $k_y$  but also  $t$ . Thus  $U$  defines a map from  $S_1 \times S_1 \times S_1 \rightarrow U(N)$  and such a map can be classified by ‘winding number’,

$$W[U] = \frac{1}{8\pi^2} \int dt dk_x dk_y \times \text{Tr} \left\{ U^{-1} \partial_t U [U^{-1} \partial_{k_x} U, U^{-1} \partial_{k_y} U] \right\}. \quad (1.7)$$

For a general unitary evolution, we can decompose it into a unitary loop  $L$  and a constant Hamiltonian evolution  $C$ , as noted in Section 1.1.1. Then we can use this ‘winding number’ to classify the unitary loop, the dynamical part. Besides giving this bulk invariant, Rudner et al. show that the number of chiral edge modes  $n_{\text{edge}}$  which propagate across the quasi-energy spectrum at any boundary is equal to  $W[U]$ [5]. In this way, a rigorous proof of bulk-edge correspondence in 2D Floquet systems is formulated. Later, Graf et al. extend the discussions to disordered systems in Reference [7].

### 1.1.4 Periodic table for Floquet topological insulators

The RLBL model described in Section 1.1.2 is an example of a Floquet Topological Insulator. These modes cannot be created or removed from the system through any locally generated perturbation confined to the edge of the system. Since the generating Hamiltonian in this example does not require any additional symmetry requirements (other than translation symmetry in space and time), this system belongs to class A of the Altland-Zirnbauer class. In static systems, Hamiltonians in this symmetry class are fully classified with the Chern number of the filled bands. As shown in Eq. (1.7), in the Floquet systems, however, we need additional topological invariants like the winding number to detect the topology fully.

The difference between Floquet systems and static systems pushes us to find a new classification and new topological invariants for Floquet systems. To catalog these new topological phases, we can extend the well-known ‘periodic table’ of topological insulators and superconductors to periodically driven systems.

Before going into details of the periodic table for Floquet topological insulators, we need to introduce symmetry classes of the AZ classification scheme. These classes are characterized by combinations of time-reversal  $\mathcal{T}$ , particle-hole (charge conjugation)  $\mathcal{C}$ , and chiral symmetry  $\mathcal{S}$ . To understand the meaning of these symmetry classes, let’s see how these symmetry operators act on the band Hamiltonians and the time evolution operators with translation invariance.

In systems with particle-hole symmetry (PHS),

$$\mathcal{C}H(\mathbf{k}, t)\mathcal{C}^{-1} = -H(-\mathbf{k}, t), \quad (1.8)$$

$$\mathcal{C}U(\mathbf{k}, t)\mathcal{C}^{-1} = U(-\mathbf{k}, t). \quad (1.9)$$

Similarly, in systems with time-reversal symmetry (TRS),

$$\mathcal{T}H(\mathbf{k}, t)\mathcal{T}^{-1} = H(-\mathbf{k}, T - t), \quad (1.10)$$

$$\mathcal{T}U(\mathbf{k}, t)\mathcal{T}^{-1} = U(-\mathbf{k}, T - t)U^\dagger(-\mathbf{k}, T), \quad (1.11)$$

With the presence of both PHS and TRS, chiral symmetry appear as an additional unitary

symmetry. It can also exist solely without the companion of PHS and TRS. This is how it acts on Hamiltonians and

$$\mathcal{S}H(\mathbf{k}, t)\mathcal{S}^{-1} = -H(\mathbf{k}, T - t), \quad (1.12)$$

$$\mathcal{S}U(\mathbf{k}, t)\mathcal{S}^{-1} = U(\mathbf{k}, T - t)U^\dagger(\mathbf{k}, T), \quad (1.13)$$

We can extend these symmetry constraints to real-space unitary operators,

$$\mathcal{C}H(t)\mathcal{C}^{-1} = -H(t), \quad (1.14)$$

$$\mathcal{T}U(t)\mathcal{C}^{-1} = U(t), \quad (1.15)$$

$$\mathcal{T}H(t)\mathcal{T}^{-1} = H(T - t), \quad (1.16)$$

$$\mathcal{T}U(t)\mathcal{T}^{-1} = U(T - t)U^\dagger(T), \quad (1.17)$$

$$\mathcal{S}H(t)\mathcal{S}^{-1} = -H(T - t), \quad (1.18)$$

$$\mathcal{S}U(t)\mathcal{S}^{-1} = U(T - t)U^\dagger(T), \quad (1.19)$$

The presence or absence of these symmetries, and whether the antiunitary symmetry operators  $\Theta$  and  $P$  square to  $\pm 1$ , define the 10 AZ symmetry classes. In Reference [1], Roy and Harper build a periodic table for Floquet topological insulators from the ten Altland-Zirnbauer symmetry classes across all dimensions using the K-theory method. This periodic table, as shown in Table 1.1, incorporates all previous studies of Floquet topological phases and can also be used to discover new phases. However, it only indicates what Abelian group a topological invariant in a specific symmetry class belongs to. The mathematical formulas to calculate these topological invariants are still missing. So in this thesis, we will show how to calculate topological invariants in some symmetry classes.

### 1.1.5 Effective edge unitary

As shown in Section 1.1.2, in an open system, the unitary evolution will differ from that of the closed system at the edge, giving rise to an effective edge unitary. In this section, we will give a rigorous definition of effective edge unitary.

AZ Class	$\mathcal{T}$	$\mathcal{C}$	$\mathcal{S}$	$d = 0$	1	2	3	4	5	6	7
A	0	0	0	$\mathbb{Z} \times \mathbb{Z}$	0	$\mathbb{Z} \times \mathbb{Z}$	0	$\mathbb{Z} \times \mathbb{Z}$	0	$\mathbb{Z} \times \mathbb{Z}$	0
AIII	0	0	1	0	$\mathbb{Z} \times \mathbb{Z}$						
AI	+	0	0	$\mathbb{Z} \times \mathbb{Z}$	0	0	0	$\mathbb{Z} \times \mathbb{Z}$	0	$\mathbb{Z}_2 \times \mathbb{Z}_2$	$\mathbb{Z}_2 \times \mathbb{Z}_2$
BDI	+	+	1	$\mathbb{Z}_2 \times \mathbb{Z}_2$	$\mathbb{Z} \times \mathbb{Z}$	0	0	0	$\mathbb{Z} \times \mathbb{Z}$	0	$\mathbb{Z}_2 \times \mathbb{Z}_2$
D	0	+	0	$\mathbb{Z}_2 \times \mathbb{Z}_2$	$\mathbb{Z}_2 \times \mathbb{Z}_2$	$\mathbb{Z} \times \mathbb{Z}$	0	0	0	$\mathbb{Z} \times \mathbb{Z}$	0
DIII	-	+	1	0	$\mathbb{Z}_2 \times \mathbb{Z}_2$	$\mathbb{Z}_2 \times \mathbb{Z}_2$	$\mathbb{Z} \times \mathbb{Z}$	0	0	0	$\mathbb{Z} \times \mathbb{Z}$
AII	-	0	0	$\mathbb{Z} \times \mathbb{Z}$	0	$\mathbb{Z}_2 \times \mathbb{Z}_2$	$\mathbb{Z}_2 \times \mathbb{Z}_2$	$\mathbb{Z} \times \mathbb{Z}$	0	0	0
CII	-	-	1	0	$\mathbb{Z} \times \mathbb{Z}$	0	$\mathbb{Z}_2 \times \mathbb{Z}_2$	$\mathbb{Z}_2 \times \mathbb{Z}_2$	$\mathbb{Z} \times \mathbb{Z}$	0	0
C	0	-	0	0	0	$\mathbb{Z} \times \mathbb{Z}$	0	$\mathbb{Z}_2 \times \mathbb{Z}_2$	$\mathbb{Z}_2 \times \mathbb{Z}_2$	$\mathbb{Z} \times \mathbb{Z}$	0
CI	+	-	1	0	0	0	$\mathbb{Z} \times \mathbb{Z}$	0	$\mathbb{Z}_2 \times \mathbb{Z}_2$	$\mathbb{Z}_2 \times \mathbb{Z}_2$	$\mathbb{Z} \times \mathbb{Z}$

Table 1.1: The periodic table for Floquet topological insulators by symmetry class and spatial dimension  $d$  in Reference [1]. Each entry is equal to one of the Abelian groups  $\{0, \mathbb{Z} \times \mathbb{Z}, \mathbb{Z}_2 \times \mathbb{Z}_2\}$ . If a specific symmetry class in a dimension hosts no nontrivial topological phases, then the corresponding entry is zero. For entry that is not zero, it's composed by two identical factors. The first one represents the classification result of the static component and the second one represents the classification result of the dynamical component.

Assume an open system is inside a large region  $D$  in our lattice. Then the Hamiltonian and evolution operator in this open system is defined as:

$$U_o(T) = \mathcal{T} \exp \left( -i \int_0^T dt H_o(t) \right); H_o(t) = P_D H_c(t) P_D. \quad (1.20)$$

This is because we truncated the whole system to region  $D$  after opening the boundary, changing from the Hamiltonian in the close system  $H_c(t)$  to the Hamiltonian in the open system  $H_o(t)$ .

For a unitary loop, the evolution operator generated by  $H_c(t)$  over a complete driving cycle  $U_c(T)$  is precisely the identity matrix. After opening the boundary, nontrivial edge modes may arise from such unitary evolutions. These modes are just eigenstates of  $U_o(T)$ . In the bulk,  $U_o(T)$  is the same as  $U_c(T)$  since the truncation operation we do in Eq. (1.20) is a local operation and can only affect the boundary of the region  $D$ . Therefore,  $U_o(T)$  is nontrivial only along the edge. In this way, we call  $U_o(T)$  the effective edge unitary.

Generally, a unitary evolution can be decomposed into a unitary loop and a constant-Hamiltonian evolution generated by the effective Hamiltonian  $H_F$ . As a result, the unitary can be written as a product of two factors, where the first factor is due to this unitary loop, and the second factor is corresponding to constant Hamiltonian evolution. That is,

$$U_o(T) = U_{eff} e^{-iH_F^o T}$$

where the effective unitary  $U_{eff}$  derives from the loop component of the evolution. Therefore it's nontrivial only along the edge given the same reason as before. We call  $U_{eff}$  the effective edge unitary.

Since  $U_{eff}$  represents the edge behavior of a Floquet system, we will study it in details in the following chapters.

## 1.2 Outline of this thesis

In this thesis, we mainly focus on the classification of Floquet systems. In chapter 2, we build a complete topological classification of local unitary operators in free fermionic systems. Effective edge unitary operators, which belongs to local unitary operators, are fully understood in this way. And in the following chapters, we use the topological invariants of effective edge unitary operators as edge invariants.

Besides, we show that a locally generated unitary is topological trivial as it can be contacted to the identity matrix smoothly. Then in chapter 3, we use the decoupling theory to show how to find the possible generating Hamiltonians for locally generated unitaries.

For the next three chapters 4,5,6, we develop methods to classify bulk unitary evolutions and use the machines introduced in chapter 2 to diagnose topology associated with edge unitaries. Afterwards, we set up a rigorous connection between bulk and edge properties.

In the last chapter 7, after treating a static system as a Floquet system with a constant Hamiltonian, we employ the tools we developed in Floquet systems to classify the edge behaviors in static cases.

## CHAPTER 2

# Classification of Local Unitary Operators

### 2.1 Motivations

Periodic driving serves as a powerful tool to realize nontrivial topological phases of matter which does not exist in its corresponding static counterpart. In particular, driven systems of free fermions have been found to form dynamical analogues of TIs known as Floquet topological insulators (FTIs)[1, 5, 6, 8–20]. Several of these phases have now been realized experimentally inside different systems like ultracold matter and acoustic systems[21, 22], photonic and acoustic systems [23–25]. In these systems, topologically protected edge states can appear at the boundary after one complete unitary evolution. Such modes are robust against a wide range of perturbations; thus, they play critical roles in the fascinating quantized responses exhibited by materials in experiments.

To better understand the topology associated with each edge mode, we study effective edge unitary operators that govern the edge behavior. These operators are defined as the difference between unitary evolutions in open systems and the corresponding closed systems at the edge[18, 26, 27]. Such edge unitaries are described by unitaries that can keep locality. Namely, unitaries that map local operators to nearby local operators[28–30]. These unitaries are called local unitary operators, the focus of this chapter. They can be expressed in a matrix product way in interacting systems, at least for one-dimensional systems[28, 29]. While in non-interacting systems, they are represented by quasideagonal matrices with sufficiently rapidly decaying off-diagonal elements[31]. In this chapter, we will focus on local unitary operators constrained to non-interacting systems.

In recent years, the classification of local unitary operators has attracted a lot of interest.

Most work has been done in the context of quantum walks, which are discrete-time analogs "hopping" on a lattice[30]. The classification of one-dimensional quantum walks with and without symmetries has been well studied[32–35], and formulas for calculating the topological invariants in one-dimensional systems are provided. A well-known example is the flow index of a one-dimensional system proposed by Kitaev[31], measuring net charge pumping from left to right in one direction. This index is physically motivated, locally computable, and robust to local perturbations. One application of this flow index is to classify co-propagating chiral edge modes generated by shift operators that are supported on the boundary of two-dimensional Floquet systems. In this chapter, we extend the notion of flow index to higher dimensions by classifying local unitary matrices without any symmetries. Furthermore, we build a complete classification of local unitary operators from the ten Altland-Zirnbauer symmetry classes across all dimensions.

Our classification of local unitary operators can shed light on the study of the bulk-edge correspondence between bulk unitary evolutions and their protected edge states, an important property of Floquet topological insulators. To set up a rigorous connection between bulk and edge properties, we need to develop methods to classify bulk unitary evolutions and edge unitaries separately. The topological classification of bulk unitary evolutions in Floquet systems with different symmetries have been intensively studied[1, 7, 29, 36–40], both in the translation-invariant systems and disordered systems. These papers focus on the entire driving process. Thus, the calculated topological invariants depend on the full-time evolution throughout the driving cycle rather than just a unitary at a specific time point in general. Unlike these studies, our method is applicable to edge unitaries, providing an alternative way to look at Floquet systems. In this chapter, we classify driven systems in terms of their corresponding Floquet operators, i.e., their unitary evolution operators, after one complete drive. We demonstrate that nontrivial edge modes can only occur on the boundary if the corresponding edge unitary, the Floquet operator constrained to the edge, belong to a nontrivial topological class. While traditional classification and topological invariants characterize the topological features of the bulk, our method captures the properties of edge

behaviors. Combining these two results, we can derive explicit bulk-boundary correspondences for a wide class of Floquet systems.

In this chapter, we encode the topological classification of local unitary operators into a "periodic table". The periodic table was first used to summarize a complete classification of all topological insulators and superconductors, which is obtained by using the idea of random matrix theory or K-theoretical approach[2, 41]. For Floquet systems, a generalized periodic table of quantum dynamics related to the full-time evolution has already been produced[1]. We, however, produce a new periodic table which characterizes the topological properties of local unitary operators. Like the other two periodic tables, this table provides a connection between the Bott periodicity in K-theory and the topological phases of non-interacting local unitary operators. In addition, it indicates topological invariants for local unitary operators in each dimension and each symmetry class of the Altland-Zirnbauer symmetry. Therefore, we can discover new topological phases that have not been discussed before from this periodic table.

In this work, we present a complete topological classification of local unitary operators in free fermionic systems. We are applying a similar method to that for Floquet Topological insulators given in Refs. [42]. While this assumes translational invariance, our approach applies to disordered systems with more rigorous proof provided. In addition, we define equivalence classes of pairs of unitaries and use the classification result to determine whether a unitary can be generated by a sequence of local Hamiltonians. Although topological invariants associated with all local unitary operators are only given in some symmetry classes, we can obtain the missing parts quickly with the topological invariants of Hamiltonians discovered in literature[3, 43, 44]. Since quantum walks can be realized in periodically driven systems, our work is also applicable to quantum walks.

The rest of the chapter is organized as follows. We begin, in section 2.2, by giving a definition of local unitary operators. Besides, we demonstrate that a local unitary operator is not necessarily the finite-time evolution operator of a local Hamiltonian. In section 2.3, we reviewed the previous studies of the flow index and extended it to higher dimensions. Then in

Sec. 2.4, we propose a definition of homotopy equivalence classes in all AZ symmetry classes. In Sec. 2.5 and 2.6, after building a one to one correspondence between Hermitian operators and unitary operators, we obtain a topological classification of local unitary operators with and without chiral symmetry separately. Then we give some examples of nontrivial unitary operators in section 2.7 and show how to diagnose their topology via mapping to Hermitian operators. Finally, we summarize our results and discuss future directions motivated by work done in this chapter in Sec. VI.

## 2.2 preliminary discussion

In this work, we are interested in obtaining a topological classification of local unitary operators, which are usually represented by local unitary matrices. Such operators arise naturally in systems where a quantum (Hermitian) Hamiltonian evolves in time and describes unitary operations in more general contexts, such as in quantum walks. In this section, we introduce the definitions and preliminary ideas that will underpin the arguments given in the rest of the chapter.

We begin by defining a unitary operator  $U$  as one which satisfies the usual definition

$$U^\dagger U = U U^\dagger = \mathbb{I}, \quad (2.1)$$

where  $\dagger$  indicates the Hermitian conjugate and  $\mathbb{I}$  is the identity operator. For concreteness, we will assume that the unitary operator has matrix elements  $U_{jk}$ , where  $j$  and  $k$  label unit cells in some (formally infinite) real-space lattice. For example, the element  $U_{jk}$  may give the propagation amplitude for a fermion to travel from the site with position  $\mathbf{r}_k$  to the site with position  $\mathbf{r}_j$  under the action of  $U$ . In this chapter, the unitary operators we consider will be independent of time. To connect our discussion to time evolution operators (which often arise in quantum systems), we can interpret our results as the instantaneous time-evolution operator at some specified time  $t_c$ .

We define a *local* unitary operator to be a unitary operator whose matrix elements decay

exponentially (or faster) in this space. Explicitly, we require that

$$|U_{jk}| \leq C e^{-|j-k|/\ell} \quad (2.2)$$

for some positive constants  $C$  and  $\ell$  and for large enough  $|j - k|$ , where  $|j - k|$  is shorthand for the distance between the unit cells labelled  $j$  and  $k$ . In this way,  $\ell$  is (a bound on) the localization length of the unitary operator. Note that we have suppressed any additional labels such as orbital or spin in the expressions above.

For later use, we also define Hermitian operators (e.g. Hamiltonians) as operators which satisfy  $H^\dagger = H$ , and local Hermitian operators as Hermitian operators whose real-space matrix elements decay as in Eq. (2.2). We define a *gapped* Hermitian operator as one whose eigenvalue spectrum has a finite gap around zero. Explicitly, if  $\{E_i\}$  are the (necessarily real) eigenvalues of a Hermitian operator  $H$ , then  $H$  is gapped if and only if

$$|E_i| > E_c \quad (2.3)$$

for some positive  $E_c$ , for all indices  $i$ . We define a *flattened* Hermitian operator as one whose eigenvalues satisfy

$$E_i \in \{-1, +1\} \quad (2.4)$$

for all indices  $i$ . In particular, we note that this is true if and only if  $H^2 = \mathbb{I}$ . Flattened Hermitian operators are useful in the context of classifying Hamiltonians, as any local Hamiltonian can be brought into a flattened form without breaking the locality [44, 45] (albeit at the expense of introducing longer-ranged hopping terms).

The classification we will ultimately derive will describe unitaries that are local but which are not necessarily *locally generated*. For our purposes, we define a locally generated unitary operator as one which may be written as a finite-time evolution with a local Hamiltonian [27]

$$U = \mathcal{T} \exp \left[ -i \int_0^T H_{loc}(t) dt \right], \quad (2.5)$$

where  $H_{loc}(t)$  is a time dependent local Hermitian operator (or ‘Hamiltonian’) as defined above. Indeed, a consequence of Eq. 2.5 is that a locally generated unitary operator may be

continuously connected to the identity operator through a local evolution. Importantly, we require a locally generated unitary to satisfy Eq. 2.5 in the thermodynamic limit. Specially, if we apply symmetry constraints to  $H_{loc}(t)$ , we say that the unitary operator is locally generated in the same symmetry classes. These will be discussed in details in section Sec. 2.4.

The locally generated unitary evolution introduced here is closely related to finite time evolution which can be simulated by finite depth quantum circuits in the quantum information context. In some chapters, they call a given time evolution local implementable if can be achieved by a sequence of block unitaries, i.e., quantum gates. Because of their equivalence, we use *locally generated unitary evolution* to represent both finite depth quantum circuits and local implementable unitary.

## 2.3 Flow of quantum systems

### 2.3.1 Nontrivial flow in one dimension

In this section, we will review one interesting property of unitary matrices, known as ‘flow’ introduced by Kitaev [31]. This index measures a charge pumping from the left side of a system to the right side of a system passing through a ‘cross section’.

For a noninteracting unitary matrix  $U = (U_{jk})$ , where  $j$  and  $k$  label sites on a one-dimensional lattice and the matrix elements  $U_{jk}$  represents the hopping of a particle from site  $k$  to  $j$ . An intuitive notion of ‘current’ from position  $k$  to position  $j$  induced by the unitary operator may then be defined as

$$f_{jk} = |U_{jk}|^2 - |U_{kj}|^2 \quad (2.6)$$

Then the total current through a cross-section (at position  $x_0$ ) can be written as the summation of this site-to-site current:

$$F(U) = \sum_{j \geq x_0} \sum_{k < x_0} f_{jk}. \quad (2.7)$$

The flow index of a unitary matrix can also be rewritten in terms of two projectors  $P_R$  for the half axis  $x \geq x_0$  and  $P_L$  for the other half axis  $x < x_0$ .

$$\begin{aligned}
F(U) &= \text{Tr}(U^\dagger P_R U P_L - U^\dagger P_L U P_R) \\
&= \text{Tr}(U^\dagger P_R U - P_R) \\
&= \text{Tr}(U^\dagger [P_R, U]).
\end{aligned} \tag{2.8}$$

This invariant is locally computable for local unitary matrices, even for those acting on systems with infinite size. In other words, this invariant can be obtained on an interval with a large enough size close to the cross-section and remain the same for any interval we may select.

To illustrate how nonzero "flow" can emerge, we give two simple examples, including one trivial unitary and one nontrivial unitary. First, we study the case of the identity operator,  $U = \mathbb{I}$ . It is clear that the flow of this operator will be zero, since each projector commutes with  $U$  in Eq. (2.8) and the overlap between two orthogonal projections is zero, namely,  $P_L P_R = 0$ . Next, we consider the 1d translation  $\hat{t}$  operator which moves particle one site right.

$$\hat{t}|j\rangle = |j+1\rangle, \tag{2.9}$$

Since  $\hat{t}$  is strictly zero for  $|i-j| > 1$ , the only sites that can be effective in calculation when applying Eq (4.4) are two neighboring sites splitting by a cross section, labelled by -1 and 0.

$$\begin{aligned}
F(U) &= \text{Tr} \left[ \left( \hat{t}^\dagger |0\rangle\langle 0| \hat{t} |-1\rangle\langle -1| \right) - \left( \hat{t}^\dagger |-1\rangle\langle -1| \hat{t} |0\rangle\langle 0| \right) \right] \\
&= 1.
\end{aligned} \tag{2.10}$$

In this chapter, we aim to extend the notion of this flow index to higher-dimensional systems and search for locally computable invariants. By establishing a connection between local unitary operators and Hermitian operators, we obtain the higher-dimensional index for local unitary operators.

### 2.3.2 Equivalence Classes of Unitary Operators

Before moving on to generalize the flow index to dimensions greater than one, we first define equivalence classes of local unitary operators that are related to each other through a notion of homotopy.

Two local unitary operators  $U_0$  and  $U_1$  (possibly with symmetries) are in the same equivalence class ( $U_0 \approx U_1$ ) if there is a homotopy

$$U(s) = V_\alpha(s)U_0V_\beta(s) \quad (2.11)$$

where two unitary transformation operators

$$V_{\alpha/\beta}(s) = \mathcal{T} \exp \left[ -i \int_0^s \tilde{H}_{\alpha/\beta}(g) dg \right], \quad (2.12)$$

are locally generated unitary operators such that  $U(0) = U_0$  and  $U(1) = U_1$ , and where  $U(s)$  remains in the appropriate symmetry class throughout the homotopy. Note that this condition is different from the homotopy condition for Hermitian operators given in Eq. (2.37): in the current case, the transformed operator  $U(s)$  must remain unitary throughout the transformation, but not necessarily Hermitian, and so the two transformation unitaries  $V_\alpha(s)$  and  $V_\beta(s)$  may differ. From our definition, if  $U(s)$  is locally generated, then  $U(s)$  is homotopic equivalent to the Identity matrix and vice versa.

There are some different definitions of equivalence relations in previous studies. We will prove that these definitions are equivalent to our definition. In one statement,  $U_1$  and  $U_n$  belong to the same equivalence class, if there is a sequence of unitaries  $U_1, U_2, \dots, U_n$  smoothly connecting  $U_1$  and  $U_n$ . For any two consecutive unitaries,  $U_i$  and  $U_{i+1}$  act in the same way in a large enough area after the choice of a suitable isomorphism[30]. In other words, the difference between two unitaries  $U_i$  and  $U_{i+1}$  represented as  $\gamma(i) = U_{i+1}^\dagger U_i$  is equal to (almost) the identity at a large area. Because  $\gamma(i)$  is bounded in a finite region,  $\gamma(i)$  can be generated by a local Hamiltonian, which can be the logarithm of  $\gamma(i)$ . Therefore,  $U_1$  and  $U_n$  can be connected via a locally generated unitary. Besides this "share the patch" definition,

another more homotopic definition says that  $U_1$  and  $U_2$  are homotopic equivalent if two unitary operators can be continuously deformed into each other[46]. Since small physical deformations can be viewed as a dressing of the original operator by a locally generated unitary, this one also matches our definition.

In order to compare unitaries with different numbers of bands, we consider *stable homotopy* here (i.e. the addition of arbitrary numbers of trivial bands). We define  $U_1 \sim U_2$  if and only if there exist two trivial unitaries,  $U_{n_1}^0$  and  $U_{n_2}^0$ , such that

$$U_1 \oplus U_{n_1}^0 \approx U_2 \oplus U_{n_2}^0 \quad (2.13)$$

where  $\oplus$  is the direct sum and we need to add  $n_1$  and  $n_2$  number of bands to two unitaries separately. The two trivial unitaries are in the same symmetry class in order to follow the homotopy equivalence.

To illustrate these ideas, we now give a simple example of some local unitary operators that belong to different equivalence classes in one dimension. We first consider the operator  $U_A$  which is block diagonal, consisting of repeating blocks of the Pauli operator  $\sigma_x$ , i.e.

$$U_A = \bigoplus_b \begin{pmatrix} 0 & 1 \\ 1 & 0 \end{pmatrix}_b. \quad (2.14)$$

In a physical system, this could be interpreted as a single-particle fermionic operator which enacts hoppings between neighbouring sites, as illustrated in Fig. 2.1. It is clearly a local operator, since  $U_{ij}$  is strictly zero for  $|i - j| > 1$ . It is also locally generated, as it may be written as the exponential of a local (block diagonal) Hamiltonian, through

$$U_A = \exp \left[ -i \bigoplus_b H(b) \right], \quad (2.15)$$

where

$$H_A(b) = \frac{\pi}{2} \begin{pmatrix} -1 & 1 \\ 1 & -1 \end{pmatrix}_b \quad (2.16)$$

and with  $H(b)_{ij}$  again strictly zero for  $|i - j| > 1$ . The unitary  $U_A$  belongs to the same universality class as the identity operator  $\mathbb{I}$ , as shown by the homotopy  $U_A = e^{-iH_A} \mathbb{I} * \mathbb{I}$ .

An example of a unitary operator belonging to a different universality class is the translation operator  $U_B$ , as defined in Eq. (2.9), which has matrix elements

$$[U_B]_{ij} = \delta_{i,j+1}. \quad (2.17)$$

In matrix form, it consists of ones on the first upper diagonal and in the lower left-hand corner (assuming periodic boundary conditions). In a physical system, this can be interpreted as a single-particle fermionic operator, which enacts a hopping to the right for each lattice site, as illustrated in Fig. 2.1.

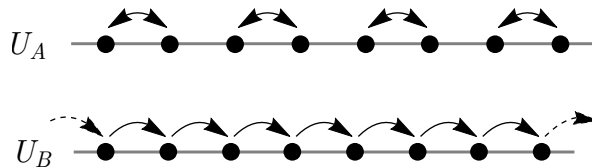


Figure 2.1: Illustration of the actions of example unitary operators  $U_A$  and  $U_B$  defined in Eqs. (2.14) and (2.17).  $U_A$  is local and locally generated, and may be interpreted as particle hops between neighbouring sites.  $U_B$  is local but not locally generated, and may be interpreted as particle translation in one direction.  $U_A$  and  $U_B$  belong to different equivalence classes.

$U_B$  is again a local operator, as  $[U_B]_{ij}$  is strictly zero for  $|i - j| > 1$ . However, it is not locally generated, as may be verified naively by taking the matrix logarithm of  $U_B$  and studying its matrix elements as a function of system size. More fundamentally, this property stems from the fact that chiral translation is anomalous on a 1D lattice [27, 27, 31].

Since  $U_B$  is not locally generated, it can't become the multiplication of  $U_A$  and other locally generated unitaries, and so  $U_A$  and  $U_B$  belong to different universality classes. In this simple 1D case, unitary operators can be assigned to different universality classes based on their winding number or unitary flow given in Eq. (2.8), which gives an integer-valued invariant in each case.

Before moving on, we note that this definition of equivalence will lead to a different classification from that which arises in the study of Floquet systems (such as Refs. [1]). In

previous studies of time-dependent systems, topological classifications are usually concerned with the presence of protected edge modes in gaps in the quasienergy spectrum. However, since these unitary operators are obtained by evolving with a local Hamiltonian, they are trivial according to our definition. Instead, the homotopic classification we study in this chapter will lead to unitary operators that are nonlocal and gapless. In this way, the nontrivial unitaries we discuss may only arise at the *boundary* of a time-evolved physical system.

### 2.3.3 Mapping from Unitary Operators to Flattened Hermitian Operators

In this section, we show how unitary operators may be mapped uniquely onto local Hermitian operators with chiral symmetry. To do this, we use a mapping introduced in the context of Floquet topological phases in Ref. [1], defining the Hermitian operator

$$H_U = \begin{pmatrix} 0 & U \\ U^\dagger & 0 \end{pmatrix}. \quad (2.18)$$

It is clear from Eq. (2.18) that  $H_U$  has twice as many degrees of freedom as the original operator  $U$ . We can interpret this doubling as effectively adding a sublattice or orbital degree of freedom on each site, which we label  $A$  and  $B$ . In this way, the two nonzero blocks of  $H_U$  on the antidiagonal connect  $A$  sites with  $B$  sites.

With this interpretation,  $H_U$  is a local operator, inheriting its locality from the underlying unitary operator  $U$ . Specifically, since the matrix elements  $U_{ij}$  satisfy the locality condition in Eq. 2.2, so do the matrix elements  $[H_U]_{\alpha i, \beta j}$ , where we have included the sublattice indices  $\alpha, \beta \in \{A, B\}$ . We also see that  $H_U^2 = \mathbb{I}$ , and so  $H_U$  is a flattened Hermitian operator as discussed in Sec. 2.3.1. In addition, from its  $2 \times 2$  block form, it must have equal numbers of  $\pm 1$  eigenvalues (see Appendix 2.C).

This mapping automatically introduces a new unitary chiral (or sublattice) symmetry, which we define as

$$\mathcal{S}' = \eta \begin{pmatrix} \mathbb{I} & 0 \\ 0 & -\mathbb{I} \end{pmatrix}, \quad (2.19)$$

(i.e. proportional to  $\sigma_z$  in the new basis) where  $\eta \in \{1, i\}$  and will be determined later. This operator squares to  $(\mathcal{S}')^2 = \mathbb{I}$  and has the action

$$\mathcal{S}' H_U (\mathcal{S}')^{-1} = \begin{pmatrix} 0 & -U \\ -U^\dagger & 0 \end{pmatrix} = -H_U, \quad (2.20)$$

and so agrees with the definition of chiral symmetry in Eq. (2.32). Indeed, a flattened Hermitian operator with unitary symmetry  $\mathcal{S}'$  *must* take the form of  $H_U$  given in Eq. (2.18). In section. 2.5, we will show that this mapping is one-to-one; namely, the mapping from Hermitian operators to local unitary operators is also unique. Besides, we show that the homotopic equivalence between two Hermitian operators  $H_U$  implies a homotopic equivalence between the corresponding two unitary operators  $U$ , and vice versa. In other words, if two Hamiltonians are topologically equivalent, then we can find  $V_\alpha$  or  $V_\beta$  which smoothly connects the corresponding two unitary operators due to the definition of equivalence classes of unitaries given in Eq. (2.11).

### 2.3.4 Flow index in higher dimensional systems

Now we can apply the correspondence between flattened Hamiltonians and unitary operators to find the flow indices for unitary operators in higher-dimensional systems. Let us consider a local unitary  $U$  acting on an infinite  $d$ -dimensional lattice (where  $d = 2n + 1$  is odd). We then start by mapping a local unitary operator without any symmetries and a Hermitian operator with chiral symmetry. According to what we have analyzed, we can construct a flattened Hamiltonian with chiral symmetry shown in Eq. (2.18). Then the topological invariant of this Hamiltonian which is also the flow index of this unitary can be written as

$$\nu^{2n+1}[U] = \frac{(\pi i)^n}{(2n+1)!!} \sum_{\sigma} \quad (2.21)$$

$$(-1)^\sigma \text{Tr} \left( U^\dagger [P_{\mathbf{a}}^{(\sigma_1)}, U] U^\dagger [P_{\mathbf{a}}^{(\sigma_2)}, U] \dots U^\dagger [P_{\mathbf{a}}^{(\sigma_{2n+1})}, U] \right)$$

where  $\sigma$  is a permutation given by

$$\sigma = \begin{pmatrix} 1, 2, \dots, 2n \\ \sigma_1, \sigma_2, \dots, \sigma_{2n} \end{pmatrix} \quad (2.22)$$

with the signature  $(-1)^\sigma$ . Similar to one dimension, we define right half axis projectors acting on all  $d$  directions,

$$P_{\mathbf{a}}^i |\mathbf{r}, \alpha\rangle = \begin{cases} |\mathbf{r}, \alpha\rangle & \text{if } r_i \geq a_i \\ 0 & \text{if } r_i < a_i \end{cases}, \quad (2.23)$$

This flow index reduces to the same formula as Eq.(4.4) when setting  $n = 0$ . While this index is associated with unitary matrices of odd dimensional systems, the unitary operators of even dimensional systems can also be classified by a lower dimensional index(e.g.  $\nu^1[U]$  for two dimensional systems, see Appendix 2.B).

Especially, if  $U$  possesses a translational symmetry, these real-space invariants which reduces to winding numbers defined by [47], can be written as

$$\nu^{2n+1}[U] = (-1)^n \left(\frac{i}{2\pi}\right)^{n+1} \frac{n!}{(2n+1)!} \sum_{\sigma} (-1)^{\sigma} \quad (2.24)$$

$$\int d\mathbf{k} \text{Tr} \left( (U^\dagger \partial_{\sigma_1} U) (U^\dagger \partial_{\sigma_2} U) \cdots (U^\dagger \partial_{\sigma_{2n+1}} U) \right) \quad (2.25)$$

Our results agree with the topological invariants associated with homotopy groups  $\pi_d[U(m)]$  because  $U$  defines a map from  $d$ -dimensional torus to  $m \times m$  unitary matrices,  $U(m)$ [8].

This invariant has some fundamental properties. First, it is a conserved quantity, in the sense that it is independent of the choice of  $\mathbf{a}$ , the location of the reference point. Second, it is locally computable since it can be (almost) determined by the truncation of unitary matrices inside a finite interval. Third, the flow index of a local unitary is zero if and only if it is locally generated. Last, this unitary index is additive under both composition and product of the unitaries:

$$\nu[U_1 \oplus U_2] = \nu[U_1] + \nu[U_2]$$

$$\nu[U_1 U_2] = \nu[U_1] + \nu[U_2]$$

The first two properties directly stem from the results of Hamiltonian with chiral symmetry[4]. The proof for the last two rules will be presented in the Appendix. Here we will give an example to illustrate this property. Since  $\hat{t}^2$  moves a particle two sites right, we expect the flow index of  $\hat{t}^2$  to be 2. In addition,  $\hat{t} \oplus \hat{t}$  moves two states across the cut, and thus we can expect the flow index of  $\hat{t}^2$  to be 2. This flow index, sharing the same properties with the current measure, could be used to gauge a flow transporting a conserved quantity.

### 2.3.5 Three Dimensional Quantum Flow

We now introduce a model [48] which can generate nontrivial Hamiltonians from where we can construct nontrivial unitary.

$$\tilde{H}(k) = \begin{pmatrix} 0 & 0 & -iq_0 + q_3 & q_1 - iq_2 \\ 0 & 0 & q_1 + iq_2 & -iq_0 - q_3 \\ iq_0 + q_3 & q_1 + iq_2 & 0 & 0 \\ q_1 - iq_2 & iq_0 - q_3 & 0 & 0 \end{pmatrix}, \quad (2.26)$$

Where  $q_0 = h + \cos k_x + \cos k_y + \cos k_z$ ,  $q_1 = t \sin k_x$ ,  $q_2 = \sin k_y$ ,  $q_3 = \sin k_z$  with  $h, t$  being control parameters. This Hamiltonian is strictly local, with nonzero hopping only existing between nearest neighboring sites. Then we can flatten the bands of this Hamiltonian by introducing the Q matrix,

$$Q(k) = \frac{1}{E(k)} \tilde{H}(k) \quad (2.27)$$

where the absolute energy spectrum of  $\tilde{H}(k)$  is  $E(k) = [t^2(\sin k_x)^2 + \sin^2 k_y + \sin^2 k_z + (\cos k_x + \cos k_y + \cos k_z + h)^2]^{\frac{1}{2}}$ . Then the off-diagonal part of the flattened Hamiltonian can become an unitary

$$U = \frac{1}{E(k)} \begin{pmatrix} -iq_0 + q_3 & q_1 - iq_2 \\ q_1 + iq_2 & -iq_0 - q_3 \end{pmatrix}. \quad (2.28)$$

After plugging into Eq. (2.24) and let n=1, the quantity  $\nu[U]$  can be simplified as

$$\nu[U] = \frac{1}{8\pi^2} \int dk_x dk_y dk_z \text{Tr} \left( U^\dagger \partial_{\sigma_{k_x}} U [U^\dagger \partial_{k_y} U, U^\dagger \partial_{k_z} U] \right)$$

which could be calculated analytically for this model. The topological index could take values  $0, \pm 1, \pm 2$  given different values of parameters  $h$  and  $t$ , calculated by [48],

$$\nu[U] = \begin{cases} -2\text{sign}(t) & |h| < 1 \\ \text{sign}(t) & 1 < |h| < 3 \\ 0 & |h| > 3 \end{cases} \quad (2.29)$$

This shows how nontrivial flow could be generated in three dimensional systems. While the first order flow index describes the net pumping of charges in one direction, what is being transported described by this three dimensional index is not clear yet and will be interesting subjects for future work.

## 2.4 Classification of Unitary Operators with Symmetries

In this section, we generalize our method in the above discussion and build a complete classification of unitary operators with symmetries in all dimensions. We are applying a similar method to that for Floquet Topological insulators given in Refs. [1, 42]. These papers are mainly focused on translational invariant systems, while our method applies to disordered systems with more rigorous proof is provided. We will first discuss the equivalence classes of Hermitian operators and unitary operators separately, and then obtain a one-to-one mapping between them.

### 2.4.1 Symmetry Operators and Symmetry Classes for Hermitian Operators

The well-known periodic table of topological insulators and superconductors [2] is a classification of gapped free-fermion Hamiltonians, arranged according to spatial dimension and symmetry class. The symmetry classes included in the table label the presence or absence of three physically relevant symmetries: time-reversal symmetry ( $\mathcal{T}$ ), particle-hole conjugation symmetry ( $\mathcal{C}$ ), and chiral (or sublattice) symmetry ( $\mathcal{S}$ ). The first two of these symmetries are antiunitary (i.e., proportional to the complex conjugation operator), and if present, act

on a real-space Hamiltonian according to

$$\mathcal{T}H\mathcal{T}^{-1} = H \quad (2.30)$$

$$\mathcal{C}H\mathcal{C}^{-1} = -H. \quad (2.31)$$

Chiral symmetry is a unitary symmetry which is present automatically if both time-reversal and particle-hole symmetries are present, but may also be present independently. This has the action

$$\mathcal{S}H\mathcal{S}^{-1} = -H. \quad (2.32)$$

The value of  $\mathcal{S}^2$  can be varied arbitrarily by adding a complex phase to the operator, but the antiunitary symmetries  $\mathcal{T}$  and  $\mathcal{C}$  may only square to either  $+\mathbb{I}$  or  $-\mathbb{I}$ . The presence or absence of each symmetry, along with the sign of its square, yields the ten Altland-Zirnbauer (AZ) symmetry classes [49]. We note that unitary commuting symmetries are ignored in this classification, as if present, they simply allow the Hamiltonian to be block diagonalised. For completeness, we also give the action of the symmetry operators on the momentum-space (Bloch) Hamiltonian, which may be used when the system has translational symmetry:

$$\mathcal{T}H(\mathbf{k})\mathcal{T}^{-1} = H(-\mathbf{k}) \quad (2.33)$$

$$\mathcal{C}H(\mathbf{k})\mathcal{C}^{-1} = -H(-\mathbf{k}) \quad (2.34)$$

$$\mathcal{S}H(\mathbf{k})\mathcal{S}^{-1} = -H(\mathbf{k}). \quad (2.35)$$

Since the value of  $\mathcal{S}^2$  can be varied, it is often chosen to satisfy  $\mathcal{S}^2 = 1$ . However, in some symmetry classes, this can cause  $\mathcal{S}$  to anticommute (rather than commute) with the other symmetries present. To see this, we observe that if  $\mathcal{S} = \mathcal{C}\mathcal{T}$ , then

$$\mathcal{S}^2 = \mathcal{C}\mathcal{T}\mathcal{C}\mathcal{T}. \quad (2.36)$$

For this to be consistent, the three symmetry operators would need to anticommute if  $\mathcal{T}^2 = -\mathcal{C}^2$ . To simplify the calculations, in this chapter, we use the convention that all symmetry operators commute if present, so that  $\mathcal{S}^2$  takes the value  $+1$  or  $-1$  as required by

adding a phase factor  $\eta$  to the definition of the chiral symmetry operator  $\mathcal{S} = \eta\mathcal{CT}$ . We can set  $\eta = 1$  when  $\mathcal{T}^2 = \mathcal{C}^2$  and  $\eta = i$  when  $\mathcal{T}^2 = -\mathcal{C}^2$  in order to make all symmetry operators commute.

### 2.4.2 Equivalence Classes of Hermitian Operators

Within each symmetry class, two gapped, flattened Hamiltonians are topologically equivalent if one can be continuously deformed into the other without closing the spectral gap, without breaking any protected symmetries, and possibly allowing the addition of an arbitrary number of trivial bands (through ‘stable homotopy’). To simplify the discussion, we ignore the latter condition in this text and assume that all Hamiltonians have the same number of bands with an equal number of  $\pm 1$  eigenvalues, but the arguments can be extended straightforwardly to the more general case. Overall, this defines a set of equivalence classes for Hermitian operators belonging to each symmetry class.

In general, we can write the topological equivalence between two flattened Hamiltonians  $H_0$  and  $H_1$  as the homotopy [50]

$$H(s) = V(s)H_0V(s)^\dagger, \quad (2.37)$$

where  $V(s)$  is a locally generated unitary operator

$$V(s) = \mathcal{T} \exp \left[ -i \int_0^s \tilde{H}(g) dg \right], \quad (2.38)$$

with  $H(0) = H_0$  and  $H(1) = H_1$ . If this relationship does not hold, then  $H_0$  cannot be continuously transformed into  $H_1$  without becoming nonlocal, which takes it outside the space of gapped, flattened Hamiltonians. Note that the exact form of  $\tilde{H}_g$  is given in Ref. [50, 51], and the detailed discussion will be given in Appendix 2.D. In general, the Hamiltonians  $\tilde{H}(g)$  that generated the unitary transformation  $V(s)$  is different from the path  $H(s)$  that smoothly connects  $H_0$  and  $H_1$ . [50]

For two gapped Hamiltonians that are not flattened, we say that these two Hamiltonians  $H_1$  and  $H_2$  are topologically equivalent if and only if there exists a continuous path  $H(s)$ ,

with  $s \in [0, 1]$ , which connects  $H_1$  and  $H_2$  smoothly without ever closing the energy gap and with some symmetries preserved. Then we can define a chain of flattened Hamiltonians

$$H'(s) = 1 - 2P(s) \quad (2.39)$$

where the spectral projector  $P(s)$  specifies a subspace of the total Hilbert space spanned by the occupied Bloch wave functions of  $H(s)$ . Here  $H'(s)$  will absolutely follows our topological equivalence definition given in Eq. (2.37).

In addition to satisfying these equations, the transformed Hamiltonian must also preserve any symmetries required by the AZ symmetry class throughout the transformation, which places restrictions on the form of the unitary operator  $V(s)$ . Recalling Eqs. (2.30–2.32), we find that each symmetry operator (if present) must commute with  $V(s)$  (see Appendix 2.D for a deviation),

$$\mathcal{T}V(s)\mathcal{T}^{-1} = V(s) \quad (2.40)$$

$$\mathcal{C}V(s)\mathcal{C}^{-1} = V(s) \quad (2.41)$$

$$\mathcal{S}V(s)\mathcal{S}^{-1} = V(s). \quad (2.42)$$

The question of how many such equivalence classes exist in a given AZ symmetry class can be posed in the language of Clifford algebras, and answered using methods from K-theory [2, 52]. The result is that in a given symmetry class in a specified number of spatial dimensions, equivalence classes are in one-to-one correspondence with elements from one of the Abelian groups  $\mathbb{Z}$ ,  $\mathbb{Z}_2$  or 0. The appropriate element can be found by calculating (or measuring) a suitable topological invariant. For example, class A in two dimensions is classified by the group of integers  $\mathbb{Z}$ , which indicates that different topological phases can be labelled by different integers. These correspond to the quantized Hall conductance in (integer) quantum Hall or Chern insulator phases. In Table 2.1, we give the definitions of the AZ symmetry classes and reproduce the full periodic table of topological insulators and superconductors for reference.

We note that the derivation of Table 2.1 using K-theory formally requires the underlying system to have translational symmetry, so that the periodicity of the Brillouin zone may be

used. However, the entries in the classification (which describe strong topological phases) hold even when this symmetry is broken (e.g., by disorder). A rough argument for why this is the case is that topological phases are labeled by discrete invariants that cannot vary continuously and are protected by a bulk energy gap. Adding weak disorder to a translationally symmetric system acts as a small perturbation, which cannot change the value of this invariant unless it is strong enough to close the energy gap. The classification therefore naturally extends to systems with weak (symmetry-respecting) disorder. However, even with a strong disorder, topological phases can survive the closure of a spectral gap provided there remains a mobility gap [44]. In these situations, real-space expressions for topological invariants may be used to diagnose the topology of a phase [44].

### 2.4.3 Symmetry Operators and Symmetry Classes for Unitary Operators

Equations (2.30), (2.31) and (2.32) give the actions of the three relevant symmetries on a Hamiltonian. To obtain the action of the symmetries on a unitary operator, we recall that we can obtain a unitary operator by taking the (imaginary) exponential of a Hermitian one. Acting on such an exponential, we find

$$\mathcal{T}e^{-iH}\mathcal{T}^{-1} = e^{+iH} \quad (2.43)$$

$$\mathcal{C}e^{-iH}\mathcal{C}^{-1} = e^{-iH} \quad (2.44)$$

$$\mathcal{S}e^{-iH}\mathcal{S}^{-1} = e^{+iH}. \quad (2.45)$$

We therefore define the action of the three symmetries on a unitary operator (if present) to be

$$\mathcal{T}U\mathcal{T}^{-1} = U^\dagger \quad (2.46)$$

$$\mathcal{C}U\mathcal{C}^{-1} = U \quad (2.47)$$

$$\mathcal{S}U\mathcal{S}^{-1} = U^\dagger. \quad (2.48)$$

AZ Class	$\mathcal{T}$	$\mathcal{C}$	$\mathcal{S}$	$d = 0$	1	2	3	4	5	6	7
A	0	0	0	$\mathbb{Z}$	0	$\mathbb{Z}$	0	$\mathbb{Z}$	0	$\mathbb{Z}$	0
AIII	0	0	1	0	$\mathbb{Z}$	0	$\mathbb{Z}$	0	$\mathbb{Z}$	0	$\mathbb{Z}$
AI	+	0	0	$\mathbb{Z}$	0	0	0	$\mathbb{Z}$	0	$\mathbb{Z}_2$	$\mathbb{Z}_2$
BDI	+	+	1	$\mathbb{Z}_2$	$\mathbb{Z}$	0	0	0	$\mathbb{Z}$	0	$\mathbb{Z}_2$
D	0	+	0	$\mathbb{Z}_2$	$\mathbb{Z}_2$	$\mathbb{Z}$	0	0	0	$\mathbb{Z}$	0
DIII	-	+	1	0	$\mathbb{Z}_2$	$\mathbb{Z}_2$	$\mathbb{Z}$	0	0	0	$\mathbb{Z}$
AII	-	0	0	$\mathbb{Z}$	0	$\mathbb{Z}_2$	$\mathbb{Z}_2$	$\mathbb{Z}$	0	0	0
CII	-	-	1	0	$\mathbb{Z}$	0	$\mathbb{Z}_2$	$\mathbb{Z}_2$	$\mathbb{Z}$	0	0
C	0	-	0	0	0	$\mathbb{Z}$	0	$\mathbb{Z}_2$	$\mathbb{Z}_2$	$\mathbb{Z}$	0
CI	+	-	1	0	0	0	$\mathbb{Z}$	0	$\mathbb{Z}_2$	$\mathbb{Z}_2$	$\mathbb{Z}$

Table 2.1: Periodic table of topological insulators and superconductors [2]. The leftmost column gives the letter label for each AZ symmetry class. The next three columns indicate the presence / absence of time-reversal symmetry ( $\mathcal{T}$ ), particle-hole symmetry ( $\mathcal{C}$ ) and chiral symmetry ( $\mathcal{S}$ ) for each symmetry class, along with whether they square to  $+\mathbb{I}$  or  $-\mathbb{I}$ . The rightmost eight columns indicate the topological classification for each symmetry class in dimension  $d$ . Note that the classification depends only on  $d \bmod 8$  ( $d \bmod 2$  for classes A and AIII) due to Bott periodicity [2]. See main text for details.

If there is translational symmetry, then these relations can be written in terms of the Bloch unitary  $U(\mathbf{k})$  as

$$\mathcal{T}U(\mathbf{k})\mathcal{T}^{-1} = U^\dagger(-\mathbf{k}) \quad (2.49)$$

$$\mathcal{C}U(\mathbf{k})\mathcal{C}^{-1} = U(-\mathbf{k}) \quad (2.50)$$

$$\mathcal{S}U(\mathbf{k})\mathcal{S}^{-1} = U^\dagger(\mathbf{k}), \quad (2.51)$$

based on Eqs. (2.33–2.35). With these symmetry definitions, we can assign unitary operators to the same ten AZ symmetry classes as static Hamiltonians. As discussed in Sec. 2.4.1, we will continue to use the assumption that all symmetry operators commute if they are present (so that  $\mathcal{S}^2 = \pm 1$  as required). Our result also works for periodic driven systems, where we study unitary at the end of one complete cycle

$$U(T) = \mathcal{T} \exp \left[ -i \int_0^T H(t') dt' \right], \quad (2.52)$$

generated by a time-periodic Hamiltonian satisfying  $H(t) = H(t + T)$  [1].

#### 2.4.4 Equivalence Classes of Unitary Operators

Our aim is to classify local unitary operators belonging to one of the AZ symmetry classes for any number of spatial dimensions  $d$ . First we generalize the definition of unitary equivalence in Sec. 2.3.2 to unitary operators with symmetries.

The discussion of unitary operators in Sec. 2.3.2 still applies here with some constraints on the locally generated unitary operators  $V_\alpha(s)$  and  $V_\beta(s)$ . Importantly, these two operators will generally be related to one another through the actions of the symmetry operators. If the system has time-reversal symmetry, then the requirement of Eq. (2.46) imposes the condition

$$\mathcal{T}V_\alpha(s)\mathcal{T}^{-1} = V_\beta(s)^\dagger, \quad (2.53)$$

while the presence of chiral symmetry [Eq. (2.48)] imposes the similar condition

$$\mathcal{S}V_\alpha(s)\mathcal{S}^{-1} = V_\beta(s)^\dagger. \quad (2.54)$$

If there is particle-hole symmetry, then the requirement of Eq. (2.47) instead imposes commutativity through

$$\mathcal{C}V_{\alpha/\beta}(s)\mathcal{C}^{-1} = V_{\alpha/\beta}(s). \quad (2.55)$$

Now with these constraints, if  $U(s)$  is locally generated in some symmetry classes, then  $U(s)$  is homotopic equivalent to the Identity matrix and vice versa.

## 2.5 Classification of Unitary Operators without Chiral Symmetry

With these definitions, we now begin a formal topological classification of local unitary operators. Our approach will be to obtain a one-to-one mapping between local unitary operators and local Hermitian operators, at which point the machinery used to classify static Hamiltonians can be employed. In order to do this, we split the AZ symmetry classes into those for which chiral symmetry is absent (classes A, AI, D, AII, and C) and those for which it is present (classes AIII, BDI, DIII, CII, and CI), and begin by studying the first set.

### 2.5.1 Mapping from Unitary Operators to Flattened Hermitian Operators

We will use the same mapping discussed in Section 2.3.3. We know that the mapping process can automatically generate a new chiral symmetry. In addition to this new chiral symmetry, the operator  $H_U$  may also inherit symmetries from the original unitary  $U$ . If the original unitary operator had time-reversal symmetry as defined in Eq. (2.46), then we can define a modified time-reversal symmetry operator  $\mathcal{T}'$  through

$$\mathcal{T}' = \begin{pmatrix} 0 & \mathcal{T} \\ \mathcal{T} & 0 \end{pmatrix}, \quad (2.56)$$

This acts on  $H_U$  according to

$$\mathcal{T}'H_U(\mathcal{T}')^{-1} = \begin{pmatrix} 0 & \mathcal{T}U^\dagger\mathcal{T}^{-1} \\ \mathcal{T}U\mathcal{T}^{-1} & 0 \end{pmatrix} = H_U, \quad (2.57)$$

with  $(\mathcal{T}')^2$  taking the sign  $\mathcal{T}^2$ . In this way,  $\mathcal{T}'$  has the same action as  $\mathcal{T}$  in Eq. (2.30), and so  $H_U$  inherits time-reversal symmetry from the underlying unitary operator. The commutator between  $\mathcal{S}'$  and  $\mathcal{T}'$  is

$$[\mathcal{S}', \mathcal{T}'] = (\eta + \eta^*) \begin{pmatrix} 0 & \mathcal{T} \\ -\mathcal{T} & 0 \end{pmatrix}, \quad (2.58)$$

and so we should set  $\eta = i$  for the operators to commute (following our assumption that all symmetry operators should commute discussed in Sec. 2.4.1).

However, if  $H_U$  has both time-reversal symmetry and chiral symmetry, then it also has a particle-hole symmetry defined through

$$\mathcal{C}' = \mathcal{S}'\mathcal{T}'. \quad (2.59)$$

It may be verified that this has required action of a particle-hole symmetry as defined in Eq. (2.47),

$$\mathcal{C}'H_U(\mathcal{C}')^{-1} = \mathcal{S}'\mathcal{T}'H_U(\mathcal{T}')^{-1}(\mathcal{S}')^{-1} = -H_U, \quad (2.60)$$

and further, that  $\mathcal{C}'$  commutes with both  $\mathcal{S}'$  and  $\mathcal{T}'$ . It follows that

$$(\mathcal{C}')^2 = \mathcal{S}'\mathcal{T}'\mathcal{S}'\mathcal{T}' = \eta^2(\mathcal{T}')^2 = -(\mathcal{T}')^2, \quad (2.61)$$

and so  $(\mathcal{C}')^2$  has the opposite sign to  $(\mathcal{T}')^2$ . [At this point, we note that different definitions of the symmetry operators are possible, but that the final results end up being unchanged]. Overall, the AZ symmetry class of  $H_U$  is different to that of the original unitary operator  $U$ , as detailed below in Eq. (2.68).

On the other hand, the original unitary operator may have particle-hole symmetry as defined in Eq. (2.47). If this is the case, then we define the modified particle-hole symmetry operator  $\mathcal{C}'$  through

$$\mathcal{C}' = \begin{pmatrix} \mathcal{C} & 0 \\ 0 & -\mathcal{C} \end{pmatrix}, \quad (2.62)$$

which acts on  $H_U$  according to

$$\mathcal{C}' H_U \mathcal{C} = \begin{pmatrix} 0 & -\mathcal{C} U \mathcal{C}^{-1} \\ -\mathcal{C} U^\dagger \mathcal{C}^{-1} & 0 \end{pmatrix} = -H_U \quad (2.63)$$

and squares to give  $(\mathcal{C}')^2 = \mathcal{C}^2 \otimes \mathbb{I}_2$  where  $\mathbb{I}_2$  is an identity matrix of size 2. In this way,  $\mathcal{C}'$  has the same action as  $\mathcal{C}$  in Eq. (2.31), and  $H_U$  inherits particle-hole symmetry from the underlying unitary operator. This time, the commutator between  $\mathcal{S}'$  and  $\mathcal{C}'$  is

$$[\mathcal{S}', \mathcal{C}'] = (\eta - \eta^*) \begin{pmatrix} \mathcal{C} & 0 \\ 0 & \mathcal{C} \end{pmatrix}, \quad (2.64)$$

and so in this case we should set  $\eta = 1$  for the operators to commute.

As before, the presence of two symmetries implies the presence of the third, and so we can define a time-reversal symmetry operator  $\mathcal{T}'$  through

$$\mathcal{T}' = \mathcal{S}' \mathcal{C}'. \quad (2.65)$$

This again has the required action

$$\mathcal{T}' H_U (\mathcal{T}')^{-1} = \mathcal{S}' \mathcal{C}' H_U (\mathcal{C}')^{-1} (\mathcal{S}')^{-1} = +H_U, \quad (2.66)$$

and squares to

$$(\mathcal{T}')^2 = \mathcal{S}' \mathcal{C}' \mathcal{S}' \mathcal{C}' = \eta^2 (\mathcal{C}')^2 = +(\mathcal{C}')^2, \quad (2.67)$$

which is the same as the original particle-hole symmetry operator.

In all cases, the mapping from  $U$  to  $H_U$  introduces an additional chiral symmetry while preserving any existing symmetries. If there was an existing symmetry, then this mapping also introduces a third symmetry as the product of the other two as summarised in Table. 2.2. Overall, the mapping shifts the AZ symmetry class according to

$$\begin{aligned} A &\rightarrow AIII & AI &\rightarrow CI & D &\rightarrow BDI \\ AII &\rightarrow DIII & C &\rightarrow CII, \end{aligned} \quad (2.68)$$

which is equivalent to cyclically moving one row upwards in Table 2.1 (considering the complex and real classes independently). Note that this is a mapping from the symmetry class of the original unitary operator  $U$  to the symmetry class of the resulting Hermitian operator  $H_U$ .

### 2.5.2 Mapping from Flattened Hermitian Operators to Unitary Operators

In the previous subsection, we demonstrated that a local unitary  $U$  from symmetry classes A, AI, D, AII, and C may be mapped uniquely onto a local flattened Hermitian operator from classes AIII, BDI, DIII, CII, and CI through Eq. (2.18). We now show that the mapping is one-to-one, by demonstrating the inverse mapping from local flattened Hermitian operators to local unitary operators.

It may be verified that a flattened Hermitian operator with chiral symmetry  $\mathcal{S}'$  defined through Eq. (2.19) necessarily takes the form of Eq. (2.18). If the chiral symmetry operator is not of this form, then a rotation can always be performed to bring it into this basis. We will assume that the phase factor  $\eta = 1$  in the definition of  $\mathcal{S}'$  for Hermitian operators in class AIII, BDI, CII, and that  $\eta = i$  for Hermitian operators in classes CI and DIII, consistent with the previous discussion.

For class AIII, the inverse mapping is now complete: a flattened Hermitian operator  $H_U$  with chiral symmetry uniquely defines a local unitary operator  $U$  through its off-diagonal blocks. Since there are no other constraints on  $U$ , the unitary belongs to class A. For the other symmetry classes, however, we must verify that the actions of the other symmetry operators on  $H_U$  map consistently onto symmetry actions on  $U$ .

We first consider classes BDI and CII, for which  $\eta = 1$ . Since we have assumed (without loss of generality) that all symmetry operators commute, the time reversal symmetry operator  $\mathcal{T}'$  must be block diagonal, in order to commute with  $\mathcal{S}' = \sigma_z$  [we are labelling our symmetry operators with primes so that notation is consistent with the previous section]. By performing a second basis transformation within each sublattice (which is therefore consistent with chiral symmetry), we can bring the operator  $\mathcal{T}'$  into a canonical form in which each block is identical. We write this as

$$\mathcal{T}' = \begin{pmatrix} \mathcal{C} & 0 \\ 0 & \mathcal{C} \end{pmatrix}, \quad (2.69)$$

where  $\mathcal{C}$  is some antiunitary operator that we have labelled  $\mathcal{C}$  in anticipation of its action of

$U$ . Indeed, the action of  $\mathcal{T}'$  on  $H_U$  leads to the condition

$$\begin{pmatrix} 0 & \mathcal{C}U\mathcal{C}^{-1} \\ \mathcal{C}U^\dagger\mathcal{C}^{-1} & 0 \end{pmatrix} = \begin{pmatrix} 0 & U \\ U^\dagger & 0 \end{pmatrix}. \quad (2.70)$$

By equating the blocks of the matrix equation, this demonstrates that  $U$  must possess particle-hole symmetry as in Eq. (2.47), with  $\mathcal{C}^2 \otimes \mathbb{I}_2 = (\mathcal{T}')^2$ .

With our basis choice, the particle-hole symmetry operator for  $H_U$  then takes the form

$$\mathcal{C}' = \begin{pmatrix} \mathcal{C} & 0 \\ 0 & -\mathcal{C} \end{pmatrix}, \quad (2.71)$$

which reproduces the same condition on  $U$  as above. In this way, a local flattened Hamiltonian in class BDI or CII is mapped uniquely (modulo basis changes) onto a local unitary operator in class D or C, respectively.

For classes CI and DIII, on the other hand, we take  $\eta = i$  in the definition of  $\mathcal{S}'$ . In these cases, the time reversal symmetry operator  $\mathcal{T}'$  only commutes  $\mathcal{S}' = i\sigma_z$  if its diagonal blocks are zero. By performing another basis rotation, we can again make these blocks identical so that

$$\mathcal{T}' = \begin{pmatrix} 0 & \mathcal{T} \\ \mathcal{T} & 0 \end{pmatrix}, \quad (2.72)$$

where we have again written the nonzero blocks as  $\mathcal{T}$  in anticipation of their action on  $U$ . Specifically, the requirement of time-reversal symmetry for  $H_U$  now leads to

$$\begin{pmatrix} 0 & \mathcal{T}U^\dagger\mathcal{T}^{-1} \\ \mathcal{T}U\mathcal{T}^{-1} & 0 \end{pmatrix} = \begin{pmatrix} 0 & U \\ U^\dagger & 0 \end{pmatrix}, \quad (2.73)$$

which, after comparing with Eq. (2.46), demonstrates that  $U$  must possess time reversal symmetry under  $\mathcal{T}$ , with  $\mathcal{T}^2 = (\mathcal{T}')^2$ .

Finally,  $H_U$  must also possess particle-hole symmetry  $\mathcal{C}' = \mathcal{S}'\mathcal{T}'$ , which in our basis takes the form

$$\mathcal{C}' = \begin{pmatrix} 0 & \mathcal{T} \\ -\mathcal{T} & 0 \end{pmatrix}. \quad (2.74)$$

The action of  $\mathcal{C}'$  on  $H_U$  reproduces the same symmetry action on  $U$  as before, and so  $H_U$  is mapped onto a unitary  $U$  that only exhibits time-reversal symmetry. In this way, local, flattened Hermitian operators from classes CI and DIII are mapped onto local unitary operators from classes AI and AII, respectively. This completes the demonstration of the one-to-one correspondence between local unitary operators without chiral symmetry and local, flattened Hermitian operators with chiral symmetry.

### 2.5.3 Topological Classification of Local Unitary Operators

We showed previously that there is a one-to-one mapping between a local unitary  $U$  and a Hermitian operator  $H_U$ , which is a gapped, flattened ‘Hamiltonian’ belonging to one of five AZ symmetry classes.  $H_U$  is therefore classified according to the periodic table of topological insulators (Table 2.1), which we will now show permits an equivalent topological classification of the underlying unitary operator  $U$ . Specifically, we will demonstrate that homotopic equivalence between two Hermitian operators  $H_U$  implies a homotopic equivalence between the corresponding unitary operators  $U$ , and vice versa.

As discussed in Sec. 2.4.2, two gapped, flattened Hamiltonians belong to the same symmetry class if one can be continuously transformed into the other without closing the gap and without breaking any protecting symmetries. We represented this transformation as the homotopy given in Eq. (2.37). In our case, the relevant Hermitian operators are of the form of  $H_U$ , and the homotopy relation should connect two such operators  $H_{U_0}$  and  $H_{U_1}$  through

$$H_U(s) = V(s)H_{U_0}V(s)^\dagger, \quad (2.75)$$

with  $H_U(0) = H_{U_0}$  and  $H_U(1) = H_{U_1}$ .

In the present symmetry classes,  $H_U$  has sublattice symmetry  $\mathcal{S}'$  and possibly an additional pair of symmetries  $\{\mathcal{T}', \mathcal{C}'\}$ , which should be preserved throughout the homotopy. To ensure that  $\{\mathcal{S}', H(s)\} = 0$  for any value of  $s$ , we require that  $[\mathcal{S}', V(s)] = 0$ , shown in Eq. (2.40).

$U$				$H_U$					
AZ Class	$\mathcal{T}$	$\mathcal{C}$	$\mathcal{S}$	$H_U$	Symmetry Operators	$\mathcal{T}'$	$\mathcal{C}'$	$\mathcal{S}'$	AZ Class
A	0	0	0	$U \hat{\oplus} U^\dagger$	$\mathcal{S}' = \sigma_z$	0	0	1	AIII
AIII	0	0	1	$SU$	None	0	0	0	A
AI	+	0	0	$U \hat{\oplus} U^\dagger$	$\mathcal{T}' = \mathcal{T}\sigma_x, \mathcal{C}' = -i\mathcal{T}\sigma_y, \mathcal{S}' = i\sigma_z$	+	-	1	CI
BDI	+	+	1	$SU$	$\mathcal{T}' = \mathcal{C}$	+	0	0	AI
D	0	+	0	$U \hat{\oplus} U^\dagger$	$\mathcal{T}' = \mathcal{C}, \mathcal{C}' = \mathcal{C}\sigma_z, \mathcal{S}' = \sigma_z$	+	+	1	BDI
DIII	-	+	1	$iSU$	$\mathcal{C}' = \mathcal{C}$	0	+	0	D
AII	-	0	0	$U \hat{\oplus} U^\dagger$	$\mathcal{T}' = \mathcal{T}\sigma_x, \mathcal{C}' = -i\mathcal{T}\sigma_y, \mathcal{S}' = i\sigma_z$	-	+	1	DIII
CII	-	-	1	$SU$	$\mathcal{T}' = \mathcal{C}$	-	0	0	AII
C	0	-	0	$U \hat{\oplus} U^\dagger$	$\mathcal{T}' = \mathcal{C}, \mathcal{C}' = \mathcal{C}\sigma_z, \mathcal{S}' = \sigma_z$	-	-	1	CII
CI	+	-	1	$iSU$	$\mathcal{C}' = \mathcal{C}$	0	-	0	C

Table 2.2: Summary of the mapping between a local unitary operator  $U$  and a local, flattened Hermitian operator  $H_U$  for each symmetry class. We use the shorthand  $U \hat{\oplus} U^\dagger$  to represent the doubled Hermitian operator obtained from  $U$  and  $U^\dagger$  through Eq. (2.18). For these cases, the Pauli operators  $\sigma_j$  are expressed in the chiral basis of  $H_U$ . See main text for details.

From the expression for  $\mathcal{S}'$  in Eq. (2.19), it follows that  $V(s)$  must be of the form

$$V(s) = \begin{pmatrix} V_{AA}(s) & 0 \\ 0 & V_{BB}(s) \end{pmatrix}, \quad (2.76)$$

where  $V_{AA}(s)$  and  $V_{BB}(s)$  only connect sites within the specified sublattice. This decomposition means that the homotopy relation for  $H_U$  can be written in terms of its constituent blocks,

$$U(s) = V_{AA}(s)U_0V_{BB}^\dagger(s) \quad (2.77)$$

$$U(s)^\dagger = V_{BB}(s)U_0^\dagger V_{AA}^\dagger(s), \quad (2.78)$$

(where the two relations are equivalent under Hermitian conjugation). Relabelling  $V_{AA} \rightarrow V_\alpha$  and  $V_{BB} \rightarrow V_\beta^\dagger$ , we see that this homotopy relation between  $U_0$  and  $U_1$  is exactly the same as that used in the definition of equivalence classes of unitaries in Sec. 2.3.2.

If the pair of symmetries  $\{\mathcal{T}', \mathcal{C}'\}$  are also present in  $H_U$ , then these must also commute with  $V(s)$  throughout the homotopy. For the case where the operators are defined as in Eqs. (2.69) and (2.71), this leads to the conditions

$$\mathcal{T}V_{AA}(s)\mathcal{T}^{-1} = V_{BB}(s) \quad (2.79)$$

$$\mathcal{T}V_{BB}(s)\mathcal{T}^{-1} = V_{AA}(s). \quad (2.80)$$

On the other hand, when the operators are defined as in Eqs. (2.72) and (2.74), the unitary operator must satisfy

$$\mathcal{C}V_{AA}(s)\mathcal{C}^{-1} = V_{AA}(s) \quad (2.81)$$

$$\mathcal{C}V_{BB}(s)\mathcal{C}^{-1} = V_{BB}(s). \quad (2.82)$$

We note that both of these sets of conditions involve just the original symmetry operator (either  $\mathcal{T}$  or  $\mathcal{C}$ ), even though the Hermitian operator  $H_U$  has additional symmetries. With the relabelling  $V_{AA} \rightarrow V_\alpha$  and  $V_{BB} \rightarrow V_\beta^\dagger$ , we see that these equations give the usual symmetry requirements used in the homotopic equivalence of unitary operators discussed in Sec. 2.4.4

In this way, a topological classification of local unitary operators from these symmetry classes *directly follows* from the topological classification of Hermitian operators  $H_U$  from

the appropriate modified symmetry classes. Conversely, a topological classification of local unitary operators  $U$  implies a corresponding classification of Hermitian operators of the form  $H_U$  in a modified symmetry class, which may be verified by following the steps in the transformation above in reverse. We can therefore fill in half of the elements of Table 2.3, the periodic table for local unitary operators.

## 2.6 Unitary Operators with Chiral Symmetry

We now turn to those AZ symmetry classes which *do* possess chiral symmetry, namely classes AIII, BDI, DIII, CII, and CI. Our approach will again be to form a one-to-one mapping between local unitary operators from one of these classes and Hermitian operators from a modified symmetry class, and thereby obtain a topological classification.

### 2.6.1 Mapping from Unitary Operators to Flattened Hermitian Operators

We begin by obtaining another mapping from local unitary operators to local Hermitian operators. As there is already a chiral symmetry present, we cannot augment the symmetry class with chiral symmetry using the doubling trick from Sec. 2.5. Instead, we will make use of the existing chiral symmetry operator, which we assume is written in the canonical form

$$\mathcal{S} = \eta \begin{pmatrix} \mathbb{I} & 0 \\ 0 & -\mathbb{I} \end{pmatrix}. \quad (2.83)$$

If this is not already the case, then a local basis transformation can be performed to bring the chiral symmetry operator into this canonical form. We take the phase factor  $\eta$  to be 1 or  $i$ , depending on the symmetry class: since we assume all symmetry operators commute, the value of  $\mathcal{S}^2 = \mathcal{T}^2\mathcal{C}^2$  depends on the values of  $\mathcal{T}^2$  and  $\mathcal{C}^2$  (if present). For classes AIII, BDI, and CII, we take  $\eta = 1$  so that  $\mathcal{S}^2 = 1$ , while for classes DIII and CI, we take  $\eta = i$  so that  $\mathcal{S}^2 = -1$ , consistent in both cases with the value of  $\mathcal{T}^2\mathcal{C}^2$ .

For the first case, with  $\mathcal{S}^2 = +1$ , we define a Hermitian operator through

$$H_U = \mathcal{S}U, \quad (2.84)$$

which is clearly local if the underlying unitary operator  $U$  is also local. It may be verified that this operator is Hermitian by noting that  $\mathcal{S}^{-1} = \mathcal{S} = \mathcal{S}^\dagger$  and recalling that  $\mathcal{S}U = U^\dagger\mathcal{S}$  from Eq. (2.48). We also see that  $H_U$  is a flattened operator, through

$$H_U^2 = \mathcal{S}U\mathcal{S}U = U^\dagger U = \mathbb{I}. \quad (2.85)$$

More specifically,  $H_U$  has an equal number of eigenstates with energies  $+1$  and  $-1$ , stemming from the chiral symmetry of the underlying unitary (see Appendix 2.C for a constructive proof of this). In this way,  $H_U$  has a well-defined gap, which can be associated with a topological invariant. However,  $H_U$  itself no longer has chiral symmetry, since in general

$$\mathcal{S}H_U\mathcal{S}^{-1} = U\mathcal{S} = \mathcal{S}U^\dagger = UH_UU^\dagger \neq \pm H_U. \quad (2.86)$$

If the original unitary had time-reversal or particle-hole symmetry, then these are also modified under this mapping to  $H_U$ . We find that

$$\begin{aligned} \mathcal{T}H_U\mathcal{T}^{-1} &= \mathcal{S}\mathcal{T}U\mathcal{T}^{-1} = \mathcal{S}U^\dagger = UH_UU^\dagger \neq \pm H_U \\ \mathcal{C}H_U\mathcal{C}^{-1} &= \mathcal{S}\mathcal{C}U\mathcal{C}^{-1} = \mathcal{S}U = H_U. \end{aligned} \quad (2.87)$$

In this way, any prior time-reversal symmetry does not carry through to  $H_U$ , while any prior particle-hole symmetry now acts as a time-reversal symmetry,  $\mathcal{C} \rightarrow \mathcal{T}'$ , according to Eq. (2.30). The value of  $(\mathcal{T}')^2$  for the new time-reversal symmetry operator is equal to the value of  $\mathcal{C}^2$  of the original particle-hole symmetry operator. Overall, this maps the symmetry class of the original local unitary  $U$  onto a symmetry class for the Hermitian operator  $H_U$  according to

$$AIII \rightarrow A \quad BDI \rightarrow AI \quad CII \rightarrow AII. \quad (2.88)$$

This is again equivalent to cyclically moving one row upwards in Table 2.1 (considering the complex and real classes independently).

We now turn to the case where  $\mathcal{S}^2 = -1$ , and define a local, flattened Hermitian operator through

$$H_U = i\mathcal{S}U. \quad (2.89)$$

Hermiticity follows this time by noting that  $\mathcal{S}^{-1} = \mathcal{S}^\dagger = -\mathcal{S}$ , and again using the relation  $\mathcal{S}U = U^\dagger\mathcal{S}$ . Flatness follows by observing that

$$H_U^2 = -SUSU = +SUS^{-1}U = U^\dagger U = \mathbb{I}. \quad (2.90)$$

Recalling that the symmetry operators  $\mathcal{T}$  and  $\mathcal{C}$  are antiunitary, their action on  $H_U$  becomes

$$\begin{aligned} \mathcal{T}H_U\mathcal{T}^{-1} &= -i\mathcal{S}\mathcal{T}U\mathcal{T}^{-1} = -i\mathcal{S}U^\dagger = -UH_UU^\dagger \neq \pm H_U \\ \mathcal{C}H_U\mathcal{C}^{-1} &= -i\mathcal{S}\mathcal{C}U\mathcal{C}^{-1} = -i\mathcal{S}U = -H_U. \end{aligned} \quad (2.91)$$

In this way, we see that the time-reversal symmetry again disappears, but the particle-hole symmetry is retained (and squares to the same value as before). This maps the symmetry class of the original local unitary  $U$  onto a symmetry class for the Hermitian operator  $H_U$  according to

$$DIII \rightarrow D \quad CI \rightarrow C, \quad (2.92)$$

which is again equivalent to cyclically moving one row upwards in the periodic table (Table 2.1). The transformation between  $U$  and  $H_U$  and associated new symmetry operators are summarised in Table 2.2.

### 2.6.2 Mapping from Flattened Hermitian Operators to Unitary Operators

In the previous subsection, we showed that a local unitary  $U$  from symmetry classes AIII, BDI, DIII, CII, or CI can be mapped uniquely onto a local flattened Hermitian operator from classes A, AI, D, AII, or C (respectively) through Eqs. (2.84) or (2.89). The resulting operators  $H_U$  have an equal number of  $\pm 1$  eigenstates (see Appendix 2.C). As before, in order to demonstrate that this mapping is one-to-one, we now show that the inverse mapping from  $H_U$  to  $U$  is also unique (up to choices of basis).

For this direction, we start with a local Hermitian operator  $H_U$  which is flattened (so that  $H_U^2 = 1$ ), which possibly has a single time-reversal or particle-hole symmetry ( $\mathcal{T}'$  or  $\mathcal{C}'$ ), and which has an equal number of  $\pm 1$  eigenvalues. Note that for symmetry classes without

particle-hole symmetry, Hermitian operators are not required to have this last eigenvalue property. However, operators which do have this property exhaust all topological classes, and so our restriction to this case does not change the resulting classification. More generally, Hamiltonians with different numbers of positive and negative eigenvalues can be related to the balanced case through the notion of stable homotopy.

Our approach will be to multiply  $H_U$  with a unitary operator which essentially undoes the original mapping and introduces an (artificial) ‘sublattice’ degree of freedom. For class A, we simply multiply with a chiral symmetry operator  $\mathcal{S} = \sigma_z$ , which is consistent with Eq. (2.83). In general, there are many different basis choices for this  $\sigma_z$ : since we ultimately require  $\mathcal{S}$  to behave as a symmetry operator, we will demand that  $\sigma_z$  is strictly local and acts in a translationally invariant manner across the system. For example, we could alternately label unit cells in a 1D lattice as  $A$  and  $B$ , and choose  $\sigma_z$  to act in this basis. Whichever basis choice is used for  $\mathcal{S}$ , we then define the operator

$$U = \mathcal{S}H_U, \tag{2.93}$$

which is unitary (but generally no longer Hermitian) since  $\mathcal{S}^{-1} = \mathcal{S}^\dagger = \mathcal{S}$ . The operator  $U$  defined in this way has chiral symmetry, since

$$\mathcal{S}U\mathcal{S}^{-1} = H_U\mathcal{S} = U^\dagger. \tag{2.94}$$

We have therefore mapped a Hermitian operator in class A onto a unitary operator from class AIII, which is unique given a particular choice of ‘sublattice’ defining the operator  $\sigma_z$ .

For the other symmetry classes, we perform a similar mapping, but where the form of  $\mathcal{S}$  must now be consistent with the existing symmetries. Classes AI and AII already have a time-reversal symmetry operator  $\mathcal{T}'$ , which (by assumption) must commute with the new operator  $\mathcal{S}$  that we introduce. This can be achieved by again artificially doubling the unit cell size, so that  $\mathcal{S} = \sigma_z \otimes \mathbb{I}$  in some basis, and  $\mathcal{T}' \rightarrow \mathbb{I} \otimes \mathcal{T}'$ . In these expressions, the left-hand operator in the product acts in ‘sublattice’-space, and the right-hand operator acts in the time-reversal space. For example,  $\mathcal{T}'$  might act on opposite spin species, while  $\sigma_z$  acts on pairs of neighbouring lattice sites, each of which supports both types of spin.

With this choice, we again define a unitary operator through  $U = \mathcal{S}H_U$ . This time, the unitary operator has chiral symmetry and also a particle-hole symmetry inherited through the original time-reversal symmetry  $\mathcal{T}'$  of  $H_U$ . Specifically, we define  $\mathcal{C} = \mathbb{I} \otimes \mathcal{T}'$  so that

$$\mathcal{C}U\mathcal{C}^{-1} = \mathcal{T}'\mathcal{S}H_U(\mathcal{T}')^{-1} = \mathcal{S}H_U = U. \quad (2.95)$$

As usual, the presence of two symmetries implies the presence of the third, and so the local unitary operator  $U$  also has a time-reversal symmetry  $\mathcal{T} = \mathcal{S}\mathcal{C}$ . This squares to the same value as the original time-reversal symmetry,  $(\mathcal{T}')^2$ , and so Hermitian operators from classes AI and AII are mapped uniquely (up to a local basis choice) onto local unitary operators from classes BDI and CII, respectively.

For classes  $D$  and  $C$ , the original Hermitian operator  $H_U$  has an existing particle-hole symmetry  $\mathcal{C}'$ . In these cases, we choose  $\mathcal{S} = i\sigma_z \otimes \mathbb{I}$ , again chosen to be strictly local and such that  $\mathcal{S}$  commutes with  $\mathcal{C}'$ . Note that in this case, a local basis rotation may need to be performed on  $\mathcal{C}'$  to achieve commutativity with  $\mathcal{S}$  (owing to the antiunitary property  $\mathcal{S}$  and the factor of  $i$  in  $\mathcal{S}$ ). An example of such a rotation is given in Sec. 2.7.

With these definitions, we then use the mapping

$$U = -i\mathcal{S}H_U, \quad (2.96)$$

to define a local operator  $U$ . This is unitary (since  $\mathcal{S}^\dagger = -\mathcal{S}$ ) and has chiral symmetry through

$$\mathcal{S}U\mathcal{S}^{-1} = -i\mathcal{S}^2H_U\mathcal{S}^\dagger = iH_U\mathcal{S}^\dagger = U^\dagger. \quad (2.97)$$

This time,  $U$  inherits a particle-hole symmetry from the underlying particle-hole symmetry of  $H_U$ . Writing  $\mathcal{C} = \mathcal{C}'$ , we see that

$$\mathcal{C}U\mathcal{C}^{-1} = i\mathcal{S}\mathcal{C}'H_U(\mathcal{C}')^{-1} = -i\mathcal{S}H_U = U, \quad (2.98)$$

with  $\mathcal{C}^2 = (\mathcal{C}')^2$ . As before, the combination of chiral symmetry and particle-hole symmetry leads to a time-reversal symmetry through  $\mathcal{T} = \mathcal{S}\mathcal{C}$ , which squares to  $\mathcal{T}^2 = -(\mathcal{C}')^2$ . In this

way, flattened Hermitian operators from classes D and C are mapped uniquely (up to a local basis choice) onto local unitary operators from classes DIII and CI, respectively. Overall, these mappings between symmetry classes are equivalent to moving *downwards* by one row in the periodic table. This completes the demonstration of one-to-one correspondence between local unitary operators and local, flattened Hermitian operators (with equal numbers of positive and negative eigenvalues).

### 2.6.3 Topological Classification of Local Unitary Operators

Finally, as in Sec. 2.5, we now study the homotopic properties of  $H_U$  and use these to obtain a topological classification of the underlying unitary operator  $U$ .

We first recall that two Hermitian operators  $H_{U_0}$  and  $H_{U_1}$  are topologically equivalent if they satisfy the homotopy relation

$$H_U(s) = V(s)H_{U_0}V(s)^\dagger, \quad (2.99)$$

with  $H_U(0) = H_{U_0}$  and  $H_U(1) = H_{U_1}$ . This can be rewritten as a homotopy relation for the underlying unitary  $U$  through the replacement  $H_U = (i)SU$ , which gives

$$\begin{aligned} H_U(s) &= V_\beta^\dagger(s) [(i)SU_0] V_\beta(s) \\ &= (i)\mathcal{S} [V_\alpha(s)U_0V_\beta(s)] \\ &= (i)\mathcal{S}U(s), \end{aligned} \quad (2.100)$$

where we have relabelled  $V(s) \rightarrow V_\beta^\dagger(s)$  and defined

$$V_\alpha(s) = \mathcal{S}V_\beta^\dagger(s)\mathcal{S}^\dagger \quad (2.101)$$

so that the notation is consistent with Sec. 2.3.2. Explicitly, the homotopy relation for  $U$  can be extracted from Eq. (2.100) as

$$U(s) = V_\alpha(s)U_0V_\beta(s), \quad (2.102)$$

with  $U(0) = U_0$  and  $U(1) = U_1$ . In this way, a homotopic deformation of  $H_U$  is equivalent to a homotopic deformation of the underlying  $U$ . The inverse relation also holds, as can be shown reversing the procedure above and using the fact that  $U_0$  possesses chiral symmetry.

All that remains is for us to check that the action of the symmetry operators is consistent. The operator  $H_U$  may have time-reversal symmetry or particle-hole symmetry (but not both). These are required to commute with the transformation unitary  $V(s)$  (see Sec. 2.4.2), which in turn means that they must commute with  $V_\beta(s)$  and  $V_\alpha(s)$ . This is consistent with a particle-hole symmetry for the underlying unitary  $U$  (and can also be shown in reverse). On the other hand, the underlying unitary will have sublattice symmetry and time-reversal symmetry too. The sublattice symmetry ensures that the homotopy for  $U(s)$  is equivalent to the homotopy for  $H_U(s)$ , while the time-reversal symmetry does not impose any new constraints on  $V(s)$ .

In this way, a topological classification of local unitary operators implies and is implied by a topological classification of the corresponding Hermitian operators, where the AZ symmetry classes are mapped onto each other following the discussion above. We can therefore fill in the remaining entries in Table 2.3, the periodic table for local unitary operators.

## 2.7 Examples of Nontrivial Local Unitary Operators

In the previous sections, we obtained a topological classification of local unitary operators based on the topological classification of Hermitian operators from a modified symmetry class. We now give some examples of nontrivial unitary operators, and show how the mapping to Hermitian operators allows their topology to be diagnosed.

### 2.7.1 One Dimension

#### 2.7.1.1 Unitary Operators without Sublattice Symmetry

We first consider local unitary operators in one dimension (which may be interpreted as quantum walks). In Sec. 2.3.2, we discussed a pair of local unitary operators without symmetry (and so belonging to class A), and noted that they belong to different equivalence classes. To connect these to the classification above, we now rewrite these unitary operators

AZ Class	$\mathcal{T}$	$\mathcal{C}$	$\mathcal{S}$	$d = 0$	1	2	3	4	5	6	7
A	0	0	0	0	$\mathbb{Z}$	0	$\mathbb{Z}$	0	$\mathbb{Z}$	0	$\mathbb{Z}$
AIII	0	0	1	$\mathbb{Z}$	0	$\mathbb{Z}$	0	$\mathbb{Z}$	0	$\mathbb{Z}$	0
AI	+	0	0	0	0	0	$\mathbb{Z}$	0	$\mathbb{Z}_2$	$\mathbb{Z}_2$	$\mathbb{Z}$
BDI	+	+	1	$\mathbb{Z}$	0	0	0	$\mathbb{Z}$	0	$\mathbb{Z}_2$	$\mathbb{Z}_2$
D	0	+	0	$\mathbb{Z}_2$	$\mathbb{Z}$	0	0	0	$\mathbb{Z}$	0	$\mathbb{Z}_2$
DIII	-	+	1	$\mathbb{Z}_2$	$\mathbb{Z}_2$	$\mathbb{Z}$	0	0	0	$\mathbb{Z}$	0
AII	-	0	0	0	$\mathbb{Z}_2$	$\mathbb{Z}_2$	$\mathbb{Z}$	0	0	0	$\mathbb{Z}$
CII	-	-	1	$\mathbb{Z}$	0	$\mathbb{Z}_2$	$\mathbb{Z}_2$	$\mathbb{Z}$	0	0	0
C	0	-	0	0	$\mathbb{Z}$	0	$\mathbb{Z}_2$	$\mathbb{Z}_2$	$\mathbb{Z}$	0	0
CI	+	-	1	0	0	$\mathbb{Z}$	0	$\mathbb{Z}_2$	$\mathbb{Z}_2$	$\mathbb{Z}$	0

Table 2.3: Periodic table for local unitary operators. The leftmost four columns define the AZ symmetry classes as described in the main text and in Table 2.1. The rightmost eight columns indicate the topological classification for local unitary operators from each symmetry class in dimension  $d$ . Note that this table is a permutation of the periodic table for topological Hamiltonians. See main text for details.

in momentum space as

$$U_A^{(A)}(k) = \begin{pmatrix} 0 & 1 \\ 1 & 0 \end{pmatrix} \quad (2.103)$$

$$U_B^{(A)}(k) = e^{ik}. \quad (2.104)$$

We recall that  $U_A^{(A)}$  enacts a hop between two sites within each unit cell, while  $U_B^{(A)}$  performs a chiral translation to a neighbouring unit cell in a single direction, with a lattice spacing we take equal to 1 (see Fig. 2.1). While we have implicitly assumed translational symmetry by writing these operators in terms of  $k$ , this is just to simplify the notation: the discussion which follows extends straightforwardly to the disordered case by working in real space.

As motivated in Sec. 2.5, these unitary operators can be mapped onto Hermitian operators in class AIII through Eq. (2.18), yielding

$$H_{U_A^{(A)}}(k) = \begin{pmatrix} 0 & 0 & 0 & 1 \\ 0 & 0 & 1 & 0 \\ 0 & 1 & 0 & 0 \\ 1 & 0 & 0 & 0 \end{pmatrix} \quad (2.105)$$

$$H_{U_B^{(A)}}(k) = \begin{pmatrix} 0 & e^{ik} \\ e^{-ik} & 0 \end{pmatrix} \quad (2.106)$$

Physically, the mapping to Hermitian operators may be interpreted as adding a sublattice degree of freedom to the system, where  $H_{U_A^{(A)}}$  then performs intracell hops, while  $H_{U_B^{(A)}}$  performs hopping in opposite directions for each sublattice (see Fig. 2.2).

By calculating the Class AIII topological invariant for these Hamiltonians [53], it may be verified that the first is trivial, while the second is topological with an invariant of 1, and so the topology of each local unitary operator is preserved in the mapping to Hamiltonians. Indeed, the invariant for these Hamiltonians is simply the winding number of the off-diagonal block—equivalent to the winding number for a 1D local unitary operator discussed in Ref. [30, 31]. The mapping between unitary and Hermitian operators proceeds in a similar manner for more complicated cases in these symmetry classes, and the mapping between topological invariants remains the same.

A similar picture also holds for 1D local unitary operators belonging to the nontrivial classes A, D and C, all of which can be mapped onto Hermitian operators with chiral symmetry and a winding number invariant. In class AII, a local unitary is mapped onto a Hermitian operator from class DIII, which also has chiral symmetry. The corresponding  $\mathbb{Z}_2$  topological invariant in this case (for both unitaries and Hermitian operators) may loosely be thought of as the winding number taken modulo 2. More formally, a constrained version of the Fu-Kane invariant may be used instead [54].

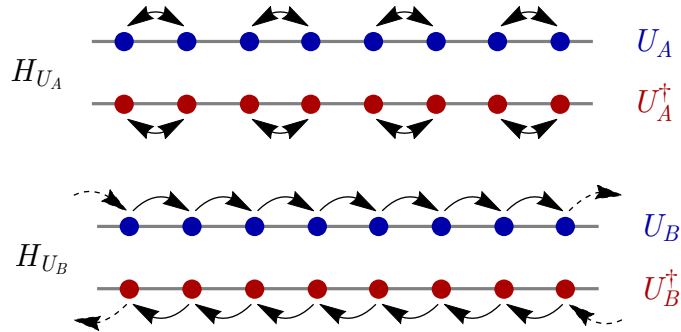


Figure 2.2: Illustration of the actions of the Hermitian operators  $H_{U_A}$  and  $H_{U_B}$  defined in Eqs. (2.105) and (2.106). In contrast to the underlying unitary operators (see Fig. 2.1, these Hermitian operators have twice the degrees of freedom. As discussed in the main text,  $H_{U_A}$  and  $H_{U_B}$  belong to different equivalence classes.

### 2.7.1.2 Unitary Operators in Class DIII

The one remaining nontrivial case in 1D corresponds to unitary operators in class DIII, which are mapped onto Hermitian operators in Class D. Topological Hamiltonians in class D are exemplified by the well-known  $p$ -wave superconducting chain [55]: we will take this as our starting point and work backwards to obtain a nontrivial local unitary operator belonging to class DIII.

The Hamiltonian for the  $p$ -wave superconductor may be written [55]

$$\begin{aligned} \hat{H}_K &= -\mu \sum_j \left[ c_j^\dagger c_j - \frac{1}{2} \right] \\ &\quad - \frac{1}{2} \sum_j \left[ t c_j^\dagger c_{j+1} + \Delta e^{i\phi} c_j c_{j+1} + \text{H.c.} \right], \end{aligned} \quad (2.107)$$

where  $\mu$  is the chemical potential,  $t$  is the hopping parameter, and  $\Delta e^{i\phi}$  is the superconducting pairing strength. We will take the two easily solvable (and flattened) points of this model as examples of trivial and topological flattened Hamiltonians from class D. In BdG form and in momentum space, these fixed points have the Hamiltonians

$$H_{\text{triv}}^{(D)}(k) = \begin{pmatrix} 1 & 0 \\ 0 & -1 \end{pmatrix} \quad (2.108)$$

$$H_{\text{top}}^{(D)}(k) = \begin{pmatrix} -\cos(k) & i \sin(k) \\ -i \sin(k) & \cos(k) \end{pmatrix}, \quad (2.109)$$

which it may be verified square to the identity matrix, and satisfy particle-hole symmetry with  $\mathcal{C} = \sigma_x \mathcal{K}$ . [These fixed point Hamiltonians also have additional symmetries, but this does not affect the arguments that follow]. It may be verified (e.g. by transforming to the Majorana fermion basis and calculating the Pfaffian [55]) that these Hamiltonians have invariants 0 and 1, respectively.

To construct distinct local unitary operators from these Hamiltonians, we can perform the (inverse) mapping described in Sec. 2.6: we should introduce a sublattice degree of freedom and then define  $U = -i\mathcal{S}H$ , where  $\mathcal{S} = i\sigma_z \otimes \mathbb{I}$  is a chiral symmetry operator that acts in the new sublattice basis. We introduce the artificial sublattice degree of freedom by labelling unit cells alternately as sublattice A and B. In this step, we coarse grain the system by enlarging the unit cell by a factor 2. Then the new coarse grained Hamiltonian after regrouping cells

can be rewritten as

$$\begin{aligned}\hat{H}_K &= -\mu \sum_j \left[ c_{j,A}^\dagger c_{j,A} + c_{j,B}^\dagger c_{j,B} - \frac{1}{2} \right] \\ &\quad - \frac{1}{2} \sum_j \left[ t(c_{j,A}^\dagger c_{j,B} + c_{j,B}^\dagger c_{j+1,A}) + \text{H.c.} \right]\end{aligned}\tag{2.110}$$

$$- \frac{1}{2} \sum_j \left[ \Delta e^{i\phi} (c_{j,A} c_{j,B} + c_{j,B} c_{j+1,A}) + \text{H.c.} \right],\tag{2.111}$$

In momentum space, this leads to the Hamiltonians

$$\tilde{H}_{triv}^{(D)}(k) = \begin{pmatrix} 1 & 0 & 0 & 0 \\ 0 & -1 & 0 & 0 \\ 0 & 0 & 1 & 0 \\ 0 & 0 & 0 & -1 \end{pmatrix}\tag{2.112}$$

$$\tilde{H}_{top}^{(D)}(k) = -\frac{1}{2} \begin{pmatrix} 0 & 0 & 1 + e^{-ik} & -1 + e^{-ik} \\ 0 & 0 & 1 - e^{-ik} & -1 - e^{-ik} \\ 1 + e^{ik} & 1 - e^{ik} & 0 & 0 \\ -1 + e^{ik} & -1 - e^{ik} & 0 & 0 \end{pmatrix},\tag{2.113}$$

which now act on the operators  $\left( c_{Ak} \quad c_{A-k}^\dagger \quad c_{Bk} \quad c_{B-k}^\dagger \right)^T$ .

The detailed calculations are shown in appendix 2.E. Both Hamiltonians continue to square to the identity, and satisfy particle-hole symmetry as in Eq. (2.34) with the symmetry operator now given by  $\mathcal{C} = \mathbb{I} \otimes \sigma_x \mathcal{K}$ .

While we could work with these Hamiltonians directly, we will instead perform a basis rotation so that the chiral symmetry operator takes the canonical form  $\mathcal{S} = i\sigma_z \otimes \mathbb{I}$  and commutes with the existing particle-hole symmetry. Specifically, we will rotate the Hamiltonians with the unitary operator

$$V = \frac{1}{\sqrt{2}} \begin{pmatrix} 0 & i & 1 & 0 \\ i & 0 & 0 & 1 \\ 0 & -i & 1 & 0 \\ -i & 0 & 0 & 1 \end{pmatrix},\tag{2.114}$$

through  $H \rightarrow VHV^\dagger$ . The particle-hole symmetry operator then becomes  $\mathcal{C} = \sigma_x \otimes \sigma_x \mathcal{K}$ , which commutes with a chiral symmetry operator defined through  $\mathcal{S} = i\sigma_z \otimes \mathbb{I}$ . Finally, after performing this rotation, we calculate the corresponding unitary operators through  $U = -i\mathcal{S}H$  to find

$$U_{triv}^{DIII}(k) = \begin{pmatrix} 0 & 0 & 1 & 0 \\ 0 & 0 & 0 & -1 \\ -1 & 0 & 0 & 0 \\ 0 & 1 & 0 & 0 \end{pmatrix} \quad (2.115)$$

and a nontrivial unitary

$$U_{top}^{DIII}(k) = \frac{1}{2} \begin{pmatrix} \sin(k) & i + i \cos(k) & -i + i \cos(k) & \sin(k) \\ -i - i \cos(k) & -\sin(k) & -\sin(k) & i - i \cos(k) \\ -i + i \cos(k) & \sin(k) & \sin(k) & i + i \cos(k) \\ -\sin(k) & i - i \cos(k) & -i - i \cos(k) & -\sin(k) \end{pmatrix}. \quad (2.116)$$

It may be verified that these are unitary operators with particle-hole symmetry ( $\mathcal{C} = \sigma_x \otimes \sigma_x \mathcal{K}$ ), chiral symmetry ( $\mathcal{S} = i\sigma_z \otimes \mathbb{I}$ ), and time-reversal symmetry ( $\mathcal{T} = -\sigma_y \otimes \sigma_x \mathcal{K}$ ), belonging to class DIII of the periodic table, although the rotation obscures its interpretation in terms of simple fermion operators. The nontrivial topology of  $U_{top}^{DIII}$  is evident from the spectra of the two operators: while the spectrum of  $U_{triv}^{DIII}(k)$  is gapped, the eigenvalues of  $U_{top}^{DIII}(k)$  wrap around the unit circle as a function of momentum, as shown in Fig. 2.3.

We now introduce another way to construct local unitary operators by directly turning the internal degree of freedom of Hamiltonian into sublattice degree of freedom. In this example, there is a nature degree of freedom generated by BdG forms. Therefore, we can define chiral symmetry operator as  $S = i\sigma_z$ . Then these two Hamiltonians can be mapped to two unitaries:

$$U_{triv2}^{DIII}(k) = \begin{pmatrix} 1 & 0 \\ 0 & 1 \end{pmatrix} \quad (2.117)$$

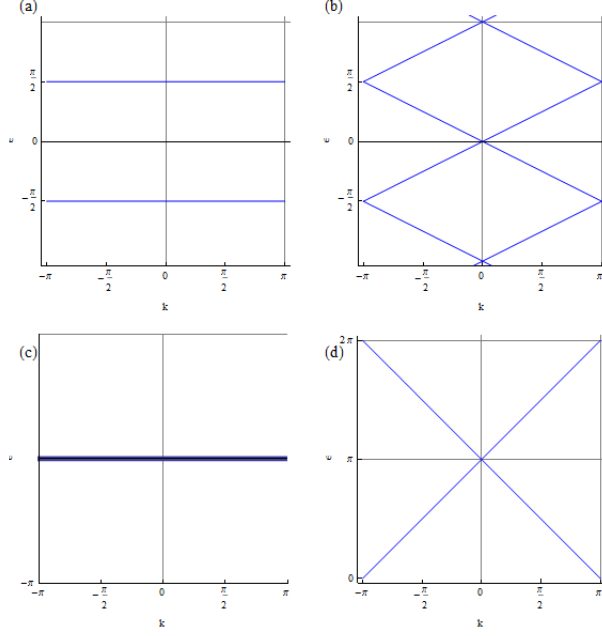


Figure 2.3: Spectrum of the unitaries (a)  $U_{triv}^{DIII}(k)$ , (b)  $U_{top}^{DIII}(k)$ , (c)  $U_{triv2}^{DIII}(k)$  and (d)  $U_{top2}^{DIII}(k)$  given in the main text. The plots show the complex phase of the eigenvalues  $\epsilon$  as a function of momentum  $k$ .

and

$$U_{top2}^{DIII}(k) = \begin{pmatrix} -\cos(k) & i \sin(k) \\ i \sin(k) & -\cos(k) \end{pmatrix} \quad (2.118)$$

It's obvious that  $U_{triv2}^{DIII}(k)$  is trivial since it's an identity matrix. In addition, we can deduce the nontrivial topology of  $U_{top2}^{DIII}$  from the nontrivial winding of the eigenspectrum of  $U_{top2}^{DIII}$  as shown in Fig.3.

This mapping to unitary operators provides an alternative method for diagnosing the topology of a gapped Hamiltonian.

## 2.7.2 Two Dimensions

### 2.7.2.1 Unitary Operators in Class AIII

We now study a two-dimensional example, again using the inverse mapping from topological Hamiltonians to nontrivial unitary operators. To obtain a nontrivial unitary in class AIII, we start from a nontrivial Hermitian operator from class A, which we take to be the simple flattened Chern insulator model

$$H^A(k) = \frac{1}{|E(\mathbf{k})|} \begin{pmatrix} \Delta + \cos(k_x) + \cos(k_y) & \sin(k_x) - i \sin(k_y) \\ \sin(k_x) + i \sin(k_y) & -\Delta - \cos(k_x) - \cos(k_y) \end{pmatrix}, \quad (2.119)$$

with

$$E(\mathbf{k}) = \sqrt{(\Delta + \cos(k_x) + \cos(k_y))^2 + (\sin(k_x) + \sin(k_y))^2}. \quad (2.120)$$

In real space, this Hamiltonian satisfies the definition of locality given in Sec. 2.3.1, but the hoppings will formally extend to infinity (with an exponentially decaying amplitude) to ensure perfectly flat bands. As shown in Ref [56], when  $-2 < \Delta < 0$ , the Chern number of the model equals  $-1$  and while  $0 < \Delta < 2$ , the Chern number is equal to  $1$ . For other values of  $\Delta$ , this model turns out to be trivial. Since this model describes a particle with two internal states hopping on a lattice, we can relabel these two states as states acting on sublattice A and sublattice B separately. Then chiral symmetry operator equals  $\sigma_z$  in the original basis. Then this Hamiltonian can be mapped to a unitary with an expression

$$U^A(k) = \frac{1}{|E(\mathbf{k})|} \begin{pmatrix} \Delta + \cos(k_x) + \cos(k_y) & \sin(k_x) - i \sin(k_y) \\ -\sin(k_x) - i \sin(k_y) & \Delta + \cos(k_x) + \cos(k_y) \end{pmatrix}, \quad (2.121)$$

The numerical computation of the quasienergy spectrum of Unitary  $U^A(k)$  reveals the appearance of Dirac cones (that is, of isolated points on the Brillouin zone where the gap closes with linear dispersion) at the surface of the system. This is illustrated in Fig. 2.4.

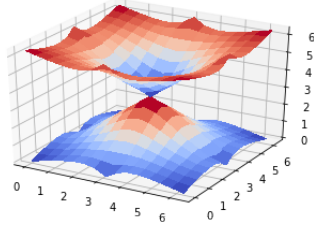


Figure 2.4: Three-dimensional view of the Dirac cone in gap  $\pi$  of the quasienergy spectrum of  $U^A(\mathbf{k})$  when  $\Delta = 1$ . The dispersion is clearly linear in the neighborhood of the Dirac cone (located approximately at  $k_x = \pi$  and  $k_y = \pi$ ).

## 2.8 Conclusion

In this work, we introduce a method to classify local unitaries. By mapping local unitary operators to Hermitian operators, we can obtain a topological classification based on the topological classification of Hermitian operators. For unitary operators without chiral symmetry, we apply the so-called ‘doubling trick’ by adding a sublattice or orbital degree of freedom on each site. On the other hand, for unitary operators with chiral symmetry, we make use of the existing chiral symmetry operator, which connects unitary operators and Hermitian operators. In general, a pair of Hermitian operators and unitary operators fall within different symmetry classes, and these mapping between symmetry classes are equivalent to moving downwards by one row in the periodic table. After showing the existence of one to one correspondence mapping between Hermitian operators and unitary operators, we also demonstrate that homotopic equivalence between two Hermitian operators implies a homotopic equivalence between the corresponding unitary operators. In the process, we discovered a number of new topological phases. It would be interesting to see if these can be realized in experimental settings.

To calculate topological invariants for models, we can combine our results with formulas for the topological invariants in static systems. By mapping a local unitary operator to a Hermitian operator, we can use the topological invariant of the Hermitian operator as the topological invariant of the unitary operator.

Our work raises many interesting problems. First, as claimed before in this chapter, our work classifies all edge unitaries in Floquet systems. Then a rigorous connection between bulk and edge properties can be explored in the future. Second, this chapter only gives a complete classification of noninteracting local unitaries with different symmetries. It would be interesting to study whether this classification can be extended to interacting Floquet phases. Progress in this direction has already been made for one-dimensional local unitaries via index theory and the matrix product unitary approach, which was first discussed in quantum cellular automata and then was used to classify interacting Floquet phases. However, the classification of quantum cellular automata and interacting Floquet phases in higher dimensions are not complete and remains an exciting avenue for future research.

## 2.A Deviations of flow index

In this section, we derive the flow index of local unitary matrices given in Eq. (2.21) and then prove some of the claims on the properties of the flow index  $\nu^{2n+1}[U]$ .

As what's shown in Ref.[44], the topological invariant of a flattened Hamiltonian with a format of Eq. (2.18) can be written as

$$\text{Ind}[H_U] = \frac{2^{2n}(\pi i)^n}{(2n+1)!!} \sum_{\sigma} (-1)^{\sigma} \text{Tr} S H_U [P_{\mathbf{a}}^{\sigma_1}, P_-] [P_{\mathbf{a}}^{\sigma_2}, P_-] \cdots [P_{\mathbf{a}}^{\sigma_{2n+1}}, P_-] \quad (2.122)$$

where we define the projector onto the lower bands as  $P_-$ . Since  $H_U$  is a flattened Hamiltonian, satisfying  $H_U = 1 - 2P_-$ , we can substitute  $P_-$  as a function of  $H_U$  in the above function:

$$\text{Ind}[H_U] = (-1)^{n+1} \frac{(\pi i)^n}{(2n+1)!!} * \frac{1}{2} \sum_{\sigma} (-1)^{\sigma} \text{Tr} S H_U [P_{\mathbf{a}}^{\sigma_1}, H_U] [P_{\mathbf{a}}^{\sigma_2}, H_U] \cdots [P_{\mathbf{a}}^{\sigma_{2n+1}}, H_U] \quad (2.123)$$

After inserting Eq. (2.18) and simplifying this expression, the multiplication of all operators inside the trace becomes a block diagonal matrix and the trace of this block diagonal matrix becomes

$$\begin{aligned} & \text{Tr} \left[ U [P_{\mathbf{a}}^{\sigma_1}, U^{\dagger}] [P_{\mathbf{a}}^{\sigma_2}, U] \cdots [P_{\mathbf{a}}^{\sigma_{2n+1}}, U^{\dagger}] \right] \\ & - \text{Tr} \left[ U^{\dagger} [P_{\mathbf{a}}^{\sigma_1}, U] [P_{\mathbf{a}}^{\sigma_2}, U^{\dagger}] \cdots [P_{\mathbf{a}}^{\sigma_{2n+1}}, U] \right] \end{aligned}$$

Then we utilize the identity  $[P_{\mathbf{a}}^{\sigma_1}, U^{\dagger}] = -U^{\dagger} [P_{\mathbf{a}}^{\sigma_1}, U] U^{\dagger}$  and rewrite the above subtraction of trace of two matrices as

$$2 * (-1)^{n+1} \text{Tr} \left[ U^{\dagger} [P_{\mathbf{a}}^{\sigma_1}, U] U^{\dagger} [P_{\mathbf{a}}^{\sigma_2}, U] \cdots U^{\dagger} [P_{\mathbf{a}}^{\sigma_{2n+1}}, U] \right]$$

Finally, by inserting it back into Eq. (2.122), we obtain the topological invariant of  $H_U$  in terms of its off-diagonal block  $U$ , which could be used as the flow index of  $U$ , showing in Eq.

(2.21)

$$\text{Ind}[H_U] = \frac{(\pi i)^n}{(2n+1)!!} \sum_{\sigma} (-1)^{\sigma} \text{Tr} \left[ U^{\dagger}[P_{\mathbf{a}}^{\sigma_1}, U] U^{\dagger}[P_{\mathbf{a}}^{\sigma_2}, U] \cdots U^{\dagger}[P_{\mathbf{a}}^{\sigma_{2n+1}}, U] \right] \quad (2.124)$$

We can know that the flow index can only take integer values directly from the properties of the topological invariants of Hermitian operators.

In the rest of this section we provide a deviation of some properties of the flow index.

First, similar to one-dimensional cases, this invariant is local computable because of the local computability of the topological invariants given in Eq. (2.122)[44]. We will explain this idea by providing the intuition rather than giving a rigorous mathematical proof. For every direction  $i$ , the matrix elements of  $U^{\dagger}[P_{\mathbf{a}}^i, U] = U^{\dagger}P_{\mathbf{a}}^iU - P_{\mathbf{a}}^i = U^{\dagger}P_{\mathbf{a}}^iU(1 - P_{\mathbf{a}}^i) - U^{\dagger}(1 - P_{\mathbf{a}}^i)UP_{\mathbf{a}}^i$  will decay exponentially with  $i$ -direction distance between the sites involved and the cut  $\mathbf{a}$ . Then the multiplication of  $U^{\dagger}[P_{\mathbf{a}}^i, U]$  for all  $i$  is bounded by a rapidly decaying function of the distance from the cut  $\mathbf{a}$ . In other words, most contributions to the calculation of the flow index come from the regions close to the cross section.

Second, we need to prove that the flow index is zero if and only if a unitary operator is locally generated. If a unitary operator  $U$  is local generated by a sequence of local Hamiltonians  $H_{loc}(t)$  ( $0 < t < T$ ), then we can define  $V_{\alpha}(s)$  as

$$V_{\alpha}(s) = U(s) = \mathcal{T} \exp \left[ -i \int_0^s H_{loc}(t) dt \right] \quad (2.125)$$

and  $V_{\beta}(s)$  as Identity matrix  $\mathbb{I}$ . So the homotopy relation between  $U$  and  $\mathbb{I}$

$$U(s) = V_{\alpha}(s)\mathbb{I}V_{\beta}(s) \quad (2.126)$$

is the same as that used in the definition of equivalence classes of unitaries in Sec. 2.3.2. Therefore the topological invariant of  $U$  is the same as the one for  $\mathbb{I}$  which is zero. Two unitaries share the same flow index if and only if they are topologically equivalent, inheriting this property from their parenting Hamiltonians. Then if the flow index of a unitary  $U$  is zero, this unitary is topologically equivalent to  $\mathbb{I}$ , namely,

$$U(s) = V_{\alpha}(s)\mathbb{I}V_{\beta}(s) \quad (2.127)$$

Therefore  $U$  is locally generated. Last, this unitary index is additive under composition and product. It's additive because of the following property of the trace:  $\text{Tr}\{U_1 \oplus U_2\} = \text{Tr}(U_1) + \text{Tr}(U_2)$ . A rigorous mathematical proof of why it's additive under matrix multiplication is given in Section 5.A.1. Here we use the same method in [30]. First, for a stacked chain, it's clear that  $\nu[U \oplus V] = \nu[U] + \nu[V]$ . Then we can construct a special unitary  $(U \oplus \mathbb{I})S_+(\mathbb{I} \oplus V)S_+$  acting on two chains where  $S_+$  denote the unitary which acts as the swap of these two chains on the right side  $r_{2n+1} > a_{2n+1}$  and leaves the left side  $r_{2n+1} < a_{2n+1}$  unchanged. Then this constructed unitary works like  $U \oplus V$  on the right subspaces and  $UV \oplus \mathbb{I}$  on the left spaces. Because this invariant is both local computable and independent of positions,  $\nu[UV] = \nu[U \oplus V] = \nu[U] + \nu[V]$ .

## 2.B Weak topological invariants of unitary operators

In the main context, we only consider strong topological invariants of Hamiltonian and thus only obtain strong topological invariants of unitary operators. In this appendix, we discuss how to extend the notion of weak topological invariants to unitary operators.

Motivated by the studies done in disordered static systems [57], we directly apply the corresponding formulas for strong invariants in lower dimensions to classify higher dimensional systems with the absence of strong invariants. We will demonstrate this idea by giving an example in a two-dimensional system.

While no strong topological invariants exist for Hamiltonians in two-dimensional class AIII systems, strong one-dimensional topological invariants can be used as weak indices to classify two-dimensional systems. As a result, we apply the flow index in Eq. (2.8) to classify our systems. We use the same method to define weak indices as Ref. [57]. We consider the two-dimensional systems as a stack of one-dimensional systems. To calculate the 1D index in the  $x$ -direction, we treat the full system as a one-dimensional system infinite in the  $x$ -direction and with width  $N_y$  in the  $y$ -direction. Finally, we could get a well defined

topological invariant if it has converged as  $N_y \rightarrow \infty$ , namely,

$$\nu_x[U] = \lim_{N_y \rightarrow \infty} \frac{1}{N_y} \text{Tr}(U^\dagger [P_R^x, U] P_{\text{trunc}}^{N_y}) \quad (2.128)$$

where  $P_{\text{trunc}}^{N_y}$  is used to truncate the original unitary of the full system to a strip which has  $N_y$  layers in  $y$ - direction labeled from  $-N_y/2$  to  $N_y/2 - 1$ . In addition, a similar topological invariant can be defined in  $y$ - direction,

$$\nu_y[U] = \lim_{N_x \rightarrow \infty} \frac{1}{N_x} \text{Tr}(U^\dagger [P_R^y, U] P_{\text{trunc}}^{N_x}) \quad (2.129)$$

where  $P_{\text{trunc}}^{N_x}$  projects onto a vertical strip including  $N_x$  layers in  $x$ - direction labeled from  $-N_x/2$  to  $N_x/2 - 1$ . Finally, these two invariants can be massaged into one vector  $n_x \mathbf{x} + n_y \mathbf{y}$ , which can be used to classify this two dimensional system.

In a translation invariant system, consider a two-dimensional  $U(k_x, k_y)$  that now is a Laurent polynomial of  $e^{ik_x}$  and  $e^{ik_y}$  [30]. Therefore,  $\det U$  is also a polynomial function of  $e^{ik_x}$  and  $e^{ik_y}$ , namely,  $\det U = e^{in_x k_x + in_y k_y}$ . Then we calculate topological invariants in two directions separately, getting  $n_x$  and  $n_y$ . From our discussion of real-space formula,  $n_x \mathbf{x} + n_y \mathbf{y}$  can be called the index, independent of basis vectors  $\mathbf{x}$  and  $\mathbf{y}$ . As a simple example, we take the unitary operator to be  $e^{ik_x}$ , which is simply stacks of one-dimensional shift operator in  $x$ - direction. For this operator, the index vector is  $\mathbf{x}$  since the winding number is 1 in  $x$ -direction and 0 in  $y$ -direction.

## 2.C Eigenstate Properties of Flattened Operators

In this appendix we prove that the flattened Hermitian operators  $H_U$  defined in the main text have equal numbers of positive and negative eigenvalues. They therefore have a well-defined energy gap and fit into the usual topological classification. For completeness, we also note that in certain symmetry classes, Hermitian operators may have different numbers of positive and negative eigenvalues. While these cannot be obtained through the mappings from unitary operators used in the main text, this does not affect our conclusions, as cases with equal eigenvalues exhaust all topological classes. The one-to-one mappings we describe are in this

way between local unitary operators, and local flattened Hermitian operators *with equal numbers of positive and negative eigenvalues*.

We first consider the symmetry classes discussed in Sec. 2.5, where  $H_U$  is defined through the doubling trick,

$$H_U = \begin{pmatrix} 0 & U \\ U^\dagger & 0 \end{pmatrix}. \quad (2.130)$$

In these cases, we can expand the underlying unitary operator in its eigenstate basis as

$$U = \sum_j e^{i\theta_j} |v_j\rangle\langle v_j|. \quad (2.131)$$

By taking the Hermitian conjugate of this equation, it follows that if  $|v_j\rangle$  is an eigenstate of  $U$  with eigenvalue  $e^{i\theta_j}$ , then it is also an eigenstate of  $U^\dagger$  with eigenvalue  $e^{-i\theta_j}$ . We can therefore construct pairs of states

$$|\psi_j^\pm\rangle = \frac{1}{\sqrt{2}} \begin{pmatrix} 1 \\ \pm e^{-i\theta_j} \end{pmatrix} |v_j\rangle \quad (2.132)$$

which are eigenstates of  $H_U$  with eigenvalue  $\pm 1$ . In this way, each eigenstate of the original unitary operator  $U$  generates a pair of eigenstates for  $H_U$  with eigenvalues  $\pm 1$ .

On the other hand, the symmetry classes discussed in Sec. 2.6 possessed chiral symmetry, and generated Hermitian operators through  $H_U = \eta \mathcal{S} U$  (where  $\eta \in \{1, i\}$  depending on the specific symmetry class). In these cases, the symmetry relation  $\mathcal{S} U \mathcal{S}^{-1} = U^\dagger$  means that we can expand  $U$  in terms of its eigenstates through

$$U = \sum_j \left[ e^{i\theta_j} |v_j\rangle\langle v_j| + e^{-i\theta_j} |\bar{v}_j\rangle\langle \bar{v}_j| \right], \quad (2.133)$$

where pairs of eigenstates are related to each other through  $\mathcal{S} |v_j\rangle = \eta^* |\bar{v}_j\rangle$  (and where the factor of  $\eta^*$  is necessary to ensure that  $\mathcal{S}^2$  takes the correct value). Note that we are assuming that the system is closed here, as topological eigenstates at a boundary can be mapped onto themselves under the action of  $\mathcal{S}$  [37].

With this setup, we can write the Hamiltonian as

$$H = \eta \mathcal{S} U = \sum_j \left[ e^{i\theta_j} |\bar{v}_j\rangle\langle v_j| + e^{-i\theta_j} |v_j\rangle\langle \bar{v}_j| \right]. \quad (2.134)$$

Then, similar to before, we can construct pairs of states

$$|\psi_j^\pm\rangle = \frac{1}{\sqrt{2}} \left[ |v_j\rangle \pm e^{i\theta_j} |\bar{v}_j\rangle \right], \quad (2.135)$$

which are eigenstates of  $H_U$  with eigenvalues  $\pm 1$ . In this way, each eigenstate of the original unitary operator  $U$  again generates a pair of eigenstates for  $H_U$  with eigenvalues  $\pm 1$ .

## 2.D Local unitary transformation

In section 2.4.2, we define the equivalence relation between two gapped quantum systems. Two Hamiltonians are in the same phase if we can find a local unitary transformation that connects their corresponding flattened Hamiltonians. Now we present a method to calculate this local unitary transformation.

This local unitary transformation defined in Eq. (2.12) is generated by  $\tilde{H}(s)$ ,  $s \in [0, 1]$  with an expression given in Ref. [51]. For two topologically equivalent quantum systems with Hamiltonians  $H_0$  and  $H_1$ , there exists a continuous path  $s \rightarrow H(s)$  that smoothly connects these two Hamiltonians. Then we can define  $\tilde{H}(s)$  as

$$\tilde{H}(s) = i \int dt F(t) e^{iH(s)t} (\partial_s H(s)) e^{-iH(s)t} \quad (2.136)$$

if the gap of Hamiltonian  $H(s)$  is larger than some finite value  $\Delta$  for all  $s$ .

Here,  $F(t)$  is a function with the following properties. First, the fourier transformation of  $F(t)$ ,  $\tilde{F}(\omega)$  obeys,  $\tilde{F}(\omega) = -\frac{1}{\omega}$  if  $|\omega| \geq \Delta$ . Second,  $F(t)$  is antisymmetric, namely,  $F(t) = -F(-t)$ .

The above expression involves a construction of  $F(t)$  and an integral over  $t$ . To simplify the above expression, we derive  $\tilde{H}(s)$  from a different perspective. First we can define a flattened Hamiltonian

$$H'(s) = 1 - 2P_g(s), \quad (2.137)$$

where the spectral projector  $P_g(s) = \sum_\alpha |\Psi^\alpha(s)\rangle \langle \Psi^\alpha(s)|$  specifies a subspace of the total Hilbert space spanned by the occupied Bloch wave functions of  $H(s)$ .

Following from Eq. (2.37), after taking derivative over  $s$ , we find how  $H'(s)$  changes with  $s$

$$\frac{\partial H'(s)}{\partial s} = i[\tilde{H}(s), H'(s)] \quad (2.138)$$

We notice that

$$\begin{aligned} & \left[ \left[ H'(s), \frac{\partial H'(s)}{\partial s} \right], H'(s) \right] \\ &= 2H'(s) \frac{\partial H'(s)}{\partial s} H'(s) - 2 \frac{\partial H'(s)}{\partial s} H'(s)^2 \end{aligned} \quad (2.139)$$

because we are considering flattened Hamiltonian  $H'(s)$  which satisfies  $H'(s)^2 = \mathbb{I}$ . To simplify above equation, we take derivative of the identity  $H'(s)^2 = \mathbb{I}$  and another equation can be derived,

$$H'(s) \frac{\partial H'(s)}{\partial s} + \frac{\partial H'(s)}{\partial s} H'(s) = 0 \quad (2.140)$$

We can rewrite Eq. (2.139) by plugging Eq. (2.140),

$$\left[ \left[ H'(s), \frac{\partial H'(s)}{\partial s} \right], H'(s) \right] = -4 \frac{\partial H'(s)}{\partial s} H'(s)^2 \quad (2.141)$$

Therefore, we can choose

$$\tilde{H}(s) = -\frac{i}{4} \left[ H'(s), \frac{\partial H'(s)}{\partial s} \right] \quad (2.142)$$

which satisfies our requirements Eq. (2.138) to be the local unitary transformation generating Hamiltonians. Because  $H'(s)$  is local and continuous,  $\tilde{H}(s)$  is also local. In general, we can also add arbitrary terms to  $\tilde{H}(s)$  which commutes with  $H'(s)$  or  $P_g(s)$  in order to satisfy Eq. (2.138). Namely, a more general form of  $\tilde{H}(g)$  can be written as

$$\begin{aligned} \tilde{H}(s) &= -\frac{i}{4} \left[ H'(s), \frac{\partial H'(s)}{\partial s} \right] \\ &+ P_g(s) H_1(s) P_g(s) + P_e(s) H_2(s) P_e(s) \end{aligned} \quad (2.143)$$

where  $P_g(s)$  is the projector in the ground states and  $P_e(s)$  is the projector in the excited states.  $P_g(s) H_1(s) P_g(s)$  and  $P_e(s) H_2(s) P_e(s)$  are two Hamiltonians which acts on occupied states and empty states separately.

Next, we want to show that these two techniques agree with each other. We can start from the first expression of  $\tilde{H}(s)$  which is given in Eq. (2.136) and expand it by inserting two identities  $\mathbb{I} = P_g(s) + P_e(s)$ . Then  $\tilde{H}(g)$  is decomposed into four parts,  $P_g(s)\tilde{H}(s)P_g(s), P_e(s)\tilde{H}(s)P_g(s), P_g(s)\tilde{H}(s)P_e(s)$  and  $P_e(s)\tilde{H}(s)P_e(s)$ . To proceed further, we express the spectral projector  $P_g(s)$  in terms of ground states  $P_g(s) = \sum_{i \in g} |\Psi^i(s)\rangle \langle \Psi^i(s)|$  and similarly,  $P_e(s) = \sum_{j \in e} |\Psi^j(s)\rangle \langle \Psi^j(s)|$ . Then the second term can be rewritten as

$$\begin{aligned} & P_e \tilde{H}(s) P_g \\ &= \sum_{j \in e} \sum_{i \in g} \langle \Psi^j(s) | \tilde{H}(s) | \Psi^i(s) \rangle | \Psi^j(s) \rangle \langle \Psi^i(s) | \end{aligned} \quad (2.144)$$

After plugging the expression of  $\tilde{H}(s)$  in Eq.(2.136), the coefficient can be simplified using the property of function  $F(t)$ ,

$$\begin{aligned} & \langle \Psi^j(s) | \tilde{H}(s) | \Psi^i(s) \rangle \\ &= i \langle \Psi^j(s) | \int dt F(t) \exp[i(E_j - E_i)t] \partial_s H(s) | \Psi^i(s) \rangle \\ &= i \tilde{F}(E_j - E_i) \langle \Psi^j(s) | \partial_s H(s) | \Psi^i(s) \rangle \\ &= i \langle \Psi^j(s) | \partial_s | \Psi^i(s) \rangle \end{aligned} \quad (2.145)$$

where  $\tilde{F}(E_j - E_i) = -\frac{1}{E_j - E_i}$  according to the assumption on the gap in the spectrum. The last equality in the above equation holds because

$$\begin{aligned} E_i \langle \Psi^j(s) | \partial_s | \Psi^i(s) \rangle &= \langle \Psi^j(s) | \partial_s (H(s) | \Psi^i(s) \rangle) \\ &= \langle \Psi^j(s) | \partial_s H(s) | \Psi^i(s) \rangle \\ &+ E_j \langle \Psi^j(s) | \partial_s | \Psi^i(s) \rangle \end{aligned} \quad (2.146)$$

Substituting (2.145) into (2.144) we have  $P_e(s)\tilde{H}(s)P_g(s) = iP_e(s)\partial_s P_g(s)$  and similarly  $P_g(s)\tilde{H}(s)P_e(s) = iP_g(s)\partial_s P_e(s)$ . After adding four parts together, we can massage  $\tilde{H}(s)$  into the desired form (2.143),

$$\begin{aligned} \tilde{H}(s) &= iP_e(s)\partial_s P_g(s) + iP_g(s)\partial_s P_e(s) \\ &+ P_g \tilde{H}(s) P_g + P_e \tilde{H}(s) P_e \end{aligned} \quad (2.147)$$

Where the addition of the first two terms become  $-\frac{i}{4}[H'(s), \frac{\partial H'(s)}{\partial s}]$  if we apply two identities  $\mathbb{I} = P_g(s) + P_e(s)$  and (2.137). Therefore, these two techniques agree with each other.

The second question in this section we want to solve is how symmetry operators act on these transformation generating Hamiltonians and their corresponding generated unitaries. In general, these Hamiltonians don't follow any symmetries because the freedom to add arbitrary local Hamiltonians that commutes with  $P_g(s)$ . However, if we have a special choice of  $\tilde{H}(s)$  given in (2.142), then symmetry operators can apply constraints on  $\tilde{H}(s)$ . Recalling Eqs. (2.30–2.32), we show how symmetry operators (if present) act on these Hamiltonians,

$$\mathcal{T}\tilde{H}(s)\mathcal{T}^{-1} = -\tilde{H}(s) \quad (2.148)$$

$$\mathcal{C}\tilde{H}(s)\mathcal{C}^{-1} = -\tilde{H}(s) \quad (2.149)$$

$$\mathcal{S}\tilde{H}(s)\mathcal{S}^{-1} = \tilde{H}(s). \quad (2.150)$$

Consequently, we can write down the action of the three symmetries (if present) on the transformation unitary operators generated by  $\tilde{H}(s)$  given in (2.142)

$$\mathcal{T}V(s)\mathcal{T}^{-1} = V(s) \quad (2.151)$$

$$\mathcal{C}V(s)\mathcal{C}^{-1} = V(s) \quad (2.152)$$

$$\mathcal{S}V(s)\mathcal{S}^{-1} = V(s). \quad (2.153)$$

Overall, we provide two techniques to construct local unitary transformation and prove that they agree with each other. Then we show how symmetry operators act on these locally generated unitaries under a particular choice of generating Hamiltonians.

## 2.E Generating nontrivial unitaries from Hamiltonians

In section 2.7, we discuss how to map from Hamiltonians without chiral symmetry to unitary operators with chiral symmetry. However, the local Hilbert spaces of these unitaries may have different dimensions with the ones of Hamiltonians. In this appendix, we only consider

when unitaries have larger internal degrees of freedom, and the opposite situation can be dealt with a similar method. To match the internal degrees of freedom, we can reorganize the cell structure by either adding trivial systems or regrouping several neighboring cells to get a new single cell with a higher internal degree of freedom.

The first method, adding trivial systems, works because the topological properties of Hamiltonians will stay the same after the addition of arbitrary numbers of trivial bands under the definition of stable homotopy. In that case, although a Hamiltonian  $H_1$  can not be transformed into a unitary with chiral symmetry  $U$ , it might be possible that there are trivial walks  $H_2$  so that  $H_1 \oplus H_2$  can be mapped to  $U$ . For example, We can define a nontrivial flattened Hamiltonian  $H_A$  acting on sublattice A and a trivial flattened Hamiltonian  $H_B$  acting on sublattice B. Then the chiral symmetry operator can be defined as  $\mathbb{I} \oplus -\mathbb{I}$  which can map a nontrivial Hamiltonian  $H_A \oplus H_B$  to a nontrivial unitary  $U = H_A \oplus -H_B$ .

Since the spatial degrees of freedom and the internal degrees of freedom are interchangeable in general, we can also regroup some finite collection of the cells to increase the size of the local Hilbert space. If we include two neighboring cells into one new unit cell, we can change the periodicity from 1 to 2 and double the dimension of the local Hilbert space. Clearly, this does not affect the topological properties of the original Hamiltonians. The main difference between new Hamiltonians and original Hamiltonians is due to different definitions of translation vectors. In section 2.7, we use this method to generate one-dimensional unitary Operators in Class DIII from Hermitian operators in Class D. Let us explain how to do the regrouping operations in this example.

In this example, we study translation-invariant systems and want to express Hamiltonians in the momentum space. Then the matrix element connecting two positions of a Hamiltonian is only dependent on distances between two positions. Explicitly, we can assume

$$f(\vec{r}) = \langle \vec{r} + \vec{x} | H | \vec{x} \rangle \quad (2.154)$$

where  $\vec{x}$  and  $\vec{x} + \vec{r}$  are two points on the lattice, and  $H$  is the Hamiltonian that we want to transform. If there is an internal degree of freedom,  $f(\vec{r})$  can become a matrix. After doing a

fourier transformation, we can express the Hamiltonian in the momentum space as

$$H(\vec{k}) = \sum_{\vec{r}} e^{-i\vec{k}\cdot\vec{r}} f(\vec{r}) \quad (2.155)$$

For one dimensional system, we label even sites as sublattice A and odd sites as sublattice B. Then the transformation has similar form as in Ref. [32]. First, the regrouped Hamiltonian  $f_r$  in the position space can be written as

$$f_r(r) = \begin{pmatrix} f(2r) & f(2r-1) \\ f(2r+1) & f(2r) \end{pmatrix} \quad (2.156)$$

and after doing fourier transformation

$$H_r(k) = M\left(\frac{k}{2}\right) \begin{pmatrix} H\left(\frac{k}{2}\right) & 0 \\ 0 & H\left(\frac{k}{2} + \pi\right) \end{pmatrix} M^\dagger\left(\frac{k}{2}\right) \quad (2.157)$$

where the unitary matrix  $M(k)$  meets  $M = \frac{1}{\sqrt{2}} \begin{pmatrix} 1 & 1 \\ e^{-ik} & -e^{-ik} \end{pmatrix}$  Then we obtain the expressions of the topological Hamiltonian after regrouping Eq. (2.113) given  $H(k)$  satisfying Eq. (2.109)

For two dimensional systems with square lattice, similarly, we label unit cells alternately. This time new translation vectors become  $e'_x = 2e_x$ ,  $e'_y = e_x + e_y$  if original lattice can be constructed by two translation vectors  $e_x$  and  $e_y$ . Then regrouping Hamiltonian becomes

$$f_r(x, y) = \begin{pmatrix} H(2x+y, y) & H(2x+y-1, y) \\ H(2x+y+1, y) & H(2x+y, y) \end{pmatrix} \quad (2.158)$$

and the regrouping Hamiltonian in momentum space becomes

$$H_r(k) = M\left(\frac{k_x}{2}\right) \begin{pmatrix} H\left(\frac{k_x}{2}, k_y - \frac{k_x}{2}\right) & \\ & H\left(\frac{k_x}{2} + \pi, k_y - \frac{k_x}{2} + \pi\right) \end{pmatrix} M^\dagger\left(\frac{k_x}{2}\right) \quad (2.159)$$

## CHAPTER 3

### Constructing locally generated unitaries

In last chapter, we provide a method which can detect whether a local unitary is locally generated. In this chapter, we want to show how to construct such locally generated unitaries.

To do this, we first apply the one-dimensional decoupling method introduced in Reference [30, 46]. Then we explain it in a new perspective and generalize this theory to higher dimensions.

#### 3.1 One-dimensional decoupling theory

In the one-dimensional decoupling theory given in Reference [46], we construct  $V$ , which decouples the left and right side of a system. Therefore,  $V$  can transform this unitary  $U$  to a new unitary  $U_L \oplus U_R$ ,

$$VU = U_L \oplus U_R \quad (3.1)$$

In other words, the decoupling condition can be expressed as  $[P_a, VU] = 0$  where  $P_a$  is a half-space projection operator. In one-dimensional system,  $P_a$  act on sites on the right of the cross-section  $a$ . If we label the one-step translation of the projector  $P_a$  as  $Q = UP_aU^\dagger$ , the decoupling condition can also be written as

$$VQ_a = P_aV \quad (3.2)$$

$V$  should be a function of  $P_a$  and  $Q_a$ . Before giving the detailed construction, we introduce the following subspaces

$$\mathcal{H}_{10} = \{\phi \in \mathcal{H} | Q_a \phi = \phi, P_a \phi = 0\}$$

$$\mathcal{H}_{01} = \{\phi \in \mathcal{H} | Q_a \phi = 0, P_a \phi = \phi\}$$

and the complement of  $\mathcal{H}_{10} \oplus \mathcal{H}_{01}$  is represented as  $\mathcal{H}_\perp$ .

With these notations, the steps to construct  $V$  is given as follows. First we study the operator  $X = 1 - P_a - Q_a + 2P_a Q_a$ . This operator meets the decoupling condition above but is not unitary. Therefore we need to modify the  $X$  operator to make it unitary. We separate Hilbert space into two parts, the null space of  $X$  which coincides with  $\mathcal{H}_{10} \oplus \mathcal{H}_{01}$  and the complement of the null space which equals  $\mathcal{H}_\perp$ . On the subspace  $\mathcal{H}_\perp$ ,  $X$  is not zero, and all its eigenvalues can be normalized. After normalizing all its nonzero eigenvalues,  $X$  is transformed to be a canonical decoupling operator  $V_{can}$  which can be written as

$$V_{can} = (X^\dagger X)^{-1/2} X \quad (3.3)$$

On the subspace  $\mathcal{H}_{10} \oplus \mathcal{H}_{01}$ , however, the normalization approach doesn't work. This time, we define a swap unitary  $V_{01}$  which swaps  $\mathcal{H}_{10}$  and  $\mathcal{H}_{01}$ , i.e.,

$$V_{01} \mathcal{H}_{10} = \mathcal{H}_{01}, V_{01} \mathcal{H}_{01} = \mathcal{H}_{10} \quad (3.4)$$

This is required by the decoupling condition. Finally we find a proper decoupling unitary  $U$  by adding  $V_{can}$  and  $V_{01}$  together

$$V = V_{can} \oplus V_{01} \quad (3.5)$$

For strictly localized systems, when away from the cut,  $P_a = Q_a = 1$  on the far right and  $P_a = Q_a = 0$  on the far left. Therefore  $X = \mathbb{I}$  far from the cut. As the function of  $X$ , the decoupling unitary  $V$  is also equal to identity away from the cut. For exponentially decaying unitaries,  $V - \mathbb{I}$  is also exponentially decaying when away from the cut. For these unitaries almost confined to a finite-size region, we can always find a Hermitian operator  $H$  which are bounded to the same region such that  $e^{iH} = V$ .

If there are symmetric constraints on  $U$  given in Eq.(2.48),  $VU$  should also be in the same symmetric class. If there is particle-hole symmetry, then the requirement of Eq. (2.47) means  $V$  commutes with the symmetry operator  $\mathcal{C}$ ,

$$\mathcal{C}V\mathcal{C}^{-1} = V. \quad (3.6)$$

If the system has time-reversal symmetry, then the requirement of Eq. (2.46) imposes the condition

$$\tilde{\mathcal{T}}V\tilde{\mathcal{T}}^{-1} = V, \quad (3.7)$$

with the modified symmetric operator  $\tilde{\mathcal{T}} = U\mathcal{T}$ . While the presence of chiral symmetry [Eq. (2.48)] imposes the similar condition

$$\tilde{\mathcal{S}}V\tilde{\mathcal{S}}^{-1} = V, \quad (3.8)$$

with the modified symmetric operator  $\tilde{\mathcal{S}} = U\mathcal{S}$ .

While  $V_{can}$  always meets all these communication relations, we need to add these additional constraints for  $V_{01}$ . We are not going to give details about how to add constraints here and suggest the reader refer Reference [46] for details.

## 3.2 One dimensional locally generated unitaries

After briefly reviewing the decoupling theory, we now show how to construct locally generated unitaries in this section. We cut the systems at locations with equal distance  $x = 0, \pm a, \pm 2a, \dots$ . At every cut  $ma$ , we can find a unitary  $V_m$  using the decoupling theory above. Let  $H_m$  denote the Hermitian operator decaying exponentially away from the cut  $m$ , such that  $V_m = e^{iH_m}$ . After multiplying by the product of these unitaries,  $\prod_m e^{iH_m}U$  will be fully decoupled, becoming  $\sum_n \tilde{U}_n$  where  $\tilde{U}_n$  only act on sites between the cut  $na$  and  $(n+1)a$  for each  $n$ . Since each unitary  $U_n$  is acting on a finite region  $[na, (n+1)a]$ , we can always find a Hermitian operator  $\tilde{H}_n$  acting on the same subspaces such that  $e^{i\tilde{H}_n} = \tilde{U}_n^\dagger$ . The whole

process can be written as

$$\prod_{n=n_{min}}^{n_{max}} e^{i\tilde{H}_n} \prod_{m=m_{min}}^{m_{max}} e^{iH_m} U = \mathbb{I} \quad (3.9)$$

Accordingly, the generating process for a local unitary  $U$  is

$$U = \prod_{m=m_{max}}^{m_{min}} e^{-iH_m} \prod_{n=n_{max}}^{n_{min}} e^{-i\tilde{H}_n} \quad (3.10)$$

Let's give an example here. Consider a translation-invariant system with two internal degrees of freedom for each site. We show how to generate the following unitary

$$U(k) = \begin{pmatrix} e^{ik} & 0 \\ 0 & e^{-ik} \end{pmatrix} \quad (3.11)$$

We first do an inverse Fourier transformation of this unitary  $U(k)$  to get a real space unitary operator  $\tilde{U}$ . As shown below, it's an addition of a left-moving translation operator and a right-moving translation operator on two separate sublattices in real space.

$$\tilde{U} = \sum_m |m+1, -1\rangle \langle m, -1| + |m, 1\rangle \langle m+1, 1| \quad (3.12)$$

where the first index denotes the position of sites and the second index represents internal degrees of freedom.

Next, we choose  $x = 0$  as a decoupling position, then the half-space projector becomes  $P_a = P_0 = \sum_{m \geq 0} |m\rangle \langle m|$ . Another projection will be the unitary transformation of  $P_0$ ,  $Q_0 = \tilde{U} P_0 \tilde{U}^\dagger$ . The two subspaces labelled by the eigenvalues of  $Q_0$  and  $P_0$  are

$$\begin{aligned} \mathcal{H}_{10} &= \{c|-1, 1\rangle | c \in \mathbb{C}\} \\ \mathcal{H}_{01} &= \{c|0, -1\rangle | c \in \mathbb{C}\} \end{aligned}$$

where  $c$  is the coefficient of a state, taking arbitrary complex number.  $V_{01}$  swap two Hilbert spaces  $\mathcal{H}_{10}$  and  $\mathcal{H}_{01}$ . This operator is of course not uniquely defined, we choose it to be

$$V_{01} = i|0, -1\rangle \langle -1, 1| + i|-1, 1\rangle \langle 0, -1| \quad (3.13)$$

Next, we calculate the decoupling operator  $X$ ,

$$\begin{aligned}
X &= 1 - P_0 - \tilde{U}P_0\tilde{U}^\dagger + 2P_0\tilde{U}P_0\tilde{U}^\dagger \\
&= \mathbb{I} - |0, -1\rangle\langle 0, -1| - |-1, 1\rangle\langle -1, 1| \\
&= \sum_{m \neq 0} |m, -1\rangle\langle m, -1| + \sum_{m \neq -1} |m, 1\rangle\langle m, 1|
\end{aligned} \tag{3.14}$$

Therefore on the complement of the null space  $\mathcal{H}_{10} \oplus \mathcal{H}_{01}$ ,  $X$  acts as the Identity matrix and thus is already a unitary. After applying the normalization process in Eq. (3.3),

$$V_{can} = X \tag{3.15}$$

Finally, we find the unitary that can decouple the left side and right side of the cut  $x = 0$  by adding  $V_{can}$  and  $V_{01}$ ,

$$V_0 = \sum_{m \neq 0} |m, -1\rangle\langle m, -1| + \sum_{m \neq -1} |m, 1\rangle\langle m, 1| + i|0, -1\rangle\langle -1, 1| + i|-1, 1\rangle\langle 0, -1| \tag{3.16}$$

which can be generated by  $H_0 = |0, -1\rangle\langle -1, 1| + |-1, 1\rangle\langle 0, -1|$ , satisfying  $V_0 = e^{iH_0}$ . This unitary is strictly local, with nonzero hopping only existing between nearest neighboring sites.

According to translation invariance, we can get decoupling unitaries  $V_n$  at every cut  $x = n$ ,

$$V_n = \sum_{m \neq n} |m, -1\rangle\langle m, -1| + \sum_{m \neq n-1} |m, 1\rangle\langle m, 1| + i|n, -1\rangle\langle n-1, 1| + i|n-1, 1\rangle\langle n, -1|$$

governed by a Hamiltonian  $H_n = \frac{\pi}{2}(|n, -1\rangle\langle n-1, 1| + |n-1, 1\rangle\langle n, -1|)$ . Since each Hamiltonian  $H_n$  are bounded to the subspaces expanded by  $|n, -1\rangle$  and  $|n-1, 1\rangle$ , different  $H_n$  and  $H_{n'}$  act on separate subspaces and don't intertwine with each other. As a result, we can do the decoupling at each cut simultaneously with a decoupling unitary,

$$V = \prod_n V_n \tag{3.17}$$

generated by a Hamiltonian

$$\begin{aligned}
H &= \sum_n H_n \\
&= \frac{\pi}{2} \sum_n |n, -1\rangle\langle n-1, 1| + |n-1, 1\rangle\langle n, -1|
\end{aligned} \tag{3.18}$$

We can do a Fourier transformation of  $H$  to express it back in the momentum space,

$$H(k) = \frac{\pi}{2} \begin{pmatrix} 0 & e^{ik} \\ e^{-ik} & 0 \end{pmatrix} \quad (3.19)$$

After applying  $V(k) = e^{iH(k)}$  to decouple the original unitary (3.11), we get

$$W(k) = V(k)U(k) = -i \begin{pmatrix} 0 & 1 \\ 1 & 0 \end{pmatrix} \quad (3.20)$$

Since  $W(k)$  is fully decoupled,  $W(k)$  can be generated by a constant Hamiltonian  $W(k) = e^{iH'(k)}$ . To recover  $H'(k)$ , we need to take a log of  $W(k)$ ,

$$H'(k) = -\frac{\pi}{2} \begin{pmatrix} 0 & 1 \\ 1 & 0 \end{pmatrix} \quad (3.21)$$

Finally, we show that  $U(k)$  can be generated by a two-step evolutions,

$$U(k) = V^\dagger(k)W(k) = e^{-iH(k)}e^{iH'(k)} \quad (3.22)$$

where  $H(k)$  and  $H'(k)$  are given in Eq. (3.19) and (3.21) separately.

### 3.3 Higher dimensional decoupling theory

In this section, we will have a different viewpoint of the decoupling theory and generalize it to higher dimensional systems. As shown in Chapter 2, there is a one-to-one correspondence between a local unitary operator and a local gapped Hermitian operator. Hence we can decouple a unitary by decoupling a Hermitian operator.

#### 3.3.1 Decoupling flattened Hermitian operators

To decouple a flattened Hermitian operator in  $d$  dimension, we need to find a  $d-1$  dimensional local unitary  $V_H$ , such that,

$$V_H H V_H^\dagger = \tilde{H} = H_R \oplus H_L. \quad (3.23)$$

Since this is a unitary transformation,  $\tilde{H}$  is also a flattened Hermitian operator. An intuitive way to do this is to have a truncation of these Hamiltonians through

$$H_{trunc} = P_{\mathbf{a}}^i H_U P_{\mathbf{a}}^i + (1 - P_{\mathbf{a}}^i) H_U (1 - P_{\mathbf{a}}^i) \quad (3.24)$$

where we cut the whole system through a cross-section located at  $\mathbf{a}$  along the direction  $i$  and the definition of  $P_{\mathbf{a}}^i$  is given in Equation (2.23). Then  $H_{trunc}$  is clearly decoupled, with no nonzero hoppings between left and right side of the cut. Clearly,

$$H_{trunc} = \begin{pmatrix} 0 & P_{\mathbf{a}}^i U P_{\mathbf{a}}^i + (1 - P_{\mathbf{a}}^i) U (1 - P_{\mathbf{a}}^i) \\ P_{\mathbf{a}}^i U^\dagger P_{\mathbf{a}}^i + (1 - P_{\mathbf{a}}^i) U^\dagger (1 - P_{\mathbf{a}}^i) & 0 \end{pmatrix} \quad (3.25)$$

Then we need to flatten this Hamiltonian as required by Eq. (3.23). If  $H_{trunc}$  is gapped then we can flatten  $H_{trunc}$  directly. If  $H_{trunc}$  is gapless, then we need to transform  $H_{trunc}$  into a gapped Hamiltonian. From the last chapter, we know that if a unitary can be locally generated, then its corresponding Hamiltonian should be topological trivial. By adding symmetry-preserving local perturbations on the edge created by the cut, we can lift the gap. This step can be done numerically. Finally, we get a gapped Hamiltonian

$$H_{gap} = H_{trunc} + H_{perturbation} \quad (3.26)$$

Then we flatten this Hamiltonian by introducing a matrix

$$H_{flat} = 1 - 2P_F \quad (3.27)$$

where  $P_F$  projectors to the lower bands of  $H_{gap}$ . Finally, we get the decoupled Hamiltonian  $\tilde{H} = H_{flat}$ .

### 3.3.2 Unitary operators without chiral symmetry

For a unitary operator  $U$  without chiral symmetry, it can be mapped to a Hermitian operator with chiral symmetry via

$$H_U = \begin{pmatrix} 0 & U \\ U^\dagger & 0 \end{pmatrix}. \quad (3.28)$$

Then the decoupling condition in Eq. (3.23) can also be written as

$$V_H H_U V_H^\dagger = \begin{pmatrix} 0 & VU \\ U^\dagger V^\dagger & 0 \end{pmatrix} = H_R \oplus H_L \quad (3.29)$$

where we define a decoupling unitary for  $H_U$  through

$$\tilde{V} = \begin{pmatrix} V & 0 \\ 0 & \mathbb{I} \end{pmatrix} \quad (3.30)$$

Hence,  $H_{flat} = H_R + H_L$  given in Equation (3.27) also follows the same chiral symmetry as  $H_U$ , taking the form of

$$H_R + H_L = H_{flat} = \begin{pmatrix} 0 & W \\ W^\dagger & 0 \end{pmatrix} \quad (3.31)$$

After comparing this equation with Eq. (3.29), we find the decoupling unitary  $V$ , satisfying

$$V = WU^\dagger \quad (3.32)$$

### 3.3.3 Unitary operators with chiral symmetry

We define a Hermitian operator through Equation (2.84) and (2.89),

$$H_U = \eta \mathcal{S} U \quad (3.33)$$

when  $\mathcal{S}^2 = 1$ ,  $\eta = 1$  and when  $\mathcal{S}^2 = -1$ ,  $\eta = i$ . Similarly, the decoupled Hamiltonian  $\tilde{H}_U = H_{flat}$  given in Eq. (3.27) can be written in a similar form,

$$\tilde{H}_U = \eta \mathcal{S} \tilde{U} \quad (3.34)$$

Therefore, the decoupled unitary  $\tilde{U}$  can be written as

$$\tilde{U} = \eta^3 \mathcal{S} \tilde{H}_U \quad (3.35)$$

$$= (\eta^3 \mathcal{S} \tilde{H}_U U^\dagger) U \quad (3.36)$$

Then we can define a local unitary  $V = \eta^3 \mathcal{S} \tilde{H}_U U^\dagger$  that meets the decoupling condition given in Eq. (3.1).

# CHAPTER 4

## Chiral flow in one-dimensional floquet topological insulator

---

*Portions of this chapter are adapted from the publication:*

Reiss, D., Harper, F., and Roy, R. *Chiral Flow in One-dimensional Floquet Topological Insulators*. Physical Review B **98**, 165116 (2018).

---

### 4.1 Preliminary Discussion

#### 4.1.1 The Flow of a Unitary Matrix

In our study of dynamical phases, we will make use of a property of unitary matrices known as ‘flow’, introduced by Kitaev in Ref. [31]. This property may be defined for any unitary operator, although we will later apply it to the special case of unitary loop evolutions.

To define this quantity, we consider a noninteracting unitary matrix  $U = (U_{jk})$ , where  $j$  and  $k$  can be interpreted as labelling sites on a (formally infinite) one-dimensional lattice. Explicitly, the matrix elements  $U_{jk}$  determine a unitary operator through the definition

$$\hat{U} = \sum_{jk} U_{jk} c_j^\dagger c_k, \quad (4.1)$$

where  $c_j^\dagger$  ( $c_j$ ) creates (annihilates) a single boson or fermion on site  $j$ . An intuitive notion of ‘current’ from position  $k$  to position  $j$  induced by the unitary operator may then be defined

as

$$f_{jk} = |U_{jk}|^2 - |U_{kj}|^2, \quad (4.2)$$

which is the difference in hopping probabilities between the two sites. In analogy with electric current, the one-dimensional flow of a unitary matrix is the total current through a cross section [31], which may be written explicitly (for a cross section at coordinate  $x_0$ ) as

$$F(U) = \sum_{j \geq x_0} \sum_{k < x_0} f_{jk}. \quad (4.3)$$

This is shown schematically in Fig. 4.1.

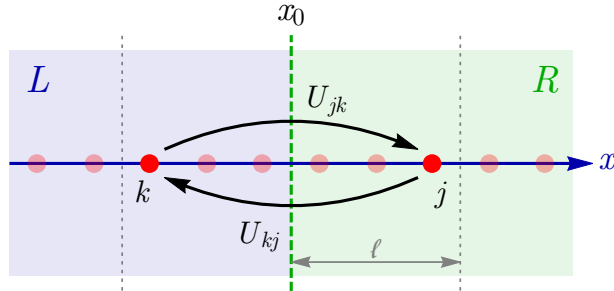


Figure 4.1: The flow of a unitary matrix. Vertical dashed green line indicates the coordinate of the cross section  $x_0$ , defining regions  $L$  and  $R$ . Red points indicate 1D lattice sites, while black arrows represent the current between sites  $j$  and  $k$  across the cut. The flow is defined by summing over all particle currents that cross the cut, as in Eq. (4.3). If the unitary is strictly local, only sites within a distance  $\ell$  of the cut will contribute to the flow, delimited by grey dotted lines. (Figure adapted from Reference [37] with permission from the *American Physical Society*.)

Following Ref. [31], we now introduce a projector  $P_R$  for the half axis  $x \geq x_0$  and a projector  $P_L$  for the other half axis  $x < x_0$ , so that  $P_L = \mathbb{I} - P_R$ . In terms of these projectors, the flow of a unitary matrix may equivalently be rewritten as

$$\begin{aligned} F(U) &= \text{Tr}(U^\dagger P_R U P_L - U^\dagger P_L U P_R) \\ &= \text{Tr}(U^\dagger P_R U - P_R) \\ &= \text{Tr}(U^\dagger [P_R, U]). \end{aligned} \quad (4.4)$$

It may be verified that these expressions reduce to Eq. (4.3). Importantly, in these expressions we cannot use the cyclic property of the trace  $\text{Tr}(AB) = \text{Tr}(BA)$ , since this holds only if one of the matrices has a finite number of nonzero elements [31].

In a physical system, the underlying Hamiltonian must satisfy certain locality constraints, which in turn places constraints on the form of the time-evolution operator. We can use these properties to our advantage when calculating the flow of a unitary operator that corresponds to time evolution. The usual definition of a local operator is one whose matrix elements decay exponentially (or faster) with the distance between the sites involved (see, for example, Ref. [7]). To simplify our discussion in the main text, however, we will assume that the time-evolution operator is *strictly* local, i.e. that  $U_{jk} = 0$  for  $|j - k| > \ell$  beyond some localisation length  $\ell$  (where  $j$  and  $k$  label unit cell positions). In Appendix 4.A we extend our arguments to the more general definition of locality.

Under this assumption of strict locality, it is clear that only the regions close to the cross section will contribute to the calculation of flow in Eq. (4.4). Setting the cross section coordinate to be  $x_0 = 0$ , we can therefore restrict our projectors to the relevant interval  $[-\ell, \ell]$ . Specifically, we define the projector  $P_L^\ell$  for the region  $[-\ell, 0)$  and the projector  $P_R^\ell$  for the region  $[0, \ell)$  and substitute  $P_L \rightarrow P_L^\ell$  and  $P_R \rightarrow P_R^\ell$  in Eq. (4.4). It is clear that the result will not be affected by this truncation, and we arrive at the expression

$$F(U) = \text{Tr}(U^\dagger P_R^\ell U P_L^\ell - U^\dagger P_L^\ell U P_R^\ell). \quad (4.5)$$

With this truncation, we have an expression for  $F(U)$  that can now be applied to finite systems.

To develop some intuition for this index, we now consider two simple examples. First, we take the unitary operator to be the identity,  $U = \mathbb{I}$ . It is clear that the flow will be zero in this case, since each projector commutes with  $U$  in Eq. (4.5) and we can apply the result  $P_L^\ell P_R^\ell = 0$ . This is reflective of the fact that that unitary operator  $\mathbb{I}$  does not involve any particle current between the two sides of the cut.

As a second example we consider the unitary  $U = \hat{t}$ , where  $\hat{t}$  is the shift operator having

action

$$\hat{t}|j\rangle = |j+1\rangle, \quad (4.6)$$

with  $|j\rangle$  a state localised on site  $x = j$ . For this operator the localisation length is  $\ell = 1$ .

Writing  $P_L^\ell = |-1\rangle\langle -1|$  and  $P_R^\ell = |0\rangle\langle 0|$ , we see that

$$\begin{aligned} F(U) &= \text{Tr} \left[ (\hat{t}^\dagger |0\rangle\langle 0| \hat{t} |-1\rangle\langle -1|) - (\hat{t}^\dagger |-1\rangle\langle -1| \hat{t} |0\rangle\langle 0|) \right] \\ &= 1. \end{aligned} \quad (4.7)$$

This quantifies the non-zero current of particles across the cut effected by the operator  $\hat{t}$ .

The flow of a unitary operator, using any of the definitions above, is quantized to take integer values [31]. It is therefore robust to any continuous change of the system, and can be used for the purposes of topological classification. When  $U$  possesses translational symmetry, it was shown by Kitaev [31] that  $P_R$  in Eq. (4.4) may be replaced with the position operator  $\hat{X}$  so that

$$F(U) = \text{tr} \left( U^\dagger [\hat{X}, U] \right), \quad (4.8)$$

where ‘tr’ now indicates the trace per unit cell. We can then use the Fourier transform

$$\hat{U}(q) = \sum_x U_{0x} e^{iqx} \quad (4.9)$$

to rewrite the flow as the integral

$$F(U) = \frac{i}{2\pi} \int_{-\pi}^{\pi} dq \text{Tr} \left[ \hat{U}(q)^\dagger \frac{d\hat{U}}{dq} \right], \quad (4.10)$$

where ‘Tr’ is once again the usual matrix trace [31]. In this way, we see that for translationally invariant systems, the flow is equal to the familiar momentum-space winding number  $w[U]$  that captures the topology of the mapping from the space  $S^1$  to the space of unitary matrices.

In this paper, we aim to find and classify time-evolution operators with nontrivial unitary flow. However, many of the systems we might hope would host such phases can be shown to have a trivial flow index. In particular, a 1D unitary generated by a local 1D Hamiltonian can be shown to always have zero flow index [30]. In addition, for a unitary operator with a

finite number of nonzero elements, we can use the cyclic property of the trace to show that Eq. (4.4) vanishes.

One way to achieve a nonzero flow is to consider higher-dimensional systems, where, for example, robust chiral edge modes may exist at the boundary of a 2D periodic drive [5]. In this work, we will instead consider inherently 1D systems with a protected chiral symmetry, which leads to a definition of ‘chiral flow’.

## 4.2 Driven Systems with Chiral Symmetry

### 4.2.1 Chiral Symmetry

In this section, we will study topological drives with chiral symmetry, corresponding to Class AIII of the AZ classification scheme [1, 49, 58]. We will introduce a notion of chiral flow that can be used to characterise such systems and describe a nontrivial model drive that may be used to generate phases with different chiral flow indices. We begin by recalling that a system has chiral symmetry if its (time-dependent) Hamiltonian satisfies the relation

$$CH(t)C^{-1} = -H(-t) \quad (4.11)$$

for some chiral symmetry operator  $C$ , which is a unitary operator satisfying  $C^2 = \mathbb{I}$  [1]. The eigenvalues of such an operator are  $\pm 1$ , and so we can write it in diagonal form as

$$C = \begin{pmatrix} \mathbb{I} & 0 \\ 0 & -\mathbb{I} \end{pmatrix} = C_+ - C_-, \quad (4.12)$$

where  $C_{\pm}$  are projectors onto the  $\pm 1$  eigenspace. In this basis, the instantaneous Hamiltonian is off-diagonal. It follows from Eq. (4.11) that chiral symmetry acts on the unitary time-evolution operator as

$$CU(t)C^{-1} = U(T-t)U^{\dagger}(T), \quad (4.13)$$

where we have used the fact that the Hamiltonian is periodic in time with period  $T$  [1]. At the end of one cycle, the time-evolution operator satisfies

$$CU(T)C^{-1} = U^{\dagger}(T). \quad (4.14)$$

### 4.2.2 A Model Drive with Chiral Symmetry

We now build a model drive with chiral symmetry that has nontrivial flow properties. Inspired by the static Su-Schrieffer-Heeger (SSH) model [59], we take a 1D bipartite chain of  $N$  unit cells, with sublattices labelled ‘A’ and ‘B’. For a closed chain, we define the SSH-like Hamiltonian

$$H_{SSH} = v \sum_{m=1}^N \left[ |m, B\rangle \langle m, A| + \text{H.c.} \right] + w \sum_{m=1}^N \left[ |(m+1)N, A\rangle \langle m, B| + \text{H.c.} \right], \quad (4.15)$$

where  $|m, \alpha\rangle$  denotes a state of the chain where the particle is on sublattice  $\alpha$  in unit cell  $m$ . The parameter  $v$  controls the hopping of particles between sublattice A and B within the same cell, while the parameter  $w$  controls the hopping between unit cells. In this static case, the Hamiltonian is trivial (topological) when  $|v| > |w|$  ( $|w| > |v|$ ) [59]. It may be verified that this Hamiltonian satisfies the chiral symmetry constraint

$$CH_{SSH}C^{-1} = -H_{SSH},$$

where  $C$  is defined in the canonical way through  $C = \prod_j \tau_j^z$ , and where  $\tau_j^z$  is a Pauli  $z$ -matrix acting in the sublattice space on site  $j$ .

For our model drive, we take a piecewise constant Hamiltonian of the form

$$H(t) = \begin{cases} H_1 & 0 \leq t < \frac{1}{4}T \\ H_2 & \frac{1}{4}T \leq t < \frac{1}{2}T \\ H_2 & \frac{1}{2}T \leq t < \frac{3}{4}T \\ H_1 & \frac{3}{4}T \leq t < T, \end{cases}, \quad (4.16)$$

where

$$H_1 = \frac{2\pi}{T} \sum_{m=1}^N (|m, B\rangle \langle m, A| + h.c.) \quad (4.17)$$

$$H_2 = -\frac{2\pi}{T} \sum_{m=1}^{N-1} (|m+1, A\rangle \langle m, B| + h.c.)$$

are of the form in Eq. (4.15).<sup>1</sup> The hopping terms of the drive are indicated in Fig. 4.2(a).

In each of the four steps of the drive, a particle moves with probability one between neighboring sites, following the trajectory shown in Fig. 4.2(b). After a complete cycle, each particle in the closed system returns to its initial position, so that  $U(T) = \mathbb{I}$  and the unitary is a loop. After cutting the chain open, however, some terms from the Hamiltonian are removed, and one particle on each edge no longer moves during the second and third steps. At the end of the evolution, these particles have instead gained a phase of  $\pi$ , and will show up in the quasienergy spectrum as protected edge modes at  $\epsilon = \pi$ .

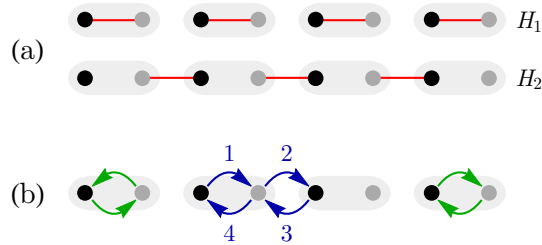


Figure 4.2: Schematic picture of the model drive given in Eqs. (4.16) and (4.17). (a) Driving protocol. The phase with Floquet edge states is obtained by driving with a trivial Hamiltonian  $H_1$  and a nontrivial Hamiltonian  $H_2$  in turn. Black (gray) points are sites on sublattice A (B). For each Hamiltonian, hopping occurs between sites indicated by red lines. Gray background indicates unit cells. (b) Drive action. Particles in the bulk move in closed trajectories indicated by the blue arrows, while particles on the boundary follow the green arrows and gain a phase of  $\pi$ . (Figure adapted from Reference [37] with permission from the *American Physical Society*.)

### 4.2.3 Winding Number Invariant

We now obtain a classification of this model drive which may be extended to more general systems with chiral symmetry. We first observe that at  $t = T/2$  in the model drive, particles that started on an A site have moved to another A site (unless they are near the boundary)

---

<sup>1</sup>The relative minus sign is added for convenience so that hopping phases gained during steps one and two cancel out in the bulk.

and similarly, particles that started on sublattice B have moved to another B site. More specifically, particles appear to ‘flow’ within each sublattice, and the action of the half-period evolution  $U(T/2)$  resembles a combination of shift operators  $\hat{t} \oplus \hat{t}^\dagger$ , introduced in Eq. (4.6). This is shown schematically in Fig. 4.3(a).

This sublattice decoupling is a general feature of Floquet drives with chiral symmetry at the half-period point. We can see this by substituting  $t = T/2$  into Eq. (4.13) to find

$$U^\dagger(T/2) C U(T/2) C^{-1} = U^\dagger(T). \quad (4.18)$$

If the drive is a loop, then

$$C U(T/2) C^{-1} = U(T/2), \quad (4.19)$$

which means that  $U(T/2)$  commutes with the chirality operator and hence is block-diagonal in the chiral basis,

$$U(T/2) = \begin{pmatrix} U_+ & 0 \\ 0 & U_- \end{pmatrix}. \quad (4.20)$$

For the model drive, we see that  $U_+ = \hat{t}$  and  $U_- = \hat{t}^\dagger$ .

Now, we know that any translationally symmetric (closed-system) unitary in 1D has a winding number as given in Eq. (4.10). Applying this formula to the block-diagonal unitary  $U(T/2)$ , we find

$$w[U(T/2)] = w[U_+] + w[U_-] = 0, \quad (4.21)$$

which must vanish because the evolution is one-dimensional: Specifically, the winding number is a homotopy invariant and  $U(t)$  is smooth, and so  $w[U(t)]$  must be independent of time [14]. Then, since  $w[U(0)] = w[\mathbb{I}] = 0$  at the beginning of the evolution, it follows that  $w[U(T/2)] = 0$  too.

However, we observed for the model drive in Sec. 4.2.2 a ‘chiral flow’ within each sublattice for which  $w \neq 0$ , and so in general  $w[U_+]$  and  $w[U_-]$  might not be zero individually. We identify the quantity  $w[U_+]$  as the topological invariant  $\nu[U]$  for a chiral Floquet system,

which may be written in full as

$$\begin{aligned}\nu[U] &= \frac{i}{2\pi} \int_{-\pi}^{\pi} dk \operatorname{tr} \left[ U_+^{-1}(k) \partial_k U_+(k) \right] \\ &= \frac{i}{4\pi} \int_{-\pi}^{\pi} dk \operatorname{tr} \left[ C U^{-1}(k, T/2) \partial_k U(k, T/2) \right].\end{aligned}\tag{4.22}$$

In the second line we have inserted the chiral symmetry operator and used the fact that  $w[U_+] = -w[U_-]$ . For the model drive above, it may be verified that  $\nu[U] = 1$ . Other integer values of  $\nu[U]$  can be obtained by running this model drive in sequence (being sure to preserve chiral symmetry), or by running the model drive in reverse.

Since the winding number is quantised to take integer values, it is robust to local perturbations and is a well-defined topological index for chiral symmetric Floquet systems with translational invariance. The topological invariant for 1D Floquet systems in class AIII has previously been expressed in this form in Ref. [14].

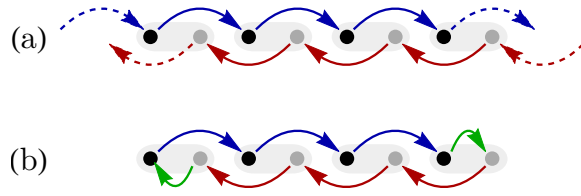


Figure 4.3: Schematic picture of the chiral flow for the model drive introduced in Sec. 4.2.2. (a) The chiral flow in the closed system generated by  $U(T/2)$ . Black (grey) circles indicate sublattice A (B). Blue (red) lines show the motion of particles on sublattice A (B) after a half period. (b) The chiral flow in the corresponding open system after a half period. Note that on each edge, particles are forced to hop between sublattices (green arrows). (Figure adapted from Reference [37] with permission from the *American Physical Society*.)

#### 4.2.4 Chiral Flow Invariant

The winding number above functions as a topological invariant for Floquet systems with both chiral symmetry and translational invariance. We now seek to construct a real-space

topological invariant that continues to hold even in disordered systems, using the connection between flow and winding number discussed in Sec. 4.1.1.

From Eq. (4.10), we see that the winding number  $w(U_+)$  is related to the flow of the unitary  $U_+$ , which acts only on the positive chirality eigenspace. We can therefore use Eqs. (4.4) and (4.5) to replace  $w[U_+]$  with  $F[U_+]$ , so that

$$\begin{aligned}\nu[U] &= \text{Tr}(U_+^{-1}P_R U_+ P_L) - \text{Tr}(U_+^{-1}P_L U_+ P_R) \\ &= \text{Tr}(U_+^{-1}P_R^\ell U_+ P_L^\ell) - \text{Tr}(U_+^{-1}P_L^\ell U_+ P_R^\ell).\end{aligned}\tag{4.23}$$

This describes the flow from the left side of a cut to the right, using the definitions of projectors introduced in Sec. 4.1.1. In the second line, we have again assumed that the unitary operator is *strictly* local, so that the truncation to a region of width  $2\ell$  around the cut has no effect on the calculation of  $\nu[U]$ . In Appendix 4.A, we consider the more general case where  $U$  is only exponentially localised.

As in the translationally invariant case, the total flow of the unitary must be zero and so  $F[U_+] = -F[U_-]$ . We can therefore write the real-space invariant more symmetrically as

$$\begin{aligned}\nu[U] &= \frac{1}{2} \left[ \text{Tr} \left( C U^{-1} P_R U P_L \right) - \text{Tr} \left( C U^{-1} P_L U P_R \right) \right] \\ &= \frac{1}{2} \left[ \text{Tr} \left( C U^{-1} [P_R, U] \right) \right] \\ &= \frac{1}{2} \left[ \text{Tr} \left( C U^{-1} P_R^\ell U P_L^\ell \right) - \text{Tr} \left( C U^{-1} P_L^\ell U P_R^\ell \right) \right]\end{aligned}\tag{4.24}$$

where we have used the shorthand  $U = U(T/2)$ .

These (equivalent) expressions for  $\nu[U]$  define what we refer to as *chiral flow*, a bulk topological invariant that quantifies the particle flow on a single sublattice at the midpoint of a Floquet evolution belonging to class AIII. For the model drive introduced in Sec. 4.2.2, this flow is evident from the form of the unitary operator at  $t = T/2$ , but  $\nu[U]$  may be calculated for any evolution in the symmetry class. In particular, the real-space expression for the chiral flow is applicable to unitary evolutions with disorder.

Before concluding this section, we note that there is another way of interpreting the chiral flow in this model drive. In Ref. [5], the authors construct a 2D Floquet loop drive belonging

to class A (which has no protecting symmetries). Under the action of their drive, a particle in the bulk will follow a closed path around a square plaquette, returning to its initial position. However, a particle at the boundary will be unable to complete a closed path, and will instead propagate along the edge, as shown in Fig. 4.4.

At  $t = T/2$ , our 1D class AIII model drive exhibits bulk chiral flow that looks very similar to the edge behaviour (at  $t = T$ ) of the 2D class A model of Ref. [5]. In fact, our class AIII model can be interpreted as an open-system class A drive collapsed down to a single layer. In this interpretation, the edge modes of the model of Ref. [5] undergo chiral flow at the boundary.

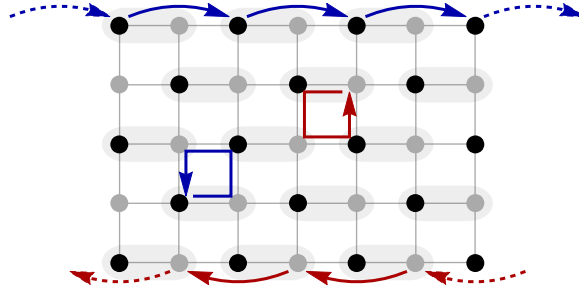


Figure 4.4: Action of the 2D class A drive introduced in Ref. [5]. During each step, particles hop between sites on a bipartite lattice following the paths indicated by red and blue arrows. Sublattices are indicated by gray and black points, while gray shaded regions indicate unit cells. After a complete cycle, a particle in the bulk returns to its initial position, while a particle at the edge is translated by one unit cell. The 1D class AIII model we introduce in Sec. 4.2.2 can be obtained by collapsing this 2D model onto a single chain. (Figure adapted from Reference [37] with permission from the *American Physical Society*.)

## 4.3 Dynamical Edge Modes with Chiral Symmetry

### 4.3.1 Protected Dynamical Edge Modes in the Model Drive

In the previous section, we introduced chiral flow as a robust topological quantity that describes the bulk properties of a Floquet evolution in class AIII halfway through the driving cycle. However, topological phases also exhibit robust edge behaviour that is closely related to the physics in the bulk, a feature known as bulk-boundary correspondence. In this section, we study the form of the dynamical edge modes present at the end of a topological drive in class AIII, and introduce an invariant that may be used to count them. This will be used in Sec. 4.4 when we derive an explicit bulk-edge correspondence.

In general, protected edge states arise at interfaces between topological phases where bulk topological numbers change. In this paper, we will mostly consider edge modes at the boundary of an open system, which may be viewed as an interface with the (topologically trivial) vacuum. As motivated in Sec. 4.1, inherently dynamical edge modes are associated with bulk unitary loops, and occur at quasienergy  $\epsilon = \pi$ .

As an example, we first revisit the model drive introduced in Sec. 4.2.2. We recall that halfway through the drive, the time-evolution operator takes the block-diagonal form

$$U_c(T/2) = \begin{pmatrix} \hat{t} & 0 \\ 0 & \hat{t}^\dagger \end{pmatrix},$$

where  $\hat{t}$  ( $\hat{t}^\dagger$ ) is the unit translation operator to the right (left), and each translation operator acts within a single sublattice. We have added the subscript  $c$  to emphasise that the unitary operator here is for the closed system. In this way, the unitary  $U_c(T/2)$  generates a chiral flow with index  $\nu[U] = 1$ , shown schematically in Fig. 4.3.

In order to find the number and form of the edge modes of the model, we must evolve with the drive in an open system until  $t = T$ . Using Eqs. (4.15) and (4.16), we find

$$U_o(T) = -|1, B\rangle \langle 1, B| - |N, A\rangle \langle N, A| + \sum_{m=1}^{N-1} |m, A\rangle \langle m, A| + \sum_{m=2}^N |m, B\rangle \langle m, B|, \quad (4.25)$$

where the subscript  $o$  indicates this is the evolution for the open system (i.e. with terms in the generating Hamiltonian which connect sites across the boundary omitted). Then, writing

$$U_o(T) = \sum_n e^{-i\epsilon_n T} |\phi_n\rangle\langle\phi_n|, \quad (4.26)$$

we see that there is a single edge mode at  $\epsilon = \pi$  on each boundary. Focussing on the right-hand edge at  $x = N$ , we find that there is one edge mode with wavefunction  $|N, A\rangle$ , and that the total number of  $\pi$  modes is  $n_\pi = 1$ . In general, we write the net number of  $\pi$  edge modes at a single boundary as

$$n_\pi = n_\pi^A - n_\pi^B, \quad (4.27)$$

which is the number of edge modes on sublattice A minus the number of edge modes on sublattice B. This definition is justified in that a pair of degenerate states at the same edge on different sublattices can be gapped out by a chiral-symmetric Hamiltonian acting only at the edge, as proved below in Sec. 4.3.2.

For our model drive, it follows that at the right edge  $n_\pi^R = 1$ , while at the left edge  $n_\pi^L = -1$ . In this way, at least for the model drive, we see that the number of edge modes is equal to the *change* in the bulk chiral flow invariant across the interface,

$$n_\pi = n_\pi^A - n_\pi^B = \Delta\nu. \quad (4.28)$$

We will show below that this bulk-edge correspondence holds in general.

### 4.3.2 Edge Invariants

We now extend this discussion of edge modes to more general drives with chiral symmetry. First, we note from Eq. (4.14) that the quasienergy spectrum of a chiral-symmetric Floquet operator  $U(T)$  is symmetric about  $\epsilon = 0$  and  $\epsilon = \pi$ . Specifically, if  $|\phi_n\rangle$  is an eigenstate of  $U(T)$  with quasienergy  $\epsilon_n \pmod{2\pi}$ , then using Eq. (4.14) we can write

$$U(T)C|\phi_n\rangle = CU^\dagger(T)|\phi_n\rangle = e^{-i\epsilon_n T}C|\phi_n\rangle, \quad (4.29)$$

which shows that  $C|\phi_n\rangle$  is also an eigenstate of  $U(T)$  with quasienergy  $-\epsilon_n \pmod{2\pi}$ . In this way, eigenstates at  $\epsilon = 0$  and  $\epsilon = \pi$  are special, in that the chiral symmetry operator

maps them onto states with the same quasienergy. These spectral properties are illustrated in Fig. 4.5.

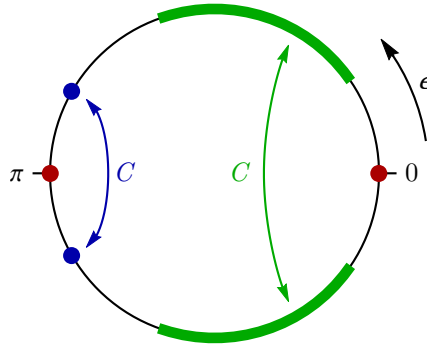


Figure 4.5: Schematic quasienergy spectrum for a Floquet operator  $U(T)$  with chiral symmetry. Since quasienergies are defined modulo  $2\pi$ , the spectrum may be visualised on the unit circle. The chiral symmetry operator  $C$  maps states with quasienergy  $\epsilon$  onto states with quasienergy  $-\epsilon$  (green band and blue points). In this way, the spectrum is symmetric about  $\epsilon = 0$  and  $\epsilon = \pi$ . States at these special values map onto states with the same quasienergy under the action of  $C$ , and possibly map onto themselves (red points). (Figure adapted from Reference [37] with permission from the *American Physical Society*.)

For the open-system Floquet operator  $U_o(T)$  of the model drive given in Eq. (4.25), we see that each edge state has support on a single sublattice, and is mapped onto itself under the action of  $C$ . In fact, eigenstates at  $\epsilon = \pi$  can always be chosen to have support on a single sublattice, as we now show. First, we write the projector onto sublattice A/B as

$$P_{A/B} = \frac{\mathbb{I} \pm C}{2}, \quad (4.30)$$

which follows from Eq. (4.12). Then, given an eigenstate

$$U_o(T) |\phi\rangle = -|\phi\rangle, \quad (4.31)$$

we see that

$$\begin{aligned} U_o(T) P_A |\phi\rangle &= U_o(T) \left[ \frac{\mathbb{I} + C}{2} \right] |\phi\rangle \\ &= \frac{1}{2} [U_o(T) + C U_o^\dagger(T)] |\phi\rangle \\ &= -P_A |\phi\rangle, \end{aligned} \quad (4.32)$$

where we have made use of Eq. (4.14). In this way,  $P_A |\phi\rangle$  is either an eigenstate of  $U_o(T)$  at  $\epsilon = \pi$  or  $|\phi\rangle$  is annihilated by  $P_A$ . In either case, we can split the state  $|\phi\rangle$  into components  $P_A |\phi\rangle$  and  $P_B |\phi\rangle$ , each of which has support on a single sublattice or vanishes. A state with support on a single sublattice is mapped onto itself by the action of  $C$ .

Now, a dynamical topological phase is indicated by the presence of *protected* edge modes at  $\epsilon = \pi$ . In order to be protected, it should not be possible to gap out the edge modes with a local, symmetry-respecting evolution acting only in the edge region. We now demonstrate that for edge modes to be protected, they must all have support on the same sublattice. Specifically, we will show that a pair of edge modes (at the same edge) with support on different sublattices may be gapped out, providing justification for the edge-mode counting defined in Eq. (4.27).

We assume we have two eigenstates  $|\phi_A\rangle$  and  $|\phi_B\rangle$  at quasienergy  $\epsilon = \pi$ , with support on sublattice A and B, respectively. While the states do not need to have support on the same sites, they should each be localised to the same boundary. We then consider the local, chiral-symmetric Hamiltonian

$$H' = |\phi_A\rangle\langle\phi_B| + |\phi_B\rangle\langle\phi_A|, \quad (4.33)$$

which generates the evolution,

$$e^{-itH'} = \begin{pmatrix} \cos(t) & -i \sin(t) \\ -i \sin(t) & \cos(t) \end{pmatrix}, \quad (4.34)$$

where we have used the basis  $\{|\phi_A\rangle, |\phi_B\rangle\}$ . To form a chiral-symmetric unitary evolution, we prepend and append this new evolution to the original unitary  $U_o(T)$ . Considering the action of this new evolution on the edge-state subspace, we find

$$\begin{aligned} e^{-itH'} U_o(T) e^{-itH'} &= e^{-itH'} \begin{pmatrix} -1 & 0 \\ 0 & -1 \end{pmatrix} e^{-itH'} \\ &= \begin{pmatrix} -\cos(2t) & i \sin(2t) \\ i \sin(2t) & -\cos(2t) \end{pmatrix}. \end{aligned} \quad (4.35)$$

This new unitary evolution has quasienergies  $\epsilon = \pi \pm 2t$ , and so even for an infinitesimal perturbation, the edge states are mixed and gap out. In this way, a pair of edge modes at  $\epsilon = \pi$  on different sublattices can be gapped out by a local, symmetric perturbation, and are not protected. The number of protected edge modes at a given edge is the *difference* between the number of edge modes on sublattice A and the number of edge modes on sublattice B, as defined in Eq. (4.27).

With these definitions, we can now obtain a general expression for the number of protected edge modes present at the boundary of an arbitrary chiral drive. An open-system drive (derived from a unitary loop evolution) will have a thermodynamically large number of eigenstates at  $\epsilon = 0$  corresponding to states in the bulk, and a smaller number of states with  $\epsilon \neq 0$  near each boundary. The number of edge modes is the net number of eigenstates on a single sublattice at quasienergy  $\epsilon = \pi$  on a single boundary.

We project to just the right-hand boundary with the real-space projector  $P_R$ , where the boundary region need not be exact but should include all states on the right-hand edge with  $\epsilon \neq 0$ . We also define a projector  $P_\pi$  onto the space of states with quasienergy  $\epsilon = \pi$  (we give an explicit expression for this operator below). In terms of these projectors, the number of protected dynamical edge modes at the right-hand edge is given by

$$n_\pi^R = n_\pi^{R,A} - n_\pi^{R,B} = \text{Tr} [P_A P_\pi P_R] - \text{Tr} [P_B P_\pi P_R]. \quad (4.36)$$

Recalling that the chiral symmetry operator takes the form  $C = P_A - P_B$ , this expression can be rewritten as

$$n_\pi^R[U] = \text{Tr} [C P_\pi P_R] = -\frac{1}{2} \text{Tr} [C (U_o(T) - \mathbb{I}) P_R], \quad (4.37)$$

where in the final equality we have replaced  $P_\pi = -\frac{1}{2} [U_o(T) - \mathbb{I}]$  under the trace.

This replacement can be justified as follows, by expanding  $U_o(T)$  in its basis of eigenstates,

$$U_o(T) = \sum_n e^{-i\epsilon_n T} |\phi_n\rangle\langle\phi_n|. \quad (4.38)$$

First, subtracting the identity removes all states with  $\epsilon = 0$  from the expansion of  $U_o(T)$ , meaning that these states do not contribute to the trace. The states with  $\epsilon = \pi$ , however,

have a coefficient of  $-1$  in the expansion of  $U_o(T)$ , and so end up with a coefficient of  $-2$  after subtracting the identity. States at  $\epsilon = \pi$  will therefore each contribute  $-2$  to the trace (if they are not annihilated by  $P_R$  or  $C$ ). Finally, if there are any states with  $\epsilon \neq 0$  and  $\epsilon \neq \pi$ , they must occur as chiral pairs with quasienergy  $\pm\epsilon$ . However, the chiral symmetry operator  $C$  acts as  $\sigma_x$  on these eigenvectors (mapping each state onto its chiral partner), and is therefore traceless in this subspace.

Overall, the only subspace that contributes to the trace of  $C(U_o(T) - \mathbb{I})P_R$  is the  $\pi$  eigenspace of the right-hand edge, and we divide by  $-2$  to calculate the number of states in this subspace. As long as the chosen region  $R$  is larger than the localisation length of any edge modes, the trace will be integer valued. It follows that Eq. (4.37) is a robust topological edge invariant which may be used to calculate the number of protected edge modes at the right-hand edge of any chiral-symmetric Floquet operator  $U_o(T)$ .

## 4.4 Bulk-Edge Correspondence

### 4.4.1 Bulk-Edge Correspondence at half period

In this section, we will prove that the bulk chiral flow invariant of a chiral unitary loop drive ( $\nu[U]$ ) is equal to the number of protected edge modes at the right-hand edge at the end of the evolution ( $n_\pi^R$ ). Our argument has two parts: first, we will show that a nonzero chiral flow in the bulk at  $t = T/2$  leads to chiral-symmetry-breaking flow at the boundary, also at  $t = T/2$ . Then, we will show that this symmetry-breaking boundary flow at  $t = T/2$  is responsible for nontrivial edge modes at the end of the cycle.

As in the previous section, it will be useful to distinguish between the closed-system evolution and the open-system evolution, which we write as  $U_c(t)$  and  $U_o(t)$ , respectively. These two evolutions are identical apart from in a finite (Lieb-Robinson bounded) region near the edges. In particular, since we are considering unitary loop evolutions,  $U_c(T) = \mathbb{I}$  everywhere, while  $U_o(T)$  is the identity away from the boundary regions.

We identify the three relevant spatial regions (left edge, middle, and right edge) as  $L$ ,  $M$

and  $R$ , respectively, as shown in Fig. 4.6. The bulk region  $M$  should be defined far enough away from the edges (i.e. larger than the Lieb-Robinson length away) that  $U_c(t)$  and  $U_o(t)$  act identically within this region. For concreteness, a chain of length  $N$  can be split into the regions

$$\begin{aligned}
L : & \quad x \leq N/3 \\
M : & \quad N/3 < x \leq 2N/3 \\
R : & \quad x > 2N/3,
\end{aligned} \tag{4.39}$$

rounding the fractions if necessary.

We recall that halfway through a chiral-symmetric drive, the unitary operator  $U_c(T/2)$  takes a block diagonal form (see Eq. (4.20)), indicating that the two sublattices become decoupled. This motivated the notion of chiral flow, which we defined in Eq. (4.24). In the open system, however,  $U_o(T/2)$  will not in general take this block-diagonal form. Instead, at the edges of the system there may be coupling between the two sublattices, as we found for the model drive and as illustrated schematically in Fig. 4.6. However, within the bulk region  $M$ , both closed- and open-system drives are identical. In this way, we can calculate the chiral flow invariant  $\nu[U]$  in the bulk even for the open system.

We now use the properties of chiral flow to relate the bulk behaviour to the boundary behaviour of the open system at  $t = T/2$ . As noted in Sec. 4.1.1, chiral flow builds on the notion of unitary flow from Ref. [31], and inherits many of its properties. Importantly, the unitary flow invariant is independent of location, and may be calculated across any imaginary cut in the 1D system. In turn, this implies that unitary flow is constant and conserved throughout the system.

In the bulk at  $t = T/2$ , chiral flow is similarly constant and conserved. However, at the edge region  $R$ , unitary flow corresponding to one sublattice flows from region  $M$  to region  $R$ , while flow corresponding to the other sublattice flows from  $R$  to  $L$ . Since unitary flow is conserved, there must be flow between sublattices at some point within the edge region. This is the coupling between sublattices that is shown schematically in Fig. 4.6. We show below that this inter-sublattice flow at the edges is *exactly* equal to the chiral flow in the bulk.

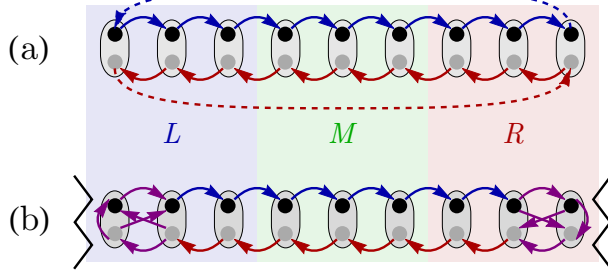


Figure 4.6: Action of the general chiral unitaries  $U_c(T/2)$  and  $U_o(T/2)$  within the left edge ( $L$ ), middle ( $M$ ) and right edge ( $R$ ) regions of a 1D chain. Sublattices are shown as black and gray points. (a) The unitary action of the closed system  $U_c(T/2)$  acts on each sublattice independently. (b) In the open system, the unitary  $U_o(T/2)$  acts on each sublattice independently in the bulk but couples the two sublattices in the edge regions. (Figure adapted from Reference [37] with permission from the *American Physical Society*.)

We write the open-system half-period unitary  $U_o(T/2)$  using the shorthand  $U$  and consider the trivial trace

$$0 = \text{Tr} [U^{-1}P_{R,A}U - P_{R,A}], \quad (4.40)$$

where  $P_{R,A} = P_R P_A$  is a projector onto sublattice  $A$  in region  $R$ . This trace vanishes because, for an open system, we can use the cyclic property of the trace to bring  $U$  next to  $U^{-1}$  and replace  $UU^{-1} = \mathbb{I}$ . Defining the complementary projector  $\bar{P}_{R,A} = \mathbb{I} - P_{R,A}$ , we can rewrite the above trace as

$$0 = \text{Tr} [U^{-1}P_{R,A}U\bar{P}_{R,A} - U^{-1}\bar{P}_{R,A}UP_{R,A}]. \quad (4.41)$$

The complementary projector can be expanded as a sum over all other sublattices and regions,

$$\bar{P}_{R,A} = P_{L,A} + P_{L,B} + P_{M,A} + P_{M,B} + P_{R,B}. \quad (4.42)$$

However, assuming the unitary has some finite strict localisation length, there can be no overlap between  $U^{-1}P_R U$  and  $P_L$ , and so we can ignore  $P_L$  in the complementary projector. In addition, in the bulk the unitary preserves chiral symmetry, and so  $U^{-1}P_{R,A}U$  can have

overlap with  $P_{M,A}$  but not with  $P_{M,B}$ . Expanding the remaining projectors, we find

$$\begin{aligned}
0 &= \text{Tr} \left[ U^{-1} P_{R,A} U P_{M,A} - U^{-1} P_{M,A} U P_{R,A} \right] \\
&\quad + \text{Tr} \left[ U^{-1} P_{R,A} U P_{R,B} - U^{-1} P_{R,B} U P_{R,A} \right] \\
&\equiv \nu_1[U] - \nu_2[U],
\end{aligned} \tag{4.43}$$

where we have defined  $\nu_{1/2}[U]$  as the first/second traces in the equation above. Referring back to Sec. 4.2.4, we identify  $\nu_1[U]$  as the chiral flow invariant  $\nu[U]$ , measured across the boundary between regions  $M$  and  $R$ . Explicitly, we use the relation  $P_A = (\mathbb{I} + C)/2$  and the fact that  $C$  commutes with the bulk unitary to rewrite the first trace as

$$\begin{aligned}
\nu_1[U] &= \text{Tr} \left[ U^{-1} P_R P_A U P_M P_A - U^{-1} P_M P_A U P_R P_A \right] \\
&= \frac{1}{2} \text{Tr} \left[ (\mathbb{I} + C) U^{-1} P_R U P_M - (\mathbb{I} + C) U^{-1} P_M U P_R \right] \\
&= \frac{1}{2} \text{Tr} \left[ C U^{-1} P_R U P_M - C U^{-1} P_M U P_R \right],
\end{aligned} \tag{4.44}$$

which recovers  $\nu[U]$  from Eq. (4.24). Note that the terms involving  $\mathbb{I}$  in the expression above do not contribute because they describe a (non-chiral) unitary flow, which must vanish in a 1D Floquet system.

We now identify the second trace  $\nu_2[U]$ , equal to  $\nu_1[U]$ , as an edge invariant which captures the flow between sublattices within the region  $R$ ,

$$\nu_{edge}^R[U] = \text{Tr} \left[ U^{-1} P_{R,B} U P_{R,A} - U^{-1} P_{R,A} U P_{R,B} \right]. \tag{4.45}$$

This can be written equivalently as

$$\nu_{edge}^R[U] = \text{Tr} \left[ U^{-1} P_B U P_A P_R - U^{-1} P_A U P_B P_R \right], \tag{4.46}$$

where we have dropped two projectors onto  $R$ , which are unnecessary because any flow into region  $M$  must conserve sublattice. We can define a similar edge invariant at the left edge, which is equal in magnitude but opposite in direction to  $\nu_{edge}^R[U]$ .

Since  $\nu_1[U]$  and  $\nu_2[U]$  are equal, we see that the bulk chiral flow invariant (Eq. (4.24)) is equal to the half-period edge invariant (Eq. (4.46)), i.e. that

$$\nu[U_c(T/2)] = \nu[U_o(T/2)] = \nu_{edge}^R[U_o(T/2)]. \tag{4.47}$$

This is the first step in our derivation of bulk-edge correspondence.

#### 4.4.2 Bulk-Edge Correspondence after a complete cycle

To complete the derivation, we now show that the half-period edge invariant is equal to the number of protected edge modes present at the right-hand edge at the end of the evolution,  $n_\pi^R$ .

To do this, we rewrite our expression for  $\nu_{edge}^R[U]$  in terms of  $C$  by substituting Eq. (4.30) into Eq. (4.46). Writing out  $U = U_o(T/2)$  in full, this gives

$$\nu_{edge}^R[U] = \frac{1}{2} \left[ \text{Tr} [CP_R] - \text{Tr} \left[ U_o^{-1}(T/2) C U_o(T/2) P_R \right] \right]. \quad (4.48)$$

However, Eq. (4.18) gives a relation between a generic half-period unitary and the corresponding full-period unitary, which we can use to rewrite the expression above as

$$\begin{aligned} \nu_{edge}^R[U] &= \frac{1}{2} \left[ \text{Tr} [CP_R] - \text{Tr} \left[ U_o^{-1}(T) C P_R \right] \right] \\ &= -\frac{1}{2} \text{Tr} \left[ C \left( U_o^{-1}(T) - \mathbb{I} \right) P_R \right], \end{aligned} \quad (4.49)$$

where in the second line we have used that  $C$  commutes with  $P_R$  and grouped together the expressions under the trace. Finally, we identify the expression above as  $n_\pi^R$  from Eq. (4.37), noting that either  $U_o(T)$  or  $U_o^{-1}(T)$  may be used to count edge modes at  $\epsilon = \pi$ .

Overall, we have shown that chiral flow in the bulk at  $t = T/2$  leads to chiral symmetry-breaking flow at the boundary, which in turn generates edge modes at  $\epsilon = \pi$  at the end of the evolution. This bulk-boundary correspondence is summarised by the three equal invariants

$$\nu[U_{c/o}(T/2)] = \nu_{edge}^R[U_o(T/2)] = n_\pi^R[U_o(T)]. \quad (4.50)$$

## 4.5 Conclusion

In this work, we have introduced chiral flow (Eq. (4.24)) as a physically motivated, locally computable bulk invariant, which describes the topological properties of unitary evolutions with chiral symmetry. While the invariant itself is defined only for unitary loop evolutions,

we argued in Sec. 4.1 and in Appendix 4.B that *any* chiral evolution (with a gap at  $\epsilon = \pi$ ) is related to a characteristic unitary loop. In this way, chiral flow provides a topological characterisation of any (gapped and non-interacting) driven system belonging to class AIII. This invariant is an improvement on previous invariants, discussed in Sec. 5.3, in that it applies to systems with disorder and is locally computable. In addition, it has the intuitive physical interpretation of describing the unitary flow [31] on each sublattice at the half-period point.

We went on to derive an explicit bulk-boundary correspondence which relates the chiral flow to the number of protected dynamical edge modes present at the end of the evolution. To do this, we first introduced an edge invariant (Eq. (4.46)) which quantifies the chiral-symmetry-breaking flow that arises at a boundary at the midpoint of the evolution. This was found to be exactly equal to the chiral flow invariant in the bulk. It is interesting to note that the behaviour of a chiral drive at  $t = T/2$  offers much more information about its topological properties than its behaviour at  $t = T$ .

Finally, we equated this half-period edge invariant to the full-period edge invariant (Eq. (4.37)), which directly counts the number of protected edge modes at  $\epsilon = \pi$  at the end of the evolution. In this way, our work provides the first explicit bulk-edge correspondence for one-dimensional Floquet systems with chiral symmetry. In passing, we note that the full-period edge invariant we introduced may be used to count the number of modes at  $\epsilon = \pi$  in general, and is applicable beyond unitary loop evolutions.

Our work raises a number of interesting open questions. First, Floquet system in class AIII have been shown to host nontrivial topological phases in all odd (spatial) dimensions, but have thus far only been studied in cases with translational symmetry or in one dimension. In future work, we will extend the notion of chiral flow, and the associated bulk-boundary correspondence, to the higher dimensional case. In the process, we hope to provide insight into the boundary behaviour of Floquet topological phases in even dimensions. Our work also extends Kitaev's notion of unitary flow [31] to systems with chiral symmetry. It would be interesting to study whether this quantity can be similarly extended to the other symmetry

classes in the 10-fold way. Finally, an information-theoretic extension of the notion of flow was applied to many-body unitary evolutions in Ref. [30], in the context of quantum cellular automata. The resulting topological invariant underpins the classification of interacting Floquet topological phases in two and three dimensions introduced in Refs. [26, 27, 60]. An extension of this many-body invariant to systems with chiral symmetry, and indeed in other symmetry classes and dimensions, remains an interesting avenue for future research.

## APPENDIX

### 4.A Extension to Exponentially Decaying Unitaries

In the main text, the unitary operators we considered were assumed to be strictly local with some localization length  $\ell$ , i.e., we assumed that  $U_{jk} = 0$  for  $|j - k| > \ell$  (where  $j$  and  $k$  label unit cell positions). In this appendix, we extend our results to the more general definition of locality in which matrix element magnitudes decay exponentially with distance. Specifically, we will assume that for large enough  $|j - k|$ , the unitary operator satisfies

$$|U_{jk}| \leq C e^{-|j-k|/\ell}, \quad (4.51)$$

for some positive constant  $C$  and localization length  $\ell$ . If we evolve a local Hamiltonian in time, the unitary time-evolution operator will generically take this form [7].

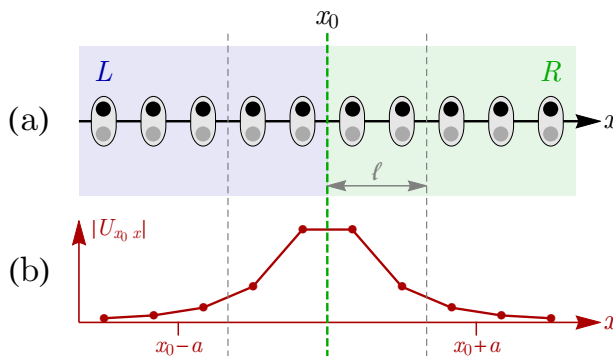


Figure 4.7: Calculation of the chiral flow invariant for a local unitary satisfying Eq. (4.51). (a) We split the region near a cut at  $x = x_0$  into left ( $L$ ) and right ( $R$ ) pieces. (b) Matrix elements which connect sites across the cut are bounded by an exponentially decaying envelope function. By truncating projectors to sites within a distance  $a$  from the cut, we neglect contributions which are of size  $O(e^{-a/\ell})$ . By taking  $a$  much larger than  $\ell$  these errors can be made exponentially small.

### 4.A.1 Bulk Invariants

We now study how this looser definition of locality affects the definition and calculation of invariants introduced in the main text. We recall that the bulk chiral flow invariant (Eq. (4.24)) may be written for a formally infinite system as

$$\nu[U] = \frac{1}{2} \left[ \text{Tr} \left( CU^{-1} P_R U P_L \right) - \text{Tr} \left( CU^{-1} P_L U P_R \right) \right], \quad (4.52)$$

where  $U = U(T/2)$  and  $P_L$  and  $P_R$  are projectors onto the semi-infinite regions  $x \leq x_0$  and  $x > x_0$ , respectively. For the infinite system, this equation continues to give a well-defined quantised chiral flow index, even for exponentially localised unitaries satisfying Eq. (4.51) [31]. For practical purposes, however, infinite system sizes cannot be achieved, and we must necessarily consider a finite system with projectors truncated to a finite region around the cut at  $x_0$ .

In the main text, the unitary operators we considered were strictly local, and we could truncate to the region  $[x_0 - \ell, x_0 + \ell]$  without changing the value of  $\nu[U]$ . In addition,  $\nu[U]$  could be calculated using either the closed-system unitary  $U_c(T/2)$  or the open-system unitary  $U_o(T/2)$ , since these had identical action within the truncated region (as long as the edges were far enough away from  $x_0$ ). In the current case, the open and closed system unitaries will have actions which differ at  $x_0$ , even if only by an exponentially small amount. In addition, truncation to a region around a cut at  $x_0$  will introduce other (exponentially small) errors, and so too will having a finite system size. All of these sources of error will need to be taken into account and quantified.

First, we consider a closed system with  $N$  sites in total (which we write as  $c[N]$ ) and attempt to calculate the bulk invariant using a truncation to the region  $[x_0 - a, x_0 + a]$ , with  $a \leq N/2$ .<sup>2</sup> Explicitly, we set  $x_0 = 0$  and define

$$\nu_{c[N],a}[U] = \frac{1}{2} \left[ \text{Tr} \left( CU^{-1} P_R^a U P_L^a \right) - \text{Tr} \left( CU^{-1} P_L^a U P_R^a \right) \right], \quad (4.53)$$

---

<sup>2</sup>For a finite system, we require  $a \leq N/2$  so that only the flow across the cut is measured, and not contributions which pass around the ‘back’ of the system.

where  $P_L^a$  projects onto the range  $[-a, 0)$ ,  $P_R^a$  projects onto the range  $[0, a)$ , and  $U$  is shorthand for the closed-system unitary  $U_{c[N]}(T/2)$ . It is clear that

$$\lim_{a \rightarrow \infty} \lim_{N \rightarrow \infty} \nu_{c[N],a}[U] = \nu[U], \quad (4.54)$$

as this recovers Eq. (4.52) which gives the exact, quantised invariant.

For large but finite values of  $a$  and  $N$ , this expression will neglect contributions from the unitary operator with magnitudes less than or equal to  $O(e^{-a/\ell})$  and  $O(e^{-N/(2\ell)})$ , respectively. Since  $a \leq N/2$ , the errors due to finite system size will be smaller than those due to truncation, and so we can safely ignore them. The total error in the calculated value of  $\nu_{c[N],a}[U]$  is bounded by the sum of all neglected terms, and so overall we expect

$$\nu_{c[N],a}[U] = \nu[U] + O(e^{-a/\ell}). \quad (4.55)$$

In this way, by taking the truncation length  $a \gg \ell$  (and increasing the system size correspondingly), it is possible to calculate the chiral flow invariant to arbitrary accuracy. This idea is shown schematically in Fig. 4.7.

We now consider a finite open system  $o[N]$ , which has  $N$  sites labelled from  $-N/2$  to  $N/2 - 1$ . We again try to calculate the bulk invariant using a truncation to the region  $[-a, a]$ , and this time define

$$\nu_{o[N],a}[U] = \frac{1}{2} \left[ \text{Tr} \left( C U^{-1} P_R^a U P_L^a \right) - \text{Tr} \left( C U^{-1} P_L^a U P_R^a \right) \right], \quad (4.56)$$

where definitions are as before except  $U$  is now shorthand for the open-system unitary  $U_{o[N]}(T/2)$ . As for the closed system, we can take the limit  $N \rightarrow \infty$  followed by the limit  $a \rightarrow \infty$  to find

$$\lim_{a \rightarrow \infty} \lim_{N \rightarrow \infty} \nu_{o[N],a}[U] = \nu[U], \quad (4.57)$$

which again recovers Eq. (4.52) (since boundary conditions are negligible in the infinite system limit). At finite system sizes, there are errors due to the truncation and errors due the finite size. The scaling follows as before, and we find

$$\nu_{o[N],a}[U] = \nu[U] + O(e^{-a/\ell}). \quad (4.58)$$

In this way, although calculations of the chiral flow invariant in the closed system and in the open system may be different, both values tend towards the same quantised value in the limit of infinite system size and infinite truncation region. At finite sizes the calculated values differ from the true value by errors of size  $O(e^{-a/\ell})$ , and correspondingly may differ from each other by a similar amount.

#### 4.A.2 Edge Invariants

We now consider the effects of the new definition of locality on the edge invariants defined in the main text. To aid the discussion, we formally consider a semi-infinite system extending from negative infinity to  $x = a$ , as shown in Figure. 4.8. Recalling Eq. (4.46), we write the edge invariant for the semi-infinite system as

$$\nu_{\text{edge},a}^R[U] = \text{Tr} \left[ U^{-1} P_B U P_A P_R^a - U^{-1} P_A U P_B P_R^a \right]. \quad (4.59)$$

where  $U = U_o(T/2)$  is the open-system unitary and  $P_R^a$  is a projector onto the right-hand edge region of the system, the interval  $[0, a]$ . For a strictly local unitary (as considered in the main text), the expression above gives an exact, quantised value, as long as  $a > \ell$ . For exponentially decaying unitary operators satisfying Eq. (4.51), however, the definition of  $R$  amounts to a truncation. In this case, the ‘edge region’ should formally include exponentially small contributions (set by the length scale  $\ell$ ) even on sites outside of the range  $[0, a]$ . The truncation in Eq. (4.59) neglects these contributions of size  $O(e^{-a/\ell})$ , leading to a total error (bounded by a sum of these pieces), which is also of size  $O(e^{-a/\ell})$ . In the thermodynamic limit we take  $a \rightarrow \infty$  and find

$$\lim_{a \rightarrow \infty} \left[ \nu_{\text{edge},a}^R[U] \right] = \nu_{\text{edge}}^R[U]. \quad (4.60)$$

We will verify that this is indeed the true, quantised edge invariant below.

We first use a similar method as in the main text to show that the bulk and edge invariants are equal in the thermodynamic limit. Starting from the trivial trace

$$0 = \text{Tr} \left[ U^{-1} P_{R,A}^a U - P_{R,A}^a \right], \quad (4.61)$$

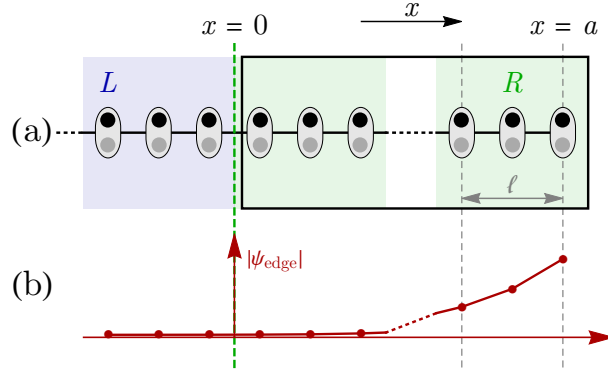


Figure 4.8: Semi-infinite system used in the construction of truncated edge invariants. (a) Boxed region indicates the region where  $P_R^a$  is nonzero, extending from  $x = 0$  to  $x = a$ . To reduce truncation errors, this should be much larger than the Lieb-Robinson length of the unitary  $\ell$ . (b) Edge modes decay exponentially away from  $x = 0$ . Truncating to the boxed region means contributions of size  $O(e^{-a/\ell})$  are neglected.

we insert the complementary projector  $\overline{P_{R,A}^a} = P_{R,B}^a + P_{L,A} + P_{L,B}$ , where  $P_L$  projects onto the region  $x \leq 0$ , and find

$$\begin{aligned}
0 &= \text{Tr} \left[ U^{-1} P_{R,A}^a U \overline{P_{R,A}^a} - P_{R,A}^a \overline{P_{R,A}^a} \right] \\
&= \tilde{\nu}_a^R[U] - \nu_{\text{edge},a}^R[U],
\end{aligned} \tag{4.62}$$

where

$$\begin{aligned}
\nu_{\text{edge},a}^R[U] &= \text{Tr} \left[ U^{-1} \left( P_{R,B}^a + P_{L,B} \right) U P_{R,A}^a \right. \\
&\quad \left. - U^{-1} P_{R,A}^a U \left( P_{R,B}^a + P_{L,B} \right) \right]
\end{aligned} \tag{4.63}$$

recovers Eq. (4.59) and

$$\tilde{\nu}_a^R[U] = \text{Tr} \left[ U^{-1} P_{R,A}^a U P_{L,A} - U^{-1} P_{L,A} U P_{R,A}^a \right] \tag{4.64}$$

is equivalent to Eq. (4.53) up to corrections of size  $O(e^{-a/\ell})$  (due to the fact that the system is now semi-infinite). In this way, in the thermodynamic limit we find

$$\lim_{a \rightarrow \infty} \left[ \nu_{\text{edge},a}^R[U] \right] = \lim_{a \rightarrow \infty} \left[ \tilde{\nu}_a^R[U] \right] = \nu[U], \tag{4.65}$$

which recovers the quantised bulk invariant. In this way, we have defined truncated edge and bulk invariants at  $t = T/2$  which are equal to each other and to their values in the thermodynamic limit up to exponentially small corrections. By taking the truncation region  $a \gg \ell$ , the corrections can be made exponentially small. This is illustrated schematically in Fig. 4.8.

Finally, we define the invariant which counts the number of edge modes at  $t = T$  in a similar way to Eq. (4.37). In the semi-infinite system, however, there is only one edge, and we can formally define the exact (quantised) number of edge modes as

$$n_{\pi}^R[U] = -\frac{1}{2} \text{Tr} [C (U_o(T) - \mathbb{I})], \quad (4.66)$$

where  $U_o(T)$  is obtained by removing terms from the generating Hamiltonian that connect sites across the boundary at  $x = a$ . In contrast to Eq. (4.37), there is no projector  $P_R$ , which previously served to remove any contributions from the left edge. This expression formally gives the exact number of edge modes, even for exponentially decaying unitaries satisfying Eq. (4.51).

For any finite system, however, we must introduce a truncation, and so we define

$$n_{\pi,a}^R[U] = -\frac{1}{2} \text{Tr} [C (U_o(T) - \mathbb{I}) P_R^a], \quad (4.67)$$

where  $P_R^a$  again projects onto the region between  $x = 0$  and  $x = a$ . This expression differs from the exact value by an error with size  $O(e^{-a/\ell})$ , as it neglects the exponential tails of the edge modes that permeate beyond  $x = 0$ . However, these corrections are again of size  $O(e^{-a/\ell})$ , and can be made arbitrarily small by taking  $a$  much larger than  $\ell$ . In this way,

$$\lim_{a \rightarrow \infty} [n_{\pi,a}^R[U]] = n_{\pi}^R[U]. \quad (4.68)$$

As in the main text, we can use Eq. (4.18) to show that expressions for  $n_{\pi,a}^R[U]$  and  $\nu_{\text{edge},a}^R[U]$  are equivalent. This argument is very similar to that given in Sec. 4.4.2, and so we do not reproduce it here.

Overall, we find that bulk and edge invariants can be defined even for unitary operators satisfying the looser definition of locality given in Eq. 4.51. While these invariants take

quantised values only in the limit of infinite system size, any realistic measurement necessarily requires truncation, which will introduce exponentially small corrections. However, by taking the truncation region to be much larger than the Lieb-Robinson length of the unitary operator, these errors can be made arbitrarily small.

## 4.B Obtaining a Unitary Loop from a General Unitary Evolution

In the main text, we mostly worked with unitary loop evolutions, which satisfy  $U_c(T) = \mathbb{I}$ . Most unitary evolutions, however, will not satisfy this property. In these cases, as motivated in Sec. 4.1, we may construct a unitary loop from the evolution which captures its inherently dynamical component. In this appendix, we outline this construction in more detail.

We consider an arbitrary closed-system evolution with chiral symmetry which, at  $t = T = 1$ , has a gap in the quasienergy spectrum at  $\epsilon = \pi$ . [In order for there to be protected dynamical edge modes, we require a gap at  $\epsilon = \pi$  in the closed system, and so we only consider this case here]. We can then define a Floquet Hamiltonian corresponding to this gap as

$$H_F = \frac{i}{T} \log_\pi U_c(T), \quad (4.69)$$

where  $\log_\pi$  is the complex logarithm defined as

$$\log_\pi(e^{i\psi}) = i\psi \quad (4.70)$$

for

$$-\pi < \psi < \pi. \quad (4.71)$$

Explicitly, if we express the full unitary evolution  $U_c(T)$  in its eigenbasis,

$$U_c(T) = \sum_j \lambda_j |\Psi_j\rangle\langle\Psi_j|, \quad (4.72)$$

then the Floquet Hamiltonian may be written

$$H_F = \frac{i}{T} \sum_j \log_\pi(\lambda_j) |\Psi_j\rangle\langle\Psi_j|. \quad (4.73)$$

As shown in Ref. [7], a Floquet Hamiltonian defined in this way is local (in that the magnitudes of its matrix elements decay exponentially with distance). In addition, since the underlying evolution is chiral symmetric, the Floquet Hamiltonian satisfies

$$CH_FC^{-1} = -H_F. \quad (4.74)$$

We can deform the full unitary evolution  $U_c(t)$  into a unitary loop followed by an evolution with  $H_F$ . First, we define a (chiral-symmetric) unitary loop through the generating Hamiltonian

$$H_L(t) = \begin{cases} -2H_F & 0 \leq t < \frac{1}{4}T \\ 2H(2(t - \frac{1}{4}T)) & \frac{1}{4}T \leq t < \frac{3}{4}T \\ -2H_F & \frac{3}{4}T \leq t < T, \end{cases} \quad (4.75)$$

where  $H(t)$  is the original generating Hamiltonian for  $U_c(t)$ . It may be verified that the evolution

$$V_c(t) = \mathcal{T} \exp \left[ -i \int_0^t H_L(t') dt' \right] \quad (4.76)$$

satisfies  $V_c(T) = \mathbb{I}$ . To recover  $U_c(T)$ , we can evolve with  $H_F$  for time  $T/2$  before and after the evolution with  $H_L(t)$  and note that

$$e^{-iH_FT/2} V_c(T) e^{-iH_FT/2} = e^{-iH_FT} \equiv U_c(T). \quad (4.77)$$

This complete evolution has chiral symmetry and is homotopically connected to the original evolution  $U_c(t)$  [1]. Dynamical edge modes can only arise during the evolution with  $H_L(t)$ , as it is only in this part of the evolution that the gap at  $\epsilon = \pi$  can close. In this way, the dynamical properties of  $U_c(t)$  are equivalent to the dynamical properties of the loop evolution  $V_c(t)$ .

The loop evolution  $V_c(t)$  can be used directly in the calculation of the bulk chiral flow invariant in Eq. (4.24). For the edge invariants, we require the corresponding open system evolution,  $V_o(t)$ . This can be obtained by truncating the loop generating Hamiltonian  $H_L(t)$  in Eq. (4.75) by removing terms which connect sites across the boundary. Evolution with

this open-system Hamiltonian then yields  $V_o(t)$ . This can be used in the calculation of the half-period edge invariant in Eq. (4.46) and in the calculation of the number of edge modes at  $t = T$  in Eq. (4.37).

## CHAPTER 5

### Bulk edge correspondence in high dimensional class

#### AIII

##### 5.1 A three-dimensional Model Drive with Chiral Symmetry

We now build a model drive with chiral symmetry. Inspired by the three dimensional tight-binding model for chiral topological insulators[61], we take a 3D bipartite chain of  $N_x \times N_y \times N_z$  unit cells, with spin 1/2 on a crystal with two sublattices(or orbitals) labelled ‘A’ and ‘B’. For our model drive, we take a piecewise constant Hamiltonian of the form

$$H(t) = \begin{cases} H_1 & 0 \leq t < \frac{1}{4}T \\ H_2 & \frac{1}{4}T \leq t < \frac{1}{2}T \\ H_2 & \frac{1}{2}T \leq t < \frac{3}{4}T \\ H_1 & \frac{3}{4}T \leq t < T, \end{cases} \quad (5.1)$$

where  $H_1$  is a swap operator only including the hopping of particles between sublattice A and B within the same cell

$$H_1 = \begin{pmatrix} 0 & 0 & \mathbb{I} & 0 \\ 0 & 0 & 0 & \mathbb{I} \\ \mathbb{I} & 0 & 0 & 0 \\ 0 & \mathbb{I} & 0 & 0 \end{pmatrix} \quad (5.2)$$

$$H_2(k_x, k_y) = -\frac{2\pi}{T} \frac{1}{E(k)} \begin{pmatrix} 0 & 0 & -iq_0 + q_3 & q_1 - iq_2 \\ 0 & 0 & q_1 + iq_2 & -iq_0 - q_3 \\ iq_0 + q_3 & q_1 + iq_2 & 0 & 0 \\ q_1 - iq_2 & iq_0 - q_3 & 0 & 0 \end{pmatrix} \quad (5.3)$$

in basis  $(A \uparrow, A \downarrow, B \uparrow, B \downarrow)$  and where  $q_0 = h + \cos k_x + \cos k_y + \cos k_z$ ,  $q_1 = t \sin k_x$ ,  $q_2 = \sin k_y$ ,  $q_3 = \sin k_z$  with  $h, t$  being control parameters.

This model, similar to the one-dimensional model we discussed in last section, can generate Dirac cones on the edge by tuning the parameters  $h$  and  $t$ . At half-period, this evolution operator becomes,

$$U(k_x, k_y, \frac{T}{2}) = i \frac{1}{E(k)} \begin{pmatrix} -iq_0 + q_3 & q_1 - iq_2 & 0 & 0 \\ q_1 + iq_2 & -iq_0 - q_3 & 0 & 0 \\ 0 & 0 & iq_0 + q_3 & q_1 + iq_2 \\ 0 & 0 & q_1 - iq_2 & iq_0 - q_3 \end{pmatrix} \quad (5.4)$$

where each block can generate the three dimensional quantum flow as defined in Section 2.3.5. In the following sections, we will study the connection between this flow and the edge behavior.

## 5.2 Edge invariants

We use  $U_c(t)$  and  $U_o(t)$  to distinguish between the closed-system evolution and the open-system evolution respectively. These two evolutions are identical apart from in a finite (Lieb-Robinson bounded) region near the edges. In particular, since we are considering unitary loop evolutions,  $U_c(T) = \mathbb{I}$  everywhere, while  $U_o(T)$  is the identity away from the boundary regions.

To describe the edge behavior, we only need to consider the boundary of the open system, which could be a  $2n$  dimensional surface of a  $2n + 1$  cubic(or other shape) with a thickness at least larger than double the Lieb-Robinson length.

We identify the two relevant spatial regions (edge and center) as  $E$ ,  $M$ , respectively.

The bulk region  $M$  should be defined far enough away from the edges (i.e. larger than the Lieb-Robinson length away) that  $U_c(t)$  and  $U_o(t)$  act identically within this region. In general, this system can be split into the regions

$$\begin{aligned} E : & \quad |r| \geq R \\ M : & \quad |r| \leq R \end{aligned} \tag{5.5}$$

Then  $M$  is a  $2n+1$  dimensional ball. we now introduce a projector  $P_E$  acting on the edge. Then the edge unitary can be the truncation of the unitary  $U_o(T)$ :

$$U_E(T) = P_E U_o(T) P_E \tag{5.6}$$

To simplify our discussion, we consider a semi-infinity open-system extending from  $x_{2n+1} = 0$  to positive infinity. Then there is only one edge located at  $x_{2n+1} = 0$ . We can directly use  $U_o(T)$  as edge unitary.

To classify an edge unitary, we can map this unitary to a flattened Hamiltonian without the chiral symmetry through Chapter 2

$$H_U = S U_o(T) \tag{5.7}$$

and then use the classification of  $H_U$  (in  $2n$ -dimensional Class A)[4]

$$\begin{aligned} \nu_E = & -\frac{(2\pi i)^n}{n!} \sum_{\sigma} \\ & (-1)^{\text{sign}(\sigma)} \text{Tr} \left( P_F [P_{\mathbf{a}}^{(\sigma_1)}, P_F] [P_{\mathbf{a}}^{(\sigma_2)}, P_F] \cdots [P_{\mathbf{a}}^{(\sigma_{2n})}, P_F] \right) \end{aligned} \tag{5.8}$$

where  $\sigma$  is a permutation given by

$$\sigma = \begin{pmatrix} 1, 2, \dots, 2n \\ \sigma_1, \sigma_2, \dots, \sigma_{2n} \end{pmatrix} \tag{5.9}$$

with the parity  $\text{sign}(\sigma)$ . We define  $P_F$  as the projector onto the lower bands, satisfying  $P_F = \frac{1-H_U}{2}$ . In addition, we define right half axis projectors acting on all  $d$  directions,

$$P_{\mathbf{a}}^i |\mathbf{r}, \alpha\rangle = \begin{cases} |\mathbf{r}, \alpha\rangle & \text{if } r_i \geq a_i \\ 0 & \text{if } r_i < a_i \end{cases}, \tag{5.10}$$

After plugging Eq. (5.7) and  $P_F = \frac{1-H_U}{2}$ , we can rewrite the edge invariant as the function of the edge unitary

$$\begin{aligned} \nu_E &= -\frac{(\pi i)^n}{2^{n+1}n!} \sum_{\sigma} \\ &(-1)^{\text{sign}(\sigma)} \text{Tr}(1 - \mathcal{S}U_o(T)) [P_{\mathbf{a}}^{(\sigma_1)}, \mathcal{S}U_o(T)] [P_{\mathbf{a}}^{(\sigma_2)}, \mathcal{S}U_o(T)] \cdots [P_{\mathbf{a}}^{(\sigma_{2n})}, \mathcal{S}U_o(T)] \end{aligned} \quad (5.11)$$

This can be further simplified as as

$$\begin{aligned} \nu_E &= \frac{(\pi i)^n}{2^{n+1}n!} \sum_{\sigma} \\ &(-1)^{\text{sign}(\sigma)} \text{Tr} \mathcal{S}U_o(T) [P_{\mathbf{a}}^{(\sigma_1)}, \mathcal{S}U_o(T)] [P_{\mathbf{a}}^{(\sigma_2)}, \mathcal{S}U_o(T)] \cdots [P_{\mathbf{a}}^{(\sigma_{2n})}, \mathcal{S}U_o(T)] \end{aligned} \quad (5.12)$$

This invariant is independent of the reference point  $\mathbf{a}$  because the topological invariants of  $H_U$  doesn't depend on the choice of  $\mathbf{a}$ .

### 5.3 Bulk invariants

Same as one-dimensional system, the classification of a higher-dimensional system with chiral symmetry is determined by the unitary evolution at half period  $U_c(\frac{T}{2})$ . Every  $U_c(\frac{T}{2})$  is block-diagonal in the chiral basis as shown in Eq. (4.20), we can associate each block unitary with a flow index which is given in Eq. (2.21). The flow index for the block unitary on sublattice A is

$$\begin{aligned} \nu^{2n+1}[U_+] &= \frac{(\pi i)^n}{(2n+1)!!} \sum_{\sigma} \\ &(-1)^{\text{sign}(\sigma)} \text{Tr} \left( U_+^{\dagger}[P_{\mathbf{a}}^{(\sigma_1)}, U_+] U_+^{\dagger}[P_{\mathbf{a}}^{(\sigma_2)}, U_+] \cdots U_+^{\dagger}[P_{\mathbf{a}}^{(\sigma_{2n+1})}, U_+] \right) \end{aligned} \quad (5.13)$$

Where  $P_{\mathbf{a}}^{(\sigma_1)}$  and  $\sigma$  are defined in last section. Substituting  $U_+$  as  $P_A U_c(T/2) P_A$ , we can therefore write down the real space invariant as

$$\begin{aligned} \nu^{2n+1}[U_+] &= \frac{(\pi i)^n}{(2n+1)!!} \sum_{\sigma} \\ &(-1)^{\text{sign}(\sigma)} \text{Tr} \left( P_A \tilde{U}^{\dagger}[P_{\mathbf{a}}^{(\sigma_1)}, \tilde{U}] \tilde{U}^{\dagger}[P_{\mathbf{a}}^{(\sigma_2)}, \tilde{U}] \cdots \tilde{U}^{\dagger}[P_{\mathbf{a}}^{(\sigma_{2n+1})}, \tilde{U}] \right) \end{aligned} \quad (5.14)$$

where we have used the shorthand  $\tilde{U} = U_c(T/2)$ . This real-space expression for the flow is applicable to unitary evolutions with disorder. As we proved in Chapter 2, the flow index

associated with a locally generated unitary  $U$  is zero. In addition,  $U_c(T/2)$  is locally generated which can be written as a finite-time evolution with a local Hamiltonian

$$U_c(T/2) = \mathcal{T} \exp \left[ -i \int_0^{T/2} H_c(t) dt \right] \quad (5.15)$$

Thus the total flow which can be written as  $\nu^{2n+1}[U_+] + \nu^{2n+1}[U_-]$  in the  $2n+1$  dimensional system is zero. This can also be understood in this way: The winding number is a homotopy invariant and  $U(t)$  is smooth, and so  $w[U(t)]$  must be independent of time [14]. Then, since  $w[U(0)] = w[\mathbb{I}] = 0$  at the beginning of the evolution, it follows that  $w[U(T/2)] = 0$  too. Therefore, there are opposite flow on sublattice A and B. That's why we call it 'chiral flow'.

## 5.4 Bulk-Edge Correspondence

In this section, we will prove the bulk edge correspondence similar as what we did in one-dimensional system. We will prove that the bulk chiral flow invariant of a chiral unitary loop drive ( $\nu^{2n+1}[U]$ ) is equal to the number of protected edge modes denoted by  $\nu_E$ .

### 5.4.1 truncated edge invariants

In order to connect the bulk and edge, we introduce a truncated edge invariant. We take a cut-off in direction  $x_{2n+1}$  by using  $Q_{0,r}$ , a projector onto the interval  $[0, r]$  at the left-hand edge region of the system. Then we can express the truncated edge invariant as,

$$\nu_E^r = \frac{(\pi i)^n}{2^{n+1} n!} \sum_{\sigma} \quad (5.16)$$

$$(-1)^{\text{sign}(\sigma)} \text{Tr} \left[ \mathcal{S}U_o(T) \left[ P_{\mathbf{a}}^{(\sigma_1)}, \mathcal{S}U_o(T) \right] \left[ P_{\mathbf{a}}^{(\sigma_2)}, \mathcal{S}U_o(T) \right] \cdots \left[ P_{\mathbf{a}}^{(\sigma_{2n})}, \mathcal{S}U_o(T) \right] Q_{0,r} \right]$$

Note that  $Q_{0,r} = P_{\mathbf{0}}^{2n+1} - P_{r\hat{e}_{2n+1}}^{2n+1}$  where the definition of these two projectors  $P_{\mathbf{0}}^{2n+1}$  and  $P_{r\hat{e}_{2n+1}}^{2n+1}$  are given in Eq. (5.10). For a strictly local unitary, the expression above equals  $\nu_E$ , taking a quantized value, as long as  $r$  is larger than the localized length  $l$ . For exponentially

decaying operators, this truncated edge invariant differ from  $\nu_E$  by exponentially small contributions (with a size  $O(e^{-r/l})$ ) from regions outside the interval  $[0, r]$ . Therefore, in the thermodynamic limit, by taking a limit,

$$\nu_E = \lim_{r \rightarrow \infty} \nu_E^r \quad (5.17)$$

To connect the edge invariants at the end of a complete cycle ( $t = T$ ) with the half-period bulk invariants, we rewrite our expression for  $\nu_E^r$  by substituting Eq. (4.18) into Eq. (5.16),

$$\begin{aligned} \nu_E^r &= \frac{(\pi i)^n}{2^{n+1} n!} \sum_{\sigma} \\ &(-1)^{\text{sign}(\sigma)} \text{Tr} \left[ U^\dagger \mathcal{S}U \left[ P_{\mathbf{a}}^{(\sigma_1)}, U^\dagger \mathcal{S}U \right] \left[ P_{\mathbf{a}}^{(\sigma_2)}, U^\dagger \mathcal{S}U \right] \dots \left[ P_{\mathbf{a}}^{(\sigma_{2n})}, U^\dagger \mathcal{S}U \right] Q_{0,r} \right] \end{aligned} \quad (5.18)$$

using the shorthand  $U$  to represent  $U_o(T/2)$ .

#### 5.4.2 Bulk-Edge Correspondence

As what we discussed in Sec 5.2, the difference between two unitary operators  $U_c(t)$  and  $U_o(t)$  is bounded near the edge. We define the difference as

$$D(t) = U_o(t) - P_{\mathbf{0}}^{2n+1} U_c(t) P_{\mathbf{0}}^{2n+1} \quad (5.19)$$

where we use  $P_{\mathbf{0}}^{2n+1}$  to confine  $U_b(t)$  to the semi-infinity system. This operator  $D(t)$  is exponentially decaying in direction  $2n + 1$ . Namely,

$$|D(t)_{\mathbf{r}_1, \mathbf{r}_2}| \leq C e^{-\lambda |\mathbf{r}_2 - \mathbf{r}_1|} e^{-\lambda |\mathbf{r}_1|^{2n+1}} \quad (5.20)$$

with a decaying length  $1/\lambda$ . Then we can use the localization properties of  $D(t)$  to connect the bulk invariant and edge behavior at half-period. Similar as the bulk invariant for  $U_c(t)$  in the closed system, we can also define a ‘bulk invariant’ for  $U_o(t)$  in the open system,

$$\begin{aligned} \nu_b^r &= \frac{(\pi i)^n}{(2n-1)!!} \sum_{\sigma} \\ &(-1)^{\text{sign}(\sigma)} \text{Tr} \left( P_A U^\dagger \left[ P_{r\hat{e}_{2n+1}}^{(\sigma_1)}, U \right] U^\dagger \left[ P_{r\hat{e}_{2n+1}}^{(\sigma_2)}, U \right] \dots U^\dagger \left[ P_{r\hat{e}_{2n+1}}^{(\sigma_{2n})}, U \right] U^\dagger \left[ P_{r\hat{e}_{2n+1}}^{(2n+1)}, U \right] \right) \end{aligned} \quad (5.21)$$

using the shorthand  $U$  to represent  $U_o(T/2)$ . Since the difference between open system and local system mainly exists on the boundary as indicated in Eq. (5.19), this invariant should agree with the bulk invariant of  $U_c(t)$  as we increase  $r$  and move projectors away from the edge. In the appendix, we will show that

$$\nu_b^r = \nu_E^r \tag{5.22}$$

when away from the edge. After taking limit ( $r \rightarrow \infty$ ) for both sides, we prove the bulk-edge correspondence.

## 5.A Projector Calculus

In this section, we introduce Projector Calculus method to study the properties of bulk and edge invariants.

Consider a general  $p$ -form

$$\begin{aligned} A &= a_{i_1 \dots i_p} dx^{i_1} \wedge \dots \wedge dx^{i_p} \\ &= a_I dx^I. \end{aligned} \tag{5.23}$$

where the operator  $a_I = a_{i_1 \dots i_p}$  is skew symmetric in  $i_1 \dots i_p$ . We define operators  $\hat{P}_j$  which act on such a form through conjugation as

$$\begin{aligned} \hat{P}_j A &= [P_j, a_I] dx^j \wedge dx^I \\ &= dx^j \wedge [P_j, A] \end{aligned}$$

where the wedge product acts from the left and we define the commutator  $[P_j, A] := [P_j, a_I] dx^I$ .

On a 0-form, we define the action of  $\hat{P}_i$  to be

$$\hat{P}_j A = dx^j [P_j, A].$$

The summation of  $\hat{P}_j$  over all directions become

$$\hat{P} = \sum_j^n \hat{P}_j.$$

where we consider a  $n$ -dimensional system. This operator works like exterior differentiation but uses commutator instead of differentiation operator. While the differentiation form is used to encode the topology of Floquet systems in momentum space [14], we can apply this ‘commutator form’ to real-space unitary evolutions.

**Lemma 5.A.1** *The operator  $\hat{P}$  takes an  $p$ -form to an  $(p + 1)$ -form, satisfying*

*(i)  $\hat{P}$  is additive, namely,  $\hat{P}(A + B) = \hat{P}A + \hat{P}B$*

(ii)  $\hat{P}^2 A = 0$  for any  $p$ -form  $A$

(iii)  $\hat{P}(AB) = [\hat{P}(A)]B + (-1)^{n_A}A[\hat{P}(B)]$ , where  $A$  is a  $n_A$  form and we use the shorthand  $AB$  to represent the wedge product between  $A$  and  $B$ , i.e.,  $A \wedge B$ .

(iv)  $\hat{P}(A^{-1}) = -A^{-1}\hat{P}(A)A^{-1}$  if  $A$  is a 0-form

**Proof:** (i) can be proved directly from the definition of the operator  $\hat{P}$ .

$$\begin{aligned}\hat{P}_j(A+B) &= dx^j \wedge [P, A+B] \\ &= \hat{P}_j A + \hat{P}_j B\end{aligned}$$

(ii) We note that

$$\begin{aligned}\hat{P}^2 A &= \sum_i \hat{P}_i \left( \sum_j \hat{P}_j A \right) \\ &= \sum_i \hat{P}_i \left( \sum_j dx^j \wedge [P_j, A] \right) \\ &= \sum_{ij} dx^i \wedge dx^j \wedge [P_i, [P_j, A]].\end{aligned}$$

Terms with  $i = j$  vanish because  $dx^i \wedge dx^i = 0$ , while for terms with  $i \neq j$  we find

$$\begin{aligned}& dx^i \wedge dx^j \wedge [P_i, [P_j, A]] \\ &= dx^i \wedge dx^j \wedge [P_i P_j A - P_i A P_j - P_j A P_i + A P_j P_i] \\ &= -dx^j \wedge dx^i \wedge [P_i P_j A - P_i A P_j - P_j A P_i + A P_j P_i],\end{aligned}$$

where in the final line, we have used the antisymmetric property of the wedge product.

However, we can relabel  $i \leftrightarrow j$  in the summation to write

$$\begin{aligned}& dx^i \wedge dx^j \wedge [P_i, [P_j, A]] \\ &= -dx^j \wedge dx^i \wedge [P_i P_j A - P_i A P_j - P_j A P_i + A P_j P_i] \\ &= -dx^i \wedge dx^j [P_j P_i A - P_j A P_i - P_i A P_j + A P_i P_j].\end{aligned}$$

Then, since  $P_i$  and  $P_j$  commute, this term is equal to its negative, and so must vanish.

(iii) We consider how  $\hat{P}_j$  acts on a product of forms, writing

$$\begin{aligned}
\hat{P}_j(AB) &= dx^j \wedge [P_j, AB] \\
&= dx^j \wedge [P_j AB - ABP_j] \\
&= dx^j \wedge [P_j AB - AP_j B + AP_j B - ABP_j] \\
&= dx^j \wedge \left[ [P_j, A] B \right] + dx^j \wedge \left[ A [P_j, B] \right] \\
&= \left[ dx^j \wedge [P_j, A] \right] \wedge B + (-1)^{n_A} A \wedge \left[ dx^j \wedge [P_j, B] \right] \\
&= \left[ \hat{P}_j(A) \right] B + (-1)^{n_A} A \left[ \hat{P}_j(B) \right],
\end{aligned}$$

where the possible relative negative sign is important. In addition, since  $\hat{P}$  is a sum over  $\hat{P}_i$ , we find

$$\hat{P}(AB) = \left[ \hat{P}(A) \right] B + (-1)^{n_A} A \left[ \hat{P}(B) \right],$$

(iv) If  $A$  is a 0-form

$$\begin{aligned}
\hat{P}_i(A^{-1}) &= dx^i [P_i A^{-1} - A^{-1} P_i] \\
&= dx^i \left[ -A^{-1} (P_i A - A P_i) A^{-1} \right] \\
&= -A^{-1} \hat{P}_i(A) A^{-1}.
\end{aligned}$$

By doing a summation over all directions,

$$\hat{P}(A^{-1}) = -A^{-1} \hat{P}(A) A^{-1}$$

□

We now introduce the trace operator as

$$\text{Tr}(A) = \text{Tr}(a_{s(I)})$$

if  $A$  is a  $p$ -form defined in (5.23). We use the symbol  $s(I)$  to represent a sorting of the indices in  $I$ , organizing them in increasing order,

$$s(i_1, i_2, \dots, i_p) = (i'_1 < \dots < i'_p) \quad (5.24)$$

For instance,  $s(3, 1, 2) = (1, 2, 3)$ . Here are two important properties of the trace operator:

**Lemma 5.A.2** (i) *The trace of any commutator form is always zero. In other words,  $\text{Tr}(\hat{P}(A)) = 0$  holds for any  $p$ -form  $A$ .*

(ii) *The cyclic property of the trace operator acting on the exterior forms:  $\text{Tr}(BA) = (-1)^{n_A n_B} \text{Tr}(AB)$ .*

**Proof:** Then

$$\text{Tr}(\hat{P}(A)) = \text{Tr}([P_j, a_{s(I)}]) = 0$$

using the cyclic property of the trace operator. This property is very useful especially when we need to construct zero-trace operators.

(vi) Consider two exterior forms  $A$  and  $B$ :

$$\begin{aligned} A &= a_{i_1 \dots i_n} dx^{i_1} \wedge \dots \wedge dx^{i_n} \\ B &= b_{j_1 \dots j_n} dx^{j_1} \wedge \dots \wedge dx^{j_n} \end{aligned}$$

Then the wedge product between them:

$$\begin{aligned} AB &= A \wedge B \\ &= a_{i_1 \dots i_n} b_{j_1 \dots j_n} (dx^{i_1} \wedge \dots \wedge dx^{i_n} \wedge dx^{j_1} \wedge \dots \wedge dx^{j_n}) \\ BA &= B \wedge A \\ &= b_{j_1 \dots j_n} a_{i_1 \dots i_n} (dx^{j_1} \wedge \dots \wedge dx^{j_n} \wedge dx^{i_1} \wedge \dots \wedge dx^{i_n}) \\ &= (-1)^{n_A n_B} b_{j_1 \dots j_n} a_{i_1 \dots i_n} (dx^{i_1} \wedge \dots \wedge dx^{i_n} \wedge dx^{j_1} \wedge \dots \wedge dx^{j_n}) \end{aligned}$$

After taking trace of  $AB$  and  $BA$ , we get

$$\text{Tr}(BA) = (-1)^{n_A n_B} \text{Tr}(AB)$$

where we also use the cyclic property  $\text{Tr}(b_{j_1 \dots j_n} a_{i_1 \dots i_n}) = \text{Tr}(a_{i_1 \dots i_n} b_{j_1 \dots j_n})$ .

When  $n_A + n_B$  is odd,  $n_A n_B$  is always even. The following equality always holds:

$$\text{Tr}(BA) = \text{Tr}(AB)$$

□

### 5.A.1 Winding number

The winding number given in (2.21) can be expressed in the commutator form

$$W_n[U] = \frac{(\pi i)^n}{(2n+1)!!} \text{Tr} \left[ (U^{-1} \hat{P} U)^n \right], \quad (5.25)$$

where the power involves taking the wedge product between brackets. We can show that this invariant is additive.

For the one-dimensional case, we can calculate the winding number of a product easily using the methods above, finding

$$\begin{aligned} W_1[UV] &= \text{Tr} \left[ (V^{-1} U^{-1} \hat{P}(UV)) \right] \\ &= \text{Tr} \left[ V^{-1} U^{-1} (\hat{P}(U)V + (-1)^{n_U} U \hat{P}(V)) \right] \\ &= \text{Tr} \left[ V^{-1} (U^{-1} \hat{P}(U)) V \right] + (-1)^{n_U} \text{Tr} \left[ (V^{-1} \hat{P}(V)) \right]. \end{aligned}$$

However,  $U$  is a 0-form, and so there is no overall negative sign, and we can also use the cyclic property of the trace to find

$$W_1[UV] = \text{Tr} \left[ (U^{-1} \hat{P}(U)) \right] + \text{Tr} \left[ (V^{-1} \hat{P}(V)) \right] = W[U] + W[V].$$

Before we generalize this property to arbitrary odd dimensions, we first prove the following property:

**Lemma 5.A.3** *The winding number is additive, namely,  $W_n[UV] = W_n[U] + W_n[V]$ .*

**Proof:** We first write down  $W_n[VU]$ ,

$$W_n[VU] = \frac{(\pi i)^n}{(2n+1)!!} \text{Tr} \left[ (V^{-1} U^{-1} \hat{P}(UV))^n \right],$$

If we split this term,

$$V^{-1} U^{-1} \hat{P}(UV) = V^{-1} (U^{-1} \hat{P} U) V + V^{-1} \hat{P} V$$

Defining  $a = V^{-1} \hat{P} V$ ,  $b = V^{-1} U^{-1} \hat{P}(UV)$ , we want to prove

$$\text{Tr} [b^n] = \text{Tr} [a^n] + \text{Tr} [(b-a)^n] \quad (5.26)$$

First we construct "total commutator" term by studying the action of  $\hat{P}$  on all possible  $(n-1)$ -forms of  $a$  and  $b$ . These  $(n-1)$ -forms should be the multiplication of  $a$  and  $b$ . We use binomial representation to represent the multiplication of  $a$  and  $b$ ,

$$B_{q_1, q_2, \dots, q_d}^d = (a^{q_1} b^{1-q_1})(a^{q_2} b^{1-q_2}) \dots (a^{q_i} b^{1-q_i}) \dots (a^{q_d} b^{1-q_d})$$

Where  $q_i = 0$  or  $1$ . Each block  $a^{q_i} b^{1-q_i}$  can become either  $a$  or  $b$  given the value of  $q_i$ .

Let's first study how  $\hat{P}$  act on each block  $a^q b^{1-q}$ .

If  $q = 0$ ,

$$\hat{P}(a^0 b^1) = -b^2$$

If  $q = 1$ ,

$$\hat{P}(a^1 b^0) = -a^2$$

In conclusion,

$$\hat{P}(a^q b^{1-q}) = -a^q b^{1-q} a^q b^{1-q}$$

Then we act  $\hat{P}$  on this  $(n-1)$ -form operator:

$$\begin{aligned} \hat{P}(B_{q_1, q_2, \dots, q_{n-1}}^{n-1}) &= \hat{P}(a^{q_1} b^{1-q_1} a^{q_2} b^{1-q_2} \dots a^{q_{n-1}} b^{1-q_{n-1}}) \\ &= \sum_{i=1}^{n-1} (-1)^{i-1} a^{q_1} b^{1-q_1} a^{q_2} b^{1-q_2} \dots \hat{P}(a^{q_i} b^{1-q_i}) \dots a^{q_{n-1}} b^{1-q_{n-1}} \\ &= - \sum_{i=1}^{n-1} (-1)^{i-1} a^{q_1} b^{1-q_1} a^{q_2} b^{1-q_2} \dots a^{q_i} b^{1-q_i} a^{q_i} b^{1-q_i} \dots a^{q_{n-1}} b^{1-q_{n-1}} \\ &= - \sum_{i=1}^{n-1} (-1)^{i-1} B_{q_1, q_2, \dots, q_i, q_i, q_{i+1}, \dots, q_{n-1}}^n \end{aligned}$$

We can also expand the result in the basis of  $B_{q'_1, q'_2, \dots, q'_n}^n$ , the above equation becomes

$$\begin{aligned}
& - \sum_{i=1}^{n-1} (-1)^{i-1} \sum_{q'_1=0}^1 \sum_{q'_2=0}^1 \cdots \sum_{q'_n=0}^1 B_{q'_1, q'_2, \dots, q'_n}^n \delta_{q'_1, q_1} \delta_{q'_2, q_2} \cdots \delta_{q'_i, q_i} \delta_{q'_{i+1}, q_i} \delta_{q'_{i+2}, q_{i+1}} \cdots \delta_{q'_n, q_{n-1}} \\
& = - \sum_{i=1}^{n-1} (-1)^{i-1} \\
& \quad \sum_{q'_1=0}^1 \sum_{q'_2=0}^1 \cdots \sum_{q'_n=0}^1 \frac{1 + (-1)^{q'_i + q'_{i+1}}}{2} B_{q'_1, q'_2, \dots, q'_n}^n \delta_{q'_1, q_1} \delta_{q'_2, q_2} \cdots \delta_{q'_i, q_i} \delta_{q'_{i+2}, q_{i+1}} \cdots \delta_{q'_n, q_{n-1}} \\
& = \sum_{q'_1=0}^1 \sum_{q'_2=0}^1 \cdots \sum_{q'_n=0}^1 B_{q'_1, q'_2, \dots, q'_n}^n \sum_{i=1}^{n-1} (-1)^i \delta_{q'_1, q_1} \delta_{q'_2, q_2} \cdots \delta_{q'_i, q_i} \delta_{q'_{i+2}, q_{i+1}} \cdots \delta_{q'_n, q_{n-1}} \frac{1 + (-1)^{q'_i + q'_{i+1}}}{2}
\end{aligned}$$

We define a filtering function  $H(x)$  to only include  $x$  satisfying  $x \neq 0$  in the calculation. In the following calculation, we use  $H(n-1 - \sum_{j=1}^{n-2} (-1)^{q_j + q_{j+1}} - (-1)^{q_1 + q_{n-1}})$  to filter out  $(q_1, q_2, \dots, q_{n-1})$  which satisfies  $n-1 - \sum_{j=1}^{n-2} (-1)^{q_j + q_{j+1}} - (-1)^{q_1 + q_{n-1}} = 0$ .

Then taking a sum over all possible (n-1)-form operators,

$$\begin{aligned}
& \frac{\sum_{q_1=0}^1 \sum_{q_2=0}^1 \cdots \sum_{q_{n-1}=0}^1 \hat{P}(B_{q_1, q_2, \dots, q_{n-1}}^{n-1})(-1)^{\sum_{j=1}^{n-1} q_j} (-1)^{q_1}}{-2} \\
& \frac{n-1 - \sum_{j=1}^{n-2} (-1)^{q_j+q_{j+1}} - (-1)^{q_1+q_{n-1}}}{H(n-1 - \sum_{j=1}^{n-2} (-1)^{q_j+q_{j+1}} - (-1)^{q_1+q_{n-1}})} \\
= & - \sum_{q_1=0}^1 \sum_{q_2=0}^1 \cdots \sum_{q_{n-1}=0}^1 (-1)^{\sum_{j=1}^{n-1} q_j} (-1)^{q_1} \frac{-2}{n-1 - \sum_{j=1}^{n-2} (-1)^{q_j+q_{j+1}} - (-1)^{q_1+q_{n-1}}} \\
& \frac{H(n-1 - \sum_{j=1}^{n-2} (-1)^{q_j+q_{j+1}} - (-1)^{q_1+q_{n-1}})}{\sum_{q'_1=0}^1 \sum_{q'_2=0}^1 \cdots \sum_{q'_n=0}^1 B_{q'_1, q'_2, \dots, q'_n}^n \sum_{i=1}^{n-1} (-1)^i \delta_{q'_1, q_1} \delta_{q'_2, q_2} \cdots \delta_{q'_i, q_i} \delta_{q'_{i+2}, q_{i+1}} \cdots \delta_{q'_n, q_{n-1}} \frac{1 + (-1)^{q'_i+q'_{i+1}}}{2}} \\
= & \sum_{q'_1=0}^1 \sum_{q'_2=0}^1 \cdots \sum_{q'_n=0}^1 B_{q'_1, q'_2, \dots, q'_n}^n (-1)^{q'_1} \\
& \sum_{i=1}^{n-1} (-1)^i \frac{1 + (-1)^{q'_i+q'_{i+1}}}{2} (-1)^{-q'_{i+1} + \sum_{j=1}^n q'_j} \\
& \frac{H(n-1 - \sum_{j=1}^{i-1} (-1)^{q'_j+q'_{j+1}} - \sum_{j=i+2}^{n-1} (-1)^{q'_j+q'_{j+1}} - (-1)^{q'_i+q'_{i+2}} - (-1)^{q'_1+q'_n})}{-2} \\
= & \sum_{q'_1=0}^1 \sum_{q'_2=0}^1 \cdots \sum_{q'_n=0}^1 B_{q'_1, q'_2, \dots, q'_n}^n (-1)^{q'_1} \frac{H(n-1 - \sum_{j=1}^{i-1} (-1)^{q'_j+q'_{j+1}} - (-1)^{q'_1+q'_n})}{n-1 - \sum_{j=1}^{i-1} (-1)^{q'_j+q'_{j+1}} - \sum_{j=i+2}^{n-1} (-1)^{q'_j+q'_{j+1}} - (-1)^{q'_i+q'_{i+2}} - (-1)^{q'_1+q'_n}} \\
& \sum_{i=1}^{n-1} (-1)^i \frac{(-1)^{q'_{i+1}} + (-1)^{q'_i}}{2} (-1)^{\sum_{j=1}^n q'_j} \frac{-2}{n - \sum_{j=1}^{n-1} (-1)^{q'_j+q'_{j+1}} - (-1)^{q'_1+q'_n}} \\
= & \sum_{q'_1=0}^1 \sum_{q'_2=0}^1 \cdots \sum_{q'_n=0}^1 B_{q'_1, q'_2, \dots, q'_n}^n (-1)^{q'_1} \\
& (-1)^{\sum_{j=1}^n q'_j} \frac{(-1)^{q'_n} - (-1)^{q'_1}}{2} \frac{-2}{n - \sum_{j=1}^{n-1} (-1)^{q'_j+q'_{j+1}} - (-1)^{q'_1+q'_n}} \\
& \frac{H(n - \sum_{j=1}^{n-1} (-1)^{q'_j+q'_{j+1}} - (-1)^{q'_1+q'_n})}{\sum_{q'_1=0}^1 \sum_{q'_2=0}^1 \cdots \sum_{q'_n=0}^1 B_{q'_1, q'_2, \dots, q'_n}^n} \\
= & \sum_{q'_1=0}^1 \sum_{q'_2=0}^1 \cdots \sum_{q'_n=0}^1 B_{q'_1, q'_2, \dots, q'_n}^n \\
& (-1)^{\sum_{j=1}^n q'_j} \frac{1 - (-1)^{q'_1+q'_n}}{n - \sum_{j=1}^{n-1} (-1)^{q'_j+q'_{j+1}} - (-1)^{q'_1+q'_n}} H(n - \sum_{j=1}^{n-1} (-1)^{q'_j+q'_{j+1}} - (-1)^{q'_1+q'_n})
\end{aligned}$$

After taking trace of both sides, we get

$$\sum_{q'_1=0}^1 \sum_{q'_2=0}^1 \cdots \sum_{q'_n=0}^1 \text{Tr} \left[ B_{q'_1, q'_2, \dots, q'_n}^n \right] g(q'_1, q'_2, \dots, q'_n) = 0$$

where

$$g(q'_1, q'_2, \dots, q'_n) = (-1)^{\sum_{j=1}^n q'_j} \frac{1 - (-1)^{q'_1 + q'_n}}{n - \sum_{j=1}^{n-1} (-1)^{q'_j + q'_{j+1}} - (-1)^{q'_1 + q'_n}} H\left(n - \sum_{j=1}^{n-1} (-1)^{q'_j + q'_{j+1}} - (-1)^{q'_1 + q'_n}\right).$$

Then we apply the cyclic properties of  $\text{Tr} \left[ B_{q'_1, q'_2, \dots, q'_n}^n \right]$ ,

$$\begin{aligned} & n \sum_{q'_1=0}^1 \sum_{q'_2=0}^1 \cdots \sum_{q'_n=0}^1 \text{Tr} \left[ B_{q'_1, q'_2, \dots, q'_n}^n \right] g(q'_1, q'_2, \dots, q'_n) \\ &= \sum_{i=1}^n \sum_{q'_1=0}^1 \sum_{q'_2=0}^1 \cdots \sum_{q'_n=0}^1 \text{Tr} \left[ B_{q'_{i+1}, q'_{i+2}, \dots, q'_n, q'_1, q'_2, \dots, q'_i}^n \right] g(q'_1, q'_2, \dots, q'_n) \\ &= \sum_{i=1}^n \sum_{q'_1=0}^1 \sum_{q'_2=0}^1 \cdots \sum_{q'_n=0}^1 \text{Tr} \left[ B_{q'_1, q'_2, \dots, q'_n}^n \right] g(q'_{n-i+1}, q'_{n-i+2}, \dots, q'_n, q'_1, q'_2, \dots, q'_{n-i}) \\ &= \sum_{q'_1=0}^1 \sum_{q'_2=0}^1 \cdots \sum_{q'_n=0}^1 \text{Tr} \left[ B_{q'_1, q'_2, \dots, q'_n}^n \right] \sum_{i=1}^n g(q'_{i+1}, q'_{i+2}, \dots, q'_n, q'_1, q'_2, \dots, q'_i) \end{aligned}$$

Where

$$\begin{aligned} & \sum_{i=1}^n g(q'_{i+1}, q'_{i+2}, \dots, q'_n, q'_1, q'_2, \dots, q'_i) \\ &= \sum_{i=1}^n (-1)^{\sum_{j=1}^n q'_j} \frac{1 - (-1)^{q'_i + q'_{i+1}}}{n - \sum_{j=1}^{n-1} (-1)^{q'_j + q'_{j+1}} - (-1)^{q'_1 + q'_n}} H\left(n - \sum_{j=1}^{n-1} (-1)^{q'_j + q'_{j+1}} - (-1)^{q'_1 + q'_n}\right) \\ &= (-1)^{\sum_{j=1}^n q'_j} H\left(n - \sum_{j=1}^{n-1} (-1)^{q'_j + q'_{j+1}} - (-1)^{q'_1 + q'_n}\right) \end{aligned}$$

Therefore,

$$\sum_{q'_1=0}^1 \sum_{q'_2=0}^1 \cdots \sum_{q'_n=0}^1 \text{Tr} \left[ B_{q'_1, q'_2, \dots, q'_n}^n \right] (-1)^{\sum_{j=1}^n q'_j} H\left(n - \sum_{j=1}^{n-1} (-1)^{q'_j + q'_{j+1}} - (-1)^{q'_1 + q'_n}\right) = 0 \quad (5.27)$$

The screening function  $H\left(n - \sum_{j=1}^{n-1} (-1)^{q'_j + q'_{j+1}} - (-1)^{q'_1 + q'_n}\right)$  only selects the combination of  $(q'_1, q'_2, \dots, q'_n)$  which makes  $n - \sum_{j=1}^{n-1} (-1)^{q'_j + q'_{j+1}} - (-1)^{q'_1 + q'_n} \neq 0$ . The equal sign holds

only when  $q'_1 = q'_2 = \dots = q'_n$ . Therefore

$$H(n - \sum_{j=1}^{n-1} (-1)^{q'_j + q'_{j+1}} - (-1)^{q'_1 + q'_n}) = 1 - \delta_{q'_1, q'_2} \delta_{q'_2, q'_3} \dots \delta_{q'_{n-1}, q'_n} \delta_{q'_n, q'_1} \quad (5.28)$$

Combining with Eq. (5.27), we can simplify the summation below

$$\begin{aligned} & \sum_{q'_1=0}^1 \sum_{q'_2=0}^1 \dots \sum_{q'_n=0}^1 \text{Tr} \left[ B_{q'_1, q'_2, \dots, q'_n}^n \right] (-1)^{\sum_{j=1}^n q'_j} \\ = & \sum_{q'_1=0}^1 \sum_{q'_2=0}^1 \dots \sum_{q'_n=0}^1 \text{Tr} \left[ B_{q'_1, q'_2, \dots, q'_n}^n \right] (-1)^{\sum_{j=1}^n q'_j} \\ & \left[ \delta_{q'_1, q'_2} \delta_{q'_2, q'_3} \dots \delta_{q'_{n-1}, q'_n} \delta_{q'_n, q'_1} + H(n - \sum_{j=1}^{n-1} (-1)^{q'_j + q'_{j+1}} - (-1)^{q'_1 + q'_n}) \right] \\ = & \sum_{q'_1=0}^1 \sum_{q'_2=0}^1 \dots \sum_{q'_n=0}^1 \text{Tr} \left[ B_{q'_1, q'_2, \dots, q'_n}^n \right] (-1)^{\sum_{j=1}^n q'_j} \delta_{q'_1, q'_2} \delta_{q'_2, q'_3} \dots \delta_{q'_{n-1}, q'_n} \delta_{q'_n, q'_1} \\ = & \text{Tr} \left[ B_{0,0,0,\dots,0}^n \right] - \text{Tr} \left[ B_{1,1,1,\dots,1}^n \right] \\ = & \text{Tr} \left[ b^n \right] - \text{Tr} \left[ a^n \right] \end{aligned}$$

Finally, we can confirm the equality given in Eq. (5.26)

$$\begin{aligned} & \text{Tr} [a^n] + \text{Tr} [(b - a)^n] \\ = & \text{Tr} [a^n] + \sum_{q'_1=0}^1 \sum_{q'_2=0}^1 \dots \sum_{q'_n=0}^1 \text{Tr} \left[ B_{q'_1, q'_2, \dots, q'_n}^n \right] (-1)^{\sum_{j=1}^n q'_j} \\ = & \text{Tr} [b^n] \end{aligned}$$

On the other hands,

$$\begin{aligned} & \text{Tr} [(b - a)^n] \\ = & \text{Tr} \left[ (V^{-1}(U^{-1}\hat{P}U)V)^n \right] \\ = & \text{Tr} \left[ V^{-1}(U^{-1}\hat{P}U)^n V \right] \end{aligned}$$

After applying the cyclic properties of the trace operator,

$$\begin{aligned} & \text{Tr} [(b - a)^n] \\ = & \text{Tr} \left[ (U^{-1}\hat{P}U)^n \right] \end{aligned}$$

Thus,

$$\begin{aligned}
W_n[VU] &= \frac{(\pi i)^n}{(2n+1)!!} \text{Tr} \left[ \left( V^{-1} U^{-1} \hat{P}(UV) \right)^n \right] \\
&= \frac{(\pi i)^n}{(2n+1)!!} \text{Tr} [b^n] \\
&= \frac{(\pi i)^n}{(2n+1)!!} \text{Tr} [(b-a)^n] + \frac{(\pi i)^n}{(2n+1)!!} \text{Tr} [a^n] \\
&= \frac{(\pi i)^n}{(2n+1)!!} \text{Tr} \left[ (U^{-1} \hat{P} U)^n \right] + \frac{(\pi i)^n}{(2n+1)!!} \text{Tr} \left[ (V^{-1} \hat{P} V)^n \right] \\
&= W_n[U] + W_n[V]
\end{aligned}$$

We finish proving the additive properties of this winding number.  $\square$

## 5.B Bulk edge correspondence

In this appendix, we want to prove the bulk-edge correspondence given in Eq. (5.22).

### 5.B.1 Two differential forms

In this section, we introduce two differential forms that assemble the bulk invariants.

First we define a 1-form  $O = U^\dagger \hat{P} U$  and a 0-form  $P_A^U = U^\dagger P_A U$  where  $P_A$  is a projector acting on the sublattice A. We are considering 2n-dimensional system now, so  $\hat{P} = \sum_j^{2n} \hat{P}_j$ .

A set of d-form which are the multiplication of  $O$  and  $P_A^U$  takes this general expression

$$Z_{q_1, q_2, \dots, q_{s+1}}^d = O^{q_1} P_A^U O^{q_2} P_A^U \dots O^{q_s} P_A^U O^{q_{s+1}} \quad (5.29)$$

where  $\sum_{i=1}^{s+1} q_i = d$  and  $s$  is just the number of the projector  $P_A^U$  inside  $Z_{q_1, q_2, \dots, q_{s+1}}^d$ . For instance,  $Z_{1,0}^1 = O P_A^U = U^\dagger \hat{P} U U^\dagger P_A U$ .

To proceed the proof, we first show two equalities:

**Lemma 5.B.1** *Here are two equalities:*

$$(i) \hat{P}(O^q) = -\frac{1-(-1)^q}{2} O^{q+1} \text{ for } q \geq 1$$

$$(ii) \hat{P}(P_A^U) = -O P_A^U + P_A^U O$$

**Proof:** (i) We use recursion method to prove this formula. When  $q = 1$ ,

$$\begin{aligned}
\hat{P}O &= \hat{P} [U^{-1}\hat{P}(U)] \\
&= \hat{P} (U^{-1}) \hat{P}(U) + U^{-1}\hat{P}^2(U) \\
&= [-U^{-1}\hat{P}(U)U^{-1}\hat{P}(U)] \\
&= -O^2.
\end{aligned}$$

meets  $\hat{P}(O^q) = -\frac{1-(-1)^q}{2}O^{q+1}$ . If for  $q-1$ ,

$$\hat{P}(O^{q-1}) = -\frac{1-(-1)^{q-1}}{2}O^q$$

Then we can prove for  $q$ ,

$$\begin{aligned}
\hat{P}(O^q) &= \hat{P}(O^{q-1}O) \\
&= \hat{P}(O^{q-1})O + (-1)^{q-1}O^{q-1}\hat{P} \\
&= -\frac{1-(-1)^{q-1}}{2}O^{q+1} - (-1)^{q-1}O^{q+1} \\
&= -\frac{1-(-1)^q}{2}O^{q+1}
\end{aligned}$$

as expected.

(ii)

$$\begin{aligned}
\hat{P}(P_A^U) &= \hat{P} [U^{-1}P_AU] \\
&= \hat{P} (U^{-1}) P_AU + U^{-1}P_A\hat{P}(U) \\
&= -U^{-1}\hat{P}(U)U^{-1}P_AU + U^{-1}P_AUU^{-1}\hat{P}(U) \\
&= -OP_A^U + P_A^UO.
\end{aligned}$$

□

We can construct ‘total commutator’ from this  $2n - 1$  form

$$\begin{aligned}
&\hat{P}(Z_{q_1, q_2 \dots q_{s+1}}^{2n-1}) \\
&= \hat{P}(O^{q_1} P_A^U O^{q_2} P_A^U \dots O^{q_r} P_A^U O^{q_{s+1}}) \\
&= \sum_{i=1}^{s+1} (-1)^{\sum_{k=1}^{i-1} q_k} O^{q_1} P_A^U \dots \hat{P}(O^{q_i}) \dots P_A^U O^{q_{s+1}} \\
&+ \sum_{i=1}^s (-1)^{\sum_{k=1}^i q_k} O^{q_1} P_A^U \dots O^{q_i} \hat{P}(P_A^U) O^{q_{i+1}} \dots P_A^U O^{q_{s+1}}
\end{aligned}$$

After plugging in the two equalities in Lemma 5.B.1, we get

$$\begin{aligned}
& \sum_{i=1}^{s+1} -\frac{1 - (-1)^{q_i}}{2} (-1)^{\sum_{k=1}^{i-1} q_k} O^{q_1} P_A^U \dots O^{q_{i+1}} \dots P_A^U O^{q_{s+1}} \\
& + \sum_{i=1}^s (-1)^{\sum_{k=1}^i q_k} O^{q_1} P_A^U \dots O^{q_i} (P_A^U O - O P_A^U) O^{q_{i+1}} \dots P_A^U O^{q_{s+1}} \\
& = \sum_{i=1}^{s+1} -\frac{1 - (-1)^{q_i}}{2} (-1)^{\sum_{k=1}^{i-1} q_k} Z_{q_1, q_2, \dots, q_{i+1}, \dots, q_{s+1}}^{2n} \\
& + \sum_{i=1}^s (-1)^{\sum_{k=1}^i q_k} (Z_{q_1, q_2, \dots, q_{i+1}+1, \dots, q_{s+1}}^{2n} - Z_{q_1, q_2, \dots, q_i+1, \dots, q_{s+1}}^{2n})
\end{aligned}$$

Adding all these terms together,

$$\hat{P}(Z_{q_1, q_2, \dots, q_{s+1}}^{2n-1}) = \sum_{i=1}^{r+1} c_i(\mathbf{q}) Z_{q_1, q_2, \dots, q_i+1, \dots, q_{s+1}}^{2n}$$

where

$$c_i(\mathbf{q}) = \begin{cases} -\frac{1+(-1)^{q_1}}{2} & i = 1 \\ (-1)^{\sum_{k=1}^{i-1} q_k} \left( \frac{1-(-1)^{q_i}}{2} \right) & 2 \leq i \leq s \\ -\frac{1+(-1)^{q_{s+1}}}{2} & i = s+1, \end{cases} \quad (5.30)$$

If we define  $\text{Tr}(Z_{q_1, q_2, \dots, p_{s+1}}^{2n} Q_{0,r})$  as  $x_{q_1, q_2, \dots, q_{s+1}}^{2n}$ , we get the first equation by taking trace of above equation

$$\sum_{i=1}^{s+1} c_i(\mathbf{q}) x_{q_1, q_2, \dots, q_i+1, \dots, q_{s+1}}^{2n} = 0 \quad (5.31)$$

because ‘total commutator’ terms will vanish under the action of the trace according to Lemma 5.A.2.

Another set of d-forms takes this format:

$$Y_{q_1, q_2, \dots, q_{s+1}}^d = Q^{q_1} P_A Q^{q_2} P_A, \dots, Q^{q_s} P_A Q^{q_{s+1}}$$

where the 1-form  $Q = U \hat{P} U^\dagger$ .

Similar as how we deal with  $Z$ , we construct ‘total commutator’ form from  $Y$ ,

$$\begin{aligned}
& \hat{P}(Y_{q_1, q_2, \dots, q_{s+1}}^{2n-1} Q_{0,r}) \\
&= \hat{P}(Q^{q_1} P_A Q^{q_2} P_A \dots Q^{q_r} P_A Q^{q_{s+1}} Q_{0,r}) \\
&= \sum_{i=1}^{s+1} (-1)^{\sum_{k=1}^{i-1} q_k} Q^{q_1} P_A \dots \hat{P}(Q^{q_i}) \dots P_A Q^{q_{s+1}} Q_{0,r}
\end{aligned}$$

which can be simplified as

$$\hat{P}(Y_{q_1, q_2, \dots, q_{s+1}}^{2n-1} Q_{0,r}) = \sum_{i=1}^{s+1} e_i(\mathbf{q}) Y_{q_1, q_2, \dots, q_i+1, \dots, q_{s+1}}^{2n} Q_{0,r}$$

where

$$e_i(\mathbf{q}) = -\frac{1 - (-1)^{q_i}}{2} (-1)^{\sum_{k=1}^{i-1} q_k} \tag{5.32}$$

After taking trace of both sides, we get,

$$\sum_{i=1}^{s+1} e_i(\mathbf{q}) \text{Tr} \left( Y_{q_1, q_2, \dots, q_i+1, \dots, q_{s+1}}^{2n} Q_{0,r} \right) = 0 \tag{5.33}$$

### 5.B.2 Bulk invariants

Since the edge lies at  $P_{r\hat{e}_{2n+1}}^{2n+1}$ , we separate the direction  $\sigma_i = 2n + 1$  from others,

$$\begin{aligned}
\nu^{2n+1}[U_+] &= \frac{(\pi i)^n}{(2n+1)!!} \sum_i \sum_{\sigma, \sigma_i=2n+1} (-1)^{\text{sign}(\sigma)} \\
&\text{Tr} \left( U_+^\dagger [P_{r\hat{e}_{2n+1}}^{(\sigma_1)}, U_+] U_+^\dagger [P_{r\hat{e}_{2n+1}}^{(\sigma_2)}, U_+] \dots U_+^\dagger [P_{r\hat{e}_{2n+1}}^{2n+1}, U_+] \dots U_+^\dagger [P_{r\hat{e}_{2n+1}}^{(\sigma_{2n+1})}, U_+] \right)
\end{aligned} \tag{5.34}$$

Applying the cyclic properties of the trace operator,

$$\begin{aligned}
\nu^{2n+1}[U_+] &= \frac{(\pi i)^n}{(2n+1)!!} \sum_i \sum_{\sigma, \sigma_i=2n+1} (-1)^{\text{sign}(\sigma)} \\
&\text{Tr} \left( U_+^\dagger [P_{r\hat{e}_{2n+1}}^{(\sigma_{i+1})}, U_+] \dots U_+^\dagger [P_{r\hat{e}_{2n+1}}^{(\sigma_{2n+1})}, U_+] U_+^\dagger [P_{r\hat{e}_{2n+1}}^{(\sigma_1)}, U_+] \dots U_+^\dagger [P_{r\hat{e}_{2n+1}}^{(\sigma_{i-1})}, U_+] U_+^\dagger [P_{r\hat{e}_{2n+1}}^{2n+1}, U_+] \right)
\end{aligned} \tag{5.35}$$

Relabelling the indices for  $\sigma$ ,

$$\begin{aligned}
\nu^{2n+1}[U_+] &= \frac{(\pi i)^n}{(2n+1)!!} \sum_{i=1}^{2n+1} \sum_{\sigma'} & (5.36) \\
& (-1)^{\text{sign}(\sigma'_{2n-i+2}, \dots, \sigma'_{2n}, 2n+1, \sigma'_1, \dots, \sigma'_{2n-i+1})} \\
& \text{Tr} \left( U_+^\dagger [P_{r\hat{e}_{2n+1}}^{(\sigma'_1)}, U_+] U_+^\dagger [P_{r\hat{e}_{2n+1}}^{(\sigma'_2)}, U_+] \dots U_+^\dagger [P_{r\hat{e}_{2n+1}}^{2n+1}, U_+] \right) \\
&= \frac{(\pi i)^n}{(2n-1)!!} \sum_{\sigma'} \\
& (-1)^{\text{sign}(\sigma')} \text{Tr} \left( U_+^\dagger [P_{r\hat{e}_{2n+1}}^{(\sigma'_1)}, U_+] U_+^\dagger [P_{r\hat{e}_{2n+1}}^{(\sigma'_2)}, U_+] \dots U_+^\dagger [P_{r\hat{e}_{2n+1}}^{2n+1}, U_+] \right)
\end{aligned}$$

### 5.B.3 Expression bulk invariants in two differential forms

In this section, we express the truncated bulk invariant given in Eq. (5.21) using the above two differential forms.

Subsequently, we substitute  $P_{r\hat{e}_{2n+1}}^{(\sigma_{2n+1})}$  as  $P_{\mathbf{0}}^{2n+1} - Q_{0,r}$  and note that  $[P_{\mathbf{0}}^{2n+1}, U]$  since  $P_{\mathbf{0}}^{2n+1}$  acts like the identity matrix on the open system, the truncated bulk invariant can be rewritten as

$$\begin{aligned}
\nu_b^r &= -\frac{(\pi i)^n}{(2n-1)!!} \sum_{\sigma} & (5.37) \\
& (-1)^{\text{sign}(\sigma)} \text{Tr} \left( P_A U^\dagger [P_{r\hat{e}_{2n+1}}^{(\sigma_1)}, U] U^\dagger [P_{r\hat{e}_{2n+1}}^{(\sigma_2)}, U] \dots U^\dagger [P_{r\hat{e}_{2n+1}}^{(\sigma_{2n})}, U] U^\dagger [Q_{0,r}, U] \right)
\end{aligned}$$

To represent this invariant in differential forms, we may use this simple rule:

$$\sum_{\sigma} (-1)^{\text{sign}(\sigma)} [P_{r\hat{e}_{2n+1}}^{(\sigma_i)}, \cdot] \rightarrow \hat{P}$$

Thus,

$$\nu_b^r = -\frac{(\pi i)^n}{(2n-1)!!} \text{Tr} \left( P_A (U^\dagger \hat{P} U)^{2n} U^\dagger [Q_{0,r}, U] \right)$$

To simplify our discussions below, we ignore the coefficient now and focus on the operator calculations. We use  $\nu_1$  to denote everything except the coefficient,

$$\begin{aligned}
\nu_1 &= \frac{(2n-1)!!}{(\pi i)^n} \nu_b^r & (5.38) \\
&= -\text{Tr} \left( P_A (U^\dagger \hat{P} U)^{2n} U^\dagger [Q_{0,r}, U] \right)
\end{aligned}$$

We can move  $P_A$  everywhere as  $P_A$  commutes with  $U$  in the bulk, for example,

$$\nu_1 = -\text{Tr}\left(U^\dagger P_A \hat{P} U (U^\dagger \hat{P} U)^{2n} U^\dagger [Q_{0,r}, U]\right)$$

Next we split  $U^\dagger [Q_{0,r}, U]$  into two parts  $U^\dagger [Q_{0,r}, U] = U^\dagger Q_{0,r} U - Q_{0,r}$  and apply the cyclicity of trace,

$$\nu_1 = \text{Tr}\left(U^\dagger P_A U (U^\dagger \hat{P} U)^{2n} Q_{0,r}\right) - \text{Tr}\left(P_A (U \hat{P} U^\dagger)^{2n} Q_{0,r}\right)$$

Which can be represented as the function of Z-form and Y-form,

$$\nu_1 = \text{Tr}\left(Z_{0,2n}^{2n} Q_{0,r}\right) - \text{Tr}\left(Y_{0,2n}^{2n} Q_{0,r}\right) \quad (5.39)$$

Since  $P_A$  commutes with  $U$  and  $P_A^2 = P_A$ , we can insert  $P_A$  anywhere in Eq. (5.39). In this way, we generalize the above identity,

$$\nu_1 = \text{Tr}\left(Z_{q_1, q_2, \dots, q_{s+1}}^{2n} Q_{0,r}\right) - \text{Tr}\left(Y_{q_1, q_2, \dots, q_{s+1}}^{2n} Q_{0,r}\right) \quad (5.40)$$

Multiply both sides by  $\sum_{i=1}^{s+1} e_i(\mathbf{q})$ ,

$$\sum_{i=1}^{s+1} e_i(\mathbf{q}) \nu_1 = \sum_{i=1}^{s+1} e_i(\mathbf{q}) \text{Tr}\left(Z_{q_1, q_2, \dots, q_{i+1}, \dots, q_{s+1}}^{2n} Q_{0,r}\right) - \text{Tr}\left(Y_{q_1, q_2, \dots, q_{i+1}, \dots, q_{s+1}}^{2n} Q_{0,r}\right)$$

Applying Eq. (5.33),

$$\left(\sum_{i=1}^{s+1} e_i(\mathbf{q})\right) \nu_1 = -\sum_{i=1}^{s+1} e_i(\mathbf{q}) \text{Tr}\left(Z_{q_1, q_2, \dots, q_{i+1}, \dots, q_{s+1}}^{2n} Q_{0,r}\right) \quad (5.41)$$

And the summation on the left side of above equation:

$$\begin{aligned} \sum_{i=1}^{s+1} e_i &= \sum_{i=1}^{s+1} -\frac{1 - (-1)^{q_i}}{2} (-1)^{\sum_{k=1}^{i-1} q_k} \\ &= \sum_{i=1}^{s+1} -\frac{(-1)^{\sum_{k=1}^{i-1} q_k} - (-1)^{\sum_{k=1}^i q_k}}{2} \\ &= -\frac{1 - (-1)^{\sum_{k=1}^{s+1} q_k}}{2} \\ &= -\frac{1 - (-1)^{2n-1}}{2} \\ &= -1 \end{aligned} \quad (5.42)$$

Therefore

$$-\nu_1 = \sum_{i=1}^{s+1} e_i(\mathbf{q}) \operatorname{Tr} \left( Z_{q_1, q_2, \dots, q_i+1, \dots, q_{s+1}}^{2n} Q_{0,r} \right) \quad (5.43)$$

To simplify discussions, we use  $x_{q_1, q_2, \dots, q_{s+1}}^{2n}$  to denote  $\operatorname{Tr} \left( Z_{q_1, q_2, \dots, q_{s+1}}^{2n} Q_{0,r} \right)$ . Then the above equation can be rewritten as

$$-\nu_1 = \sum_{i=1}^{s+1} e_i(\mathbf{q}) x_{q_1, q_2, \dots, q_i+1, \dots, q_{s+1}}^{2n} \quad (5.44)$$

#### 5.B.4 Two cyclic properties

If we add two equations in Eq. (5.31) and (5.44) together,

$$\nu_1 = x_{q_1+1, q_2, \dots, q_i, \dots, q_{s+1}}^{2n} + x_{q_1, q_2, \dots, q_i, \dots, q_{s+1}+1}^{2n} \quad (5.45)$$

This equation shows after moving a 1-form  $O$  from the left end to the right end or from the right end to the left end, the summation of the old trace and new trace is just one. This is a special law of ‘cyclic property’. After utilizing this equation  $q_1$  times,

$$\begin{aligned} x_{0, q_2, \dots, q_i, \dots, q_{s+1}+q_1}^{2n} &= \frac{1 - (-1)^{q_1}}{2} (\nu_1 - x_{q_1, q_2, \dots, q_i, \dots, q_{s+1}}^{2n}) + \frac{1 + (-1)^{q_1}}{2} x_{q_1, q_2, \dots, q_i, \dots, q_{s+1}}^{2n} \\ &= \frac{1 - (-1)^{q_1}}{2} \nu_1 + (-1)^{q_1} x_{q_1, q_2, \dots, q_i, \dots, q_{s+1}}^{2n} \end{aligned} \quad (5.46)$$

Next, we notice another ‘cyclic property’,

$$\begin{aligned} x_{0, q_2, \dots, q_i, \dots, q_{s+1}}^{2n} &= \operatorname{Tr} \left[ P_A^U O^{q_2} P_A^U \dots O^{q_s} P_A^U O^{q_{s+1}} Q_{0,r} \right] \\ &= \operatorname{Tr} \left[ O^{q_2} P_A^U \dots O^{q_s} P_A^U O^{q_{s+1}} P_A^U Q_{0,r} \right] \\ &= x_{q_2, \dots, q_i, \dots, q_{s+1}, 0}^{2n} \end{aligned} \quad (5.47)$$

where we make use of the cyclic property of the trace operator and  $Q_{0,r}$  commutes with  $P_A^U$  as  $r \rightarrow \infty$ .

### 5.B.5 Edge invariant

We will show how the truncated edge invariant give in Eq. (5.16) agrees with the truncated bulk invariant. First, we express the edge invariant in the differential form,

$$\begin{aligned}\nu_E^r &= \frac{(2\pi i)^n}{n!} \frac{1}{2^{2n+1}} \text{Tr} \left[ U^\dagger \mathcal{S} U (\hat{P}(U^\dagger \mathcal{S} U))^{2n} Q_{0,r} \right] \\ &= \frac{(2\pi i)^n}{n!} \frac{1}{2^{2n+1}} \text{Tr} \left[ U^\dagger \mathcal{S} U (\hat{P}(U^\dagger \mathcal{S} U))^{2n} Q_{0,r} \right]\end{aligned}\tag{5.48}$$

Next, we notice that

$$\text{Tr} \left[ (\hat{P}(U^\dagger \mathcal{S} U))^{2n} Q_{0,r} \right] = 0$$

This is because

$$\hat{P} \left[ (U^\dagger \mathcal{S} U) (\hat{P}(U^\dagger \mathcal{S} U))^{2n-1} Q_{0,r} \right] = \hat{P}(U^\dagger \mathcal{S} U) (\hat{P}(U^\dagger \mathcal{S} U))^{2n-1} Q_{0,r}$$

where the trace of the left side is zero and the trace of the right side is  $\text{Tr} \left[ (\hat{P}(U^\dagger \mathcal{S} U))^{2n} Q_{0,r} \right]$ .

As a result,

$$\begin{aligned}\nu_E^r &= \frac{(2\pi i)^n}{n!} \frac{1}{2^{2n+1}} \text{Tr} \left[ U^\dagger \mathcal{S} U (\hat{P}(U^\dagger \mathcal{S} U))^{2n} Q_{0,r} \right] \\ &= \frac{(2\pi i)^n}{n!} \text{Tr} \left[ U^\dagger P_A U (\hat{P}(U^\dagger P_A U))^{2n} Q_{0,r} \right]\end{aligned}\tag{5.49}$$

where we also substitute  $\mathcal{S} = 2P_A - 1$ .

Now we expand  $\hat{P}(U^\dagger P_A U)$ ,

$$\begin{aligned}\hat{P}(U^\dagger P_A U) &= P_A^U O - O P_A^U \\ &= P_A^U O P_B^U - P_B^U O P_A^U\end{aligned}$$

where we use  $P_B^U$  to denote  $U^\dagger P_B U$  and apply the identity  $P_B + P_A = \mathbb{I}$ . Using this equation, we can simplify  $U^\dagger P_A U (\hat{P}(U^\dagger P_A U))^{2n}$ ,

$$\begin{aligned}U^\dagger P_A U (\hat{P}(U^\dagger P_A U))^{2n} &= P_A^U (P_A^U O P_B^U - P_B^U O P_A^U)^{2n} \\ &= (P_A^U O P_B^U O P_A^U)^n \\ &= (P_A^U O P_B^U O)^n P_A^U\end{aligned}$$

where we also use  $P_A^U P_B^U = 0$ .

Hence, Eq.(5.49) can be rewritten as,

$$\begin{aligned}\nu_E^r &= \frac{(2\pi i)^n}{n!} \text{Tr} \left[ (P_A^U O P_B^U O)^n P_A^U Q_{0,r} \right] \\ &= \frac{(2\pi i)^n}{n!} \text{Tr} \left[ (P_A^U O P_B^U O)^n Q_{0,r} \right]\end{aligned}\quad (5.50)$$

where we use  $[Q_{0,r}, P_A^U] = 0$ .

### 5.B.6 Express edge invariants in differential forms

In this section, we want to calculate  $\nu_E^r$  in Eq. (5.51). To do this, we need to rewrite it in terms of  $x_{q_1, q_2, \dots, q_i, \dots, q_{s+1}}^{2n}$ . We first expand this equation,

$$\begin{aligned}\nu_E^r &= \text{Tr} \left[ (P_A^U O^2 - P_A^U O P_A^U O)^n Q_{0,r} \right] \\ &= \sum_{q_1=0}^1 \sum_{q_2=0}^1 \dots \sum_{q_n=0}^1 (-1)^{n - \sum_{i=1}^n q_i} \\ &\quad \text{Tr} \left[ (P_A^U O^2)^{q_1} (P_A^U O P_A^U O)^{1-q_1} \dots (P_A^U O^2)^{q_n} (P_A^U O P_A^U O)^{1-q_n} Q_{0,r} \right]\end{aligned}\quad (5.51)$$

Only a specific collection of  $x_{q_1, q_2, \dots, q_{s+1}}^{2n}$  where  $q_1 = 0, q_2 = q_3 = \dots = q_{s+1} = 1$  or 2 contributes to above equation. To represent this subset of  $x_{q_1, q_2, \dots, q_{s+1}}^{2n}$ , we can define another set of variables,

$$y_{p_1, p_2, \dots, p_{s+1}}^d = \text{Tr} \left[ (P_A^U O)^{p_1} O (P_A^U O)^{p_2} O (P_A^U O)^{p_3} \dots (P_A^U O)^{p_s} O (P_A^U O)^{p_{s+1}} Q_{0,r} \right] \quad (5.52)$$

where  $s$  denotes the total number of  $O$  between two  $P_A^U O$ . Since the operator inside the trace is a  $d$ -form,  $\sum_{i=1}^{s+1} p_i + s = d$ . when  $s = 0$ , the only possible configuration is  $y_{2n}^{2n} = \text{Tr} \left[ (P_A^U O)^{2n} Q_{0,r} \right]$ .

Then the we can express Eq. (5.51) in terms of  $y_{p_1, p_2, \dots, p_{s+1}}^{2n}$ ,

$$\nu_E^r = (-1)^n y_{2n}^{2n} + \sum_{s=1}^n (-1)^{n-s} \sum_{l_1=0}^n \sum_{l_2=0}^n \dots \sum_{l_s=0}^n \sum_{l_{s+1}=0}^n y_{2l_1+1, 2l_2+1, \dots, 2l_s+1, 2l_{s+1}}^{2n} \delta_{\sum_{j=1}^{s+1} (2l_j+1), 2n+1-s}$$

The constraint  $\delta_{\sum_{j=1}^{s+1} (2l_j+1), 2n+1-s}$  is applied to make sure  $\sum_{j=1}^s (2l_j + 1) + 2l_{s+1} + s = 2n$  because we only consider  $2n$ -form.

### 5.B.7 Calculate edge invariants

In this part, we will show how  $\nu_E^r$  can be written as a function of  $\nu_1$ .

By restricting  $q_1 = 0$ ,  $q_i = 1$  or  $2$  for  $i \geq 2$ , we can rewrite Eq. (5.44) as

$$\nu_1 = \sum_{i=2}^{2n-s+1} (-1)^{\sum_{k=1}^{i-1} q_k} x_{0,q_2,\dots,q_i+1,\dots,q_{2n-s+1}}^{2n} \delta_{q_i,1}$$

To simplify the following discussions, we can define another set of variables,  $z_{i_1,i_2,\dots,i_s}^d$  where  $i_1, i_2, \dots, i_s$  represents the position of  $O^2$ .  $z_{i_1,i_2,\dots,i_s}^d = x_{0,q_2,\dots,q_{d-s+1}}^d$  where  $q_{i_l} = 2$  for  $1 \leq l \leq k$  and  $q_i = 1$  for others. In this new representation, we only record the position of  $O^2$ . For example,  $z_{3,4}^6 = \text{Tr} \left[ P_A^U O P_A^U O^2 P_A^U O^2 P_A^U O \right]$ . Then the above equation can be expressed as a function of  $z$  if  $\{i_1, i_2, \dots, i_{s-1}\}$  denotes the the position of  $O^2$  in  $\mathbf{q} = (0, q_2, q_3, \dots, q_{2n-s+1})$ ,

$$\sum_{j=2}^{i_1-1} (-1)^j z_{j,i_2,\dots,i_{s-1}}^{2n} + \sum_{j=i_1+1}^{i_2-1} (-1)^{j+1} z_{i_1,j,i_2,\dots,i_{s-1}}^{2n} + \dots + \sum_{j=i_{s-1}}^{2n-s+1} (-1)^{j+s-1} z_{i_1,i_2,\dots,i_{s-1},j}^{2n} = \nu_1 \quad (5.53)$$

If we label  $i_0 = 1$  and  $i_s = 2n - s + 2$ , we can simplify the above equation as

$$\sum_{k=0}^{s-1} \sum_{j=i_k+1}^{i_{k+1}-1} (-1)^{j+k} z_{i_1,i_2,\dots,i_k,j,i_{k+1},\dots,i_{s-1}}^{2n} = \nu_1 \quad (5.54)$$

Applying the cyclic properties given in Eq. (5.45) and (5.45),

$$\begin{aligned} z_{i_1,i_2,\dots,i_s}^{2n} &= x_{0,q_2,\dots,q_{d-s+1}}^{2n} \\ &= \frac{1 - (-1)^{i_1-2}}{2} \nu_1 + (-1)^{i_1-2} x_{0,q_{i_1},\dots,q_{s+1}+q_1,q_2,\dots,q_{i_1-1}}^{2n} \end{aligned}$$

Since we have moved  $i_1 - 2$  number of  $O$  from the left to the right. After representing  $x_{0,q_{i_1},\dots,q_{s+1}+q_1,q_2,\dots,q_{i_1-1}}^{2n}$  in terms of  $z$ , we get

$$z_{i_1,i_2,\dots,i_s}^{2n} = \frac{1 - (-1)^{i_1}}{2} \nu_1 + (-1)^{i_1} z_{2,i_2-i_1+2,i_3-i_1+2,\dots,i_s-i_1+2}^{2n} \quad (5.55)$$

In addition, if we continue moving  $i_2 - i_1 + 1$  number of  $O$  from the left to the right,

$$\begin{aligned} & z_{2,i_2-i_1+2,i_3-i_1+2,\dots,i_s-i_{s-1}+2}^{2n} \\ &= \frac{1 + (-1)^{i_2-i_1}}{2} \nu_1 - (-1)^{i_2-i_1} z_{2,i_3-i_2+2,i_4-i_2+2,\dots,i_s-i_2+2,(d-s)+(i_1-i_2)+2}^{2n} \end{aligned} \quad (5.56)$$

To better describe this cyclic behavior, we now define a new function:

$$f^d(d_1, d_2, \dots, d_s) = z_{i_1=2, i_2, \dots, i_s}^d$$

where we use  $d_i$  to represent the distance between two neighboring indices of  $z_{i_1=2, i_2, \dots, i_s}^d$ . Specifically,  $d_1 = i_2 - i_1, d_2 = i_3 - i_2, \dots, d_s = 2n - s - (i_s - i_1)$ . Then  $d_i$  counts the number of the projectors  $P_A^U$  between two consecutive  $O^2$  and  $s$  means the number of  $O^2$ . For example,  $f^6(1, 3) = y_{2,3}^6 = \text{Tr} \left[ P_A^U O^2 P_A^U O^2 P_A^U O P_A^U O \right]$ .

In this way, we can rewrite Eq. (5.55) as

$$z_{i_1, i_2, \dots, i_s}^{2n} = \frac{1 - (-1)^{i_1}}{2} \nu_1 + (-1)^{i_1} f^{2n}(i_2 - i_1, i_3 - i_2, \dots, i_s - i_{s-1}, 2n - s - (i_s - i_1)) \quad (5.57)$$

and Eq. (5.56) as

$$\begin{aligned} & f^{2n}(i_2 - i_1, i_3 - i_2, \dots, i_s - i_{s-1}, 2n - s - (i_s - i_1)) \\ = & \frac{1 + (-1)^{i_2 - i_1}}{2} \nu_1 - (-1)^{i_2 - i_1} f^{2n}(i_3 - i_2, \dots, i_s - i_{s-1}, 2n - s - (i_s - i_1), i_2 - i_1) \end{aligned}$$

If we let  $d_1 = i_2 - i_1, d_2 = i_3 - i_2, \dots, d_s = (2n - s) - (i_s - i_1)$ ,

$$\begin{aligned} & f^{2n}(d_1, d_2, \dots, d_s) \quad (5.58) \\ = & \frac{1 + (-1)^{d_1}}{2} \nu_1 - (-1)^{d_1} f^{2n}(d_2, d_3, \dots, d_s, d_1) \end{aligned}$$

with  $\sum_{i=1}^s d_i = 2n - s$ . After repeating this equation  $k$  times, we get,

$$\begin{aligned} & f^{2n}(d_1, d_2, \dots, d_s) \quad (5.59) \\ = & \frac{1 - (-1)^{k + \sum_{i=1}^k d_i}}{2} \nu_1 + (-1)^{k + \sum_{i=1}^k d_i} f^{2n}(d_{k+1}, \dots, d_s, d_1, d_2, \dots, d_k) \end{aligned}$$

Plugging Eq. (5.57) into Eq. (5.54),

$$\begin{aligned} \nu_1 = & \sum_{j=2}^{i_1-1} (-1)^j \left[ \frac{1 - (-1)^j}{2} \nu_1 \right. \\ & + (-1)^j f^{2n}(i_1 - j, i_2 - i_1, \dots, i_{s-1} - i_{s-2}, 2n - s - (i_{s-1} - i_1)) \left. \right] \\ & + \sum_{k=1}^{s-1} \sum_{j=i_k+1}^{i_{k+1}-1} (-1)^{j+k} \left[ \frac{1 - (-1)^{i_1}}{2} \nu_1 \right. \\ & + (-1)^{i_1} f^{2n}(i_2 - i_1, i_3 - i_2, \dots, j - i_k, i_{k+1} - j, \dots, i_{s-1} - i_{s-2}, 2n - s - (i_{s-1} - i_1)) \left. \right] \end{aligned}$$

Then applying Eq. (5.58),

$$\begin{aligned}
\nu_1 &= \sum_{j=2}^{i_1-1} (-1)^j \left[ \frac{1 - (-1)^j}{2} \nu_1 \right. \\
&\quad \left. + (-1)^j f^{2n}(i_1 - j, i_2 - i_1, \dots, i_{s-1} - i_{s-2}, 2n - s - (i_{s-1} - i_1)) \right] \\
&\quad + \sum_{k=1}^{s-1} \sum_{j=i_k+1}^{i_{k+1}-1} (-1)^{j+k} \left[ \frac{1 - (-1)^{j+k}}{2} \nu_1 \right. \\
&\quad \left. + (-1)^{j+k} f^{2n}(i_{k+1} - j, \dots, i_{s-1} - i_{s-2}, 2n - s - (i_{s-1} - i_1), i_2 - i_1, \dots, j - i_k) \right]
\end{aligned}$$

After simplifying this equation,

$$\begin{aligned}
&\sum_{k=0}^{s-1} \sum_{j=i_k+1}^{i_{k+1}-1} f^{2n}(i_{k+1} - j, \dots, i_{s-1} - i_{s-2}, 2n - s - (i_{s-1} - i_1), i_2 - i_1, \dots, j - i_k) \\
&= \left[ 1 + \sum_{k=0}^{s-1} \sum_{j=i_k+1}^{i_{k+1}-1} \frac{1 - (-1)^{j+k}}{2} \right] \nu_1 \\
&= (n - s + 1) \nu_1
\end{aligned}$$

Let  $d_1 = i_2 - i_1, d_2 = i_3 - i_1, \dots, d_{s-2} = i_{s-1} - i_{s-2}, d_{s-1} = 2n - s - (i_{s-1} - i_1)$ , then we can rewrite the above equation as

$$(n - s + 1) \nu_1 = \sum_{k=1}^{s-1} \sum_{d'=1}^{d_k-1} f^{2n}(d_k - d', d_{k+1}, \dots, d_{s-2}, d_{s-1}, d_1, \dots, d_{k-1}, d')$$

We now can prove the following equalities for  $y_{p_1, p_2, \dots, p_{s+1}}^{2n}$

**Lemma 5.B.2** (i)  $y_{2n}^{2n} = \frac{1}{2} \nu_1$

(ii) When  $s \geq 1$ ,

$$\begin{aligned}
&\sum_{l_1=0}^n \sum_{l_2=0}^n \cdots \sum_{l_s=0}^n \sum_{l_{s+1}=0}^n y_{2l_1+1, 2l_2+1, \dots, 2l_s+1, 2l_{s+1}}^{2n} \delta_{\sum_{j=1}^{s+1} (2l_j+1), 2n+1-s} \\
&= \frac{n}{2n-s} (-1)^s \frac{n!}{s!(n-s)!}
\end{aligned}$$

**Proof:** (i)

$$\begin{aligned}
y_{2n}^{2n} &= \text{Tr} \left[ (P_A^U O)^{2n} Q_{0,r} \right] \\
&= x_{0,1,1,1,1,\dots,1}
\end{aligned}$$

Applying the first cyclic property given in Eq. (5.45), we have,

$$x_{1,1,1,1,\dots,1,0} + x_{0,1,1,1,1,\dots,1} = \nu_1$$

where we let  $q_1 = q_{s+1} = 0$  and  $q_2 = q_3 = \dots = q_s = 1$  in Eq. (5.45). Subsequently, we utilize the second cyclic property given in Eq. (5.47),

$$x_{1,1,1,1,\dots,1,0} = x_{0,1,1,1,1,\dots,1}$$

where we let  $q_2 = q_3 = \dots = q_{s+1} = 1$ . Therefore,

$$y_{2n}^{2n} = x_{0,1,1,1,1,\dots,1} = \frac{\nu_1}{2}$$

(ii) Consider  $y_{p_1, p_2, \dots, p_{s+1}}^d = x_{0, q_2, q_3, \dots, q_{d-s+1}}^d$  where  $q_j = 2$  for  $j = 1 + \sum_{i=1}^k p_i (1 \leq k \leq s)$  and  $q_j = 1$  for other indices. Therefore,  $y_{p_1, p_2, \dots, p_{s+1}}^d = z_{i_1, i_2, \dots, i_s}^d$  where  $i_k = 1 + \sum_{i=1}^k p_i (1 \leq k \leq s) (1 \leq k \leq s)$ . In other words,

$$z_{i_1, i_2, \dots, i_s}^d = y_{i_1-1, i_2-i_1, \dots, i_s-i_{s-1}, 2n-s+1-i_s}^d$$

Substitute all  $y$  by  $z$  in the following summation,

$$\begin{aligned} & \sum_{l_1=0}^n \sum_{l_2=0}^n \dots \sum_{l_s=0}^n \sum_{l_{s+1}=0}^n y_{2l_1+1, 2l_2+1, \dots, 2l_s+1, 2l_{s+1}}^{2n} \delta_{\sum_{j=1}^{s+1} (2l_j+1), 2n+1-s} \\ = & \sum_{l_1=0}^n \sum_{l_2=0}^n \dots \sum_{l_s=0}^n \sum_{l_{s+1}=0}^n z_{1+\sum_{i=1}^1 (2l_i+1), 1+\sum_{i=1}^2 (2l_i+1), \dots, 1+\sum_{i=1}^s (2l_i+1)}^{2n} \delta_{\sum_{j=1}^{s+1} (2l_j+1), 2n+1-s} \end{aligned}$$

After applying (5.57), the rhs. becomes

$$\begin{aligned} & \sum_{l_1=0}^n \sum_{l_2=0}^n \dots \sum_{l_s=0}^n \sum_{l_{s+1}=0}^n \\ & f^{2n}(2l_2+1, 2l_3+1, \dots, 2l_s+1, 2n-s - \sum_{i=2}^s (2l_i+1)) \delta_{\sum_{j=1}^{s+1} (2l_j+1), 2n+1-s} \\ = & \sum_{l'_1=0}^n \sum_{l'_2=0}^n \dots \sum_{l'_s=0}^n f^{2n}(2l'_1+1, 2l'_2+1, 2l'_3+1, \dots, 2l'_s+1) \frac{2l'_s+1}{2} \delta_{\sum_{j=1}^s (2l_j+1), 2n-s} \end{aligned}$$

By relabelling indices, the lhs. becomes

$$\begin{aligned}
& \sum_{l'_1=0}^n \sum_{l'_2=0}^n \dots \sum_{l'_s=0}^n f^{2n}(2l'_1 + 1, 2l'_2 + 1, \dots, 2l'_s + 1) \frac{2l'_s + 1}{2} \delta_{\sum_{j=1}^s (2l_j+1), 2n-s} \\
&= \sum_{l'_1=0}^n \sum_{l'_2=0}^n \dots \sum_{l'_s=0}^n f^{2n}(2l'_2 + 1, 2l'_3 + 1, \dots, 2l'_s + 1, 2l'_1 + 1) \frac{2l'_1 + 1}{2} \delta_{\sum_{j=1}^s (2l_j+1), 2n-s} \\
&= \dots \\
&= \sum_{l'_1=0}^n \sum_{l'_2=0}^n \dots \sum_{l'_s=0}^n f^{2n}(2l'_s + 1, 2l'_1 + 1, 2l'_2 + 1, \dots, 2l'_{s-1} + 1) \frac{2l'_{s-1} + 1}{2} \delta_{\sum_{j=1}^s (2l_j+1), 2n-s}
\end{aligned}$$

Summarizing all equations and applying the cyclic properties in Equation (5.58), we have,

$$\begin{aligned}
& \sum_{l'_1=0}^n \sum_{l'_2=0}^n \dots \sum_{l'_s=0}^n f^{2n}(2l'_1 + 1, 2l'_2 + 1, 2l'_3 + 1, \dots, 2l'_s + 1) \frac{2l'_s + 1}{2} \delta_{\sum_{j=1}^s (2l_j+1), 2n-s} \quad (5.60) \\
&= \frac{n}{k} \sum_{l'_1=0}^n \sum_{l'_2=0}^n \dots \sum_{l'_s=0}^n f^{2n}(2l'_1 + 1, 2l'_2 + 1, 2l'_3 + 1, \dots, 2l'_s + 1) \delta_{\sum_{j=1}^s (2l_j+1), 2n-s} \quad (5.61)
\end{aligned}$$

Expand

$$(n - s + 1)\nu_1 = \sum_{d'_1} \sum_{d'_2} \dots \sum_{d'_s} f^{2n}(d'_1, d'_2, \dots, d'_s) \sum_{k=1}^{s-1} \sum_{d'=1}^{d_k-1} \delta_{d'_1, d_k-d'} \delta_{d'_2, d_{k+1}} \dots \delta_{d'_s, d'}$$

Then summerizing over all  $d_1, d_2, \dots, d_{s-1}$ ,

$$\begin{aligned}
& \sum_{d_1=1}^{2n-s} \sum_{d_2=1}^{2n-s} \dots \sum_{d_{s-1}=1}^{2n-s} (n - s + 1) \delta_{\sum_{j=1}^{s-1} d_j, 2n-s} \nu_1 \\
&= \sum_{d'_1} \sum_{d'_2} \dots \sum_{d'_s} f^{2n}(d'_1, d'_2, \dots, d'_s) (s - 1) \delta_{\sum_{j=1}^s d'_j, 2n-s}
\end{aligned}$$

After applying the cyclic properties in Equation. (5.58), we cancelled all terms with even distances ( $\exists i, d_i$  is even) on the right-hand side,

$$\begin{aligned}
& \sum_{l'_1=0}^n \sum_{l'_2=0}^n \dots \sum_{l'_s=0}^n f^{2n}(2l'_1 + 1, 2l'_2 + 1, 2l'_3 + 1, \dots, 2l'_s + 1) \delta_{\sum_{j=1}^s (2l_j+1), 2n-s} \\
&= \frac{s}{2n-s} (-1)^s \frac{n!}{s!(n-s)!} \nu_1
\end{aligned}$$

Combined with (5.61), we have

$$\begin{aligned} & \sum_{l'_1=0}^n \sum_{l'_2=0}^n \cdots \sum_{l'_s=0}^n f^{2n}(2l'_1+1, 2l'_2+1, 2l'_3+1, \dots, 2l'_s+1) \frac{2l'_s+1}{2} \delta_{\sum_{j=1}^s (2l_j+1), 2n-s} \\ &= \frac{n}{2n-s} (-1)^s \frac{n!}{s!(n-s)!} \nu_1 \end{aligned}$$

where the left hand side is equal to

$$\sum_{l_1=0}^n \sum_{l_2=0}^n \cdots \sum_{l_s=0}^n \sum_{l_{s+1}=0}^n y_{2l_1+1, 2l_2+1, \dots, 2l_s+1, 2l_{s+1}}^{2n} \delta_{\sum_{j=1}^{s+1} (2l_j+1), 2n+1-s}.$$

□

### 5.B.8 Connection between edge invariants and bulk invariants

Combining the two equations given in Lemma 5.B.2,

$$\begin{aligned} & \text{Tr} \left[ (PA^2 - PAPAPA)^n P_{2n+1} \right] \\ &= \sum_{s=0}^n \frac{n}{2n-s} (-1)^s \frac{n!}{s!(n-s)!} \\ &= \frac{(-1)^n}{(2n-1)!!} \frac{n!}{2^n} \nu_1 \end{aligned}$$

Finally, we prove the bulk edge correspondence

$$\begin{aligned} \nu_E^r &= \frac{(2\pi i)^n}{n!} \text{Tr} \left[ (PA^2 - PAPAPA)^n P_{2n+1} \right] \\ &= \nu_b^r (-1)^n \end{aligned} \tag{5.62}$$

# CHAPTER 6

## Classification of class AII

In this chapter, we characterize the topological properties of two dimensional periodic driven systems with time reversal symmetry. In addition, we obtain the bulk edge correspondence inside this system which is known as Class AII of the Altland-Zirnbauer symmetry classification [1, 49].

The rest of the chapter is organized as follows. We begin, in Sec. II, by giving some background on time-dependent systems and the concepts we will use in obtaining the bulk-boundary correspondence. In Sec. III we define a new edge invariant which is physically motivated, locally computable, and applicable to systems both with and without disorder, and give an example how to apply it in a model drive. We study the properties of the edge index in Sec. IV. Finally, we propose a bulk invariant which can be applied in the disordered systems and derive the bulk-edge correspondence in Sec. V.

### 6.1 Driven Systems with time reversal Symmetry

#### 6.1.1 Time reversal symmetry

In this section, we will study topological drives with time-reversal symmetry, corresponding to Class AII of the AZ classification scheme. For time-reversal symmetry (TRS), the symmetry operator takes the form of  $\mathcal{T} = \mathcal{K}\mathcal{T}$  where  $\mathcal{K}$  is still the complex conjugation and  $\mathcal{T}$  is unitary. Here are the constraints the operator applies to the system [1, 49]:

$$\mathcal{T}H(t)\mathcal{T}^{-1} = H(T - t) \tag{6.1}$$

$$\mathcal{T}U(t)\mathcal{T}^{-1} = U(T - t)U^\dagger(T) \tag{6.2}$$

where we have used the fact that the Hamiltonian is periodic in time with period. At the end of one cycle, the time-evolution operator satisfies

$$\mathcal{T}U(T)\mathcal{T}^{-1} = U^\dagger(T), \quad (6.3)$$

### 6.1.2 Examples

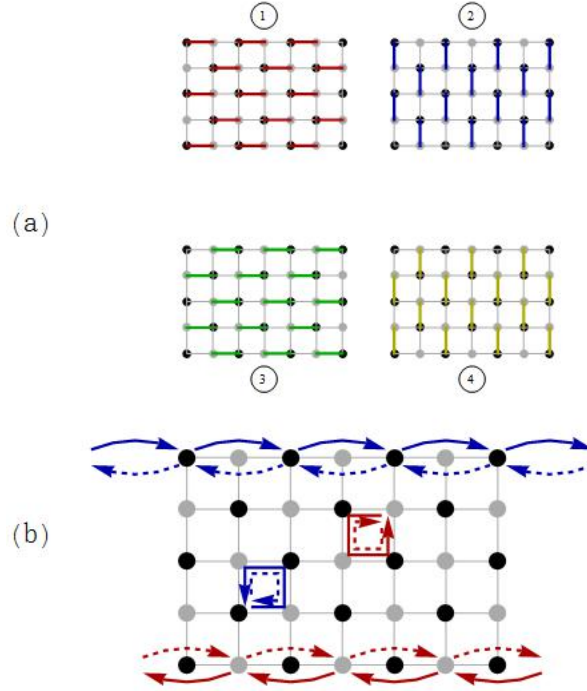


Figure 6.1: The action of the 2D class AII drive introduced in Ref. [5]. (a) Driving protocol. The only nonvanishing hopping amplitudes between sites are represented for each time step. Spin up states moves according to the sequence  $1 \rightarrow 2 \rightarrow 3 \rightarrow 4$  while spin-down states follows the opposite sequence  $4 \rightarrow 3 \rightarrow 2 \rightarrow 1$ . (b) During each step, particles hop between sites on a bipartite lattice, following the paths indicated by red and blue arrows. This is done for spin-up (solid lines) and spin-down (dashed lines). Sublattices are indicated by gray and black points. After a complete cycle, a particle in bulk returns to its initial position, while a particle at the edge is translated by one unit cell.

To better understand the time-reversal symmetric system, we construct a model drive in this symmetry class with nontrivial topological properties. A simple way to do this is to

define a nontrivial evolution for spin-up states and then deduce an evolution for spin-down states according to the time-reversal symmetry. [12] In this way, we consider a two-layer Rudner model with a piece-wise Hamiltonian. [5] During each step of the evolution, the Hamiltonian takes the diagonal form of

$$H_n = \begin{pmatrix} H_n^{\uparrow\uparrow} & 0 \\ 0 & H_n^{\downarrow\downarrow} \end{pmatrix} \quad (6.4)$$

where  $H_n^{\uparrow\uparrow}(H_n^{\downarrow\downarrow})$  controls the motion of spin up(down) states.

$$H_n^{\uparrow\uparrow} = \sum_{\vec{r} \in A} \sum_{n=1}^4 J_n(t) (c_{\vec{r}+\vec{b}_n} c_{\vec{r}} + h.c.) \quad (6.5)$$

where  $c_{\vec{r}}$  is the fermionic annihilation operator on the lattice site with coordinate  $\vec{r}$ , and the first sum runs over sites  $\vec{r}$  on sublattice A. The vectors  $\vec{b}_n$  are given by  $\vec{b}_1 = -\vec{b}_3 = (a, 0)$  and  $\vec{b}_2 = -\vec{b}_4 = (0, a)$ , where  $a$  is the lattice constant. There are four steps in total and for nth step,  $J_n(t) = J$  where all other hopping amplitudes are zero and  $J \frac{T}{4} = \frac{\pi}{2}$ . Then the evolution operator  $U(t)$  is block diagonal in the spin basis and thus can be written as:

$$U(t) = \begin{pmatrix} U_{\uparrow}(t) & 0 \\ 0 & U_{\downarrow}(t) \end{pmatrix}$$

Put our diagonal Hamiltonian into Eq. (6.1), we find that  $H^{\downarrow\downarrow}(t) = (H^{\uparrow\uparrow}(T-t))^*$ . Thus the spin down states is a time-reversed copy of the spin up states. After a full period, each particle away from the edge returns to its initial position and thus the full evolution unitary is identity. On the edge, however, spin up  $\uparrow$  moves by one unit cell to the right along the upper edge while spin down  $\downarrow$  moves in the opposite direction.

In this example, the z-component of spin is conserved. Therefore we can classify the whole system by calculating the winding number of each block unitary. According to reference [5],

$$W[U] = \frac{1}{8\pi^2} \int dt dk_x dk_y \times \text{Tr}(U^\dagger \partial_t U [U^\dagger \partial_{k_x} U, U^\dagger \partial_{k_y} U]) \quad (6.6)$$

We can see that  $W_{\uparrow} = W[U_{\uparrow}]$  is one. Namely, the net flow for the spin-up states is 1. Then the  $Z_2$  index for our time-reversal symmetric system is  $W[U_{\uparrow}] \bmod 2$  which is like a "spin winding number." However, this simple formula only works when spin-up states are decoupled from the spin-down states. If there are couplings between the spin up and spin down states, classification becomes much more complicated, and we need to derive a new set of topological invariants for these systems.

### 6.1.3 Zero Kitaev flow

In this paper, we mainly study unitary loops, satisfying  $U(0) = U(T) = \mathbb{I}$  in a close system where  $T$  is the period of this evolution. In an open system, a unitary of this form may generate nontrivial chiral edge modes along the boundary. Thus the evolution unitary at the end of a complete cycle in an open system can be decomposed as:

$$U_o(T) = U_b(T) \oplus U_e(T) = I \oplus U_e(T) \tag{6.7}$$

where the bulk and edge degrees of freedom are explicitly decoupled. Despite the apparently trivial bulk Floquet operator, the dynamics of the system may be nontrivial at the edge. Then  $U_e(T)$  is the unitary which describes the behavior on the edge. Since our system is two dimensional, the edge operator is an one dimensional operator. The first idea to classify the system is to use the quantized Kitaev flow index.[31] We have a discussion of this flow index in 4.1.1.

It's found that the kitaev flow index can be used to classify the edge behavior of two-dimensional Floquet systems. [62] The behavior related to a nontrivial index can be understood as a nonadiabatic quantized charge pumping. In other words, this index counts the net number of particles(states) that move to the right side of a cut from the left side after a complete cycle. The idea of a topological pump was first proposed by Thouless[63] and was always studied with a slow driving frequency where we can use the adiabatic theorem. But now, in Floquet systems, we can have considered systems with high frequencies, and we don't

need to assume that the Hamiltonian should be gapped all the time.

To better understand the edge behavior of systems with time reversal symmetry, first we notice that the kitaev flows for these systems are always zero. The flow of a unitary matrix maybe written as

$$\nu[U_e] = \text{Tr}(U_e^\dagger P U_e - P) \quad (6.8)$$

where the projector  $P$  acts on the left side of a cut.

Next, we apply the time reversal operator,

$$\begin{aligned} \nu[U_e] &= \text{Tr}(\mathcal{T}U_e^\dagger P U_e \mathcal{T}^{-1} - \mathcal{T}P\mathcal{T}^{-1}) \\ &= \text{Tr}(U_e P U_e^\dagger - P) \end{aligned} \quad (6.9)$$

After doing a unitary transformation,

$$\begin{aligned} \nu[U_e] &= -\text{Tr}(U_e(U_e^\dagger P U_e - P)U_e^\dagger) \\ &= -\text{Tr}(U_e^\dagger P U_e - P) \end{aligned} \quad (6.10)$$

Combined with (6.8), it's clear that

$$\text{Tr}(U_e^\dagger P U_e - P) = 0 \quad (6.11)$$

Therefore, the net flow of the whole system is always zero. We need to find a new way to construct topological invariants for systems with time-reversal symmetry.

#### 6.1.4 Construction of edge invariant

In one dimension, a nontrivial unitary can always transport some states from the left side of a cut to the right side.

To describe this transport behavior, we study this ‘flow’ operator of a a one dimensional locality-preserving unitary operator  $Y$  [33],

$$A = Q - P = Y^\dagger P Y - P \quad (6.12)$$

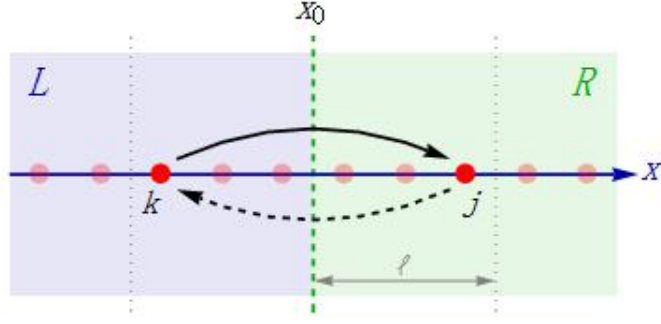


Figure 6.2: The flow of a time-reversal symmetric unitary matrix. Vertical dashed green line locates at the cross-section  $x_0$ , separating the regions  $L$  and  $R$ . Red points indicate 1D lattice sites host Hilbert space of even dimensions which includes states  $(|\phi\rangle)$  and their time-reversed partners  $(\mathcal{T}|\phi\rangle)$ . The solid black arrow represents the hoppings between states on sites  $j$  and  $k$  across the cut, while the dashed arrow denotes the movement of the corresponding time-reversed partners. For example, in the preceding section, the solid arrow corresponds to spin up states while the dashed arrow is associated with the spin-down states. Since a state moves in the opposite direction compared to its time-reversed partner, their total contribution to the Kitaev flow, associated with the charge pumping from region  $L$  to region  $R$ , is zero.

where  $P$  is a projector acting on the right side of a cut. Clearly, this operator  $A$  is the difference between two projectors  $Q$  and  $P$ . Since  $Y$  is a locality preserving unitary,  $Y^+PY$  is different from  $P$  only inside a small range. Thus  $A$  is a finite size matrix.

To have a better understanding of the information contained in operator  $A$ , we first study the eigenspaces of  $A$ . [33]

$$\begin{aligned}
 \mathcal{H}_{11}^A &= \{\phi \in \mathcal{H} | P\phi = Q\phi = \phi\} \\
 \mathcal{H}_{00}^A &= \{\phi \in \mathcal{H} | P\phi = Q\phi = 0\} \\
 \mathcal{H}_{10}^A &= \{\phi \in \mathcal{H} | Q\phi = \phi, P\phi = 0\} \\
 \mathcal{H}_{01}^A &= \{\phi \in \mathcal{H} | Q\phi = 0, P\phi = \phi\}
 \end{aligned} \tag{6.13}$$

Because the two projectors  $P$  and  $Q$  can only have eigenvalues zero and one, the eigenvalues of  $A$  are between  $-1$  and  $+1$ . The  $+1$  eigenvalue of  $A$  is reached only when there exists a

state that is both the +1 eigenvector of  $Q$  and the zero eigenvector of  $P$ . Since

$$-1 \leq \langle \phi | (Y^\dagger P Y - P) | \phi \rangle \leq 1, \quad (6.14)$$

one obtains that

$$(Y^\dagger P Y - P) | \phi \rangle = | \phi \rangle \quad (6.15)$$

if and only if  $P | \phi \rangle = 0$  and  $Y^\dagger P Y | \phi \rangle = | \phi \rangle$ . Therefore the +1 eigenspace of  $A$  is just  $\mathcal{H}_{10}^A$ .

Now, let's explain the physical meaning of these different eigenspaces. A state inside the Hilbert space  $\mathcal{H}_{00}^A$  is the eigenvector of  $P$  with eigenvalue 0 and the eigenvector of  $Q = Y^\dagger P Y$  with eigenvalue 0. That is, a state starting from the left side of a cut stays at the left side of the cut after a unitary evolution  $Y$ . Therefore  $\mathcal{H}_{00}$  includes the states 'far left from the cut'. Similarly,  $\mathcal{H}_{11}$  are related to the regions 'far-right from the cut'. To the opposite,  $\mathcal{H}_{10}$  and  $\mathcal{H}_{01}$  match the regions 'close to the cut'. Inside the Hilbert space  $\mathcal{H}_{10}$ , a state  $| \phi \rangle$  is not the eigenvector of  $P$ , which means that  $| \phi \rangle$  is related to the left side of the cut which is covered by  $1 - P$ . At the same time,  $| \phi \rangle$  is the eigenvector of  $Q$ :

$$Y^\dagger P Y | \phi \rangle = | \phi \rangle \quad (6.16)$$

which can be rewritten as

$$P Y | \phi \rangle = Y | \phi \rangle \quad (6.17)$$

Physically, the unitary  $Y$  pumps the state  $| \phi \rangle$  from the left side to the right side of the cut.

To construct the topological index of a time-reversal system, we seek a way to measure the continuous flow from the left to the right (the full shift of a particle from the left side to the right side). From the above analysis, a natural candidate is the dimension of  $\mathcal{H}_{10}$  which calculates the number of states which move from the left side to the right side across the cut.

$$\nu_1[Y] = \dim(\mathcal{H}_{10}^A) = \dim(\ker(A - 1)) \pmod{2} \quad (6.18)$$

where  $\dim \ker O$  stands for the dimension of the kernel of an operator  $O$ , i.e. the nullspace of  $O$ . This is because  $\mathcal{H}_{10}$  denotes the +1 eigenspace of  $A$ .

Similarly, the flow from the right side to the left side can be written as

$$\nu_2[Y] = \dim(\mathcal{H}_{01}) = \dim(\ker(A + 1)) \pmod{2} \quad (6.19)$$

And the relationship between the Kitaev flow index and our two new flow indexes  $\nu_1[Y]$  and  $\nu_2[Y]$  is [64]

$$\nu[Y] = \dim(\ker(A - 1)) - \dim(\ker(A + 1)) = \text{Tr}(A)$$

Combining with the fact that the Kitaev flow is zero for any systems with time-reversal symmetries, we reach the equivalence

$$\nu_1[Y] = \nu_2[Y] \quad (6.20)$$

Hence, we can use any one of them to be the  $Z_2$  index of the time-reversal symmetry system.

In a physical system, the Hamiltonian always satisfies a particular locality constraint, making the generated unitary quasi-diagonal. In other words, the matrix elements of the unitary decay exponentially (or faster) with the distance between the sites involved. In the following discussion, to simplify the proof, we consider the unitary, which is strictly local, i.e.,  $U_{jk}$  vanishes if the distance between two positions  $j$  and  $k$  is larger than the localization length  $l$ . Under the assumption of locality, it's clear that only the regions close to our cutting  $x = x_0$  will contribute to the calculation of the  $Z_2$  index.

After considering two contiguous intervals of sites  $L^l$  and  $R^l$  which are at the left and right side of the cut respectively, we can then define two projectors  $P_L^l$  and  $P_R^l$  which are hosted by Region  $L$  and  $R$  correspondingly. The size of the region  $L^l$  and  $R^l$  are both  $l$ . If we set the coordinate of the cut to be  $x_0 = 0$ , then  $L^l$  and  $R^l$  are  $[-l, 0)$  and  $[0, l]$  separately. Then we notice that the matrix

$$A = Y^\dagger P Y - P = Y^\dagger P Y (1 - P) - Y^\dagger (1 - P) Y P \quad (6.21)$$

can be simplified as

$$A = Y^\dagger P_R^l Y P_L^l - Y^\dagger P_L^l Y P_R^l \quad (6.22)$$

To develop some intuitive understanding of the index, we now consider two simple examples. If  $Y$  is the identity operator  $\mathbb{I}$ , then the only eigenvalue of  $A$  is zero. Clearly  $\dim(\ker(A - 1)) = 0$ . This is reflective of the fact that the unitary operator  $\mathbb{I}$  does not create any particle current between the two sides of the cut.

As a second example, we consider the unitary  $Y = \hat{t}S_{\uparrow} \oplus \hat{t}^{\dagger}S_{\downarrow}$  where  $\hat{t}$  is the unit right translation operator and  $\hat{t}(\hat{t}^{\dagger})$  act at the spin-up (spin-down) subspace. The Lieb-Robinson length of  $Y$  is 1 and thus the truncation length of  $L$  and  $R$  can be chosen to be 1 separately. If we cut between site  $x$  and site  $x + 1$ , then  $P_L^l = P_x$  and  $P_R^l = P_{x+1}$ .

$$\begin{aligned} A &= P_x \otimes s_+ - P_{x+1} \otimes s_- \\ &= |x, \uparrow\rangle \langle x, \uparrow| - |x + 1, \downarrow\rangle \langle x + 1, \downarrow| \end{aligned} \tag{6.23}$$

Thus the dimension of the +1 eigenspace of  $A$  is 1 and the dimension of the -1 eigenspace of  $A$  is also 1. The index  $\nu = 1$ .

## 6.2 The Edge index

### 6.2.1 Properties of the operator $A$

The preceding section has shown that the eigenspectrum of  $A$  can offer us an opportunity to understand better the transport behavior of a one dimensional unitary  $Y$ . In this section, we are going to study the properties of operator  $A$  in detail. Our derivation is inspired by an analogous derivation in Ref. [65].

First, we introduce a second operator[64]

$$B = 1 - P - Q = 1 - Y^+PY - P$$

Then as in [64],the following relation holds:

$$\begin{aligned} AB + BA &= 0 \\ A^2 + B^2 &= 1 \end{aligned} \tag{6.24}$$

Consider an eigenvector of the operator  $A$   $|\phi\rangle$  with an eigenvalue  $\lambda$  which satisfies  $0 < \lambda < 1$ . Then, the anticommutation relation of (6.24) yields

$$AB|\phi\rangle = -BA|\phi\rangle = -\lambda B|\phi\rangle$$

There is a one-to-one correspondence between the states  $|\phi\rangle$  and  $B|\phi\rangle$ , and their eigenvalues come in pairs  $\pm\lambda$ , provided  $0 < |\lambda| < 1$ .

since the unitary operator  $Y$  follows time-reversal symmetry (6.3):

$$\mathcal{T}Y\mathcal{T}^{-1} = Y^\dagger \quad (6.25)$$

Now we can build a relation between  $A$  and the time-reversal symmetric operator  $\mathcal{T}$ . After doing some algebraic calculations:

$$\begin{aligned} \mathcal{T}A &= \mathcal{T}(Y^\dagger P Y - P) \\ &= (Y P Y^\dagger - P)\mathcal{T} \\ &= Y(P - Y^\dagger P Y)Y^\dagger \mathcal{T} \\ &= -Y A Y^\dagger \mathcal{T} \end{aligned}$$

We find out an anticommutation relation

$$Y^\dagger \mathcal{T} A = -A Y^\dagger \mathcal{T} \quad (6.26)$$

Similarly, we can prove the commutation relation as follows,

$$Y^\dagger \mathcal{T} B = B Y^\dagger \mathcal{T} \quad (6.27)$$

Now let's see how the time-reversal transformation plays a similar role as the operator  $B$ . Let  $|\phi\rangle$  be an eigenvector of  $A$  with a strictly positive eigenvalue, i.e.,  $A|\phi\rangle = \lambda|\phi\rangle$ . Then according to Eq. (6.26)

$$A Y^\dagger \mathcal{T} |\phi\rangle = -Y^\dagger \mathcal{T} A |\phi\rangle \quad (6.28)$$

Therefore,

$$A Y^\dagger \mathcal{T} |\phi\rangle = -\lambda Y^\dagger \mathcal{T} |\phi\rangle \quad (6.29)$$

This implies that  $Y^\dagger \mathcal{T} |\phi\rangle$  is an eigenvector of  $A$  with eigenvalue  $-\lambda$ . Now both  $B$  and  $Y^\dagger \mathcal{T}$  define a map from the eigenspace  $\lambda$  to  $-\lambda$ . It's obvious that  $BY^\dagger \mathcal{T} |\phi\rangle$  and  $Y^\dagger \mathcal{T} B |\phi\rangle$  are both the eigenvectors of  $A$  with eigenvalue  $\lambda$ . As a result of (6.27), these two vectors are actually the same,

$$BY^\dagger \mathcal{T} |\phi\rangle = Y^\dagger \mathcal{T} B |\phi\rangle \quad (6.30)$$

Due to the anticommutation relation given in Eq. (6.24) and Eq. (6.26),

$$AY^\dagger \mathcal{T} B |\phi\rangle = -\lambda Y^\dagger \mathcal{T} B |\phi\rangle \quad (6.31)$$

two vectors  $|\phi\rangle$  and  $Y^\dagger \mathcal{T} B |\phi\rangle$  are eigenvectors of the operators  $A$  with the same eigenvalue  $\lambda$ . The dimension of the  $\lambda$  eigenspace will be even if these two vectors are linearly independent of each other. Now we show that if  $\phi$  is an eigenvector of  $A$  with eigenvalue  $\lambda$  which meets the constraint  $0 < |\lambda| < 1$ , then

$$\langle \phi | Y^\dagger \mathcal{T} B |\phi\rangle = 0 \quad (6.32)$$

First, following from the properties of an antiunitary,

$$\langle \mathcal{T} \phi | \mathcal{T} \psi \rangle = \langle \phi | \psi \rangle^* = \langle \psi | \phi \rangle \quad (6.33)$$

We substitute  $|\psi\rangle$  as  $Y^\dagger \mathcal{T} B |\phi\rangle$  then the left side of the above equation becomes

$$\begin{aligned} \langle \mathcal{T} \phi | \mathcal{T} Y^\dagger \mathcal{T} B \phi \rangle &= \langle \mathcal{T} \phi | Y \mathcal{T}^2 B \phi \rangle \\ &= -\langle \mathcal{T} \phi | Y B \phi \rangle \\ &= -\langle B Y^\dagger \mathcal{T} \phi | \phi \rangle \\ &= -\langle Y^\dagger \mathcal{T} B \phi | \phi \rangle \end{aligned}$$

And the right side becomes

$$\langle \psi | \phi \rangle = \langle Y^\dagger \mathcal{T} \phi B | \phi \rangle$$

Thus, we arrive at our desired result, two vectors are linearly independent,

$$\langle Y^\dagger B \mathcal{T} \phi | \phi \rangle = 0$$

Overall, the eigenspectrum of a transport operator  $A$  is symmetric about the eigenvalue  $\lambda = 0$ . In addition, the multiplicity of the eigenvalue  $\lambda$  of the operator  $A$  must be even when  $\lambda$  satisfies  $0 < |\lambda| < 1$ .

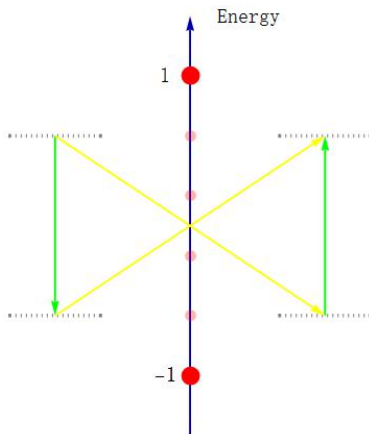


Figure 6.3: An illustration of the Eigenvalue spectrum of operator  $A$ . Red dots indicate different eigenvalues, while the dashed lines represent the eigenvectors. The green Arrow symbolizes the action of the mapping  $B$ , and the yellow arrows denote the mapping  $Y^\dagger \mathcal{T}$ , between two eigenvectors with opposite eigenvalues. After these two mappings, a state is mapped to another state with the same eigenvalue. Therefore each energy level between  $-1$  and  $+1$  is double degenerate.

### 6.2.2 Robustness of the index

Now it's natural to ask whether this index is invariant under smooth physical transformations. If it's not, then this index can not be treated as the edge invariant.

First, We can study this question from the properties of operator  $A$ . As shown in the last section, the multiplicity of the eigenvalue  $\lambda$  of the operator  $A$  must be even when  $0 < |\lambda| < 1$ . Thus, when the eigenvalues of  $A$  changes continuously under a continuous deformation of the unitary  $Y$ , the parity of the multiplicity of the  $\pm 1$  must be invariant under a smooth transformation of the unitary. There will be two possibilities: a) An even number of eigenvectors of  $A$  are lifted from the sector spanned by the eigenvectors of  $A$

with the eigenvalue  $\lambda = 1$ ; (b) an even number of eigenvectors of  $A$  with eigenvalue  $\lambda = 1$  become degenerate with the eigenvectors of  $A$  with the eigenvalue  $\lambda = 1$ . In both cases, it is enough to prove the continuity of the eigenvalues of the operator  $A$  under deformation of the Hamiltonian. The logic for the eigenvalue  $-1$  is the same.

Consider two locality-preserving unitaries which satisfies (6.3),  $U(0)$  and  $U(1)$ , together with a smooth interpolation  $U(s)$  respecting (6.3) between them, parametrized by  $s \in [0, 1]$ . Define the difference between two unitaries:

$$\gamma(s) = U(s)U^\dagger(0). \quad (6.34)$$

For small  $\delta s$ , we expand the gamma operator as:

$$\gamma(s + \delta s) = \gamma(s)(1 - i\delta s h(s) + \dots) \quad (6.35)$$

where  $h(s)$  is a Hermitian operator because  $\gamma(s)$  is also a locality preserving unitary.

$$A(s) = U^\dagger(s)PU(s) - P \quad (6.36)$$

$$A(s + \delta s) = U^\dagger(s + \delta s)P(s + \delta s) - P \quad (6.37)$$

Consider the difference between  $A(s + \delta s)$  and  $A(s)$

$$\begin{aligned} & A(s + \delta s) - A(s) \quad (6.38) \\ &= (1 + i\delta s h(s))U^\dagger(s)PU(s)(1 - i\delta s h(s)) - P \\ &- (U^\dagger(s)PU(s) - P) \\ &= i\delta s [h(s), U^\dagger(s)PU(s)] \end{aligned}$$

because  $h(s)$  is a local operator, thus  $[h(s), U^\dagger(s)PU(s)]$  is finite. Therefore,  $A(s)$  changes continuously as the parameter  $s$  changes. Together with above analysis, we know that the index of  $A(s)$  is robust.

### 6.2.3 Properties of the index

Here we provide an explicit derivation of some of the claims on the properties of the chiral unitary index.

(a) Parallel chains.

$$\nu_1[U_1 \oplus U_2] = \nu_1[U_1] + \nu_1[U_2] \quad (6.39)$$

Because for a unitary taking the block diagonal form, the dimension of its +1 eigenspace should be the addition of the dimension of +1 eigenspace for each block unitary.

(b)

$$\nu_1[U] = \nu_1[U^\dagger] \quad (6.40)$$

$P - UPU^\dagger$  is a unitary transformation of  $U^\dagger PU - P$ ,

$$P - UPU^\dagger = U(U^\dagger PU - P)U^\dagger$$

Thus the dimension of +1 eigenspace of  $P - UPU^\dagger$  should be equal to the dimension of +1 eigenspace of  $U^\dagger PU - P$ .

$$\dim \ker[(P - UPU^\dagger) + 1] \pmod{2} = \dim \ker[(U^\dagger PU - P) - 1] \pmod{2} \quad (6.41)$$

That is,

$$\nu_2[U^\dagger] = \nu_1[U] \quad (6.42)$$

according to the definition of two flow indexes. Due to the equivalence between two indexes  $\nu_1[Y]$  and  $\nu_2[Y]$  given in Eq. (6.20),

$$\nu_1[U^\dagger] = \nu_1[U] \quad (6.43)$$

This equality meets our physical intuition. As our flow index only relates to the amplitude of a flow and ignore the direction information, two flows with the same amplitudes and opposite directions should share the same index.

## 6.3 Bulk-edge correspondence

### 6.3.1 Bulk invariant

Carpentier introduced a bulk invariant that can be used to classify the translation-invariant system. They build a new unitary evolution only containing the information during the first half-period in the original unitary evolution. We denote the new evolution unitary operator as  $V(t)$  while our original unitary evolution operator is  $U(t)$ .

This new evolution unitary operator is generated by the following Hamiltonian,

$$\tilde{H}(t) = \begin{cases} H(t) & 0 \leq t \leq \frac{T}{2} \\ H'(t) & \frac{T}{2} < t \leq T \end{cases} \quad (6.44)$$

For the first half period, the Hamiltonian in the new evolution is the same as the original one. And for the second half period, the new Hamiltonian  $H'(t)$  follows particle hole symmetry which can connect  $V(\frac{T}{2})$  with identity.

Then the new constructed evolution operator satisfies:

$$V(t) = U(t) \quad (0 \leq t \leq \frac{T}{2}) \quad (6.45)$$

and

$$\mathcal{T}V(t)\mathcal{T}^{-1} = V(t) \quad (\frac{T}{2} < t \leq T) \quad (6.46)$$

with  $V(T) = \mathbb{I}$ . In this way, we construct a two-dimensional unitary loop in class A. Then we can use the bulk invariant for class A to classify this new unitary evolution  $V(t)$ . [12, 66] It will be useful to distinguish between the closed-system evolution and the open-system evolution, which we write as  $U_c(t)$ ,  $V_c(t)$  and  $U_o(t)$ ,  $V_o(t)$  respectively. In the closed system, the bulk invariant can be expressed as [7]

$$W[V_c] = \frac{1}{2} \int dt \text{Tr} \left( V_c(t)^\dagger \partial_t V_c(t) \left[ V_c(t)^\dagger [P_x, V_c(t)], V_c(t)^\dagger [P_y, V_c(t)] \right] \right) \quad (6.47)$$

The  $Z_2$ -valued index  $K$  is defined by the relation

$$K[U_c] = W[V_c] \pmod{2} \quad (6.48)$$

Because  $V(t)$  is defined from  $U(T)$ ,  $V(t)$  contains all the information inside  $U(t)$ .

However, Carpentier only proved that this method worked for translation invariant systems. In order to generalize this method to disordered systems, we need to first prove the existence of the construction and then prove the independence of the choice of  $V(t)$ .

First, to prove the construction of a new unitary  $V(t)$  exist, we only need to show  $V(\frac{T}{2})$  can be smoothly connected to Identity in any systems. Explicitly, from Equation (6.44) and  $V(T) = \mathbb{I}$ , we have

$$V(\frac{T}{2}) = \mathcal{T} \exp \left[ i \int_{\frac{T}{2}}^T H'(t') dt' \right]$$

and the corresponding hamiltonian  $\tilde{H}(t')$  follows particle hole symmetry and belongs to class C,

$$\mathcal{T} H'(t') \mathcal{T}^{-1} = -H'(t').$$

In other words,  $V(\frac{T}{2})$  can be local generated by two dimensional particle hole symmetric Hamiltonians. According to the classification of local unitaries given in Chapter 2, we need to show that all two dimensional class C unitary  $V(\frac{T}{2})$  are topologically trivial to be smoothly connected to identity through class C hamiltonians. To do this, let's have a one to one correspondence from the unitary  $V(\frac{T}{2})$  and a local hermitian operator which is in Class CII,

$$H_V = \begin{pmatrix} 0 & V(\frac{T}{2}) \\ V(\frac{T}{2})^\dagger & 0 \end{pmatrix}, \quad (6.49)$$

and the second dimensional topological index for  $H_V$  is always trivial[4]. Therefore, all  $V(\frac{T}{2})$  is topologically trivial and thus can be locally generated by class C Hamiltonians  $H'(t)$ .

Next, let's address the question whether the  $Z_2$ -valued quantity  $K[U]$  is independent of the choice of the contraction. If there are two distinct ways to do the contraction, we can prove that the final  $Z_2$ -valued index will be the same for two methods. The difference between two winding numbers  $W[V_1]$  for the first contraction and  $W[V_2]$  for the second contraction is:

$$\begin{aligned}
W[V_1] - W[V_2] &= \frac{1}{2} \int dt dk_x dk_y & (6.50) \\
&\times \text{Tr}(V_{1c}^\dagger \partial_t V_{1c} [V_{1c}(t)^\dagger [P_x, V_{1c}(t)], V_{1c}(t)^\dagger [P_y, V_{1c}(t)]] \\
&\quad - \text{Tr}(V_{2c}^\dagger \partial_t V_{2c} [V_{2c}(t)^\dagger [P_x, V_{2c}(t)], V_{2c}(t)^\dagger [P_y, V_{2c}(t)]] \\
&= \frac{1}{2} \int dt \text{Tr}(\tilde{V}^\dagger \partial_t \tilde{V} [\tilde{V}^\dagger [P_x, \tilde{V}], \tilde{V}^\dagger [P_y, \tilde{V}]]
\end{aligned}$$

where we define a unitary loop as

$$\tilde{V}(t) = \begin{cases} V_{1c}(T-t) & 0 \leq t \leq \frac{T}{2} \\ V_{2c}(t) & \frac{T}{2} < t \leq T \end{cases}.$$

Since  $V_{1c}(t)$  and  $V_{2c}(t)$  both follow particle-hole symmetry given in Eq. (1.8),  $\tilde{V}(t)$  is also a class unitary and the winding number of it should always be even. Therefore

$$W[V_1] \pmod{2} = W[V_2] \pmod{2}$$

In summary, we can generalize the method developed by Carpentier to disordered systems.

### 6.3.2 Bulk-edge correspondence

In this section, we will prove that the bulk invariant equals our  $Z_2$  edge index at the end of the evolution. We first show that the edge index in the newly built Class A system is equal to the bulk invariant, i.e., the bulk edge correspondence in class A. Then, we associate this edge index to our  $Z_2$  edge index.

We partition the lattice into three spatial regions: L which is the part  $0 \leq x < L_x/3$ , M which is  $0 \leq x < 2L_x/3$  and R which is  $2L_x/3 \leq x \leq L_x$ . The bulk part M should be far away from the edges (larger than the Lieb-Robinson length) where is not affected by the cutting operation thus  $U_c(t) = U_o(t)$  which is just Identity in this area. Then the unitary  $V_o(T)$  takes the block diagonal form

$$V_o(T) = \begin{pmatrix} V_L(T) & & \\ & \mathbb{I} & \\ & & V_R(T) \end{pmatrix} \quad (6.51)$$

According to [7], we can count the number of edge modes by using the edge invariants,

$$\nu_{\text{edge}}[V_o] = \text{Tr}[V_L^\dagger P V_L - P] \quad (6.52)$$

Then due to the one to one correspondence between the well-defined bulk invariant and the edge index as shown in [7],

$$W[V_c] = \nu_{\text{edge}}[V_o] \quad (6.53)$$

Similarly, the unitary  $U_o(T)$  takes the block diagonal form

$$U_o(T) = \begin{pmatrix} U_L(T) & & \\ & \mathbb{I} & \\ & & U_R(T) \end{pmatrix} \quad (6.54)$$

Substituting  $t = T/2$  into Eq. (6.1), we find

$$\mathcal{T}U_o\left(\frac{T}{2}\right)\mathcal{T}^{-1} = U_o\left(\frac{T}{2}\right)U_o^\dagger(T) \quad (6.55)$$

and according to the construction formula Eq. (6.45)

$$V_c\left(\frac{T}{2}, 0\right) = U_c\left(\frac{T}{2}, 0\right)$$

For the second half period (follows the particle-hole symmetry)

$$\mathcal{T}V_c\left(T, \frac{T}{2}\right)\mathcal{T}^{-1} = V_c\left(T, \frac{T}{2}\right)$$

where we use  $V_c\left(T, \frac{T}{2}\right)$  to denote the unitary evolution for the second half period, i.e.,  $V_c\left(T, \frac{T}{2}\right) = V(T)V^\dagger\left(\frac{T}{2}\right)$ .

Following these equations, we can find the relation between the new constructed unitary and our original unitary at the end of the cycle:

$$\begin{aligned} \mathcal{T}V_c(T)\mathcal{T}^{-1} &= \mathcal{T}V_c\left(T, \frac{T}{2}\right)\mathcal{T}^{-1}\mathcal{T}V_c\left(\frac{T}{2}, 0\right)\mathcal{T}^{-1} \\ &= V_c\left(T, \frac{T}{2}\right)V_c\left(\frac{T}{2}, 0\right)U_c^\dagger(T) \\ &= V_c(T)U_c^\dagger(T) \end{aligned} \quad (6.56)$$

Then after decomposing  $V_c(T)$  and  $U_c(T)$  into three blocks:

$$U_L^\dagger(T) = V_L(T)^\dagger \mathcal{T} V_L(T) \mathcal{T}^{-1} \quad (6.57)$$

Now, we want to prove the bulk edge correspondence in this class AII system which can be written as

$$K[U_c] = \nu[U_L] \quad (6.58)$$

we just need to prove that

$$\nu_{\text{edge}}[V_o] \pmod{2} = \nu[U_L] \quad (6.59)$$

which can be written as

$$\begin{aligned} & \text{Tr}(V_L^\dagger P V_L - P) \pmod{2} \\ &= \dim(\ker(U_L^\dagger P U_L - P - 1)) \pmod{2} \end{aligned} \quad (6.60)$$

because these two equalities (6.52) and (6.53).

To proceed further, define the transport operator  $A$  based on the one dimensional edge unitary  $U_L$ :

$$A = U_L^\dagger P U_L - P \quad (6.61)$$

Eq. (6.57) gives a relation between the original full-period unitary  $U(T)$  and the new constructed full-period unitary  $V(T)$ , which we can use to rewrite the expression above as

$$A = V_L(T)^\dagger \mathcal{T} V_L(T) P V_L(T)^\dagger \mathcal{T}^{-1} V_L(T) - P \quad (6.62)$$

We introduce the operator

$$B = V_L^\dagger P V_L - P \quad (6.63)$$

After doing a unitary transformation, we can get a new operator

$$C = -V_L P V_L^\dagger + P = P - Q = V_L B V_L^\dagger \quad (6.64)$$

where  $Q$  arising from the unitary evolution  $V_L$  is defined as  $V_L B V_L^\dagger$ .

Thus

$$\text{Tr}(C) = \text{Tr}(B) \quad (6.65)$$

since a unitary transformation will not change the trace of a matrix. Similarly, let's do a transformation of the operator  $A$

$$D = \mathcal{T}^{-1} V_L A V_L^\dagger \mathcal{T} \quad (6.66)$$

$$= V_L P V_L^\dagger - \mathcal{T}^{-1} V_L P V_L^\dagger \mathcal{T} \quad (6.67)$$

$$= Q - \mathcal{T}^{-1} Q \mathcal{T} \quad (6.68)$$

Thus the dimension of the  $+1$  eigenspace of  $A$  equals the dimension of the  $+1$  eigenspace of  $D$ .

$$\dim(\ker(A - 1)) = \dim(\ker(D - 1)) \quad (6.69)$$

Let's study the eigenspace of operator  $D$ :

$$\mathcal{H}_{00}^D = \{|\phi\rangle \in \mathcal{H} | Q|\phi\rangle = 0, Q\mathcal{T}|\phi\rangle = 0\} \quad (6.70)$$

$$\mathcal{H}_{11}^D = \{|\phi\rangle \in \mathcal{H} | Q|\phi\rangle = |\phi\rangle, Q\mathcal{T}|\phi\rangle = 0\}$$

$$\mathcal{H}_{10}^D = \{|\phi\rangle \in \mathcal{H} | Q|\phi\rangle = |\phi\rangle, Q\mathcal{T}|\phi\rangle = 0\}$$

$$\mathcal{H}_{01}^D = \{|\phi\rangle \in \mathcal{H} | Q|\phi\rangle = |\phi\rangle, Q\mathcal{T}|\phi\rangle = \mathcal{T}|\phi\rangle\}$$

$$\mathcal{H}_{\perp}^D = \{|\phi\rangle \in \mathcal{H} | D|\phi\rangle = \lambda|\phi\rangle, 0 < |\lambda| < 1\}$$

Where  $\mathcal{H}_{10}^D$  indicates the  $+1$  eigenspace of  $D$  and  $\mathcal{H}_{01}^D$  is the  $-1$  eigenspace of  $D$ . Each vector in  $\mathcal{H}_{\perp}^D$  is an eigenvector for  $D$  with absolute value larger than zero and less than one. In the same time, we define projectors  $P_{00}$ ,  $P_{11}$ ,  $P_{10}$ ,  $P_{01}$  and  $P_{\perp}$  correlated to the Hilbert space  $\mathcal{H}_{00}^D$ ,  $\mathcal{H}_{11}^D$ ,  $\mathcal{H}_{10}^D$ ,  $\mathcal{H}_{01}^D$  and  $\mathcal{H}_{\perp}^D$  individually.

Now we want to prove that the zero eigenspace is just the combination of  $\mathcal{H}_{11}^D$  and  $\mathcal{H}_{00}^D$ . It's easy to verify that  $D^2$  commutes with  $Q$ , namely,

$$[D^2, Q] = 0. \quad (6.71)$$

Hence, we can diagonalized  $D^2$  and  $Q$  simultaneously. If  $D|\phi\rangle = 0$ , then  $D^2|\phi\rangle = 0$ . Therefore there are two sectors in the zero-eigenspace of  $D$  which corresponds to  $Q = 1$  and  $0$  separately. The first sector is the same as  $\mathcal{H}_{11}^D$  and the second sector is identical to  $\mathcal{H}_{00}^D$ .

From the above analysis, we see that the eigenspace of  $D$  is fully constructed by the combination of  $\mathcal{H}_{00}^D$  and  $\mathcal{H}_{11}^D$  which is the same as the zero eigenspace,  $\mathcal{H}_{10}^D$  which denotes the  $+1$  eigenspace,  $\mathcal{H}_{01}^D$  which is related to the  $-1$  eigenvalue and  $\mathcal{H}_{\perp}^D$  satisfying that the absolute values of eigenvalues are between  $0$  and  $1$ .

According to the theory of pairs of projectors, we can create another operator  $E = 1 - Q - \mathcal{T}^{-1}Q\mathcal{T}$ . Then the following two relations hold:

$$ED + DE = 0 \quad (6.72)$$

and

$$E^2 + D^2 = 1 \quad (6.73)$$

The second relation means that inside the  $D^2 = 1$  subspace,  $E^2 = 0$ . This shows that the zero eigenspace of  $E$  is identical to the  $\pm 1$  eigenspace of  $D$ . And similarly, the  $\pm 1$  eigenspace of  $E$  is the same as the zero eigenspace of  $D$ . To summarize, the eigenspace of  $E$  is made up of the combination of  $\mathcal{H}_{10}^D$  and  $\mathcal{H}_{01}^D$  which contain the zero eigenstate of  $E$ ,  $\mathcal{H}_{00}^D$  which indicates the  $+1$  eigenspace of  $E$ ,  $\mathcal{H}_{11}^D$  which is associated the  $-1$  eigenvalue of  $E$  and  $\mathcal{H}_{\perp}^D$  includes eigenstates with the eigenvalues not  $0$  or  $\pm 1$ .

In addition, from Eq. (6.66) we find that  $\mathcal{T}$  anticommutes with the operator  $D$ :

$$\mathcal{T}D + D\mathcal{T} = 0 \quad (6.74)$$

Similarly, it's clear that  $E$  commutes with the time reversal symmetric operator  $\mathcal{T}$ :

$$\mathcal{T}E\mathcal{T}^{-1} = E \quad (6.75)$$

This relation yields that  $E$  is time reversal symmetric which means that every energy level of  $E$  is at least doubly degenerate due to the Kramers theorem. From (6.72) we can

define an invertible map  $D$  that maps an eigenvector with eigenvalue  $\lambda \in (0, 1)$  to that with  $-\lambda$ . Thus, there is a one-to-one correspondence between the states  $|\phi\rangle$  and  $E|\phi\rangle$ , and their eigenvalues come in pairs  $\pm\lambda$ , provided that  $0 < |\lambda| < 1$ . Combined with the fact that every eigenvalue of  $E$  is double degenerate, we know that the eigenspace  $\mathcal{H}_D^\perp$  that is associated to each eigenvalue  $\lambda$  which satisfies  $0 < |\lambda| < 1$  is four-fold, to be specific,

$$\begin{aligned} & \text{Tr}(P_\perp)/2 \pmod{2} \\ &= \dim(\mathcal{H}_D^\perp)/2 \pmod{2} \\ &= 0 \pmod{2} \end{aligned} \tag{6.76}$$

Since  $D$  anticommutes with the time reversal symmetric operator  $\mathcal{T}$  (6.74), we can prove that the eigenstates  $|\phi\rangle$  and  $\mathcal{T}|\phi\rangle$  comes in pairs with opposite eigenvalues. Upon the fact that the operator  $D$  is antisymmetric about the eigenvalue 0, the trace of  $D$  is zero on the Hilbert space  $\mathcal{H}_\perp^D$ , in other words,

$$\text{Tr}(DP_\perp) = \text{Tr}(QP_\perp) - \text{Tr}(\mathcal{T}Q\mathcal{T}^{-1}P_\perp) = 0 \tag{6.77}$$

where  $P_\perp$  is the projector to the Hilbert space  $\mathcal{H}_\perp^D$ .

Due to the existence of the mapping  $D$ , we know that the eigenvalues of  $E$  on the Hilbert space  $\mathcal{H}_\perp^D$  come in  $\pm$  pairs, the trace of  $E$  on this Hilbert space is zero.

$$\begin{aligned} \text{Tr}(EP_\perp) &= \text{Tr}((1 - Q - \mathcal{T}Q\mathcal{T}^{-1})P_\perp) \\ &= \text{Tr}(P_\perp) - \text{Tr}(QP_\perp) - \text{Tr}(\mathcal{T}Q\mathcal{T}^{-1}P_\perp) \\ &= 0 \end{aligned} \tag{6.78}$$

Therefore,

$$\text{Tr}(P_\perp) = 2\text{Tr}(QP_\perp)$$

Since  $\text{Tr}(P_\perp)$  is just the dimension of  $\mathcal{H}_\perp^D$  which is a multiple of four(6.76),  $\text{Tr}(QP_\perp)$  is an even number, that is to say,

$$\text{Tr}(QP_\perp) \pmod{2} = 0 \tag{6.79}$$

For every state  $|\phi\rangle$  belongs to  $\mathcal{H}_{11}^D$ , then

$$\begin{aligned} Q|\phi\rangle &= |\phi\rangle \\ Q\mathcal{T}|\phi\rangle &= \mathcal{T}|\phi\rangle \end{aligned} \tag{6.80}$$

Then  $\mathcal{T}|\phi\rangle$  also belongs to  $\mathcal{H}_{11}^D$  because it meets the same requirement. Since  $\mathcal{T}|\phi\rangle$  and  $|\phi\rangle$  are linearly dependent with each other, the dimension of  $\mathcal{H}_{11}^D$  is even. After some straightforward algebraic calculation, we arrive at this equality,

$$\dim(\mathcal{H}_{11}^D) = \text{Tr}(P_{11}) = \text{Tr}(QP_{11}) \tag{6.81}$$

Consequently,

$$\text{Tr}(QP_{11}) \pmod{2} = 0 \pmod{2} \tag{6.82}$$

Now we can decompose the matrix  $Q$  into five parts according to different Hilbert space,

$$\begin{aligned} \text{Tr}(Q) &= \text{Tr}((P_{11} + P_{00} + P_{10} + P_{01} + P_{\perp})Q) \\ &= \text{Tr}((P_{11} + P_{10} + P_{\perp})Q) \\ &= \text{Tr}(P_{11}Q) + \text{Tr}(P_{10}Q) + \text{Tr}(P_{\perp}Q) \end{aligned} \tag{6.83}$$

owing to the fact that  $Q$  equals 0 on the Hilbertspace  $\mathcal{H}_{00}^D$  and  $\mathcal{H}_{01}^D$ . Because both  $\text{Tr}(P_{11}Q)$  and  $\text{Tr}(P_{\perp}Q)$  are even, the parity of  $\text{Tr}(Q)$  is the same as that of  $\text{Tr}(P_{10}Q)$ .

$$\text{Tr}(Q) \pmod{2} = \text{Tr}(QP_{10}) \pmod{2} \tag{6.84}$$

The final step is to massage the expression (6.84) into the desired form (6.60). Because the projector  $P$  which acts on the right side of the cut is time reversal symmetric, it's  $+1$  eigenvalue is double degenerate, to be specific,

$$\text{Tr}(P) \pmod{2} = 0 \pmod{2} \tag{6.85}$$

Combined with the definition of the matrix  $C$  (6.64) and the equality(6.65), the left side

of Eq. (6.84) becomes

$$\begin{aligned}
& \text{Tr}(Q) \pmod{2} && (6.86) \\
& = \text{Tr}(Q) - \text{Tr}(P) \pmod{2} \\
& = \text{Tr}(C) \pmod{2} \\
& = \text{Tr}(B) \pmod{2}
\end{aligned}$$

Because the operator  $Q$  is identity on the Hilbert space  $\mathcal{H}_{10}^D$ ,  $QP_{10}$  is just  $P_{10}$  and then the right side of Eq. (6.84) can be rewritten as

$$\begin{aligned}
\text{Tr}(QP_{10}) &= \text{Tr}(P_{10}) \\
&= \dim(\ker(D - 1)) \\
&= \dim(\ker(A - 1))
\end{aligned}$$

following from Eq. (6.69).

Substituting the expression (6.86) and (6.87) into (6.84),

$$\dim(\ker(A - 1)) \pmod{2} = \text{Tr}(B) \pmod{2}$$

just as expected. The left side of the above expression is the  $Z_2$  index of our time reversal symmetric evolution unitary and the right side indicates the parity of the edge invariant of the newly constructed unitary. Then combined with the bulk edge correspondence in class A, we can set up a one to one correspondence between the number of edge modes and the bulk invariant.

## 6.A Edge invariants deviation

As we discussed in Chapter 2, there is another method to derive edge invariants. In this section, we will show how to use this method to get edge invariants. First, we map the edge unitary in class AII to a flattened Hamiltonian in class DIII through

$$H_U = \begin{pmatrix} 0 & U \\ U^\dagger & 0 \end{pmatrix}. \quad (6.87)$$

Then we get the topological invariant of  $H_U$  from [44] which is

$$\text{Ind}_2(H_U) := \frac{1}{2} \dim \ker[S(P_R - H_U P_R H_U) - 1] \pmod{2} \quad (6.88)$$

After plugging Eq.(6.87) into the above equation, we can rewrite the topological invariant as the function of  $U$ ,

$$\text{Ind}_2(H_U) = \frac{1}{2} \left[ \dim \ker[(P_R - U P_R U^\dagger) - 1] + \dim \ker[(P_R - U^\dagger P_R U) + 1] \right] \pmod{2}. \quad (6.89)$$

As we know,  $P_R - U P_R U^\dagger$  is a unitary transformation of  $U^\dagger P_R U - P_R$ ,

$$P_R - U P_R U^\dagger = U(U^\dagger P_R U - P_R)U^\dagger \quad (6.90)$$

Thus the dimension of +1 eigenspace of  $P_R - U P_R U^\dagger$  should be equal to the dimension of +1 eigenspace of  $U^\dagger P_R U - P_R$ . In addition, because  $P_R - U^\dagger P_R U = -(U^\dagger P_R U - P_R)$ , the dimension of -1 eigenspace of  $P_R - U^\dagger P_R U$  should be equal to the dimension of +1 eigenspace of  $U^\dagger P_R U - P_R$ . Therefore, we can simplify Eq. (6.89) as

$$\text{Ind}_2(H_U) = \dim \ker[(U^\dagger P_R U - P_R) - 1] \pmod{2} \quad (6.91)$$

This agrees with what we show in Eq. (6.18).

# CHAPTER 7

## classification of the edge states in static Hamiltonians

### 7.1 Motivations

In the last sections, we have talked about the classification of Floquet systems. In this section, we will discuss the classification of static Hamiltonians following the connection between Floquet systems and static Hamiltonians. Previous studies of static Hamiltonians mainly focus on the classification of bulk Hamiltonians. There is limited research on the studies of edge modes besides counting the number of edge modes from eigenspectrum. A rigorous mathematical studies of edge modes in [45], however, only gives edge invariants for so-called complex classes of topological insulators, which don't include time-reversal or particle-hole symmetries. Our method fills this gap and can be used in any symmetry classes. In this way, our work forms a vital milestone in the study and characterization of Topological insulator phases.

### 7.2 Constructing unitary loops from a static Hamiltonian

As we discussed before, we define a unitary loop to be a unitary evolution that satisfies  $U(0) = U(T) = \mathbb{I}$  where  $T$  is the period of this evolution. This unitary loop captures all the dynamic features of an unitary evolution. That's the difference between Floquet systems and static systems. A unitary of this form can be seen to act trivially on a closed system but may generate nontrivial edge modes in a system with a boundary. In chapter 2, we classifies all edge unitaries which control edge behaviors in Floquet systems. As long as we can associate a static Hamiltonian to a unitary loop, we can build a connection between the edge modes of

the static Hamiltonian and the edge unitary of the corresponding unitary loop. In this way, we can directly apply the classification of edge unitaries to classify the edge modes of static Hamiltonians. To simplify the discussion, we first discuss flattened Hamiltonians.

Consider a flattened Hamiltonian  $H_f$  with a projector  $P_F$  where  $P_F$  projects onto the lower band, then we can define a unitary evolution which is governed by  $P_F$  with a period  $2\pi$ ,

$$U(t) = e^{itP_F} \quad (7.1)$$

After expanding this time evolution operator using the identity  $P_F^2 = P_F$ , we have

$$U(t) = (e^{it} - 1)P_F + 1 \quad (7.2)$$

Hence this is a unitary loop which meets  $U(2\pi) = U(0) = \mathbb{I}$ . We can also adjust this loop to be an evolution directly evolved by  $H_f$ . By substituting  $P_F = \frac{1-H_f}{2}$  and  $t' = t/2$ , we get another expression of this evolution,

$$U(t') = e^{-it'(H_f-1)} \quad (7.3)$$

with a period  $\pi$ . The part  $e^{it}$  just gives a phase shift and the topology is encoded in  $H_f$ .

In a close system, we can see from Eq.(7.2) that  $U(t)$  takes a block diagonal form, acting as the Identity matrix on the subspaces projected by  $1 - P_F$  and  $e^{it}\mathbb{I}$  matrix on the subspaces projected by  $P_F$ .  $e^{it}$  evolves from  $e^{i*0}$  to  $e^{i*2\pi}$  as time goes. That is, the quasienergy of the +1 eigenspace of the flattened Hamiltonian is fixed at 0 while the quasienergy of the -1 eigenspace evolve from 0 to  $2\pi$ . After opening the boundary, the edge states at the gap 0 of this flattened Hamiltonian will thus be pushed to the gap  $\pi$ .

Assume the number of edge modes for this flattened Hamiltonian is  $n_{edge}^H$ . In the evolution process, we keep the edge modes structure  $n_{edge}^H = n_{\pi}^U$  since we only extend or compress the energy bands. After a complete cycle, we get an effective edge unitary  $U_{edge}$  for this unitary loop. The topological invariants for this edge unitary is  $\nu[U_{edge}]$  which counts the the number of edge modes  $\nu[U_{edge}] = n_{\pi}^U$ . Therefore,  $n_{edge}^H = n_{\pi}^U$ . Then we use the classification of the edge unitary(emerge after opening the boundary for the unitary loop) to classify the edge modes for the Hamiltonian.

### 7.3 An example: class A Hamiltonian in two dimensions

In this section, we show how our logic works by testing it in two dimensional systems without any symmetries. Reference [5] gives a similar discussion but only in translation-invariant system and we are going to discuss in a more general context, including disordered system. First, we note that the time evolution operator  $U = e^{2\pi it P_F}$  satisfies the identities

$$\begin{aligned} U &= (e^{2\pi it} - 1)P_F + 1 \\ U^{-1} &= (e^{-2\pi it} - 1)P_F + 1, \end{aligned} \quad (7.4)$$

Expanding  $U^\dagger[P_x, U]$  in terms of  $P_F$ ,

$$\begin{aligned} U^\dagger[P_x, U] &= (e^{-2\pi it} - 1)(e^{2\pi it} - 1)P_F[P_x, P_F] \\ &+ (e^{2\pi it} - 1)[P_x, P_F] \\ &\equiv a(2\pi t) \cdot P_F[P_x, P_F] + b(2\pi t) [P_x, P_F]. \end{aligned} \quad (7.5)$$

where  $P_x$  is a projector acting on the right-half plane with  $x > 0$ . Here,

$$a(\theta) = 2 - 2 \cos(\theta) , \quad b(\theta) = e^{i\theta} - 1. \quad (7.6)$$

Similarly, we have

$$\begin{aligned} U^{-1}[P_y, P_F] &= a(2\pi t) \cdot P_F[P_y, P_F] + b(2\pi t) \cdot [P_y, P_F] \\ U^{-1}\partial_t U &= 2\pi i P_F. \end{aligned} \quad (7.7)$$

Combining these results, we find

$$\begin{aligned} &\text{Tr} \left( U^{-1}\partial_t P_F \right) U^\dagger[P_x, U] U^\dagger[P_y, U] \\ &= \text{Tr} \left( 2\pi i P_F (a(2\pi t) \cdot P_F[P_x, P_F] + b(2\pi t) [P_x, P_F]) \right. \\ &\quad \left. \cdot (a(2\pi t) P_F[P_y, P_F] + b(2\pi t) [P_y, P_F]) \right) \end{aligned} \quad (7.8)$$

By making use of the identity

$$P[P_x, P]P = [P_x, P^2]P - [P_x, P]P^2 = 0$$

Similarly,

$$P[P_y, P]P = 0$$

We can simplify Eq. (7.9),

$$\begin{aligned} & \text{Tr} \left( U^{-1} \partial_t P_F U^\dagger [P_x, U] U^\dagger [P_y, U] \right) \\ &= 2\pi i [2 \cos(2\pi t) - 2] \text{Tr} \left( P_F [P_x, P_F] [P_y, P_F] \right) \end{aligned}$$

We can now compute the winding number corresponding to  $U$  given in Reference. [7]:

$$\begin{aligned} W[U] &= \frac{1}{2} \int_0^1 dt \text{Tr} \left( U^{-1} \partial_t P_F U^\dagger [P_x, U] U^\dagger [P_y, U] \right) - (x \leftrightarrow y) \\ &= \pi i \int dt [2 \cos(2\pi t) - 2] \text{Tr} \left( P_F [P_x, P_F] [P_y, P_F] \right) \end{aligned} \quad (7.9)$$

$$= -2\pi i \text{Tr} \left( P_F [P_x, P_F] [P_y, P_F] \right) \quad (7.10)$$

The latter expression is the Chern number of a real-space Hamiltonian[31]. In this way, we showed how a static Hamiltonian can be mapped to a special unitary loop. In addition, the topological invariant of such unitary loop is equal to the topological invariant used in classifying a bulk Hamiltonian.

## BIBLIOGRAPHY

- [1] Rahul Roy and Fenner Harper. Periodic table for Floquet topological insulators. *Physical Review B*, 96(15), October 2017.
- [2] Alexei Kitaev, Vladimir Lebedev, and Mikhail Feigel'man. Periodic table for topological insulators and superconductors. *AIP Conference Proceedings*, pages 22–30, 2009.
- [3] Andreas P. Schnyder, Shinsei Ryu, Akira Furusaki, and Andreas W. W. Ludwig. Classification of topological insulators and superconductors in three spatial dimensions. *Physical Review B*, 78(19):195125, November 2008.
- [4] Hosho Katsura and Tohru Koma. The Noncommutative Index Theorem and the Periodic Table for Disordered Topological Insulators and Superconductors. *arXiv:1611.01928 [cond-mat, physics:hep-lat, physics:hep-th, physics:math-ph]*, November 2016. arXiv: 1611.01928.
- [5] Mark S. Rudner, Netanel H. Lindner, Erez Berg, and Michael Levin. Anomalous Edge States and the Bulk-Edge Correspondence for Periodically Driven Two-Dimensional Systems. *Physical Review X*, 3(3), July 2013.
- [6] Fenner Harper, Rahul Roy, Mark S. Rudner, and S. L. Sondhi. Topology and Broken Symmetry in Floquet Systems. *arXiv:1905.01317 [cond-mat]*, May 2019. arXiv: 1905.01317.
- [7] Gian Michele Graf and Clément Tauber. Bulk–Edge Correspondence for Two-Dimensional Floquet Topological Insulators. *Annales Henri Poincaré*, 19(3):709–741, March 2018.
- [8] Takuya Kitagawa, Erez Berg, Mark Rudner, and Eugene Demler. Topological characterization of periodically driven quantum systems. *Physical Review B*, 82(23), December 2010.
- [9] Liang Jiang, Takuya Kitagawa, Jason Alicea, A. R. Akhmerov, David Pekker, Gil Refael, J. Ignacio Cirac, Eugene Demler, Mikhail D. Lukin, and Peter Zoller. Majorana Fermions

- in Equilibrium and in Driven Cold-Atom Quantum Wires. *Physical Review Letters*, 106(22), June 2011.
- [10] Manisha Thakurathi, Aavishkar A. Patel, Diptiman Sen, and Amit Dutta. Floquet generation of Majorana end modes and topological invariants. *Physical Review B*, 88(15), October 2013.
- [11] J. K. Asbóth, B. Tarasinski, and P. Delplace. Chiral symmetry and bulk-boundary correspondence in periodically driven one-dimensional systems. *Physical Review B*, 90(12):125143, September 2014.
- [12] David Carpentier, Pierre Delplace, Michel Fruchart, and Krzysztof Gawędzki. Topological Index for Periodically Driven Time-Reversal Invariant 2d Systems. *Physical Review Letters*, 114(10), March 2015.
- [13] Frederik Nathan and Mark S Rudner. Topological singularities and the general classification of Floquet–Bloch systems. *New Journal of Physics*, 17(12):125014, December 2015.
- [14] Michel Fruchart. Complex classes of periodically driven topological lattice systems. *Physical Review B*, 93(11), March 2016.
- [15] C. W. von Keyserlingk and S. L. Sondhi. Phase structure of one-dimensional interacting Floquet systems. II. Symmetry-broken phases. *Physical Review B*, 93(24):245146, June 2016.
- [16] Dominic V. Else and Chetan Nayak. Classification of topological phases in periodically driven interacting systems. *Physical Review B*, 93(20):201103, May 2016.
- [17] Andrew C. Potter, Takahiro Morimoto, and Ashvin Vishwanath. Classification of Interacting Topological Floquet Phases in One Dimension. *Physical Review X*, 6(4), October 2016.

- [18] Rahul Roy and Fenner Harper. Abelian Floquet symmetry-protected topological phases in one dimension. *Physical Review B*, 94(12), September 2016.
- [19] Paraj Titum, Erez Berg, Mark S. Rudner, Gil Refael, and Netanel H. Lindner. The anomalous Floquet-Anderson insulator as a non-adiabatic quantized charge pump. *Physical Review X*, 6(2), May 2016. arXiv: 1506.00650.
- [20] Manisha Thakurathi, Daniel Loss, and Jelena Klinovaja. Floquet Majorana fermions and parafermions in driven Rashba nanowires. *Physical Review B*, 95(15), April 2017.
- [21] André Eckardt. Colloquium: Atomic quantum gases in periodically driven optical lattices. *Reviews of Modern Physics*, 89(1):011004, March 2017.
- [22] Gregor Jotzu, Michael Messer, Rémi Desbuquois, Martin Lebrat, Thomas Uehlinger, Daniel Greif, and Tilman Esslinger. Experimental realization of the topological Haldane model with ultracold fermions. *Nature*, 515(7526):237–240, November 2014.
- [23] M. Esmann, F. R. Lamberti, A. Lemaître, and N. D. Lanzillotti-Kimura. Topological acoustics in coupled nanocavity arrays. *Physical Review B*, 98(16):161109, October 2018.
- [24] Zhaoju Yang, Fei Gao, Xihang Shi, Xiao Lin, Zhen Gao, Yidong Chong, and Baile Zhang. Topological Acoustics. *Physical Review Letters*, 114(11):114301, March 2015.
- [25] Tomoki Ozawa, Hannah M. Price, Alberto Amo, Nathan Goldman, Mohammad Hafezi, Ling Lu, Mikael C. Rechtsman, David Schuster, Jonathan Simon, Oded Zilberberg, and Iacopo Carusotto. Topological photonics. *Reviews of Modern Physics*, 91(1):015006, March 2019.
- [26] Dominic Reiss, Fenner Harper, and Rahul Roy. Interacting Floquet topological phases in three dimensions. *Physical Review B*, 98(4):045127, July 2018. Publisher: American Physical Society.
- [27] Hoi Chun Po, Lukasz Fidkowski, Takahiro Morimoto, Andrew C. Potter, and Ashvin

- Vishwanath. Chiral Floquet Phases of Many-body Localized Bosons. *Physical Review X*, 6(4), December 2016. arXiv: 1609.00006.
- [28] M. Burak Şahinoğlu, Sujeet K. Shukla, Feng Bi, and Xie Chen. Matrix product representation of locality preserving unitaries. *Physical Review B*, 98(24), December 2018.
- [29] Zongping Gong, Christoph Sünderhauf, Norbert Schuch, and J. Ignacio Cirac. Classification of Matrix-Product Unitaries with Symmetries. *arXiv:1812.09183 [cond-mat, physics:math-ph, physics:quant-ph]*, September 2019. arXiv: 1812.09183.
- [30] D. Gross, V. Nesme, H. Vogts, and R. F. Werner. Index Theory of One Dimensional Quantum Walks and Cellular Automata. *Communications in Mathematical Physics*, 310(2):419–454, March 2012.
- [31] Alexei Kitaev. Anyons in an exactly solved model and beyond. *Annals of Physics*, 321(1):2–111, January 2006.
- [32] C. Cedzich, T. Geib, C. Stahl, L. Velázquez, A. H. Werner, and R. F. Werner. Complete homotopy invariants for translation invariant symmetric quantum walks on a chain. *Quantum*, 2:95, September 2018. arXiv: 1804.04520.
- [33] C. Cedzich, T. Geib, F. A. Grünbaum, C. Stahl, L. Velázquez, A. H. Werner, and R. F. Werner. The topological classification of one-dimensional symmetric quantum walks. *arXiv:1611.04439 [cond-mat, physics:math-ph, physics:quant-ph]*, November 2016. arXiv: 1611.04439.
- [34] C Cedzich, F A Grünbaum, C Stahl, L Velázquez, A H Werner, and R F Werner. Bulk-edge correspondence of one-dimensional quantum walks. *Journal of Physics A: Mathematical and Theoretical*, 49(21):21LT01, May 2016.
- [35] J. K. Asboth. Symmetries, Topological Phases and Bound States in the One-Dimensional Quantum Walk. *Physical Review B*, 86(19):195414, November 2012. arXiv: 1208.2143.

- [36] Shunyu Yao, Zhongbo Yan, and Zhong Wang. Topological invariants of Floquet systems: General formulation, special properties, and Floquet topological defects. *Physical Review B*, 96(19), November 2017.
- [37] Xu Liu, Fenner Harper, and Rahul Roy. Chiral flow in one-dimensional Floquet topological insulators. *Physical Review B*, 98(16):165116, October 2018.
- [38] Bastian Höckendorf, Andreas Alvermann, and Holger Fehske. Topological invariants for Floquet-Bloch systems with chiral, time-reversal, or particle-hole symmetry. *Physical Review B*, 97(4), January 2018. arXiv: 1708.07420.
- [39] Christian Sadel and Hermann Schulz-Baldes. Topological boundary invariants for Floquet systems and quantum walks. *Mathematical Physics, Analysis and Geometry*, 20(4), August 2017.
- [40] Paolo Glorioso, Andrey Gromov, and Shinsei Ryu. Effective response theory for Floquet topological systems. *arXiv:1908.03217 [cond-mat, physics:hep-th]*, September 2019. arXiv: 1908.03217.
- [41] Shinsei Ryu, Andreas P Schnyder, Akira Furusaki, and Andreas W W Ludwig. Topological insulators and superconductors: tenfold way and dimensional hierarchy. *New Journal of Physics*, 12(6):065010, June 2010.
- [42] Sho Higashikawa, Masaya Nakagawa, and Masahito Ueda. Floquet Chiral Magnetic Effect. *Physical Review Letters*, 123(6):066403, August 2019. Publisher: American Physical Society.
- [43] Ching-Kai Chiu, Jeffrey C. Y. Teo, Andreas P. Schnyder, and Shinsei Ryu. Classification of topological quantum matter with symmetries. *Reviews of Modern Physics*, 88(3), August 2016. arXiv: 1505.03535.
- [44] Hosho Katsura and Tohru Koma. The noncommutative index theorem and the periodic table for disordered topological insulators and superconductors. *Journal of Mathematical Physics*, 59(3):031903, March 2018.

- [45] Emil Prodan and Hermann Schulz-Baldes. *Bulk and Boundary Invariants for Complex Topological Insulators*. Mathematical Physics Studies. Springer International Publishing, Cham, 2016.
- [46] C. Cedzich, T. Geib, F. A. Grünbaum, C. Stahl, L. Velázquez, A. H. Werner, and R. F. Werner. The Topological Classification of One-Dimensional Symmetric Quantum Walks. *Annales Henri Poincaré*, 19(2):325–383, February 2018.
- [47] R. Bott and R. Seeley. Some remarks on the paper of Callias. *Communications in Mathematical Physics*, 62(3):235–245, October 1978.
- [48] D.-L. Deng, S.-T. Wang, and L.-M. Duan. Systematic construction of tight-binding Hamiltonians for topological insulators and superconductors. *Physical Review B*, 89(7):075126, February 2014. Publisher: American Physical Society.
- [49] Alexander Altland and Martin R. Zirnbauer. Nonstandard symmetry classes in mesoscopic normal-superconducting hybrid structures. *Physical Review B*, 55(2):1142–1161, January 1997.
- [50] Xie Chen, Zheng-Cheng Gu, and Xiao-Gang Wen. Local unitary transformation, long-range quantum entanglement, wave function renormalization, and topological order. *Physical Review B*, 82(15), October 2010.
- [51] Sergey Bravyi, Matthew B. Hastings, and Spyridon Michalakis. Topological quantum order: Stability under local perturbations. *Journal of Mathematical Physics*, 51(9):093512, September 2010.
- [52] Max Karoubi. *K-Theory: An Introduction*. Classics in Mathematics. Springer-Verlag, Berlin Heidelberg, 2008.
- [53] Ian Mondragon-Shem, Taylor L. Hughes, Juntao Song, and Emil Prodan. Topological Criticality in the Chiral-Symmetric AIII Class at Strong Disorder. *Physical Review Letters*, 113(4):046802, July 2014.

- [54] Jeffrey C. Y. Teo and C. L. Kane. Topological defects and gapless modes in insulators and superconductors. *Physical Review B*, 82(11), September 2010.
- [55] A Yu Kitaev. Unpaired Majorana fermions in quantum wires. *Physics-Usppekhi*, 44(10S):131–136, October 2001.
- [56] Xiao-Liang Qi, Yong-Shi Wu, and Shou-Cheng Zhang. Topological quantization of the spin Hall effect in two-dimensional paramagnetic semiconductors. *Physical Review B*, 74(8):085308, August 2006. Publisher: American Physical Society.
- [57] Jahan Claes and Taylor L. Hughes. Disorder driven phase transitions in weak AIII topological insulators. *Physical Review B*, 101(22):224201, June 2020. Publisher: American Physical Society.
- [58] P. Heinzner, A. Huckleberry, and M.R. Zirnbauer. Symmetry Classes of Disordered Fermions. *Communications in Mathematical Physics*, 257(3):725–771, August 2005.
- [59] W. P. Su, J. R. Schrieffer, and A. J. Heeger. Solitons in Polyacetylene. *Physical Review Letters*, 42(25):1698–1701, June 1979.
- [60] Fenner Harper and Rahul Roy. Floquet Topological Order in Interacting Systems of Bosons and Fermions. *Physical Review Letters*, 118(11):115301, March 2017.
- [61] S.-T. Wang, D.-L. Deng, Joel E. Moore, Kai Sun, and L.-M. Duan. Quantized electromagnetic response of three-dimensional chiral topological insulators. *Physical Review B*, 91(3):035108, January 2015. Publisher: American Physical Society.
- [62] Gian Michele Graf and Jacob Shapiro. The Bulk-Edge Correspondence for Disordered Chiral Chains. *arXiv:1801.09487 [cond-mat, physics:math-ph]*, page 20, January 2018. arXiv: 1801.09487.
- [63] D. J. Thouless. Quantization of particle transport. *Physical Review B*, 27(10):6083–6087, May 1983.

- [64] J. Avron, R. Seiler, and B. Simon. The Index of a Pair of Projections. *Journal of Functional Analysis*, 120(1):220–237, February 1994.
- [65] Hosho Katsura and Tohru Koma. The  $Z_2$  Index of Disordered Topological Insulators with Time Reversal Symmetry. *Journal of Mathematical Physics*, 57(2):021903, February 2016. arXiv: 1508.05485.
- [66] D. Carpentier, P. Delplace, M. Fruchart, K. Gawędzki, and C. Tauber. Construction and properties of a topological index for periodically driven time-reversal invariant 2d crystals. *Nuclear Physics B*, 896:779–834, July 2015.
- [67] Terry Farrelly. A review of Quantum Cellular Automata. *arXiv:1904.13318 [quant-ph]*, April 2019. arXiv: 1904.13318.
- [68] Yue Yu, Yong-Shi Wu, and Xincheng Xie. Bulk–edge correspondence, spectral flow and Atiyah–Patodi–Singer theorem for the  $Z_2$ -invariant in topological insulators. *Nuclear Physics B*, 916:550–566, March 2017.
- [69] D. C. Tsui, H. L. Stormer, and A. C. Gossard. Two-Dimensional Magnetotransport in the Extreme Quantum Limit. *Physical Review Letters*, 48(22):1559–1562, May 1982.
- [70] Richard E Prange and Steven M Girvin. *The Quantum Hall Effect*. Springer New York, New York, NY, 1990. OCLC: 852790318.
- [71] K. v. Klitzing, G. Dorda, and M. Pepper. New Method for High-Accuracy Determination of the Fine-Structure Constant Based on Quantized Hall Resistance. *Physical Review Letters*, 45(6):494–497, August 1980.
- [72] Marcos Atala, Monika Aidelsburger, Julio T. Barreiro, Dmitry Abanin, Takuya Kitagawa, Eugene Demler, and Immanuel Bloch. Direct measurement of the Zak phase in topological Bloch bands. *Nature Physics*, 9:795, November 2013.
- [73] Algebraic topology 1 | Geometry and topology.

- [74] Fenner Harper, Rahul Roy, Mark S. Rudner, and S. L. Sondhi. Topology and Broken Symmetry in Floquet Systems. *arXiv:1905.01317 [cond-mat]*, May 2019. arXiv: 1905.01317.